SYNTHESES AND CHARACTERIZATIONS OF MIXED-LIGAND COPPER(I/II)

AND SILVER(I) COMPLEXES AND METALLOPOLYMERS WITH PYRAZOLATE-

AND PHENANTHROLINE-BASED LIGANDS AND POLY(4-VINYLPYRIDINE)

A THESIS

SUBMITTED IN PARTIAL FULLFILLMENT OF THE REQUIREMENTS

FOR THE DEGREE OF MASTER OF SCIENCE

IN THE GRADUATE SCHOOL OF THE

TEXAS WOMAN'S UNIVERSITY

DEPARTMENT OF CHEMISTRY AND BIOCHEMISTRY,

COLLEGE OF ARTS AND SCIENCES

BY

ALLAN KOLEK, B.S.

DENTON, TEXAS

AUGUST 2019

ACKNOWLEDGMENTS

ABSTRACT

ALLAN KOLEK

SYNTHESES AND CHARACTERIZATIONS OF MIXED-LIGAND COPPER(I/II)

AND SILVER(I) COMPLEXES AND METALLOPOLYMERS WITH PYRAZOLATE-

AND PHENANTHROLINE-BASED LIGANDS AND POLY(4-VINYLPYRIDINE)

AUGUST 2019

This thesis focuses on the syntheses and characterizations of heteroleptic Cu(I/II) and Ag(I) complexes and coordination polymers with fluorinated-pyrazolate (FPz⁻) and phenanthrolines (phen) ligands, followed by that of copper(I) iodide-based Cu(I/II) complexes and metallopolyers with the fluorinated-pyrazolate (FPz⁻) ligand and poly(4-vinylpyridine) (PVP). Chapter I provides an introduction into the chemistry of homoleptic coinage metal-pyrazolate complexes, pyrazolate ligands, phenanthroline ligands, heteroleptic coinage metal complexes, solventless syntheses, copper(I) halide complexes, and poly(4-vinylpyridine), respectively, followed by the potential applications of coinage metal complexes/coordination polymers with the aforementioned ligands. Chapter II discusses the synthetic routes of the aforementioned Cu(I/II) and Ag(I) complexes and metallopolymers with the respective ligands. Chapter III discusses structural, physical, and photophysical properties of the resulting products. Chapter IV summarizes and concludes the effects of the different synthetic routes, the metal, and the ligand on the resulting products with regard to their aforementioned properties.

TABLE OF CONTENTS

Chapter

LIST OF TABLES

LIST OF FIGURES

Figure   Page

xii

xiii

xvi

CHAPTER I

INTRODUCTION TO COINAGE METAL COMPLEXES

WITH N-HETEROCYCLIC, AROMATIC LIGANDS:

PYRAZOLATES, PHENANTHROLINES, AND POLY(4-VINYL PYRIDINE)

This thesis will primarily focus on the syntheses of heteroleptic (mixed-ligand) copper(I) and silver(I) compounds with the N-heterocyclic, aromatic ligands: fluorinated-pyrazolate (FPz$^-$) and phenanthrolines (phen), followed by their characterizations with regard to their physical, photophysical, and structural properties. In addition, alternative methods of syntheses will be explored, offering insight into the effects of solvent-mediated synthesis versus solventless ("green" solvent-free chemistry) syntheses on the resulting products. The syntheses and characterizations of copper(I) iodide-based complexes and metallopolymers will be explored with the ligands: fluorinated-pyrazolate (FPz$^-$) and poly(4-vinylpyridine).

1.1 Chemistry of Coinage Metal-Pyrazolate Complexes

Cyclic, trinuclear Au(I), Ag(I), and Cu(I) complexes possess extraordinary photophysical properties with regard to the modification of the metal center, the substituents on the ligand, and the environment and/or medium in which the complexes exist.[1] For example, in solid-state, various cyclic, trinuclear Cu(I) complexes, {[3,5-

(R,R')Pz]Cu$\}_3$, exhibit an assortment of emission colors, which were enhanced and/or tuned with regard to a change in temperature, as shown in Figure 1.[1-3] The Cu(I) complex, $\{[3,5\text{-}(CF_3)_2Pz]Cu\}_3$, exhibited a variety of vibrant emission colors when frozen solutions of the Cu(I) complex was prepared, producing a wide-range of colors across the visible region (390 nm to 780 nm).[1] This was accomplished through coarse- and fine-tuning, such as changing the identity of the solvent and/or the concentration of the Cu(I) complex, as shown in Figure 2.[1-3] These changes in photoluminescence color were attributed to the modification or disruption of the intertrimer Cu-Cu cuprophilic bonding caused by the presence of the solvent molecules.[1]
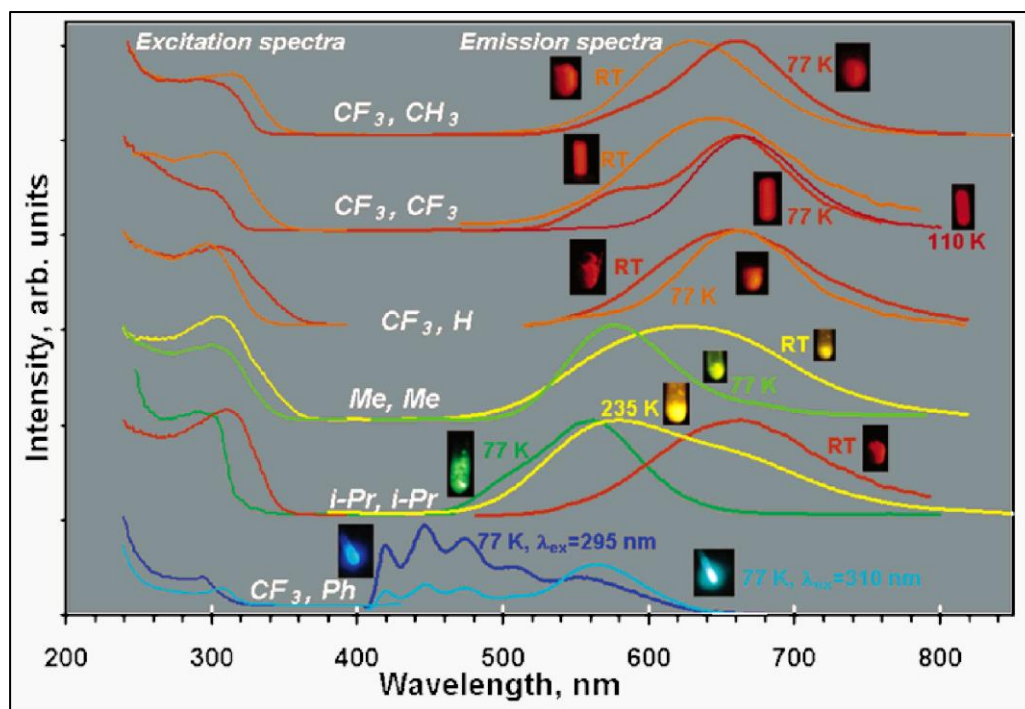
Figure 1. Solid-state photoluminescence (PL) spectra of Cu(I) trinuclear complex: $\{[3,5\text{-}$ (R,R')Pz]Cu$\}$3, varying in R,R' substituents (R,R' = CF3, CH3 / CF3, CF3 / CF3, H / CH3, CH3 / i-Pr, i-Pr / CF3, Ph) with regard to change in temperature.[1-3]
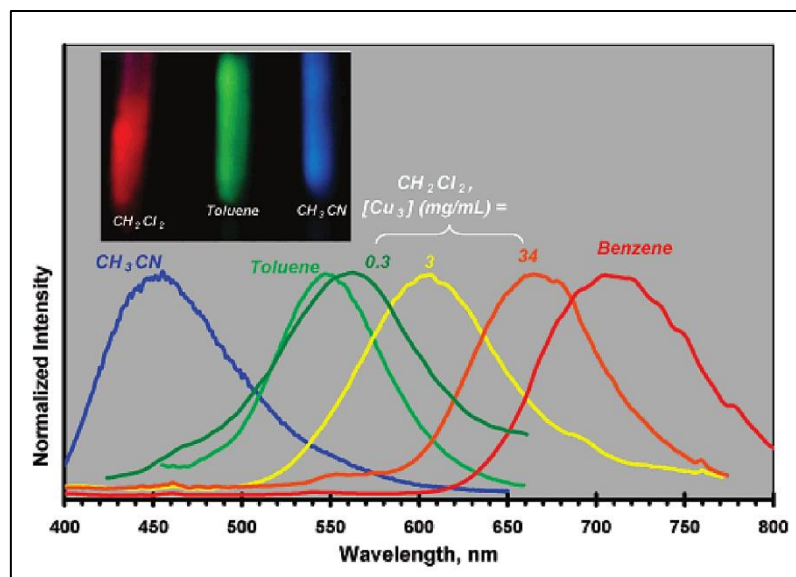
Figure 2. Photoluminescence (PL) spectra of frozen solutions of fluorinated-pyrazolate Cu(I) trinuclear complex: $\{[3,5-(CF_3)_2Pz]Cu\}_3$, with regard to change in identity of solvent and concentration of the Cu(I) complex.[1-3]

Investigations into coinage metal complexes with pyrazolate ligands (N-,N-bidentate, bridging ligands), such as $\{[3,5-(R,R')\ Pz]Cu\}_3$ and $\{[3,5-(CF_3)_2Pz]Au\}_3$, inspired the syntheses of the cyclic, trinuclear Cu(I)- and Ag(I)-pyrazolate complexes: $\{[3,5-(CF_3)_2Pz]M\}_3$, shown in Figure 3.[1,4] The resulting homoleptic, coinage metal trimers with fluorinated-pyrazolates, $\{[3,5-(CF_3)_2Pz]M\}_3$ (M = Au(I) Ag(I), and Cu(I)) are comprised of a nearly planar, nine-membered M_3N_6 ring with the metal atoms connected via the N-,N- bidentate, bridging ligand.[4-5] Although these fluorinated metal trimers appear similar in their overall molecular structure, they differ significantly with regard to their structural, photophysical, and acid-base properties, which are primarily dictated by the role/function of the metal(I) atoms.[6]
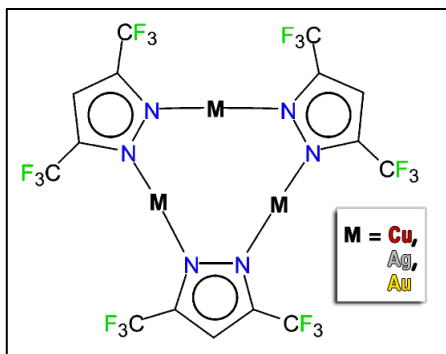
Figure 3. Structure of coinage metal trinuclear clusters (trimers) with fluorinated-pyrazolate ligand: $\{[3,5\text{-}(CF_3)_2Pz]M\}_3$ (M = Au(I) Ag(I), and Cu(I)).[1-6]

The single crystal of three trimer analogues exhibited photoluminescence thermochromism (temperature-dependent luminescence), as shown in Figure 4, which was significantly more dramatic for the Au(I) analogue, possessing orange (λ_{em} ~660 nm), green (λ_{em} ~535 nm), and UV (λ_{em} ~365 nm) phosphorescence, respectively, with regard to decreasing temperature (from room temperature (RT) to cryogenic temperatures).[5] Similarly, the Cu(I) analogue possesses bright orange (λ_{em} ~660 nm) phosphorescence at RT and cryogenic temperatures; however, the orange phosphorescence observed at 77K and 4K was due to a combination of a yellow shoulder at ~590 nm, followed by a major red peak at ~665 nm, which could neither be isolated nor significantly increased despite decreasing the temperature.[5] Although the Ag(I) analogue does not exhibit photoluminescence at room temperature, it does exhibit blue (λ_{em} ~460 nm) and UV (λ_{em} ~395 nm) phosphorescence at cryogenic temperatures with both emissions observed at 30K, which could be isolated by varying the temperature to 77K and 4K, respectively.[5] In comparison, the lack of photoluminescence observed at room temperature was due to intermolecular Ag-Ag argentophilic interaction; however,

the violet and/or blue photoluminescence that was observed at cryogenic temperatures was due to Ag-Ag covalent bonding.[1]
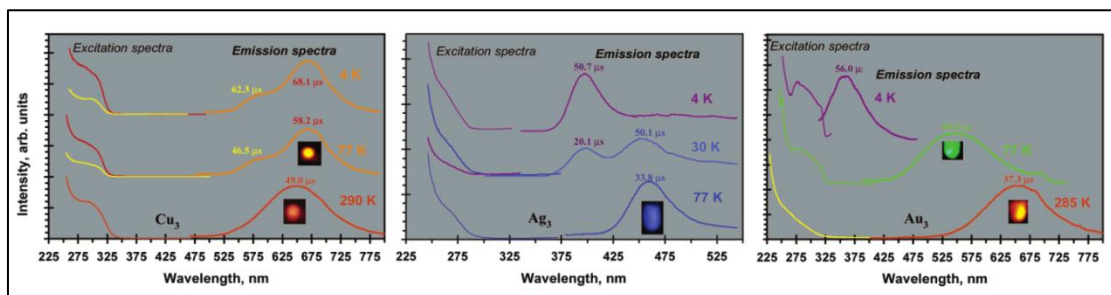
Figure 4. Photoluminescence (PL) spectra of coinage metal trinuclear clusters (trimers) with fluorinated-pyrazolate ligand: $\{[3,5-(CF_3)_2Pz]M\}_3$ (M = Au(I) Ag(I), and Cu(I)).[1]

The aforementioned trinuclear metal(I) complexes possess intermolecular M-M interactions, which increase pairwise with regard to Cu(I), Ag(I), and Au(I), respectively, thus allowing for the formation (packing) of extended supramolecular crystal structures resembling variations of extended zigzag chains, shown in Figure 5.[5] Enhanced M-M bonding in the excited state is exhibited due to the presence of these extended zigzag chains and the neighboring metal(I) centers, thus allowing for the possibility for multiple excited states.[5] As depicted in the photophysical model for the Au(I) analogue (shown in Figure 6), with regard to its photoluminescence thermochromism, three phosphorescent triplet metal-metal (^{3}MM) emitting states are involved (upon relaxation), one for each emission band: (1) the UV emission band (the highest-energy), (2) the green emission band (the second highest-energy), and (3) the orange emission band (the lowest-energy).[5] The ^{1}LMMCT absorption band can undergo intersystem-crossing from an excited singlet state to an excited triplet state.[5] Internal conversation, from a higher triplet state to a

lower triplet state, results in the change in phosphorescence with regard temperature, such as the change in phosphorescence from UV to green, upon increasing the temperature from 4K to 77K, and from green to orange, upon increasing the temperature from 77K to 285K.[5]
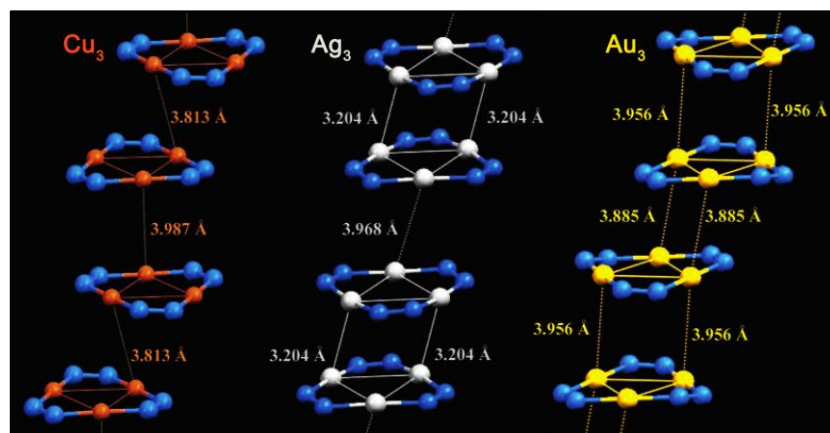
Figure 5. Crystal packing of coinage metal trinuclear clusters (trimers) with Ligand: {[3,5-(CF$_3$)$_2$Pz]M}$_3$ (M = Au(I) Ag(I), and Cu(I)).[5] The extended structures depict the two closest intermolecular M-M interactions distances for the Cu(I), Ag(I), and Au(I) analogue.[5]
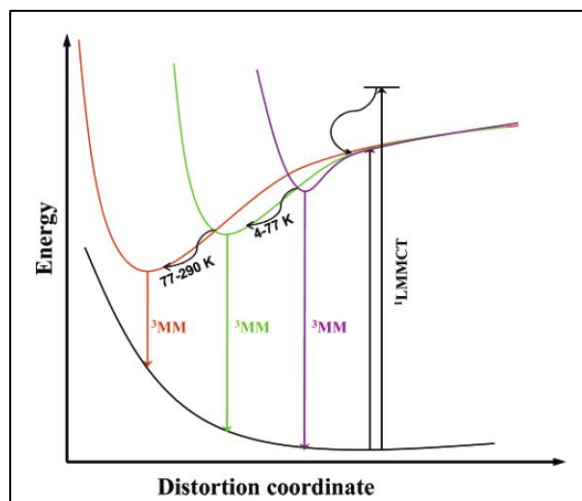
Figure 6. Photophysical model for Au(I) trinuclear cluster (Trimer) with fluorinated-pyrazolate Ligand: {[3,5-(CF$_3$)$_2$Pz]Au}$_3$, illustrating the three phosphorescent triplet metal-metal (^{3}MM) emitting states with regard to change in temperature.[5]

The acid-base properties of three methylated-pyrazolate metal(I) trimer analogues, $\{[3,5\text{-}(CH_3)_2Pz]M\}_3$ (M = Au(I), Ag(I), Cu(I)) were compared using molecular electrostatic potential (MEP), as shown in Figure 7, and although basic in nature due to the presence of their methylated substituents (base), the three anologues vary in degree of basicity with the Au(I) complex being the most basic and the Ag(I) complex being the least basic.[5] The ligand effect is visually apparent upon comparison with the fluorinated-pyrazolate metal(I) trimer $\{[3,5\text{-}(CF_3)_2Pz]Au\}_3$, acidic in nature due to the presence of the fluorinated substituents (acid).[5] The understanding of the acid-base behavior of these metal(I) trimers paved the way for the syntheses of π-acidic/ π-basic binary adducts.[5]
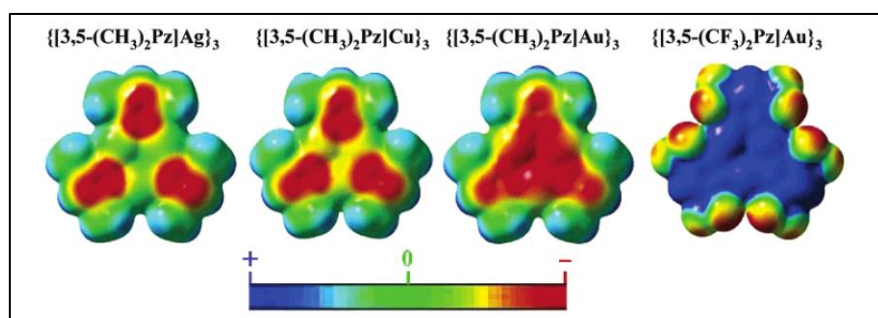
Figure 7. Molecular electrostatic potentials (MEP) of $\{[3,5\text{-}(R)_2Pz]M\}_3$ with basicity of metal (M = Ag(I), Cu(I), and Ag(I)) and R substituents (R = CH_3 and CF_3).[5]

As shown in Figure 8, the fluorinated-pyrazolate Ag(I) trimer, $\{[3,5\text{-}(CF_3)_2Pz]Ag\}_3$, exhibited vapochromic sensor properties: photoluminescence enhancement ("turn-ON") and/or photoluminescence quenching ("turn-OFF"), possessing vivid (bright) luminescent properties in the presence of small aromatic molecules (SAMs): green phosphorescence (λ_{em} = ~510 and ~520 nm) in benzene and toluene, respectively, and blue phosphorescence (λ_{em} = ~400 nm) in mesitylene.[1,6] Similar

7

photophysical properties were observed for single crystal adducts of the π-acidic Ag(I) complex grown in the respective aromatic solvents (π-basic), all of which influence the stacking/packing motif of the π-acid/base binary adduct system.[1,6]
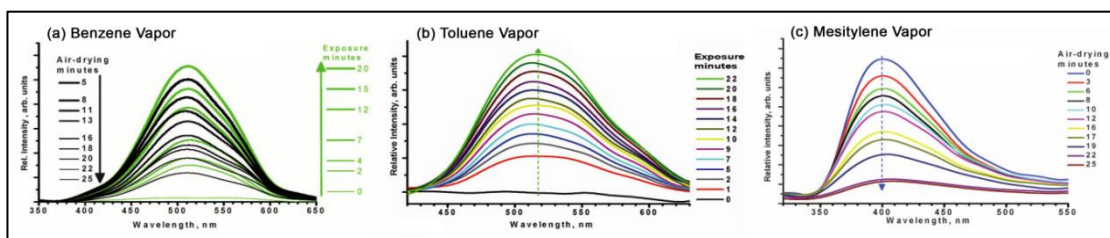
Figure 8. Photoluminescence (PL) spectra of thin-films of fluorinated- pyrazolate Ag(I) trinuclear complex: {[3,5-(CF$_3$)$_2$Pz]Ag}$_3$, with regard to exposure to/ removal of SAMs.[1,6]

1.2 Chemistry of Pyrazolate Ligands

Pyrazole (HPz), shown in Figure 9, is part of a class of N-heterocyclic, aromatic compounds, known as azoles (or azolates, the deprotonated derivatives), joined in a five-membered ring with a minimum of two nitrogen atoms.[7]   Other azoles include imidazole (Him), 1,2,4-triazole (Htz), 1,2,3-triazole (H*v*tz) and tetrazole (Httz).[7]   In coordination chemistry, the pyrazolate anion (Pz⁻ = the deprotonated derivative of pyrazole), shown in Figure 10, is a Lewis base (nucleophile) and is capable of coordinating with one or two central metal atoms and/or metalloids (Lewis acids or electrophiles) via one of three modes of coordination (shown in Figure 11): (1) monodentate, (2) *exo*-bidentate (bridging), and (3) *endo*-bidentate (chelating).[8-9]   However, pyrazole/pyrazolate ligands primarily function as a bidentate, bridging ligands.[8-9]   If a metal-pyrazole complex forms via monodentate (η-) coordination, a base (deprotonating agent), such as triethylamine, can be used to deprotonate the already coordinated pyrazole, thus increasing the basicity

8

of the pyrazole/pyrazolate and allowing it to coordinate via bridging (μ-) with another central metal atom or metalloid.[8-9] In addition to using a base, deprotonation can also be achieved via heating (i.e. high temperatures).[7]
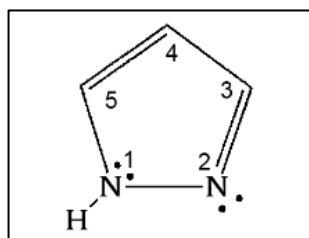
Figure 9. Structure of Pyrazole (HPz).[8,10]
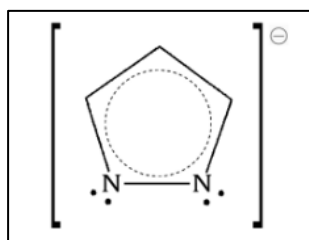
Figure 10. Structure of Pyrazolate Anion (Pz⁻).[8-10]
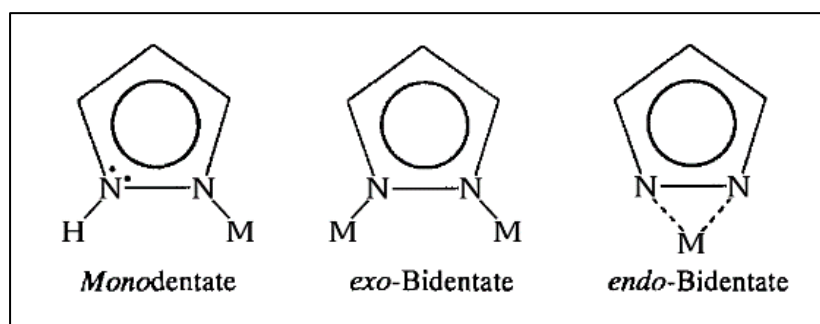
Figure 11. Modes of coordination for pyrazolate (Pz⁻) ligand.[8]

As bidentate, bridging ligands, pyrazolates can form interesting cluster and chain structures with regard to the number of bridging pyrazolates (see Figure 12): single bridging = $M(\mu\text{-}Pz^*)M$ and double bridging = $M(\mu\text{-}Pz^*)_2M$, as well as triple bridging = $M(\mu\text{-}Pz^*)_3M$.[7-10] Homoleptic, single bridging pyrazolate-metal complexes have only

been known to form with coinage metals (M = Cu, Ag, and Au), forming a variety of oligomeric clusters, such as trinuclear complexes: $[M(dpPz)]_3$ (dpPz = 3,5-diphenylpyrazole) and $[Cu(dmPz)]_3$ (dmPz = 3,5-dimethylpyrazole), tetranuclear complex: $[Cu(dpPz)]_4$, and hexanuclear complex: $[Au(dpPz)]_6$, as well as polymeric chains, such as α-$[Cu(Pz)]_n$, β-$[Cu(Pz)]_n$, and $[Ag(Pz)]_n$.[8]
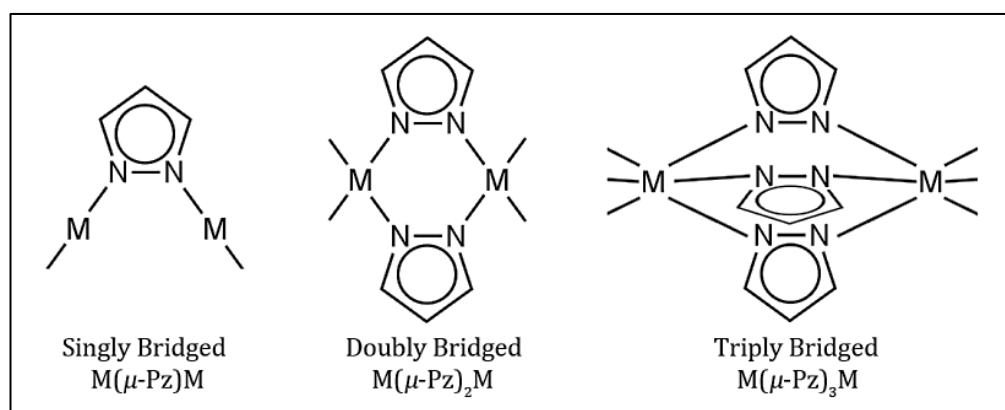
Figure 12. Variations of bidentate, bridging pyrazolates.[9-10]

As previously mentioned, pyrazolates (and azolates, in general) have a tendency to bridge between two central metal atoms, forming clusters and coordination polymers, more specifically metal-azolate frameworks (MAFs), a subtype of metal-organic frameworks (MOFs) composed primarily of azolate-based ligands.[7] In general, MOFs have a variety of potential application, which include gas storage and/or separation, energy conversion and/or storage, and chemical sensing.[11] Simple, bridging azolates (coordinated with metal centers) have fixed coordination geometries with short bridging lengths, which often decreases the possibility of forming extended superstructures (i.e. MAFs; see Figure 13).[7] However, the introduction of substituents to azolate ligands may

alter their coordination behavior, allowing adjacent substituents to cooperatively interact with one another, as well as with "guest" molecules, such as solvents.[7] Regarding the design of MAFs, it is beneficial to view it in terms of topology (or a net-like structure, with regard to metal-ligand connectivity), with metal ions, or metal-ligand clusters/chains, represented as "nodes" and ligands, such as azolates, represented as "linkers".[7] For example, as shown in Figure 14, the pyrazolate-based coinage metal trinuclear clusters (trimers): $[M(Pz)]_3$ (M = Ag(I), and Cu(I)), may serve as secondary building units (SBUs), following the replacement of the monopyrazolate ligand with a polypyrazolate ligand, such as 3,3',5,5'-tetramethyl-4,4'-bipyrazolate (bPz^{2-}).[7] Afterward, the resulting SBU, metal-polypyrazolate: $[M(bPz^-)]_3$, may covalently bond with adjacent units, thus forming a highly porous MAF (with a $[M(bPz)]_3$ core).[7] MAFs typically have simple and low topologies with coordination numbers ranging from 3 to 4, and thus, low framework node densities ($Å^{-3}$), which is essential in the design of new porous frameworks (MAFs and/or MOFs).[7] In addition, MAFs possess beneficial physical properties, such as thermal and chemical stability, ideal for potential applications involving coordination polymers.[7]
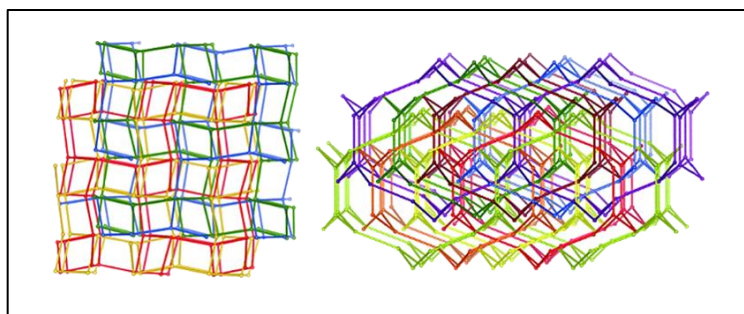
Figure 13. Crystal structures of highly porous MAFs: The 4-fold interpenetrated srs- (*right*) and 8 fold nof- (*left*) $[M_2(bPz)]$ (M = Ag(I) or Cu(I)).[7]

11
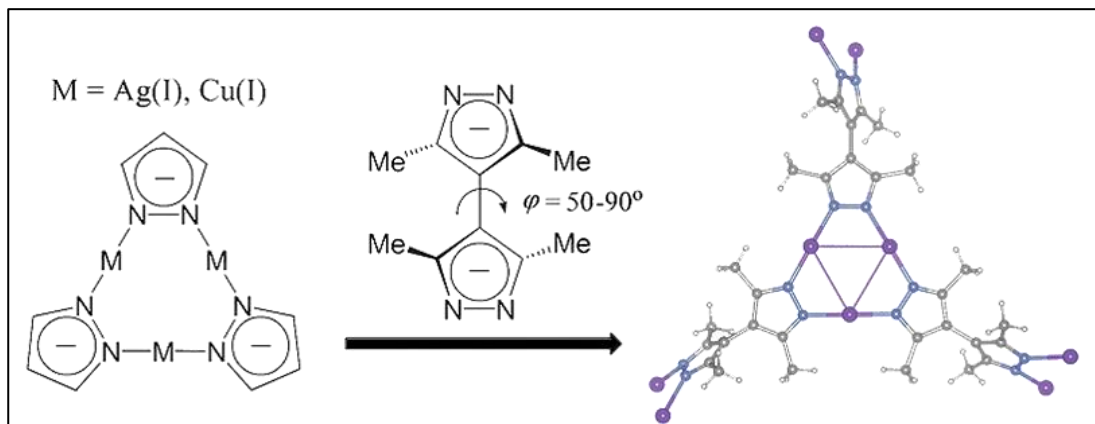
Figure 14. Formation of MAF = metal-polypyrazolate, [M(bPz)]$_3$ (Core), following modification of SBU = metal-monopyrazolate, [M(Pz)]$_3$, with polypyrazolate ligand.[7]

1.3 Chemistry of Phenanthroline Ligands

Phenanthrolines (phen) are a class of N-heterocyclic, aromatic compounds with a planar, rigid structure, comprised of three fused, six-membered rings with two nitrogen atoms.[12-15] There are a total of ten phenanthroline isomers of which the 1,10-, 1,7-, and 4,7-isomers, shown in Figure 15, are the most common and widely studied in literature.[12] In coordination chemistry, phenanthrolines are neutral ligands and function as Lewis bases that can coordinate with one or two central metal atoms and/or metalloids via one of three modes of coordination: (1) monodentate, (2) bridging bidentate, and (3) chelating bidentate.[13] More specifically, the 1,10-isomer is a chelating bidentate ligand; meanwhile, the 1,7- and 4,7-isomers (as well as the other remaining isomers) are non-chelating ligands and can coordinate as either a monodentate (η-) or a bidentate, bridging (μ-) ligand.[13] In comparison, the 1,7-isomer is more likely to coordinate as a monodentate ligand via the N7 nitrogen atom, rather than the N1 nitrogen atom, due to

N7 being more thermodynamically favorably (less sterically hindered), while the 4,7-isomer is more likely coordinate as a bridging bidentate ligand via the N4 and N7
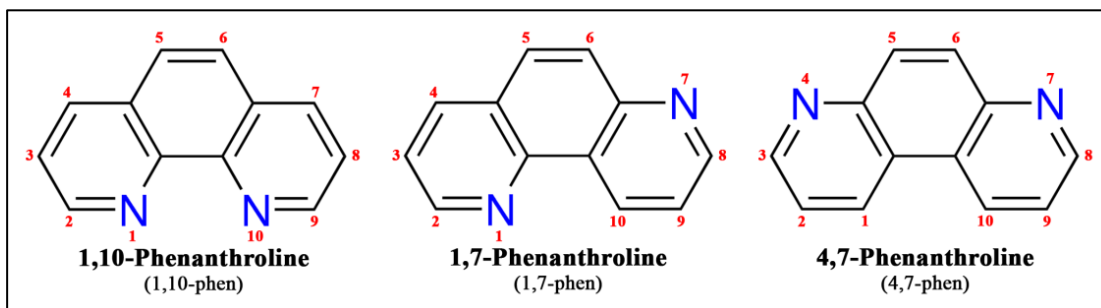
Figure 15. Structures of phenanthrolines (phen): 1,10-, 1,7-, and 4,7-isomers.[12] nitrogen atoms.[13,16-17]

In the past five decades, Cu(I) complexes have exhibited impressive photophysical properties with long-lived (S→T) metal-to-ligand charge transfer (MLCT) lifetimes that could potentially be used in the design of new molecular organic light emitting diodes (MOLED), luminescent sensors, and solar energy conversion for dye-sensitive solar cells (DSSCs), thus rivaling that of ruthenium(II) complexes in terms of both cost and abundance, as well as toxicity.[14,18-22] Upon photo-excitation (hv) to singlet MLCT excited states, the d^{10} Cu(I) center undergoes oxidation to a d^9 Cu(II) configuration.[18-19,23] In these excited states, the Cu(II) complexes are prone to flattening relaxation, shown in Figure 16, due to pseudo Jahn-Teller (PJT) distortion, that occurs in conjunction with intersystem crossing (ISC) between the transition of the excited singlet MLCT (^{1}MLCT) to triplet MLCT (^{3}MLCT) coupling, typically resulting in a planar geometry.[18-21] As a result, this exposes the metal center to donor solvent molecules, such as acetonitrile (MeCN), leading to exciplex formation with the aforementioned solvent

molecules and thereby inducing photoluminescence quenching and loss of performance (i.e., a decrease in excited state energy via internal conversion (IC) and nonradiative decay).[18-22] However, the aforementioned exciplex formation has been disputed by Capano et al. following a recent study of $[Cu(dmp)_2]^+$ in MeCN and dichloromethane (DCM, a nondonating solvent) using time-resolved X-ray absorption spectroscopy (XAS), revealing the same transient XAS spectra and leaving the true solute-solvent interaction a mystery.[22]
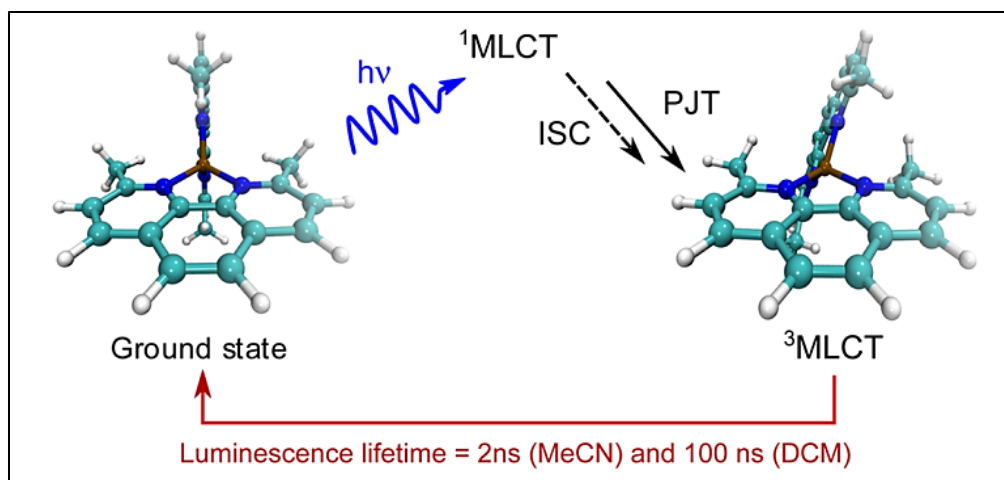
Figure 16. Diagram depicting the ground and excited states of $[Cu(dmp)_2]^+$ (dmp = 2,9-dimethyl) in the presence of acetonitrile (MeCN) and dichloromethane (DCM). Intersystem crossing (ISC) and pseudo Jahn-Teller (PJT) distortion occurs between the excited ^{1}MLCT and ^{3}MLCT, which is followed by the transition from triplet MLCT excited state to ground state.[18]

In order to overcome/suppress PJT distortion, Cu(I) complexes with rigid, N-heterocyclic, aromatic ligands, such as 1,10-phenanthroline, are ideal for improving photoluminescence, which can be further enhanced through the structural modification of the aforementioned ligands via the addition of bulky substituents/side chains (such as in structures of $[Cu(dmp)_2]^+$, $[Cu(sbmpep)_2]^+$, and $[Cu(sbmm)_2]^+$, shown in Figures 16 and

17, respectively) and/or the fusion of ring structures (such as imidazole- or pyrazine-fused derivatives, shown in Figure 18), as well as the introduction of a second ligand (preferably another N-heterocyclic, aromatic compound with a rigid structure).[19-20,22] As a chelating bidentate ligand, the parent 1,10-phenanthroline coordinates tightly with metal centers, forming somewhat rigid complexes, yet the metal center is still prone to oxidative instability.[20-21,23] This is can be prevented through the addition of bulky substituents (such as methyl, phenyl, sec-butyl substituents), primarily in the 2,9-positions (see Figures 16 and 17), followed by the 3,8- positions (see Figure 17), thus providing rigidity and cooperative steric inhibition/hindrance effects against flattening relaxation/planarization, essentially shielding the metal center and making it less susceptible to oxidation due to its interaction with solvent molecules.[19-23] In comparison between the parent phenanthroline and the substituted derivatives, the 2,9- and 3,8-substituted derivatives exhibit enhanced photoluminescence properties in terms of increased quantum yield (Φ) and lifetime (τ).[19,21,23] Moreover, the addition of aryl-substituents in the 4,7-positions (see Figure 17) may result in further enhancement via tuning of the electronic properties across the visible spectrum without hindering the long-lived MLCT lifetimes (due to π-delocalization).[19,23] With regard to structurally modified 1,10-phenanthroline ligands via fusion of heterocyclic rings, such as with an imidazole or a pyrazine (see Figures 18 and 19), the resulting Cu(I)-phenanthroline complexes may exhibit significant changes in photophysical properties due to the increase in conjugation via the addition of the fuse-ring structures (contributing to the low energy π-π* transitions).[20]
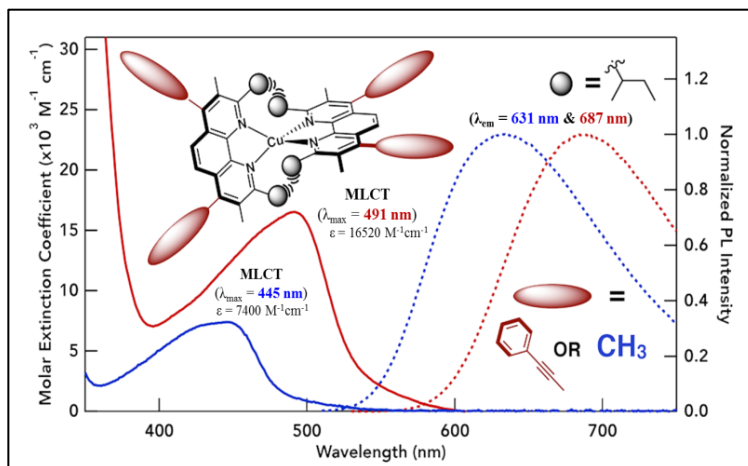
Figure 17. Structure of Cu(I) complexes with heavily substituted phenanthroline in the 2,9-, 3,8-, and 4,7-positions: [Cu(sbmpep)$_2$]$^+$ and [Cu(sbmm)$_2$]$^+$ (sb = sec-butyl, m = methyl, and pe = phenylehtynyl, respectively).[19]
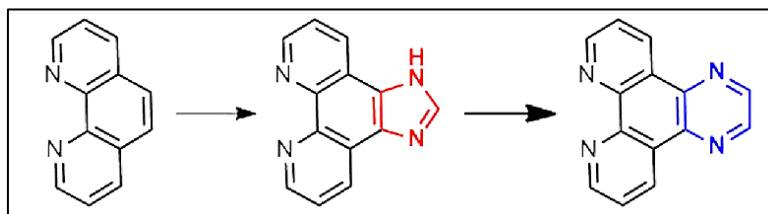
Figure 18. Structures of 1,10-phenanthroline (*left*), imidazole-fused (center) and pyrazine-fused (*right*) 1,10-phenanthroline derivatives.[20]
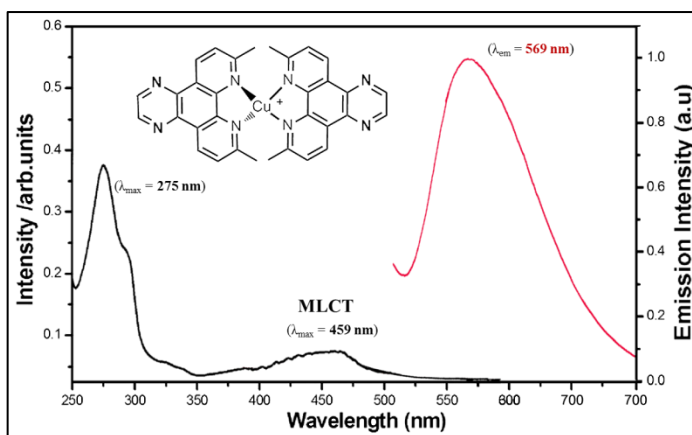
Figure 19. Structure and photoluminescence of Cu(I) complexes with pyrazine-fused phenanthroline (Pyz-phen), such as [Cu(Pyz-phen)$_2$]$^+$.[20]

Various metal complexes with phenanthroline ligands have been studied as potential anti-tumor/anti-cancer drugs as well as angiogenesis inhibitors in tumor cells.[13,16-17] With regard to anti-cancer drugs, cisplatins are the leading anti-cancer drugs, despite their negative side effects: high toxicity and drug resistance.[24-25] Of the many trace elements, copper, in particular, possesses a plethora of biological and physiological implications responsible for maintaining the human condition.[14,24] As an alternative to cisplatins, Cu(I)- and Cu(II)-phenanthroline complexes have been studied as potential anti-tumor/anti-cancer drugs due to exhibiting lower toxicity and higher specificity/targeting (attributed to the tendency of phenanthroline ligand intercalating into DNA's minor groove).[14,24,26] The production of reactive oxygen species (ROS), catalyzed by Cu(II)/Cu(I) ions, as shown in Figure 20, is responsible for DNA scission.[14,27]
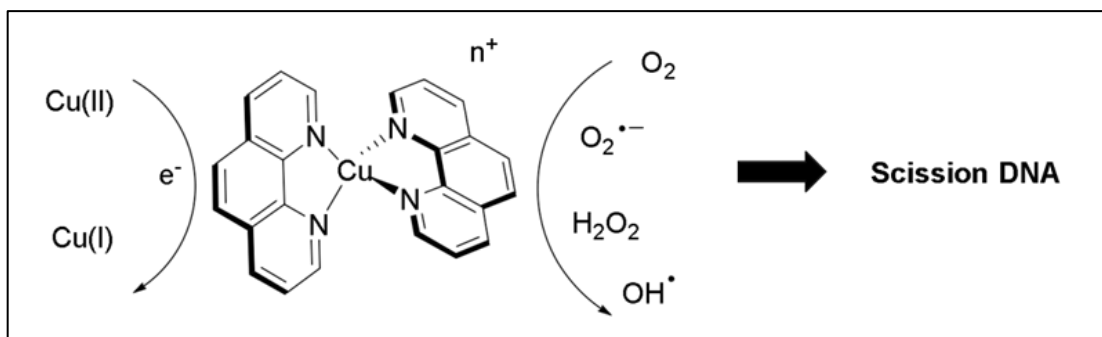
Figure 20. Representation of Cu-phenanthroline complex: $[Cu(phen)_2]^{n+}$ (n = 1 or 2) with regard to DNA Scission.[14,27] The Cu(II)/Cu(I) redox cycle is shown, catalyzing the formation of reactive oxygen species (ROS): $O_2^{\bullet-}$ (the superoxide anion), followed by $H^{\bullet}$ (the hydroxyl radical).[14,24,27]

1.4 Chemistry of Mixed-Ligand Coinage Metal Complexes

The synthesis of mixed-ligand (heteroleptic) metal complexes can be utilized as a strategy for enhancing photophysical properties (for the design of new MOLEDs), as well as forming extended coordination polymers or MOFs.[10]

With regard to pyrazolate (Pz$^-$) ligands, polymeric complexes are typically formed due to the pyrazolate's tendency to bridge between two central metal atoms and/or metalloids; however, heteroleptic, dinuclear complexes with double bridging pyrazolates, shown in Figure 21, may form following the introduction of another ligand(s), essentially acting as end caps.[10] For example, a 4-coordinated, heteroleptic, Cu(I) dimer (general structure shown in Figure 21) with double bridging pyrazolates: [(μ-dmPz)Cu(phen)]$_2$, was synthesized upon reacting the trinuclear complex: [Cu(μ-dmPz)]$_3$ (dmPz = 3,5-dimethylpyrazolate), with the chelating bidentate ligand: 1,10-phenanthroline (phen).[8] Similarly, 3-coordinated, heteroleptic Cu(I) and Ag(I) dimers with double bridging pyrazolates: {[3,5-(CF$_3$)$_2$Pz]M(2,4,6-collidine)}$_2$ (M = Cu(I), Ag(I)), were synthesized upon reacting the respective trinuclear complexes: {[3,5-(CF$_3$)$_2$Pz]M}$_3$ (M = Cu(I), Ag(I)), with the monodentate ligand: 2,4,6-collidine (2,4,6-trimethylpyridine).[28] The resulting 3-coordinated dimers were similar in their overall structure yet they differ in their geometry with the Cu(I) analogue featuring a planar, Cu(μ-N,N)Cu ring conformation, while the Ag(I) analogue features a mixed, half-planar and half-boat, Ag(μ-N,N)Ag ring conformation.[28] The resulting heteroleptic Cu(I) dimer exhibited blue (λ_{em} ~460 nm) emission, a desirable property for MOLEDs; whereas, the Ag(I) analogue featured excitation wavelength-dependent luminescence, exhibiting blue (λ_{em} ~405 nm

and ~455 nm) and UV (λ_{em} ~280 nm) emissions, as well as green emission (λ_{em} ~500 nm) for single crystals, which was attributed to the different conformations.[28]
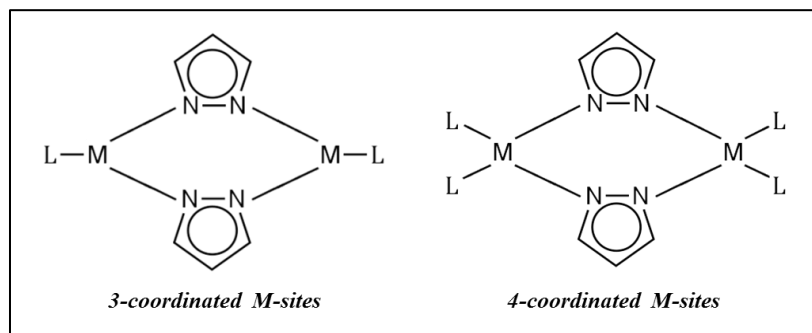
Figure 21. General structure of heteroleptic, metal(I) dimers with double bridging pyrazolates.[10]

With regard to Cu-phenanthroline complexes, the introduction of a secondary ligand, may enhance photoluminescence and/or form coordination polymers.[18,29] Neogi et al. explored the syntheses of HETPYP (heteroleptic pyridine and phenanthroline metal complexes) with various oligopyridines (specifically di- and tri-pyridyl ligands), forming Cu(I)- HETPYP-I complexes with 3-coordinated Cu(I) centers and their respective Cu(I)-HETPYP-II coordination polymers with 4-coordinated Cu(I) centers, as shown in Figure 22.[29] In addition to the aforementioned properties, Cu-phenanthroline complexes exhibit potential new anti-cancer/anti-tumor drugs via the introduction of a secondary, bidentate, chelating ligand, which provides additional specificity and stability with regard to the intercalation of the copper complex with DNA's minor grooves.[26] Recently, anti-cancer drugs known as the Casiopeìnas family, consisting of heteroleptic Cu(I) complexes (composed of an aromatic ligand: 1,10-phenanthroline [phen] or 2,2'-bipyridine [bpy], with a secondary ligand: acetylacetonate [acac] or glycinate [gly]) have exhibited

remarkable anti-tumor activity in *in vitro* studies, as well as *in vivo* studies, which revealed an extraordinary 10-fold enhancement effect versus that of known cis-platins.[26] As a result, this prompted phase I clinical trials of two (out of 21) proposed heteroleptic Cu(I) complexes.[26]
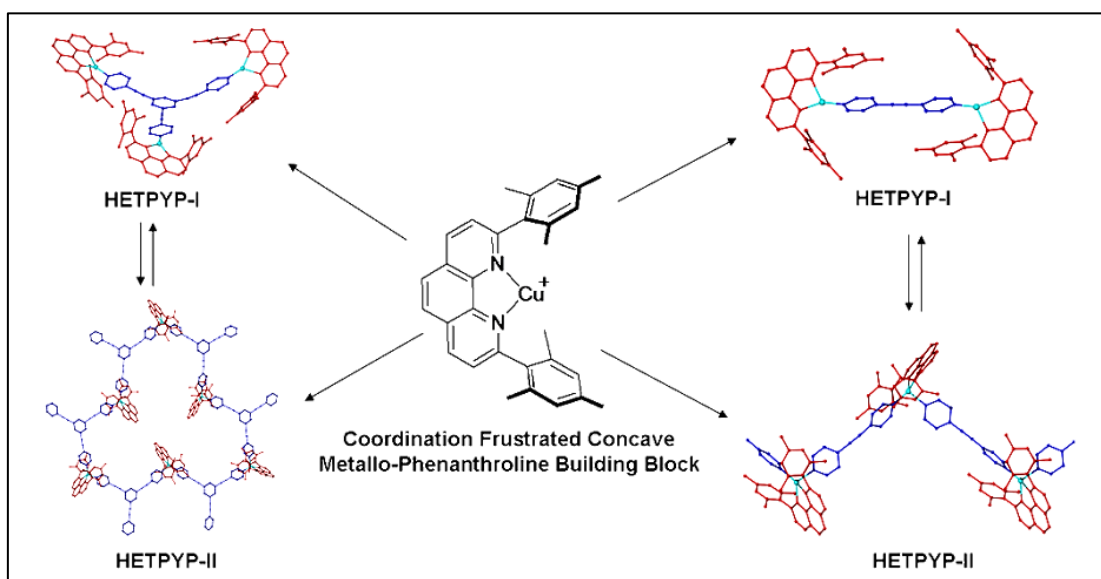
Figure 22. Structure of Cu(I)-HETPYP-I complexes and their respective Cu(I)-HETPYP-II coordination polymers, using $[Cu(phenAr_2)]^+$ as a building block.[29]

1.5 Chemistry of Solventless Syntheses

The exploration of solventless (solvent-free) syntheses have been of great interest with regard to the practice of "green" chemistry, being both environmentally and economically friendly, which is ideal for laboratory and industrial settings.[30] Solventless synthesis is a technique encompassing either mechanochemical (via mechanical grinding with heat) or sublimation (via vapor diffusion), which may be accompanied by a change in physical color and/or appearance/disappearance of luminescence, thus providing a means for monitoring the formation of the final product, as shown in Figure 23.[30]

Moreover, with regard to the mechanochemical technique, a mortar and pestle (for small scale reactions, i.e. laboratory purposes) or grinding mill (for large scale reactions, i.e. industrial) can be used to mechanically grind the solid-solid or solid-liquid reactants (starting materials) into a crude product, that can then be washed or recrystallized (using a small volume of solvent) in order to obtained a pure product.[31-32] Meanwhile, the sublimation technique involves the vapor diffusion and deposition of the ligand adduct, preferably a volatile ligand, onto the metal adduct, thereby allowing the gradual formation of the final product, as shown in Figure 23.[30,33] Although both solventless techniques are relatively simple, faster, and more efficient, in comparison to solvent-mediated syntheses, oxidation/reduction of the metal adduct or the decomposition of the ligand are possible consequences due to air and thermal instabilities, respectively.[30,33-34]
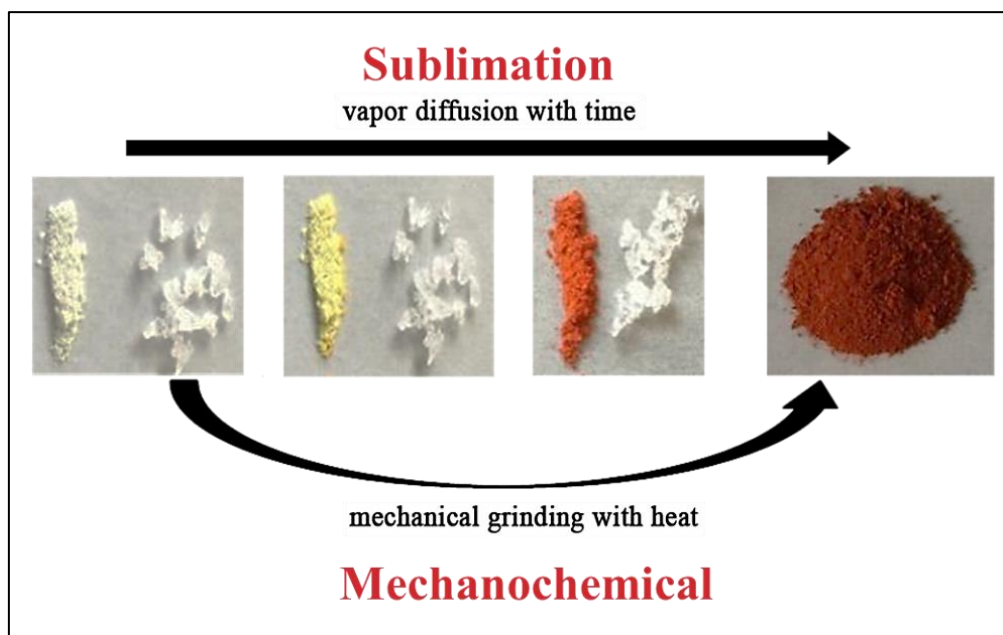
Figure 23. Solventless (solvent-free) Syntheses: mechanochemical (via mechanical grinding with heat) & sublimation (via vapor diffusion).[30]

Almotawa et al. discusses the syntheses of various Cu(I) and Ag(I) complexes with mixed ligands using both solvent-mediated and solventless syntheses, revealing that synthetic route may yield different final products.[30] Moreover, the monitoring of solventless syntheses of the Cu(I) and Ag(I) products differed greatly in that the formation of Cu(I) products were monitored via quenching of photoluminescence (characteristic of the Cu(I) starting material), as well as the dramatic change/appearance of physical color; meanwhile, the formation of Ag(I) products were monitored via the appearance of photoluminescence (characteristic of the Ag(I) product) and not via physical color change due to the absence of color change.[30]

1.6 Chemistry of Copper(I) Halide Complexes

Cu(I) halide (X = Cl, Br, I) complexes with N-heterocyclic aromatic ligands have exhibited remarkable photoluminescence properties, as well as tendencies to form various polymeric 1-, 2-, and 3-D network structures.[35] Due to Cu(I) halides' propensity to form topological, knot-like structures in the presence of monodentate, N-donor (as well as S- and P-donor) ligands, the resulting complexes may form one of the following four motifs: (1) square dimers, (2) cubane tetramers (or other oligomeric clusters), (3) polymeric zigzags, and (4) polymeric stairsteps, as shown in Figure 24 (A-D, respectively).[35] However, via the introduction of bidentate, bridging ligands, the four aforementioned motifs can be expanded upon, forming respective cross-linked, network structures, as shown in Figure 24 (E-H, respectively).[35]
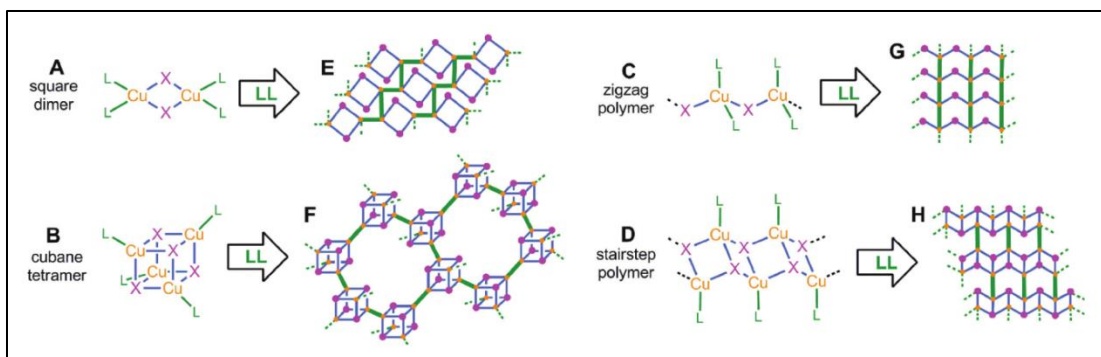
Figure 24. Possible motifs of Cu(I) halide (X = Cl, Br, I) complexes with N-, S-, and P-donor ligands.[35]

1.7 Chemistry of Poly(4-vinylpyridine)

Poly(4-vinylpyridine) (PVP, MW = 60,000 g/mol) is a N-heterocyclic, poly-dentate ligand composed of individual units of 4-vinylpyridine, which are linked to together as a polymeric chain.[36-37] As shown in Figure 25, PVP can coordinate with a metal precursor to form metallopolymers (metal-containing polymers).[36-37] Rawashdeh-Omary et al. and Hobbollahi et al., respectively, have recently synthesized Au(I)-based metallopolymers exhibiting photoluminescence upon excitation with UV light.[36-37] Regarding Rawashdeh-Omary et al., two [Au(C6F5)PVP]-based metallopolymers exhibited metal-centered photoluminescence (attributed to aurophillic interactions: intra- and interchain) capable of either fine-tuning emission with regard to a varying the excitation wavelength (λ_{ex}) or coarse-tuning emission with regard to varying the temperature (RT versus 77K).[37] Regarding Hobbollahi et al., their [AuCl(PVP)]-based metallopolymer exhibited photoluminescence, which was attributed to aurophillic interactions; however, the metallopolymer does not exhibit course- nor fine-tuning with

regard to either varying the excitation wavelength (λ_{ex}) or temperature. Brightly phosphorescent metallopolymers displaying course- and/or fine-tuning, such as the aforementioned [Au(C6F5)PVP]-based metallopolymers, may have potential applications with regard to the development of polymer light-emitting diodes (PLEDs).[37]
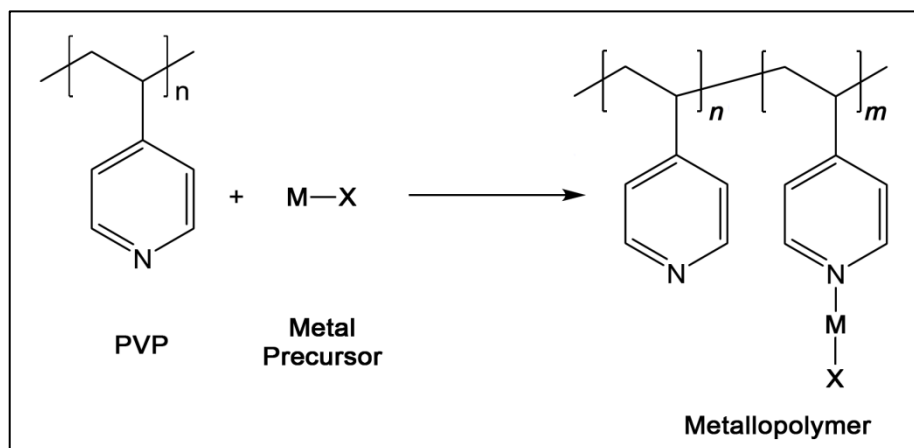
Figure 25. General synthesis of a metallopolymer using poly(4-vinylpyridine) (PVP) and a metal precursor.[36-37]

1.8 Applications

Coinage metal(I) complexes with N-heterocyclic ligands has a wide range of potential applications with regard to the design of new MOLEDs, energy-efficient DSSCs, optical sensors for VOCs, and/or highly porous MOFs, which possesses other potential applications, such as gas storage and/or separation, catalysis, and drug delivery.[7,11,14] The implementation of mixed-ligands may enhance the aforementioned properties, as well as expanded onto other potential applications, such as anti-tumor/anti-cancer drugs.[26,27]

CHAPTER II

SYNTHESES OF COPPER(I/II) AND SILVER(I) COMPLEXES AND

METALLOPOLYMERS WITH N-HETEROCYCLIC LIGANDS

This chapter focuses primarily on the syntheses of various heteroleptic Cu(I) and Ag(I) complexes or coordination polymers with the fluorinated-pyrazolate (FPz⁻) and phenanthroline (phen) ligands, followed by the syntheses of a heteroleptic Cu(II) complex using copper(I) iodide and the fluorinated-pyrazolate (FPz⁻) ligand and a homoleptic Cu(I) coordination polymer using copper(I) iodide and poly(4-vinylpyridine). Section 2.1: *Materials and Methods,* describes the various starting materials, solvents, and glassware utilized with regard to both the methods of syntheses (and crystallizations). Section 2.2: *Synthetic Procedure/Processes,* describes the various methods of syntheses, followed by the methods of crystallizations, for the copper(I/II) and silver(I) complexes and/or coordination polymers with the aforementioned N-heterocyclic ligands.

2.1 Materials and Methods

All metal and ligand starting materials were purchased from Sigma Aldrich, Alfa-Aesar, and Matrix Scientific. Copper(I) oxide (Cu_2O), copper(I) iodide (CuI), neocuproine hemihydrate (2,9-dimethyl-1,10-phenanthroline hemihydrate = dmp • 0.5 H_2O), 1,7-phenanthroline (1,7-phen), 4,7-phenanthroline (4,7-phen), and poly(4-vinylpyridine) (PVP) were purchased from Sigma Aldrich. Silver(I) oxide (Ag_2O) was purchased from Alfa-Aesar. 3,5-Bis(trifluoromethyl)pyrazole ([3,5-$(CF_3)_2$Pz]H = FPzH) was purchased from Matrix Scientific. All solvents used for these syntheses were ACS or HPLC grade and purchased from Sigma Aldrich, Fisher Chemical, VWR, and Acros Organics. Benzene (HPLC grade) was purchased from Sigma Aldrich. Toluene (Optima), hexanes (HPLC grade), and ethyl ether, anhydrous (stabilized/HPLC) were purchased from Fisher Chemical. Dichloromethane (HiPerSolv) and acetonitrile (ACS grade) were purchased from VWR. Chloroform (ACS grade) was purchased from Acros Organics. All glassware used for these syntheses were cleaned using acetone or acetonitrile (low grade solvents for general lab use), followed by DI water, aqua regia, DI water, base bath, and DI water, respectively. The clean glassware was oven-dried at ~150°C for 24 hours prior to carrying out each synthesis. The synthetic routes/methods (shown in Figures 26 and 27) for the new metal-ligand complexes or coordination polymers consisted of both solvent-mediated syntheses, via Schlenk technique under gaseous nitrogen (N_2) atmosphere (Ultra High Purity, UHP), and "green" solventless (mechanochemical) syntheses, via mechanical grinding and heating.
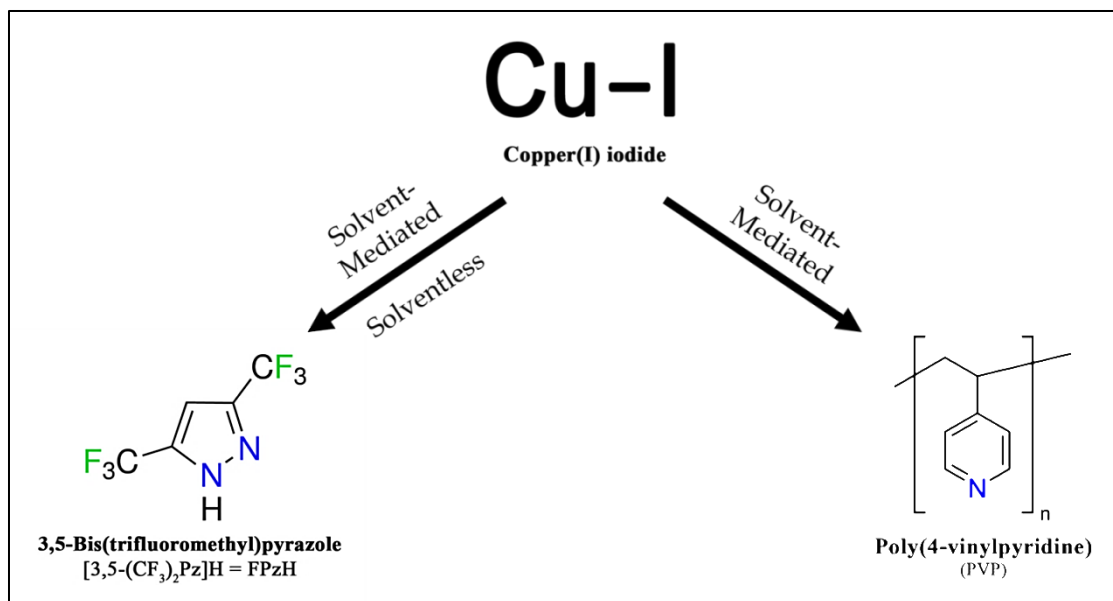
Figure 26. Synthetic routes/methods for the synthesis of copper(I) iodide-based complexes and/or coordination polymers with the FPzH ligand and PVP.
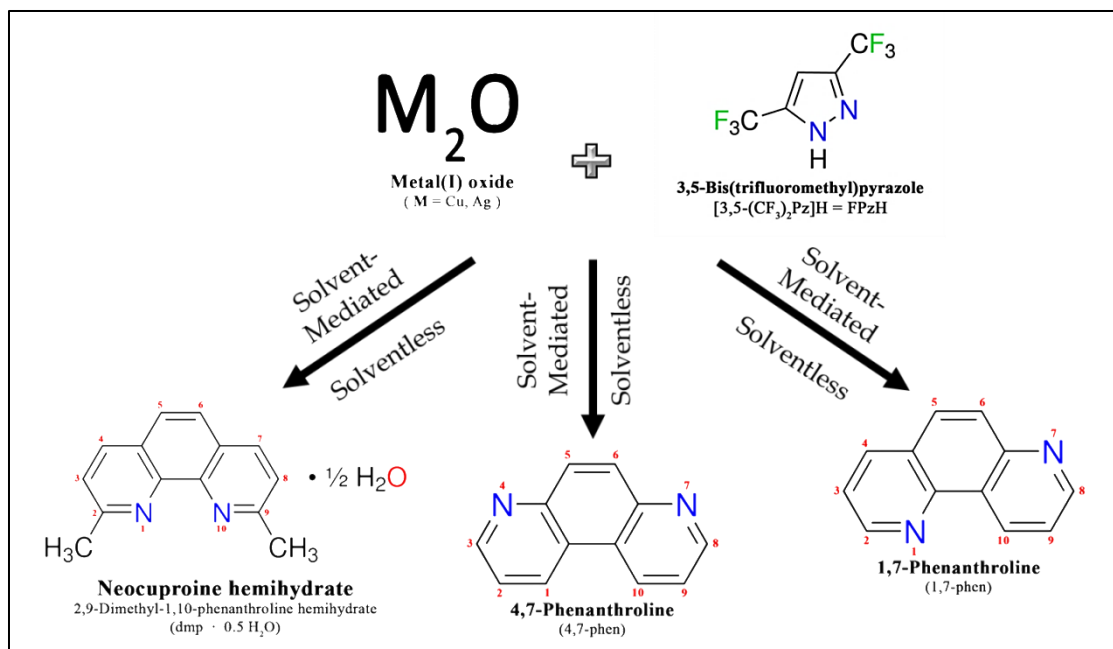
Figure 27. Synthetic routes/methods for the synthesis of copper(I) and silver(I) complexes and/or coordination polymers with pyrazolate- and phenanthroline-based ligands.

2.2 Synthetic Procedures/Processes

2.2.1 Syntheses of Compound 1: {Cu$_2$[3,5-(CF$_3$)$_2$Pz]$_2$(4,7-phen)}$_2$

2 Cu$_2$O + 4 [3,5-(CF$_3$)$_2$Pz]H + 2 (4,7-phen)

   Solvent-mediated ↓ Solventless

  {Cu$_2$[3,5-(CF$_3$)$_2$Pz]$_2$(4,7-phen)}$_2$ + 2 H$_2$O

2.2.1.1 Solvent-mediated Synthesis of {Cu$_2$[3,5-(CF$_3$)$_2$Pz]$_2$(4,7-phen)}$_2$

The synthesis of {[3,5-(CF$_3$)$_2$Pz]Cu}$_3$ was carried out as reported in the literature, via Schlenk technique and under constant gaseous nitrogen (N$_2$) atmosphere. [3,5-(CF$_3$)$_2$Pz]H (0.50 g, 2.45 mmol) and copper(I) oxide, Cu$_2$O, (0.19 g, 1.43 mmol) were mixed in 12 mL of benzene (bubbled with N$_2$), and subsequently heated (with constant stirring) under reflux at ~60°C for 24 hours. The resulting reaction mixture was filtered over a bed of celite (wet with benzene) in order to remove insoluble impurities. The filtrate was collected and placed under vacuum for ~5 hour in order to completely remove the solvent, yielding the white/colorless solid, {[3,5-(CF$_3$)$_2$Pz]Cu}$_3$.

Under constant N$_2$ atmosphere, {[3,5-(CF$_3$)$_2$Pz]Cu}$_3$ (0.2027 g, 0.2534 mmol) and 4,7-phenanthroline (0.1371 g, 0.7608 mmol) were mixed in 7 mL of toluene (bubbled with N$_2$). Upon adding {[3,5-(CF$_3$)$_2$Pz]Cu}$_3$ to 4,7-phenanthroline in toluene, an immediate color change was observed, from milky, beige to cloudy, yellow (formation of yellow precipitate). The resulting reaction mixture was allowed to stir for ~2.5 hours in order to allow the starting materials to completely react. The yellow reaction mixture was

filtered, collecting the yellow precipitate (product) on the filter. The filter product was placed under vacuum for ~4 hours in order to completely remove traces of solvent, yielding the dry product: yellow, solid (yield 84%). Mp: 216.7-218.3°C (w/ dec). IR: =C-H stretch (aromatic): 3020.13, 3163.02, 824.33, 787.26, 754.09 cm^{-1}, C=C stretch (aromatic): 1587.48, 1406.18 cm^{-1}, C=N stretch (aromatic): 1540.71, 1524.76, 1498.35 cm^{-1}, C-C stretch (aromatic): 1446.64 cm^{-1}, C-N stretch (aromatic): 1359.01, 1257.32 cm^{-1}, C-F stretch: 1218.91, 1147.09, 1101.45, 1013.74 cm^{-1}. Theoretical Anal. Calc. for C44 H20 Cu4 F24 N12 (MW = 1426.88 g/mol): C, 37.04; H, 1.41; N, 11.78; experimentally found: C, 37.37; H, 1.46; N, 11.57.

The yellow, solid product was checked under a handheld UV lamp for photoluminescence under Short Wave UV (λ_{ex} = 254 nm) and Long Wave UV (λ_{ex} = 365 nm). Yellow photoluminescence was observed under 254 nm (medium-weak, yellow luminescence) and 365 nm (medium-strong, yellow luminescence). The yellow, solid product was completely soluble in acetone, acetonitrile, toluene, methanol, and dichloromethane, and insoluble in diethyl ether, cyclohexane, and water (very hydrophobic). The product is air sensitive and oxidizes in solution with common solvents.

X-ray quality crystals (physical color: yellow) were grown from a binary solvent system using benzene and cyclohexane via slow evaporation (with slow cooling from 55-60°C to room temperature). 4 mL of benzene and 2 mL of cyclohexane were added to a graduated cylinder and transferred to a Schlenk flask. The resulting solution was bubbled with N_2 for 10 minutes. Under constant N_2 flow, ~7 mg of the yellow solid product was

added to the binary solvent system and the resulting cloudy, yellow mixture was heated in an oil bath at 50-55°C and manually swirled until the mixture became clear (the product completely dissolved). The flask was lowered back into the warm oil bath, the heat was turned off, and the solution was allowed to slowly cool and evaporate under constant, low N_2 flow. The solution was left undisturbed in order to slowly evaporate for one day, resulting in crystal growth. The yellow crystals were of uniform size and shape. Mp: 216.7-218.3°C (w/ dec). IR: =C-H stretch (aromatic): 3020.25, 3164.62, 824.08, 787.07, 754.04 cm^{-1}, C=C stretch (aromatic): 1587.10, 1406.04 cm^{-1}, C=N stretch (aromatic): 1540.74, 1524.34, 1498.13 cm^{-1}, C-C stretch (aromatic): 1446.40 cm^{-1}, C-N stretch (aromatic): 1358.61, 1257.03 cm^{-1}, C-F stretch: 1219.04, 1146.91, 1101.29, 1014.01 cm^{-1}. Theoretical Anal. Calc. for C44 H20 Cu4 F24 N12 (MW = 1426.88 g/mol): C, 37.04; H, 1.41; N, 11.78; experimentally found: C, 36.28; H, 1.42; N, 11.18.
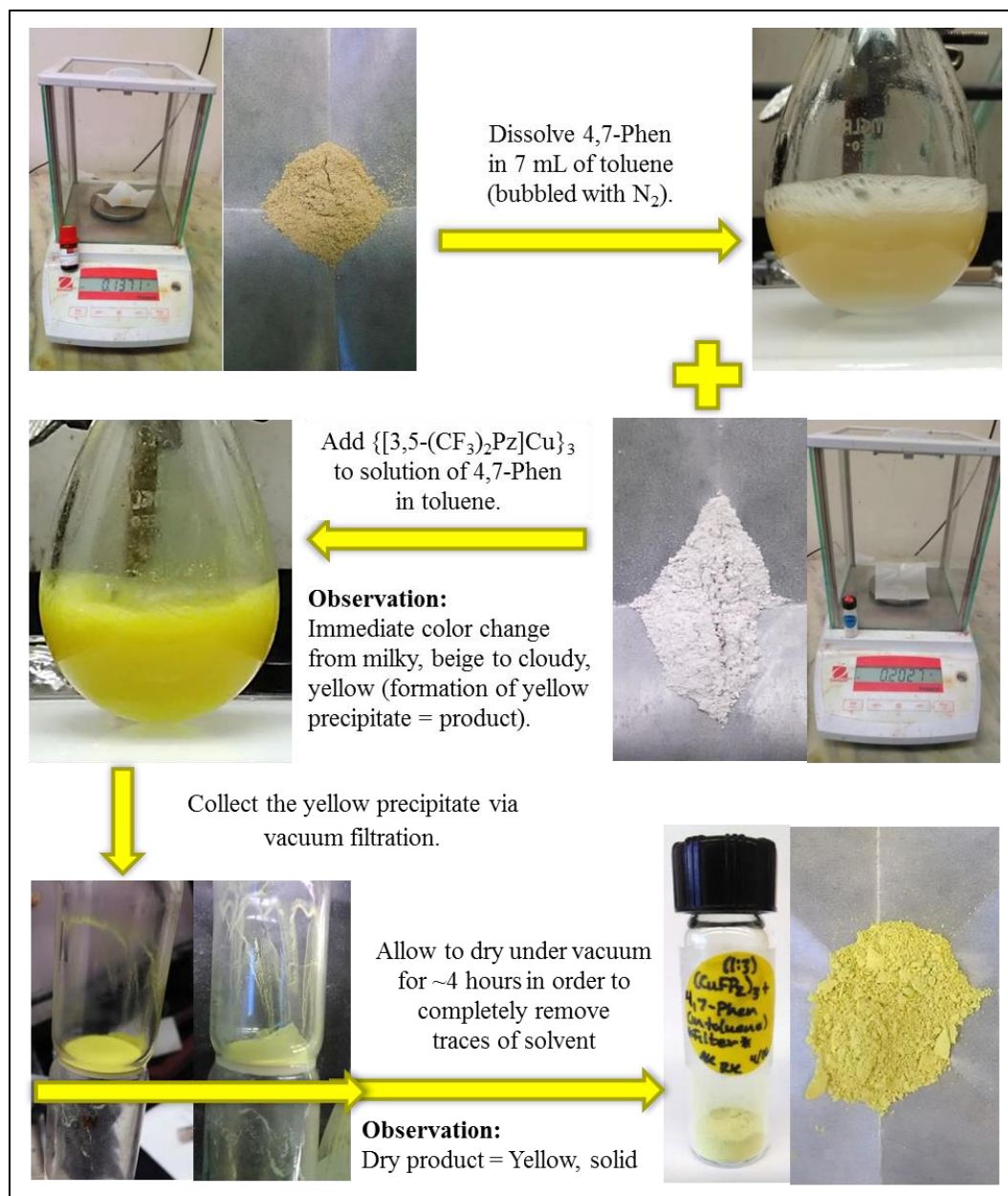
Figure 28. Solvent-mediated synthesis of $\{Cu_2[3,5-(CF_3)_2Pz]_2(4,7\text{-phen})\}_2$ powder.
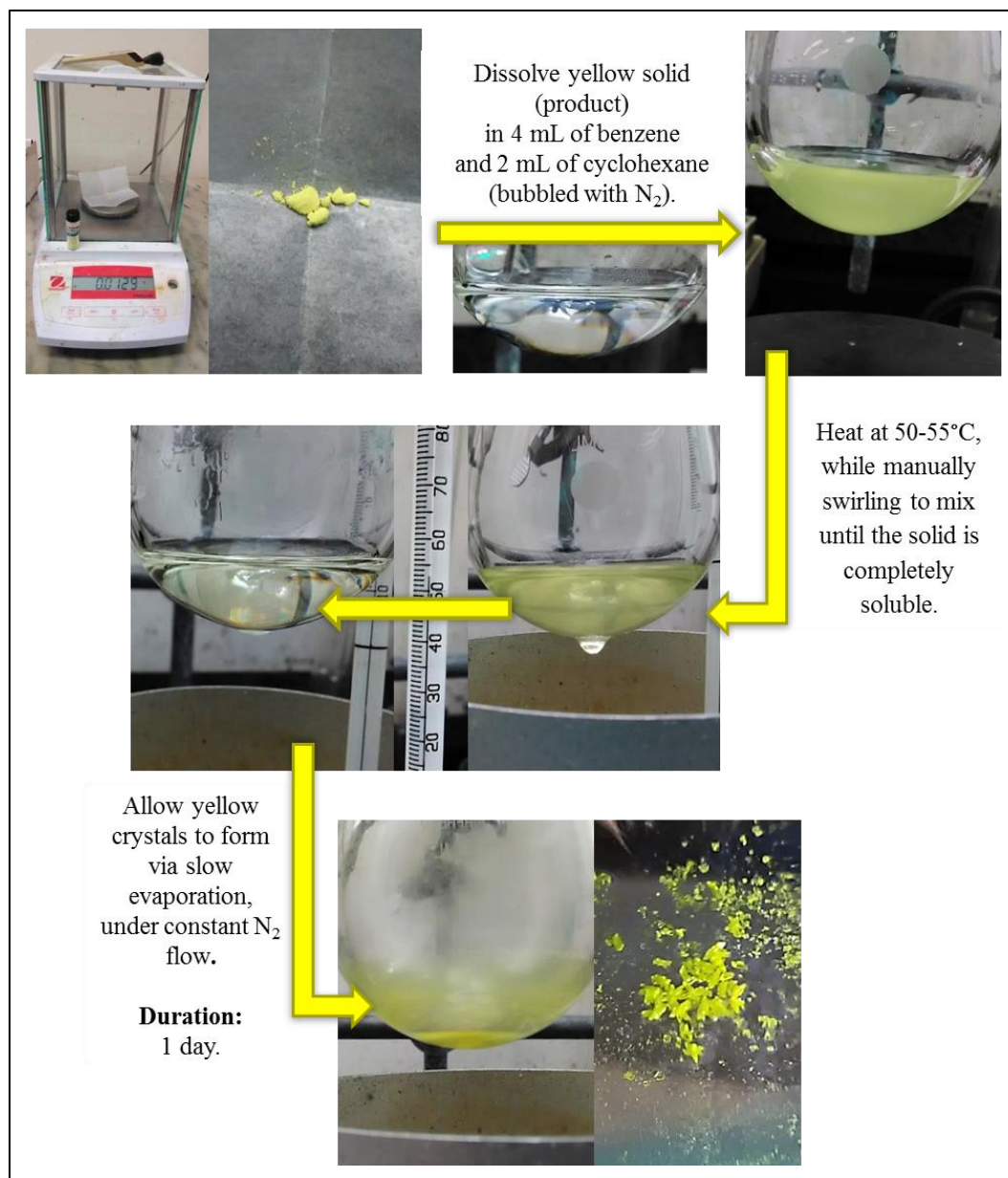
Figure 29. Crystallization of $\{Cu_2[3,5\text{-}(CF_3)_2Pz]_2(4,7\text{-}phen)\}_2$ using solvent-mediated powder.

2.2.1.2 Solventless Synthesis of {Cu$_2$[3,5-(CF$_3$)$_2$Pz]$_2$(4,7-phen)}$_2$

The synthesis of {[3,5-(CF$_3$)$_2$Pz]Cu}$_3$ was carried out as reported in the literature, via Schlenk technique and under constant gaseous nitrogen (N$_2$) atmosphere. [3,5-(CF$_3$)$_2$Pz]H (0.50 g, 2.45 mmol) and copper(I) oxide, Cu$_2$O, (0.19 g, 1.43 mmol) were mixed in 12 mL of benzene (bubbled with N$_2$), and subsequently heated (with constant stirring) under reflux at ~60°C for 24 hours. The resulting reaction mixture was filtered over a bed of celite (wet with benzene) in order to remove insoluble impurities. The filtrate was collected and placed under vacuum for ~5 hour in order to completely remove the solvent, yielding the white/colorless solid, {[3,5-(CF$_3$)$_2$Pz]Cu}$_3$.

{[3,5-(CF$_3$)$_2$Pz]Cu}$_3$ (0.1014 g, 0.1268 mmol) and 4,7-phenanthroline (0.0690 g, 0.383 mmol) were placed side by side on a glass petri dish and mechanically ground together with heat. The progress of the reaction was monitored via both a change in physical color and the disappearance/appearance of photoluminescence (checked using a handheld UV lamp). In contrast, {[3,5-(CF$_3$)$_2$Pz]Cu}$_3$ has a very strong, orange photoluminescence under Short Wave UV (λ_{ex} = 254 nm); meanwhile, 4,7-phenanthroline has a weak, blue photoluminescence under both Short Wave UV and Long Wave UV (λ_{ex} = 365 nm). Prior to heating, {[3,5-(CF$_3$)$_2$Pz]Cu}$_3$ and 4,7-phenanthroline were mechanically ground together for 10 minutes (at room temperature), resulting in a light beige physical color with light orange photoluminescence under 254 nm and blue photoluminescence under 365 nm. Afterward, the resulting powder mixture was mechanically ground while gradually increasing the temperature 25°C every 10-15 minutes, from 50°C to150°C. At 100°C, a weak green-blue photoluminescence was

observed under 254 nm, while no photoluminescence was observed under 365 nm. After mechanically grinding at 150°C, the resulting powder was yellow in color (physical) with weak, yellow photoluminescence under 254 nm and medium-strong, yellow photoluminescence under 365 nm. Further heating of the crude, solventless product was not performed in order to avoid potential oxidation or decomposition of the product. The crude, yellow, solventless product was weighed out and stored in a glass vial. Mp: 215.3-217.3°C (w/ dec). IR: =C-H stretch (aromatic): 3019.90, 3165.01, 824.45, 787.18, 753.16 cm^{-1}, C=C stretch (aromatic): 1587.24, 1406.14 cm^{-1}, C=N stretch (aromatic): 1540.82, 1524.60, 1498.26 cm^{-1}, C-C stretch (aromatic): 1446.59 cm^{-1}, C-N stretch (aromatic): 1358.77, 1257.07 cm^{-1}, C-F stretch: 1218.70, 1147.21, 1100.38, 1013.00 cm^{-1}. Theoretical Anal. Calc. for $C_{44} H_{20} Cu_4 F_{24} N_{12}$ (MW = 1426.88 g/mol): C, 37.04; H, 1.42; N, 11.18; experimentally found: C, 36.98; H, 1.41; N, 11.45.

The crude, solventless product is completely soluble in acetone, acetonitrile, toluene, methanol, and dichloromethane and insoluble in diethyl ether, cyclohexane, and water (very hydrophobic). The product is air sensitive and oxidizes in solution with common solvents. The aforementioned crude, solventless product was unwashed. A previous attempt at a solventless synthesis resulted in a crude, solventless product that was washed using DI water. Mp: 210.0-214.8°C (w/ dec). Theoretical Anal. Calc. for $C_{44} H_{20} Cu_4 F_{24} N_{12}$: C, 37.04; H, 1.42; N, 11.18; experimentally found: C, 39.29; H, 1.35; N, 11.59. The melting point and elemental analysis data showed that DI water is not a suitable solvent for washing off excess ligand.
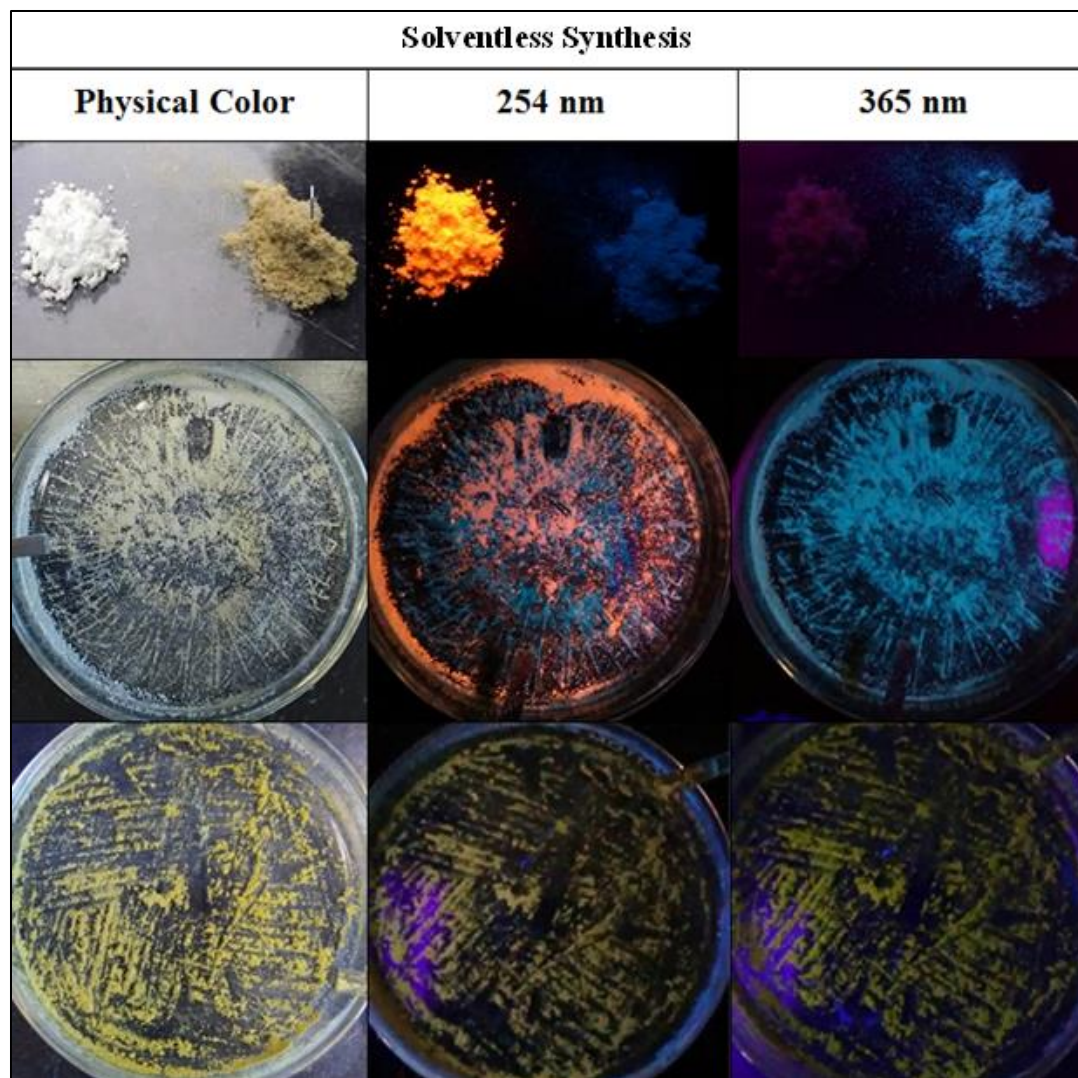
Figure 30. Solventless synthesis of $\{Cu_2[3,5\text{-}(CF_3)_2Pz]_2(4,7\text{-phen})\}_2$ powder, monitored via physical color change (yellow) and appearance of medium-strong, yellow luminescence.

2.2.2 Syntheses of Compound 2: {Ag$_5$[3,5-(CF$_3$)$_2$Pz]$_5$(4,7-phen)$_4$}$_\infty$

5 Ag$_2$O + 10 [3,5-(CF$_3$)$_2$Pz]H + 8 (4,7-phen)

   Solvent-mediated ↓ Solventless
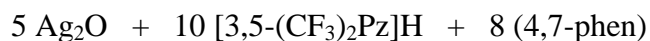
2 {Ag$_5$[3,5-(CF$_3$)$_2$Pz]$_5$(4,7-phen)$_4$}$_\infty$ + 5 H$_2$O
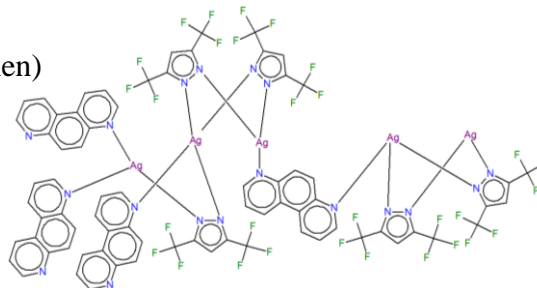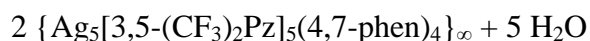
2.2.2.1 Solvent-mediated Synthesis of {Ag$_5$[3,5-(CF$_3$)$_2$Pz]$_5$(4,7-phen)$_4$}$_\infty$ using DCM

The synthesis of {[3,5-(CF$_3$)$_2$Pz]Ag}$_3$ was carried out as reported in the literature, via Schlenk technique and under constant gaseous nitrogen (N$_2$) atmosphere. [3,5-(CF$_3$)$_2$Pz]H (0.50 g, 2.45 mmol) and silver(I) oxide, Ag$_2$O, (0.31 g, 1.34 mmol) were mixed in 12 mL of toluene (bubbled with N$_2$), and subsequently heated (with constant stirring) under reflux at ~68°C for 48 hours. The resulting reaction mixture was filtered over a bed of celite (wet with toluene) in order to remove insoluble impurities. The filtrate was collected and placed under vacuum for ~2 hour in order to remove the solvent, yielding the white/colorless solid, {[3,5-(CF$_3$)$_2$Pz]Ag}$_3$.

Under constant N$_2$ atmosphere, {[3,5-(CF$_3$)$_2$Pz]Ag}$_3$ (0.3112 g, 0.3336 mmol) and 4,7-phenanthroline (0.1989 g, 1.001 mmol) were mixed in 6 mL of dichloromethane (DCM) (bubbled with N$_2$). Upon adding {[3,5-(CF$_3$)$_2$Pz]Ag}$_3$ to 4,7-Phenanthroline in toluene, an immediate color change was observed, from clear, golden brown to cloudy/milky, beige (formation of off-white precipitate). The resulting reaction mixture was allowed to stir at room temperature for ~4.5 hours in order to allow the starting materials to react. Subsequently, the resulting reaction mixture was heated (with constant

stirring) under reflux at 35-40°C for ~1.5 hours. After allotting time to cool, the off-white reaction mixture was filtered, collecting the off-white precipitate (product) on the filter. The filter product was placed under vacuum for ~5.5 hours in order to completely remove traces of solvent, yielding the dry product: off-white, solid (yield 77%). Mp: 125.3-127.2°C. IR: =C-H stretch (aromatic): 3142.65, 3059.34, 838.26, 787.01, 755.34 cm^{-1}, C=C stretch (aromatic): 1584.19, 1407.04 cm^{-1}, C=N stretch (aromatic): 1522.02, 1498.54 cm^{-1}, C-C stretch (aromatic): 1444.32 cm^{-1}, C-N stretch (aromatic): 1347.08, 1304.90, 1254.56 cm^{-1}, C-F stretch: 1219.24, 1144.30, 1094.70, 999.66 cm^{-1}. Anal. Calc. for C73 H37 Ag5 F30 N18: C, 38.53; H, 1.64; N, 11.08; found: C, 38.32; H, 1.56; N, 10.80.

A diethyl ether molecule (C4 H10 O) is present in the unit cell of the crystal structure. The empirical formula for the powder, solid product (synthesized using dichloromethane) accounts for the absence of the diethyl ether molecule. The off-white solid product was checked under a handheld UV lampfor photoluminescence under Short Wave UV (λ_{ex} = 254 nm) and Long Wave UV (λ_{ex} = 365 nm). Very weak, orange photoluminescence was observed under 254 nm. The off-white solid product was completely soluble in acetone, acetonitrile, toluene, ethanol, methanol, chloroform, dichloromethane, and diethyl ether, and insoluble in hexane, cyclohexane, and water (very hydrophobic).

X-ray quality crystals (physical color: colorless/ off-white) were grown from a binary solvent system using diethyl ether and hexane via slow evaporation. Approximately 2 mL of diethyl ether and 2 mL of hexane were added to a graduated

cylinder and transferred to a glass vial. Approximately 15 mg of the off-white solid product was added to the binary solvent system and mixed via sonication in a sonicator bath until the mixture became clear (the product completely dissolved). The solution was filtered (via pasture pipette with cotton) into a clean, glass vial and was allowed to slowly evaporate. The solution was left undisturbed in order to slowly evaporate for 14 days, resulting in crystal growth. Mp: 124.81°C. IR: =C-H stretch (aromatic): 3131.38, 3056.69, 837.87, 789.29, 755.42 cm^{-1}, C=C stretch (aromatic): 1583.44, 1392.25 cm^{-1}, C=N stretch (aromatic): 1535.98, 1517.79, 1496.34 cm^{-1}, C-C stretch (aromatic): 1444.12 cm^{-1}, C-N stretch (aromatic): 1348.94, 1304.27, 1254.92 cm^{-1}, C-F stretch: 1212.98, 1098.97, 999.15 cm^{-1}, C-H (sp^3): 2957.83, 2922.78, 2850.76 cm^{-1}, C-O stretch: 1138.93 cm^{-1}. Anal. Calc. for C77 H47 Ag5 F30 N18 O: C, 39.36; H, 2.02; N, 10.73; found: C, 39.09; H, 1.98; N, 10.38. A diethyl ether molecule (C4 H10 O) is present in the unit cell of the crystal structure and is included in the empirical formula for the crystallized product.

2.2.2.2 Solvent-mediated Synthesis of {Ag$_5$[3,5-(CF$_3$)$_2$Pz]$_5$(4,7-phen)$_4$}$_\infty$ using Toluene

The synthesis of {[3,5-(CF$_3$)$_2$Pz]Ag}$_3$ was carried out as reported in the literature, via Schlenk technique and under constant gaseous nitrogen (N$_2$) atmosphere. [3,5-(CF$_3$)$_2$Pz]H (0.50 g, 2.45 mmol) and silver(I) oxide, Ag$_2$O, (0.31 g, 1.34 mmol) were mixed in 12 mL of toluene (bubbled with N$_2$), and subsequently heated (with constant stirring) under reflux at ~68°C for 48 hours. The resulting reaction mixture was filtered

over a bed of celite (wet with toluene) in order to remove insoluble impurities. The filtrate was collected and placed under vacuum for ~2 hour in order to remove the solvent, yielding the white/colorless solid, $\{[3,5-(CF_3)_2Pz]Ag\}_3$.

Under constant N_2 atmosphere, $\{[3,5-(CF_3)_2Pz]Ag\}_3$ (0.2082 g, 0.2232 mmol) and 4,7-phenanthroline (0.1206 g, 0.6692 mmol) were mixed in 4 mL of toluene (bubbled with N_2). Upon adding $\{[3,5-(CF_3)_2Pz]Ag\}_3$ to 4,7-phenanthroline in toluene, an immediate color change was observed, from cloudy, beige to cloudy/milky light beige (formation of off-white precipitate). The resulting reaction mixture was allowed to stir at room temperature for 10 minutes in order to allow the starting materials to react. Subsequently, the resulting reaction mixture was heated (with constant stirring) under reflux at 70°C for 1 hours. After allotting time to cool, the off-white reaction mixture was filtered, collecting the off-white precipitate (product) on the filter. The filter product was placed under vacuum for 2 hours in order to completely remove the solvent, yielding the product: off-white, solid (yield 40%). Mp: 132.3-134.3°C. IR: =C-H stretch (aromatic): 3130.62, 3051.34, 836.37, 788.69, 755.23 cm^{-1}, C=C stretch (aromatic): 1583.36, 1405.51 cm^{-1}, C=N stretch (aromatic): 1536.84, 1517.26, 1496.39 cm^{-1}, C-C stretch (aromatic): 1444.40 cm^{-1}, C-N stretch (aromatic): 1348.90, 1254.02 cm^{-1}, C-F stretch: 1217.77, 1156.63, 1096.72, 998.82 cm^{-1}, C-H bending "oop": 738.79 cm^{-1}. Anal. Calc. for C80 H45 Ag5 F30 N18: C, 40.58; H, 1.92; N, 10.65; found: C, 40.35; H, 1.90; N, 10.49. As previously mentioned, a diethyl ether molecule (C4 H10 O) is present in the unit cell of the crystal structure. The empirical formula for the powder, solid product (synthesized using toluene) accounts for the presence of a toluene molecule. The

presence of the toluene molecule is due to insufficient drying of the product, leaving behind traces of toluene.

2.2.2.3 Solventless Synthesis of $\{Ag_5[3,5-(CF_3)_2Pz]_5(4,7-phen)_4\}_\infty$

A solventless synthesis of $\{Ag_5[3,5-(CF_3)_2Pz]_5(4,7-phen)_4\}_\infty$ was attempted via mechanically grinding with heat; however, the progress of the reaction was difficult to monitor via either a change in physical color or the disappearance/appearance of photoluminescence (checked using a handheld UV lamp). The resulting powder was off-white in physical color and did not exhibit photoluminescence under Short Wave UV (λ_{ex} = 254 nm) nor Long Wave UV (λ_{ex} = 365 nm).

2.2.3 Syntheses of Compound 3: {Cu[3,5-(CF$_3$)$_2$Pz](1,7-phen)}$_2$

Cu$_2$O   +   2 [3,5-(CF$_3$)$_2$Pz]H   +   2 (1,7-phen)

   Solvent-mediated ↓ Solventless

{Cu[3,5-(CF$_3$)$_2$Pz](1,7-phen)}$_2$ +   H$_2$O

2.2.3.1 Solvent-mediated Synthesis of {Cu[3,5-(CF$_3$)$_2$Pz](1,7-phen)}$_2$

The synthesis of {[3,5-(CF$_3$)$_2$Pz]Cu}$_3$ was carried out as reported in the literature, via Schlenk technique and under constant gaseous nitrogen (N$_2$) atmosphere. [3,5-(CF$_3$)$_2$Pz]H (0.50 g, 2.45 mmol) and copper(I) oxide, Cu$_2$O, (0.19 g, 1.43 mmol) were mixed in 12 mL of benzene (bubbled with N$_2$), and subsequently heated (with constant stirring) under reflux at ~60°C for 24 hours. The resulting reaction mixture was filtered over a bed of celite (wet with benzene) in order to remove insoluble impurities. The filtrate was collected and placed under vacuum for ~5 hour in order to completely remove the solvent, yielding the white/colorless solid, {[3,5-(CF$_3$)$_2$Pz]Cu}$_3$.

Under constant N$_2$ atmosphere, {[3,5-(CF$_3$)$_2$Pz]Cu}$_3$ (0.1511 g, 0.1889 mmol) and 1,7-phenanthroline (0.1022 g, 0.5671 mmol) were mixed in 6.5 mL of hexane (bubbled with N$_2$). Upon adding 1,7-phenanthroline to {[3,5-(CF$_3$)$_2$Pz]Cu}$_3$ in hexane, an immediate color change was observed, from cloudy, white to cloudy/milky, yellow (formation of yellow precipitate). The resulting reaction mixture was allowed to stir for 0.5 hours in order to allow the starting materials to completely react. The yellow reaction mixture was filtered, collecting the yellow precipitate (product) on the filter. The filter

product was placed under vacuum for 3.5 hours in order to completely remove traces of solvent, yielding the dry product: pale, yellow, solid (yield 81%). Mp: 134.4-135.7°C (w/ dec). IR: =C-H stretch (aromatic): 3174.71, 3046.36, 2962.28, 835.97, 811.82, 773.62, 727.59, 715.61 cm^{-1}, C=C stretch (aromatic): 1600.29, 1395.43 cm^{-1}, C=N stretch (aromatic): 1619.42, 1574.40, 1526.86, 1496.00 cm^{-1}, C-C stretch (aromatic): 1429.39 cm^{-1}, C-N stretch (aromatic): 1355.66, 1262.44 cm^{-1}, C-F stretch: 1210.83, 1109.87, 1015.26 cm^{-1}. Anal. Calc. for C34 H18 Cu2 F12 N8: C, 45.70; H, 2.03; N, 12.54; found: C, 45.79; H, 1.77; N, 12.31.

The pale yellow solid product was checked under a handheld UV lamp for photoluminescence under Short Wave UV (λ_{ex} = 254 nm) and Long Wave UV (λ_{ex} = 365 nm). Yellow photoluminescence was observed under 254 nm (weak, yellow-orange luminescence) and 365 nm (medium-strong, yellow luminescence). The pale yellow solid product was completely soluble in acetone, acetonitrile, benzene, toluene, ethanol, methanol, chloroform, dichloromethane, cyclohexane, and diethyl ether, partially soluble in hexane, and insoluble in water.

X-ray quality crystals (physical color: yellow) were grown from a single solvent system using hexane via slow cooling (with slow cooling from 50°C to 5°C). 4 mL of hexane were added to a graduated cylinder and transferred to a Schlenk flask. The resulting solution was bubbled with N_2 for 10 minutes. Under constant N_2 flow, 5 mg of the pale yellow solid product was added to hexane (pre-heated at 50°C), and the resulting cloudy, yellow mixture was heated in an oil bath at 50°C and manually swirled until the mixture became clear, pale yellow (the product completely dissolved). The flask was

removed from the oil bath, and the resulting solution was allowed to slowly cool to room temperature under low N_2 flow. Afterward, the flask containing the resulting solution was stored in the refrigerator and was allowed to slowly cool at 5°C. The solution was left undisturbed in order to slowly cool for 2 days, resulting in crystal growth Mp: 134.3-136.8°C (w/ dec). IR: =C-H stretch (aromatic): 3176.04, 3046.53, 2962.67, 835.70, 811.73, 773.36, 727.59, 715.59 cm^{-1}, C=C stretch (aromatic): 1600.39, 1395.55 cm^{-1}, C=N stretch (aromatic): 1619.51, 1574.40, 1527.15, 1508.39, 1496.18 cm^{-1}, C-C stretch (aromatic): 1429.58 cm^{-1}, C-N stretch (aromatic): 1355.91, 1262.15 cm^{-1}, C-F stretch: 1210.25, 1108.45, 1015.31 cm^{-1}. Anal. Calc. for C34 H18 Cu2 F12 N8: C, 45.70; H, 2.03; N, 12.54; found: C, 45.84; H, 2.00; N, 12.46.
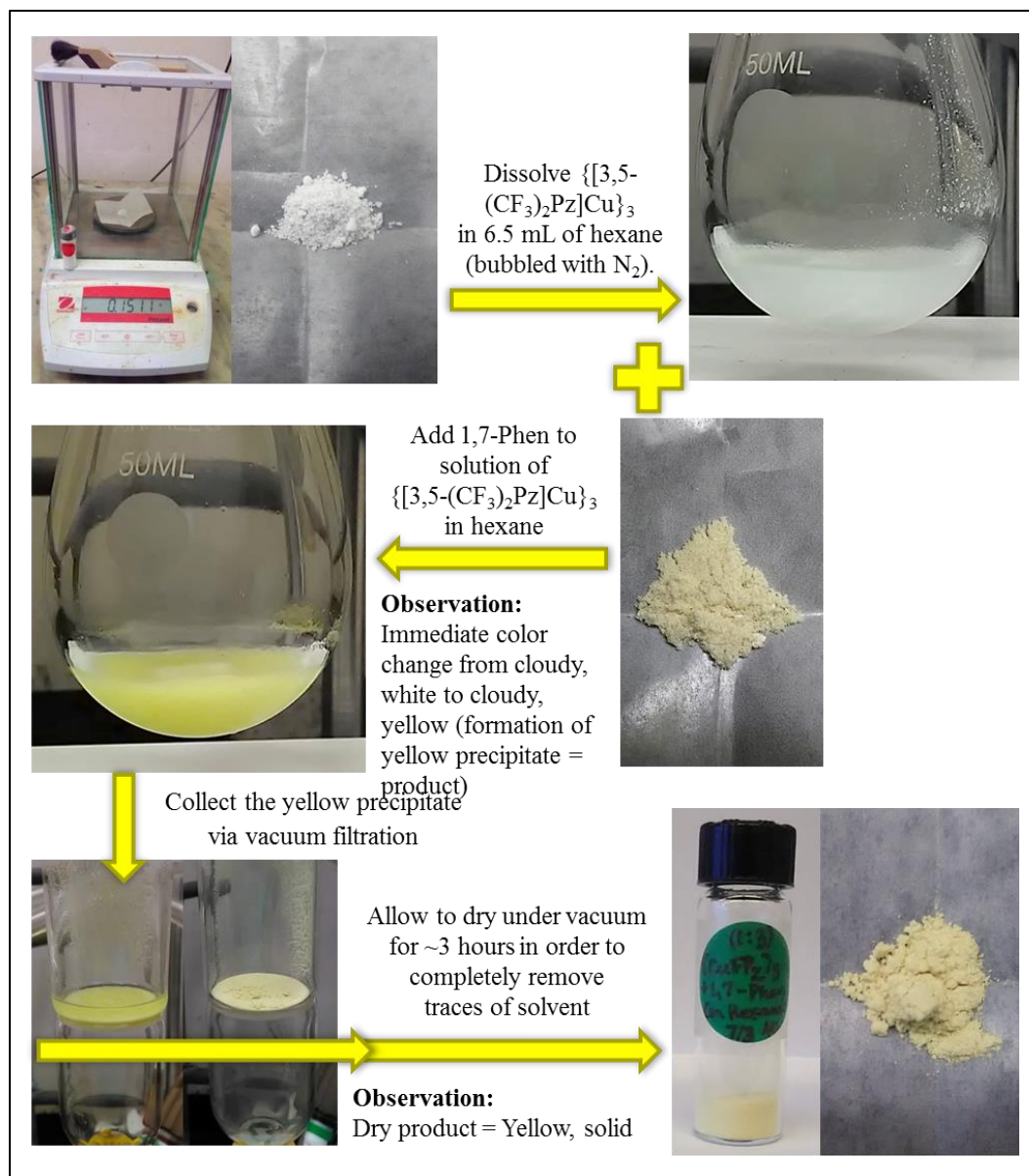
Figure 31. Solvent-mediated synthesis of {Cu[3,5-(CF$_3$)$_2$Pz](1,7-phen)}$_2$ powder.

2.2.3.2 Solventless Synthesis of {Cu[3,5-(CF$_3$)$_2$Pz](1,7-phen)}$_2$

The synthesis of {[3,5-(CF$_3$)$_2$Pz]Cu}$_3$ was carried out as reported in the literature, via Schlenk technique and under constant gaseous nitrogen (N$_2$) atmosphere. [3,5-(CF$_3$)$_2$Pz]H (0.50 g, 2.45 mmol) and copper(I) oxide, Cu$_2$O, (0.19 g, 1.43 mmol) were mixed in 12 mL of benzene (bubbled with N$_2$), and subsequently heated (with constant stirring) under reflux at ~60°C for 24 hours. The resulting reaction mixture was filtered over a bed of celite (wet with benzene) in order to remove insoluble impurities. The filtrate was collected and placed under vacuum for ~5 hour in order to completely remove the solvent, yielding the white/colorless solid, {[3,5-(CF$_3$)$_2$Pz]Cu}$_3$.

{[3,5-(CF$_3$)$_2$Pz]Cu}$_3$ (0.1001 g, 0.1251 mmol) and 1,7-phenanthroline (0.0669 g, 0.371 mmol) were placed side by side on a glass petri dish and mechanically ground together with heat. The progress of the reaction was monitored via both a change in physical color and the disappearance/appearance of photoluminescence (checked using a handheld UV lamp). In contrast, {[3,5-(CF$_3$)$_2$Pz]Cu}$_3$ has a very strong, orange photoluminescence under Short Wave UV (λ_{ex} = 254 nm); meanwhile, 1,7-phenanthroline has a weak, blue photoluminescence under both Short Wave UV and Long Wave UV (λ_{ex} = 365 nm). Prior to heating, {[3,5-(CF$_3$)$_2$Pz]Cu}$_3$ and 1,7-phenanthroline were mechanically ground together for 10 minutes at room temperature, resulting in a light pale yellow physical color with medium-strong light orange/salmon photoluminescence under 254 nm and weak, yellow-blue photoluminescence under 365 nm. Afterward, the resulting powder mixture was mechanically ground for an additional 10 minutes while heating at 50°C. After heating, the resulting powder was pale yellow in

color (physical) and exhibited yellow photoluminescence under both 254 nm (medium-strong, yellow luminescence) and 365 nm (strong, yellow luminescence). Further heating of the crude, solventless product was not performed in order to avoid potential oxidation or decomposition of the product. The crude, yellow, solventless product was weighed out and stored in a glass vial. Mp: 114.0-124.0°C (w/ dec). IR: =C-H stretch (aromatic): 3147.65, 3038.25, 836.63, 814.44, 771.28, 731.53, 713.53 cm^{-1}, C=C stretch (aromatic): 1599.86, 1397.30 cm^{-1}, C=N stretch (aromatic): 1616.13, 1575.30, 1538.53, 1496.71 cm^{-1}, C-C stretch (aromatic): 1429.16 cm^{-1}, C-N stretch (aromatic): 1356.23, 1254.96 cm^{-1}, C-F stretch: 1222.22, 1111.22, 1019.26 cm^{-1}. Anal. Calc. for C34 H18 Cu2 F12 N8: C, 45.70; H, 2.03; N, 12.54; found: C, 47.44; H, 2.00; N, 12.33.

The aforementioned crude, solventless product was completely soluble in acetone, acetonitrile, benzene, toluene, ethanol, methanol, chloroform, dichloromethane, cyclohexane, and diethyl ether, partially soluble in hexane, and insoluble in water. The product was unwashed because it oxidizes easily in all the solvents mentioned above with the exception of water.
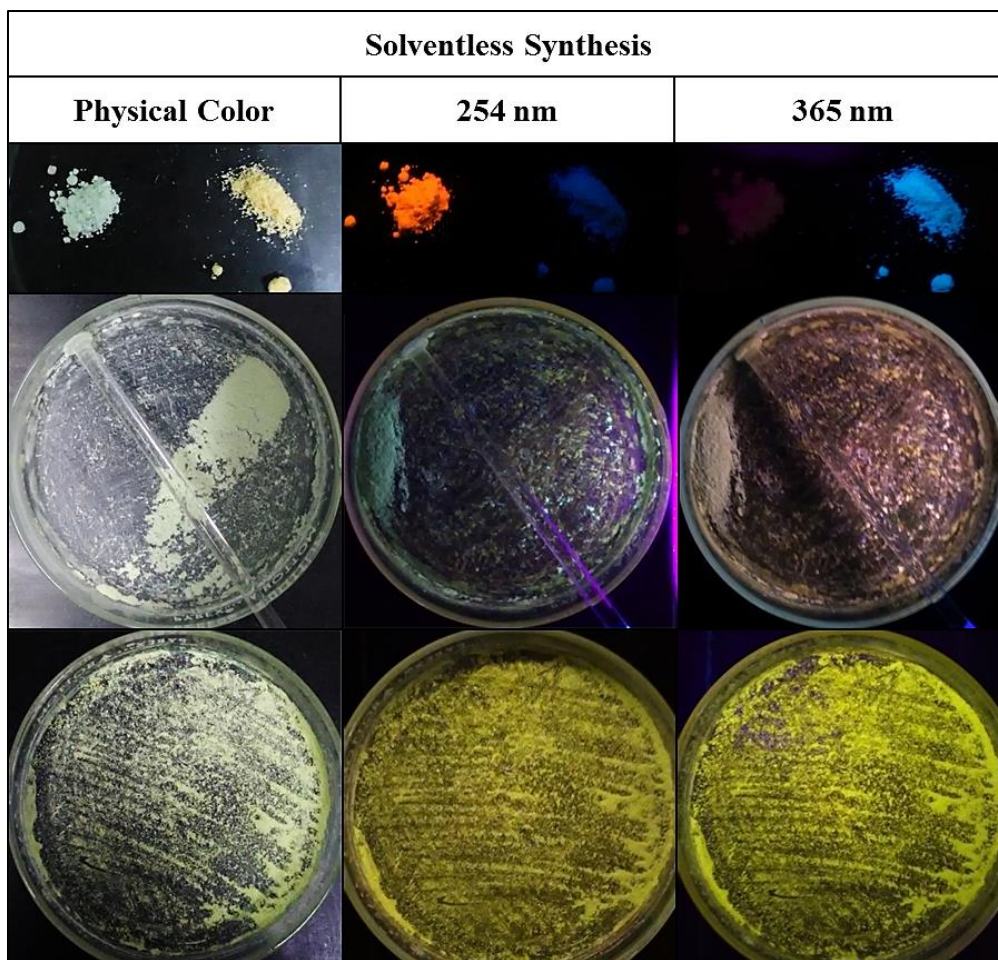
Figure 32. Solventless synthesis of {Cu[3,5-(CF$_3$)$_2$Pz](1,7-phen)}$_2$ powder, monitored via physical color change (yellow) and appearance of strong, yellow luminescence.

2.2.4 Syntheses of Compound 4: Ag$_2$[3,5-(CF$_3$)$_2$Pz]$_2$(1,7-phen)$_3$

Ag$_2$O + 2 [3,5-(CF$_3$)$_2$Pz]H + 3 (1,7-phen)

   Solvent-mediated ↓ Solventless
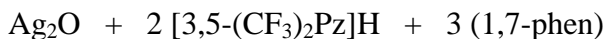
  Ag$_2$[3,5-(CF$_3$)$_2$Pz]$_2$(1,7-phen)$_3$ + H$_2$O
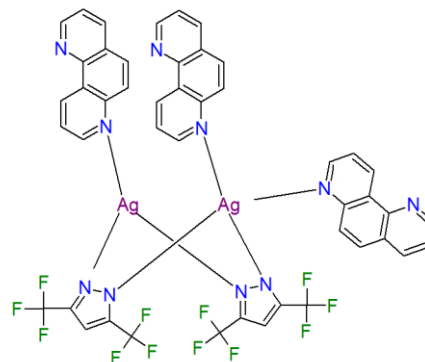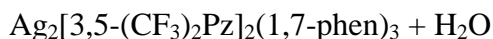
2.2.4.1 Solvent-Mediated Synthesis of Ag$_2$[3,5-(CF$_3$)$_2$Pz]$_2$(1,7-phen)$_n$, (n = 2 or 3) Using Benzene

The synthesis of {[3,5-(CF$_3$)$_2$Pz]Ag}$_3$ was carried out as reported in the literature, via Schlenk technique and under constant gaseous nitrogen (N$_2$) atmosphere. [3,5-(CF$_3$)$_2$Pz]H (0.50 g, 2.45 mmol) and silver(I) oxide, Ag$_2$O, (0.31 g, 1.34 mmol) were mixed in 12 mL of toluene (bubbled with N$_2$), and subsequently heated (with constant stirring) under reflux at ~68°C for 48 hours. The resulting reaction mixture was filtered over a bed of celite (wet with toluene) in order to remove insoluble impurities. The filtrate was collected and placed under vacuum for ~2 hour in order to remove the solvent, yielding the white/colorless solid, {[3,5-(CF$_3$)$_2$Pz]Ag}$_3$.

Under constant N$_2$ atmosphere, {[3,5-(CF$_3$)$_2$Pz]Ag}$_3$ (0.2084 g, 0.2235 mmol) and 1,7-phenanthroline (0.1248 g, 0.6925 mmol) were mixed in 7 mL of hexane (bubbled with N$_2$). Upon adding {[3,5-(CF$_3$)$_2$Pz]Ag}$_3$ to 1,7-Phenanthroline in hexane, an immediate change was observed, from a slightly turbid, solution with insoluble 1,7-phenanthroline to cloudy/milky, off-white mixture (formation of off-white precipitate). The resulting reaction mixture was allowed to stir at room temperature for 0.5 hours in

order to allow the starting materials to react. Subsequently, the resulting reaction mixture was heated (with constant stirring) under reflux at 55°C for 1.5 hours. After allotting time to cool, the off-white reaction mixture was filtered, collecting the off-white precipitate (product) on the filter. The filter product was placed under vacuum for 3.5 hours in order to completely remove traces of solvent, yielding the dry product: off-white, solid (yield 75%). Mp: 140.0-141.3°C (w/ dec). IR: =C-H stretch (aromatic): 3064.16, 3034.19, 832.87, 787.90, 767.65 cm^{-1}, C=C stretch (aromatic): 1599.74, 1394.41 cm^{-1}, C=N stretch (aromatic): 1615.90, 1573.13, 1540.28, 1494.30 cm^{-1}, C-C stretch (aromatic): 1426.95 cm^{-1}, C-N stretch (aromatic): 1348.05, 1301.03, 1254.27 cm^{-1}, C-F stretch: 1212.00, 1149.18, 1104.97, 1001.40 cm^{-1}. Anal. Calc. for C34 H18 Ag2 F12 N8: C, 41.57; H, 1.85; N, 11.41; found: C, 40.34; H, 1.78; N, 11.10.

The off-white solid product was checked under a handheld UV lamp for photoluminescence under Short Wave UV (λ_{ex} = 254 nm) and Long Wave UV (λ_{ex} = 365 nm). The solid product did not exhibit photoluminescence under either 254 nm or 365 nm at room temperature. Strong, green photoluminescence was observed under 365 nm at 77K. The off-white solid product was completely soluble in acetone, acetonitrile, toluene, ethanol, methanol, chloroform, dichloromethane, and diethyl ether, partially soluble in hexane and cyclohexane, and insoluble in water

X-ray quality crystals (physical color: colorless) were grown from a single solvent system using cyclohexane via slow evaporation. 13 mg of the off-white solid product was added to a clean, glass vial. Afterward, 3 mL of cyclohexane was measured out in a graduated cylinder and transferred to the glass vial. The resulting clear, colorless solution

and the un-dissolved product were mixed via sonication in a sonicator bath until all the product completely dissolved, resulting in a clear, colorless solution. The solution was filtered (via pasture pipette with cotton) into a clean, glass vial and was allowed to slowly evaporate. The solution was left undisturbed for four days in order to slowly evaporate, resulting in crystal growth. The colorless crystals were of uniform size and shape. Mp: 140.3-143.2°C. IR: =C-H stretch (aromatic): 3063.96, 3033.74, 833.08, 797.59, 767.78 cm^{-1}, C=C stretch (aromatic): 1599.48, 1393.93 cm^{-1}, C=N stretch (aromatic): 1615.64, 1572.80, 1540.21, 1494.07 cm^{-1}, C-C stretch (aromatic): 1426.68 cm^{-1}, C-N stretch (aromatic): 1347.47, 1300.74, 1255.18 cm^{-1}, C-F stretch: 1210.90, 1150.06, 1105.39, 1001.81 cm^{-1}. Anal. Calc. for C46 H26 Ag2 F12 N10: C, 47.53; H, 2.25; N, 12.05; found: C, 47.20; H, 2.16; N, 11.84.

The structure of the solvent-mediated powder (synthesized using dichloromethane) may possibly resemble {Ag[3,5-(CF$_3$)$_2$Pz](1,7-phen)}$_2$, the Ag(I) analogue of {Cu[3,5-(CF$_3$)$_2$Pz](1,7-phen)}$_2$, which possesses two 3-coordinated Ag(I) centers with two [3,5-(CF$_3$)$_2$Pz]$^-$ and two 1,7-phenanthroline ligands. In contrast, the structure of the single crystals resembles Ag$_2$[3,5-(CF$_3$)$_2$Pz]$_2$(1,7-phen)$_3$, which possesses 3- and 4-coordinated Ag(I) centers with two [3,5-(CF$_3$)$_2$Pz]$^-$ and three 1,7-phenanthroline ligands. The empirical formula for the solvent-mediated powder accounts for the absence of the aforementioned 1,7-phenanthroline.

In addition to the crystals above, other colorless crystals of different size and shape were grown. Anal. Calc. for C27 H11 Ag3 F18 N8: C, 29.14; H, 1.00; N, 10.07; found: C, 29.31; H, 0.92; N, 10.08. The structure of the single crystals possibly resembles

Ag$_3$[3,5-(CF$_3$)$_2$Pz]$_3$(1,7-phen), a Ag(I)-pyrazolate trimer with one 1,7-phenanthroline ligand.

2.2.4.2 Solvent-Mediated Synthesis of Ag$_2$[3,5-(CF$_3$)$_2$Pz]$_2$(1,7-phen)$_n$, (n = 2) Using Benzene

The synthesis of {[3,5-(CF$_3$)$_2$Pz]Ag}$_3$ was carried out as reported in the literature, via Schlenk technique and under constant gaseous nitrogen (N$_2$) atmosphere. [3,5-(CF$_3$)$_2$Pz]H (0.50 g, 2.45 mmol) and silver(I) oxide, Ag$_2$O, (0.31 g, 1.34 mmol) were mixed in 12 mL of toluene (bubbled with N$_2$), and subsequently heated (with constant stirring) under reflux at ~68°C for 48 hours. The resulting reaction mixture was filtered over a bed of celite (wet with toluene) in order to remove insoluble impurities. The filtrate was collected and placed under vacuum for ~2 hour in order to remove the solvent, yielding the white/colorless solid, {[3,5-(CF$_3$)$_2$Pz]Ag}$_3$.

{[3,5-(CF$_3$)$_2$Pz]Ag}$_3$ (0.1488 g, 0.1595 mmol) and 1,7-phenanthroline (0.0868 g, 0.482 mmol) were mixed in 6 mL of benzene (bubbled with N$_2$). Upon adding {[3,5-(CF$_3$)$_2$Pz]Ag}$_3$ to 1,7-Phenanthroline in hexane, no immediate change was observed (remained clear and beige in color). The resulting reaction mixture was allowed to stir at room temperature for five days in order to allow the starting materials to react. After five days, the resulting reaction mixture became slightly turbid and darker in color. The reaction mixture was placed under vacuum, and the solvent was slowly removed. As the solvent was removed, the solution became significantly more turbid. With less than 1 mL of solution remaining, the glassware containing the aforementioned solution was lightly

tapped, resulting in the immediate formation/expansion of off-white, foam-like substance from the solution. Following the complete removal of the solvent, the crude, product remained under vacuum for 2 hours in order to completely remove traces of solvent, yielding the dry, crude product: off-white, solid. Mp: 138.7-140.3°C (w/ dec). IR: =C-H stretch (aromatic): 3063.05, 3031.74, 833.02, 798.05, 767.53cm^{-1}, C=C stretch (aromatic): 1599.59, 1394.37 cm^{-1}, C=N stretch (aromatic): 1615.94, 1573.49, 1540.55, 1494.47 cm^{-1}, C-C stretch (aromatic): 1427.24 cm^{-1}, C-N stretch (aromatic): 1348.081 1301.02, 1254.37 cm^{-1}, C-F stretch: 1213.66, 1148.91, 1105.25, 1001.88 cm^{-1}. Anal. Calc. for C34 H18 Ag2 F12 N8: C, 41.57; H, 1.85; N, 11.41; found: C, 42.03; H, 1.67; N, 11.18.

2.2.4.3 Solventless Synthesis of Ag$_2$[3,5-(CF$_3$)$_2$Pz]$_2$(1,7-phen)$_n$, (n = 2 or 3)

A solventless synthesis of Ag$_2$[3,5-(CF$_3$)$_2$Pz]$_2$(1,7-phen)$_n$, (n = 2 or 3) was attempted via mechanically grinding with heat; however, the progress of the reaction was difficult to monitor via either a change in physical color or the disappearance/appearance of photoluminescence (checked using a handheld UV lamp). The resulting powder was beige/tan in physical color (similar to the 1,7-phenanthroline starting material) and did not exhibit photoluminescence under Short Wave UV nor Long Wave UV

2.2.5 Syntheses of Compound 5: {Cu[3,5-(CF$_3$)$_2$Pz](dmp)}$_2$

Cu$_2$O + 2 [3,5-(CF$_3$)$_2$Pz]H + 2 (dmp · 0.5 H$_2$O)
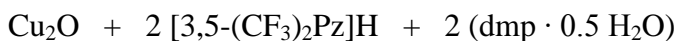
$\quad$ Solvent-mediated ↓ Solventless
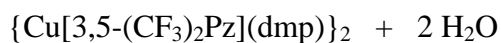
$\quad$ {Cu[3,5-(CF$_3$)$_2$Pz](dmp)}$_2$ + 2 H$_2$O

Chloroform $\qquad\qquad$ Acetone (excess)

{Cu[3,5-(CF$_3$)$_2$Pz](dmp)}$_2$ $\qquad$ [Cu(Lactate)(dmp)]$_2$
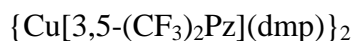
Red Crystals $\qquad\qquad$ **Green Crystals**

2.2.5.1 Solventless Synthesis of {Cu[3,5-(CF$_3$)$_2$Pz](dmp)}$_2$

The synthesis of {[3,5-(CF$_3$)$_2$Pz]Cu}$_3$ was carried out as reported in the literature, via Schlenk technique and under constant gaseous nitrogen (N$_2$) atmosphere. [3,5-(CF$_3$)$_2$Pz]H (0.50 g, 2.45 mmol) and copper(I) oxide, Cu$_2$O, (0.19 g, 1.43 mmol) were mixed in 12 mL of benzene (bubbled with N$_2$), and subsequently heated (with constant stirring) under reflux at ~60°C for 24 hours. The resulting reaction mixture was filtered over a bed of celite (wet with benzene) in order to remove insoluble impurities. The filtrate was collected and placed under vacuum for ~5 hours in order to completely remove the solvent, yielding the white/colorless solid, {[3,5-(CF$_3$)$_2$Pz]Cu}$_3$.

{[3,5-(CF$_3$)$_2$Pz]Cu}$_3$ (0.1171 g, 0.1464 mmol) and dmp · 0.5 H$_2$O (0.1055 g, 0.4858 mmol) were placed side by side on a glass petri dish and mechanically ground together with heat. The progress of the reaction was monitored via both a change in

physical color and the disappearance/appearance of photoluminescence (checked using a handheld UV lamp). In contrast, $\{[3,5\text{-}(CF_3)_2Pz]Cu\}_3$ has a very strong, orange photoluminescence under Short Wave UV (λ_{ex} = 254 nm); meanwhile, dmp · 0.5 H_2O has a weak, blue photoluminescence under Long Wave UV (λ_{ex} = 365 nm). Prior to heating, $\{[3,5\text{-}(CF_3)_2Pz]Cu\}_3$ and dmp · 0.5 H_2O were mechanically ground together for 26 minutes at room temperature, resulting in a pale orange physical color. Afterward, the resulting powder mixture was mechanically ground while gradually heated from 50°C to120°C. After mechanically grinding for 5 minutes at 50°C, the resulting powder became more orange in color (physical) with strong, hot orange (more orange-red) photoluminescence under Short Wave UV (254 nm) and very weak, red photoluminescence under Long Wave UV (365 nm). After mechanically grinding for 14 minutes at 120°C, the resulting powder became more orange (hot orange) in color (physical) with weak, red photoluminescence under both Short Wave UV (254 nm) and Long Wave UV (365 nm). Further heating of the crude, solventless product was not performed in order to avoid potential oxidation or decomposition of the product. The crude, solventless product was weighed out and stored in a glass vial. Mp: 245-259°C (w/ dec). Anal. Calc. for C38 H26 C2 F12 N8: C, 48.06; H, 2.76; N, 11:80; found: C, 49.00; H, 2.95; N, 11.55. The crude solventless product was washed five times with 3-5 mL portions of diethyl ether. The resulting solutions were mixed via sonication in a sonicator bath, and time was allotted in order for the product to settle out solution. The washed, orange solid product was allowed to dry for at least 3 hours in order for the diethyl ether traces to completely evaporate. Afterward, the solid product was re-weighed and stored in

a clean, glass vial (yield 69%). Mp: 264.0°C (w/ dec). IR: =C-H stretch (aromatic): 3140.91, 3040.92, 844.99, 802.56, 750.40, 728.67 cm^{-1}, C=C stretch (aromatic): 1607.74, 1372.22 cm^{-1}, C=N stretch (aromatic): 1590.63, 1561.12, 1500.42 cm^{-1}, C-C stretch (aromatic): 1415.32 cm^{-1}, C-N stretch (aromatic): 1354.98, 1305.52, 1252.67 cm^{-1}, C-F stretch: 1199.35, 1161.21, 1129.64, 1106.20, 1006.85, 976.41 cm^{-1}, C-H stretch (C-CH3): 2945.01, 2918.96, 2847.96, 2754.50 cm^{-1}. Anal. Calc. for C38 H26 Cu2 F12 N8: C, 48.06; H, 2.76; N, 11:80; found: C, 48.06; H, 2.72; N, 11.69.

The orange solid product was checked under a handheld UV lamp for photoluminescence under Short Wave UV (λ_{ex} = 254 nm) and Long Wave UV (λ_{ex} = 365 nm). Red photoluminescence was observed under both 254 nm (medium-weak, red luminescence) and 365 nm (medium-weak, red luminescence). The orange solid product was completely soluble in acetone, acetonitrile, benzene, methanol, chloroform, and dichloromethane, and partially soluble in toluene, ethanol, cyclohexane, diethyl ether, and water.

The petri dish and spatula used for the solventless synthesis contained remnants of the orange product, which were collected via chloroform washings and later crystallized via slow evaporation, similarly as described below. The crystals were not accounted for in the washed product's percent yield.
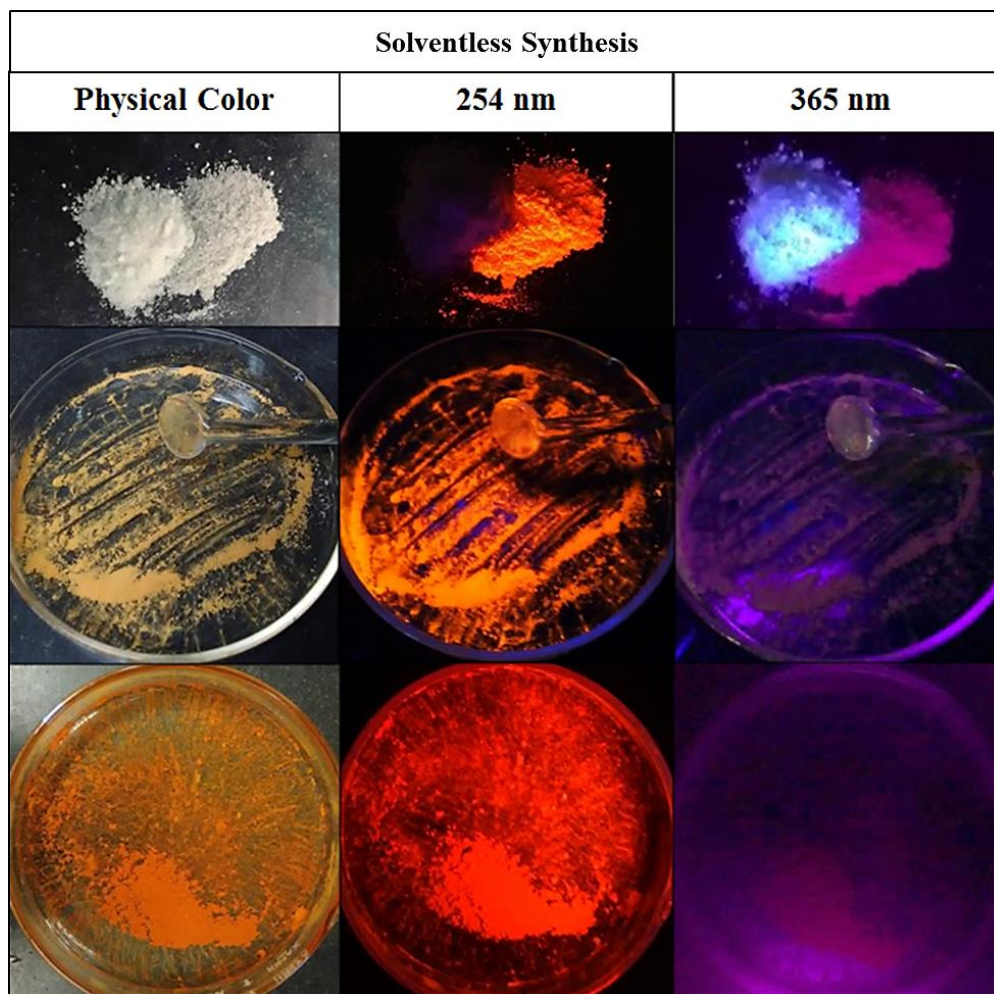
Figure 33. Solventless synthesis of {Cu[3,5-(CF$_3$)$_2$Pz](dmp)}$_2$ powder, monitored via physical color change (orange) and disappearance of strong, orange luminescence/ appearance of medium, strong, red luminescence.

X-ray quality crystals (physical color: red) were grown from a single solvent system using chloroform via slow evaporation (with slow cooling from 55°C to ambient temperature. Approximately 8 mg of the orange solid product was added to a clean, glass vial. Afterward, ~8 mL of chloroform was measured out in a graduated cylinder and transferred to the glass vial. The resulting cloudy, orange mixture was mixed via a mini

Roto and heated in an oil bath at 55°C until the mixture became clear (the product completely dissolved). The clear, orange solution was filtered (via pasture pipette with cotton) into a clean, glass vial, and the resulting solution was allowed to slowly cool and evaporate under room temperature. The red crystals were of uniform size and shape. Mp: 264.0°C (w/ dec). IR: =C-H stretch (aromatic): 3141.43, 3041.31, 844.87, 802.60, 750.65, 728.44 cm^{-1}, C=C stretch (aromatic): 1607.99, 1372.19 cm^{-1}, C=N stretch (aromatic): 1590.55, 1561.19, 1500.75 cm^{-1}, C-C stretch (aromatic): 1415.60 cm^{-1}, C-N stretch (aromatic): 1355.08, 1305.71, 1253.16 cm^{-1}, C-F stretch: 1199.62, 1161.03, 1129.36, 1106.30, 1007.36, 976.61 cm^{-1}, C-H stretch (C-CH3): 2954.35, 2918.93 cm^{-1}. Anal. Calc. for C38 H26 Cu2 F12 N8: C, 48.06; H, 2.76; N, 11:80; found: C, 48.19; H, 2.72; N, 11.73.
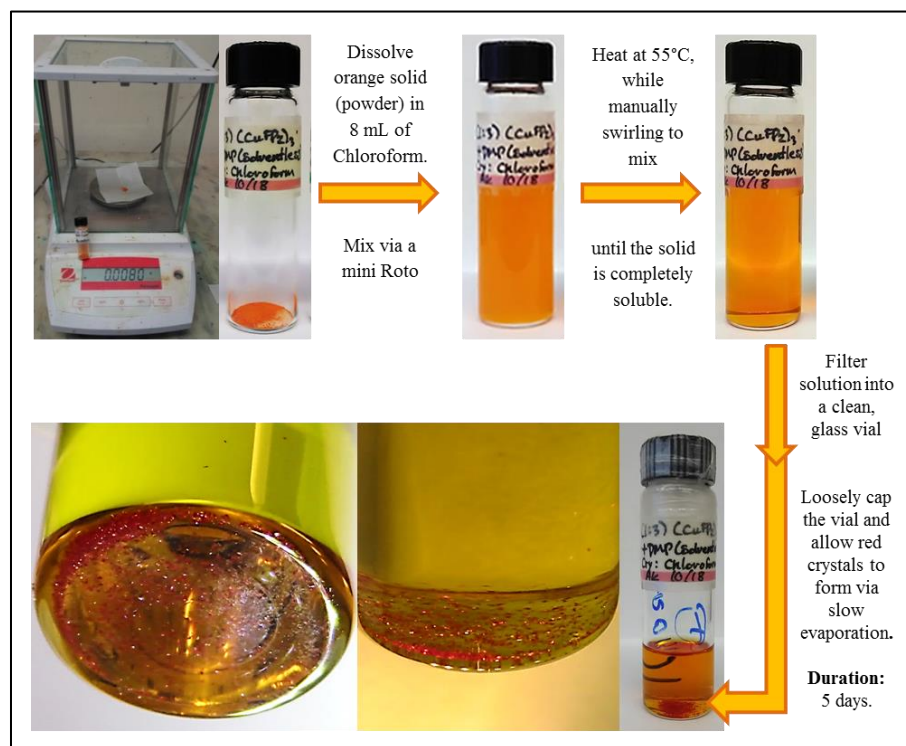
Figure 34. Crystallization of {Cu[3,5-(CF$_3$)$_2$Pz](dmp)}$_2$ using solventless powder.

2.2.5.2 Solvent-mediated Synthesis of {Cu[3,5-(CF$_3$)$_2$Pz](dmp)}$_2$

The synthesis of {[3,5-(CF$_3$)$_2$Pz]Cu}$_3$ was carried out as reported in the literature, via Schlenk technique and under constant gaseous nitrogen (N$_2$) atmosphere. [3,5-(CF$_3$)$_2$Pz]H (0.50 g, 2.45 mmol) and copper(I) oxide, Cu$_2$O, (0.19 g, 1.43 mmol) were mixed in 12 mL of benzene (bubbled with N$_2$), and subsequently heated (with constant stirring) under reflux at ~60°C for 24 hours. The resulting reaction mixture was filtered over a bed of celite (wet with benzene) in order to remove insoluble impurities. The filtrate was collected and placed under vacuum for ~5 hour in order to completely remove the solvent, yielding the white/colorless solid, {[3,5-(CF$_3$)$_2$Pz]Cu}$_3$.

Under constant N$_2$ atmosphere, {[3,5-(CF$_3$)$_2$Pz]Cu}$_3$ (0.1055 g, 0.1319 mmol) and dmp · 0.5 H$_2$O (0.0950 g, 0.437 mmol) were mixed in 6 mL of toluene (bubbled with N$_2$). Upon adding {[3,5-(CF$_3$)$_2$Pz]Cu}$_3$ to dmp · 0.5 H$_2$O in toluene, an immediate color change was observed, from clear, colorless to cloudy, red (formation of red precipitate). The resulting reaction mixture was allowed to stir for 0.5 hours in order to allow the starting materials to completely react. The red reaction mixture was filtered, collecting the red precipitate (product) on the filter. The filter product was placed under vacuum for ~4 hours in order to completely remove traces of solvent, yielding the dry product: orange, solid (yield 79%). Mp: 265.40°C (w/ dec). IR: =C-H stretch (aromatic): 3140.43, 3039.21, 845.53, 803.10, 750.94, 729.37 cm^{-1}, C=C stretch (aromatic): 1608.40, 1371.11 cm^{-1}, C=N stretch (aromatic): 1590.53, 1561.32, 1500.55 cm^{-1}, C-C stretch (aromatic): 1414.88 cm^{-1}, C-N stretch (aromatic): 1354.83, 1305.61, 1253.48 cm^{-1}, C-F stretch: 1199.31, 1162.09, 1130.57, 1106.16, 1007.57, 976.34 cm^{-1}, C-H stretch (C-CH3):

2958.23, 2917.75, 2838.71, 2756.68 cm^{-1}. Anal. Calc. for C38 H26 Cu2 F12 N8: C, 48.06; H, 2.76; N, 11:80; found: C, 48.06; H, 2.72; N, 11.69. The orange solid product was checked under a handheld UV lampfor photoluminescence under Short Wave UV (λ_{ex} = 254 nm) and Long Wave UV (λ_{ex} = 365 nm). Red photoluminescence was observed under both 254 nm (medium-weak, red luminescence) and 365 nm (medium-weak, red luminescence). The orange solid product was completely soluble in acetone, acetonitrile, benzene, methanol, chloroform, and dichloromethane, and partially soluble in toluene, ethanol, cyclohexane, diethyl ether, and water.

Figure 35. Solvent-mediated synthesis of {Cu[3,5-(CF$_3$)$_2$Pz](dmp)}$_2$ powder.

2.2.6 Synthesis of Compound 7: [Cu(Lactate)(dmp)]₂· 4 Chloroform

{Cu[3,5-(CF$_3$)$_2$Pz](dmp)}$_2$ + 2 Acetone + 2 O$_2$

↓ Acetone (excess)

Diethyl ether ↓ Chloroform

[Cu(Lactate)(dmp)]$_2$· 4 Chloroform + 2 [3,5-(CF$_3$)$_2$Pz]H
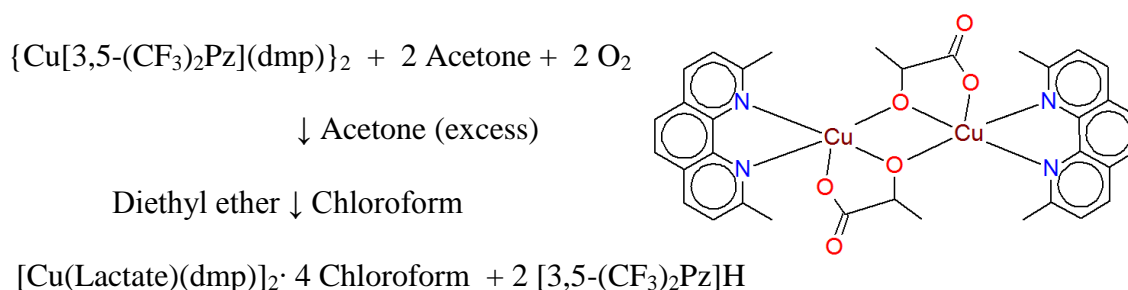
2.2.6.1 Solvent-mediated Synthesis of [Cu(Lactate)(dmp)]₂

In a glass vial, {Cu [3,5-(CF$_3$)$_2$Pz](dmp)}$_2$ (10 mg, 0.011 mmol) was mixed in 12 mL of acetone. The resulting yellow-orange solution and un-dissolved orange powder were mixed via sonication in a sonicator bath, followed by a miniRoto, until all the {Cu[3,5-(CF$_3$)$_2$Pz](dmp)}$_2$ completely dissolved in acetone, resulting in a clear, red-orange solution. Afterward, the vial, containing the resulting orange solution, was loosely capped, and the vial was stored in a fume hood for one week in order to allow the solvent to completely evaporate. After the solvent completely evaporated, the resulting brown-ish red solid (dry crystals) was re-dissolved using 10 mL of chloroform (mixed via sonication in a sonicator bath), and ~2.5 mL of the resulting orange solution was filtered (via pasture pipette with cotton) into four clean, small, glass vials, respectively. The small, glass vials (inner vials containing the filtered solution) were lowered into four clean, large, glass vials (outer vials), and ~2.5 mL of diethyl ether were added to the outer vials. The outer vials were tightly capped and wrapped with parafilm, and the resulting vial-to-vial (vapor diffusion) crystallization setups were stored in a cabinet (undisturbed)

for 25 days in order to allow crystals to form via vapor diffusion (of diethyl ether to chloroform). After 25 days (typically requires one week into the 25 days), several, small, green single crystals (X-ray quality crystals) formed out of solution. Mp: 150-190°C (loss of green physical color with shrinkage), 194.2-196.7°C (melting with w/ dec). IR: =C-H stretch (aromatic): 3061.44, 852.73, 773.62, 730.83 cm^{-1}, C=C stretch (aromatic): 1592.97 cm^{-1}, C=N stretch (aromatic): 1566.63, 1503.06 cm^{-1}, C-C stretch (aromatic): 1428.46 cm^{-1}, C-N stretch (aromatic): 1305.18, 1272.16 cm^{-1}, C-H stretch (C-CH3): 2961.71, 2920.21, 2858.86, 2796.64 cm^{-1}, C=O stretch (COO-): 1625.99 cm^{-1}, C-O stretch (COO-): 1357.35, 1116.80 cm^{-1}. Anal. Calc 1 for C38 H36 Cl12 Cu2 N4 O6: C, 38.12; H, 3.03; N, 4.68; found#1: C, 54.55; H, 4.08; N, 7.88; found#2: C, 50.93; H, 3.77; N, 7.53.

The green crystals are very unstable out of solution. The empirical formula from the X-ray crystallographic data shows that chloroform (C H Cl3) is present with [Cu(Lactate)(dmp)]$_2$ in a 4:1 molar ratio, which was used for the Anal. Calc. 1 (above). The empirical formula was adjusted to reflect the presence of chloroform with [Cu(Lactate)(dmp)]$_2$ in a 1:4 molar ratio. Anal. Calc. 2 for C137 H129 Cl3 Cu8 N16 O24: C, 54.88; H, 4.34; N, 7.47; found#1: C, 54.55; H, 4.08; N, 7.88; found#2: C, 50.93; H, 3.77; N, 7.53. In contrast to "found#2" data, "found#1" data were obtained for the green crystals with fewer impurities.
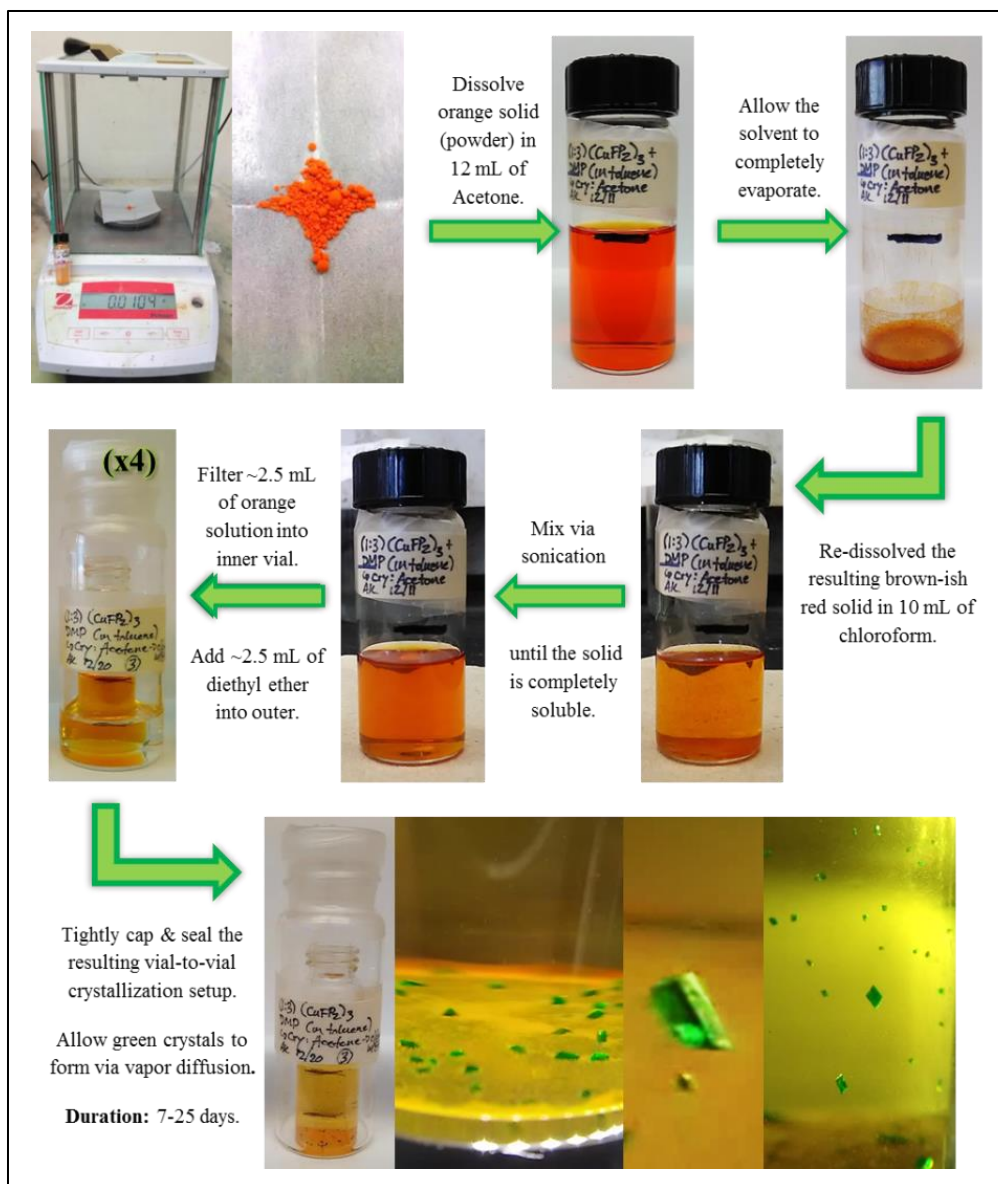
Figure 36. Crystallization of [Cu(Lactate)(dmp)]$_2$ using {Cu[3,5-(CF$_3$)$_2$Pz](dmp)}$_2$ solvent-mediated powder

2.2.7 Syntheses of Compound 6: {Ag[3,5-(CF$_3$)$_2$Pz](dmp)}$_2$

Ag$_2$O + 2 [3,5-(CF$_3$)$_2$Pz]H + 2 (dmp · 0.5 H$_2$O)
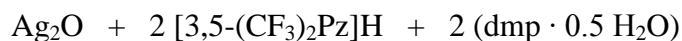
    Solvent-mediated ↓ Solventless
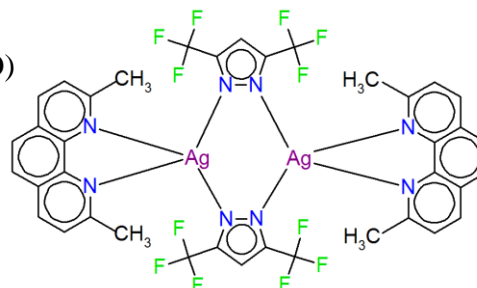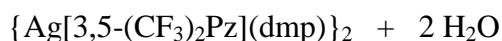
   {Ag[3,5-(CF$_3$)$_2$Pz](dmp)}$_2$ + 2 H$_2$O

2.2.7.1 Solvent-mediated Synthesis of {Ag[3,5-(CF$_3$)$_2$Pz](dmp)}$_2$

The synthesis of {[3,5-(CF$_3$)$_2$Pz]Ag}$_3$ was carried out as reported in the literature, via Schlenk technique and under constant gaseous nitrogen (N$_2$) atmosphere. [3,5-(CF$_3$)$_2$Pz]H (0.50 g, 2.45 mmol) and silver(I) oxide, Ag$_2$O, (0.31 g, 1.34 mmol) were mixed in 12 mL of toluene (bubbled with N$_2$), and subsequently heated (with constant stirring) under reflux at ~68°C for 48 hours. The resulting reaction mixture was filtered over a bed of celite (wet with toluene) in order to remove insoluble impurities. The filtrate was collected and placed under vacuum for ~2 hour in order to remove the solvent, yielding the white/colorless solid, {[3,5-(CF$_3$)$_2$Pz]Ag}$_3$.

Under constant N$_2$ atmosphere, {[3,5-(CF$_3$)$_2$Pz]Ag}$_3$ (0.1832 g, 0.1964 mmol) and dmp · 0.5 H$_2$O (0.1281 g, 0.5896 mmol) were mixed in 5.2 mL of toluene (bubbled with N$_2$). Upon adding {[3,5-(CF$_3$)$_2$Pz]Ag}$_3$ to dmp · 0.5 H$_2$O in toluene, an immediate color change was observed, from clear, colorless to cloudy/milky, white (formation of white precipitate). The resulting reaction mixture was allowed to stir for 48 hours in order to allow the starting materials to completely react. Subsequently, the resulting reaction mixture was heated (with constant stirring) under reflux at 72°C for 4 hours. After

allotting time to cool, the cloudy, white reaction mixture was filtered, collecting the white precipitate (product) on the filter. The filter product was placed under vacuum for 5.5 hours in order to completely remove the solvent, yielding the product: white/colorless, solid (yield 61%). Mp: 254.60°C (w/ dec). IR: =C-H stretch (aromatic): 3138.76, 3048.20, 847.26, 801.54, 755.15, 728.87 cm^{-1}, C=C stretch (aromatic): 1619.31, 1363.17 cm^{-1}, C=N stretch (aromatic): 1594.50, 1557.91, 1499.97 cm^{-1}, C-C stretch (aromatic): 1420.65 cm^{-1}, C-N stretch (aromatic): 1346.26, 1307.367, 1249.63 cm^{-1}, C-F stretch: 1211.85, 1164.71, 1108.25, 1001.08, 978.28 cm^{-1}, C-H stretch (C-CH3): 2919.74, 2850.71, 2754.77 cm^{-1}. Anal. Calc. for C38 H26 Ag2 F12 N8: C, 43.95; H, 2.52; N, 10.79; found: C, 43.94; H, 2.48; N, 10.69.

The white solid product was checked under a handheld UV lamp for photoluminescence under Short Wave UV (λ_{ex} = 254 nm) and Long Wave UV (λ_{ex} = 365 nm). The solid product did not exhibit photoluminescence under either 254 nm or 365 nm at room temperature. Strong, green photoluminescence was observed under 365 nm at 77K. The white solid product was completely soluble in acetone, acetonitrile, and dichloromethane.

X-ray quality crystals (physical color: colorless) were grown from a single solvent system using acetone via slow evaporation. Approximately 10 mg of the white solid product was added to a clean, glass vial. Afterward, 4 mL of acetone was measured out in a graduated cylinder and transferred to the glass vial. The resulting clear, colorless solution and the un-dissolved product were mixed via sonication in a sonicator bath until all the product completely dissolved, resulting in a clear, colorless solution. The solution

was filtered (via pasture pipette with cotton) into a clean, glass vial and was allowed to slowly evaporate. The solution was left undisturbed in order to slowly evaporate for 7 day, resulting in crystal growth. The colorless crystals were of uniform size (large) and shape. Mp: 254.6°C (w/ dec). IR: =C-H stretch (aromatic): 3138.80, 3048.41, 847.61, 801.51, 755.68, 729.15 cm^{-1}, C=C stretch (aromatic): 1619.59, 1363.38 cm^{-1}, C=N stretch (aromatic): 1594.95, 1558.11, 1499.96 cm^{-1}, C-C stretch (aromatic): 1421.06 cm^{-1}, C-N stretch (aromatic): 1346.97, 1307.67, 1250.09 cm^{-1}, C-F stretch: 1211.49, 1165.11, 1106.99, 1001.21, 978.22 cm^{-1}, C-H stretch (C-CH3): 2918.56, 2854.62, 2755.30 cm^{-1}. Anal. Calc. for C38 H26 Ag2 F12 N8: C, 43.95; H, 2.52; N, 10.79; found: C, 43.93; H, 2.45; N, 10.77.

2.2.7.2 Solventless Synthesis of {Ag[3,5-(CF$_3$)$_2$Pz](dmp)}$_2$

A solventless synthesis of {Ag[3,5-(CF$_3$)$_2$Pz](dmp)}$_2$ was attempted via mechanically grinding with heat; however, the progress of the reaction was difficult to monitor via either a change in physical color or the disappearance/appearance of photoluminescence (checked using a handheld UV lamp). The resulting powder was white (same as starting materials) in physical color and did not exhibit photoluminescence under Short Wave UV (λ_{ex} = 254 nm) nor Long Wave UV (λ_{ex} = 365 nm).

2.2.8 Synthesis of Compound 8: {Cu₃[3,5-(CF₃)₂Pz]₄(ACN)(OH)₂}₂ · ACN

$$6 \text{ CuI } + 12 \text{ [3,5-(CF}_3\text{)}_2\text{Pz]H } +$$

$$3 \text{ ACN } + 2 \text{ O}_2$$

$$\downarrow \text{ ACN } (excess)$$

$$\{Cu_3[3,5\text{-}(CF_3)_2Pz]_4(ACN)(OH)_2\}_2 \cdot ACN +$$

$$4 \text{ [3,5-(CF}_3\text{)}_2\text{Pz]H } (excess) + 3 \text{ I}_2 + 2 \text{ H}_2$$
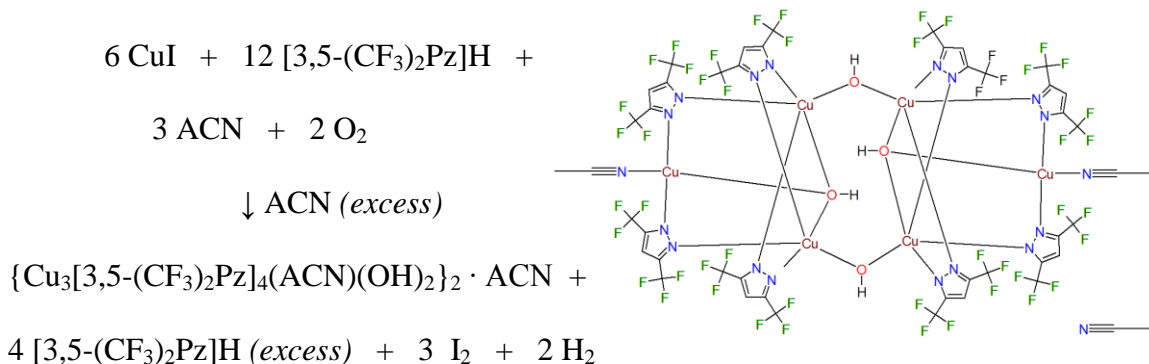
2.2.8.1 Solvent-mediated Synthesis of {Cu₃[3,5-(CF₃)₂Pz]₄(ACN)(OH)₂}₂ · ACN

In a glass vial, CuI (0.0998 g CuI, 0.5214 mmol) and [3,5-(CF₃)₂Pz]H (0.2129 g, 1.043 mmol) were mixed in 8 mL of acetonitrile (ACN). With regard to previous observations, upon adding CuI to [3,5-(CF₃)₂Pz]H in ACN, an immediate change was observed, from a clear, colorless solution to a clear, pale yellow solution. The resulting solution was mixed via sonication in a sonicator bath until all the CuI and [3,5-(CF₃)₂Pz]H completely dissolved in ACN, resulting in the clear, pale yellow solution. The resulting solution was filtered into a clean, glass vial. The vial was stored in a drawer and was left undisturbed for ~2.5 months. The vial was checked daily, observing for a change in the physical color of the solution, as well as for precipitation, if any. Within ~1.5 months, the change in the physical color of the solution was observed, from pale yellow, to yellow, to orange, to brown, to dark brown/black, respectively. The solution became dark brown/black in color after ~40 days. No precipitation was observed during the aforementioned duration. The vial containing the solution was stored in a drawer and

was left standing (undisturbed) for an additional month in order to allow for crystal growth. X-ray quality crystals (physical color: dark blue) were grown from the clear, dark brown/black solution after ~2.5 month (total duration) and eventually collected via gravity filtration (yield 39%). Mp: 40.00-283.01°C (partial loss of blue physical color), 283.01°C (complete loss of blue color w/ shrinkage), ~300°C (melting w/ decomposition). IR: =C-H stretch (aromatic): 3151.52, 815.41, 760.25, 736.44, 717.24 cm^{-1}, C=C stretch (aromatic): 1632.92 cm^{-1}, C=N stretch (aromatic): 1537.63, 1502.78 cm^{-1}, C-C stretch (aromatic): 1449.79 cm^{-1}, C-N stretch (aromatic): 1365.02, 1258.07 cm^{-1}, C-F stretch: 1224.20, 1118.88, 1021.90 cm^{-1}, O-H stretch: 3648.82 cm^{-1}, C-H stretch (C-CH3): 2940.38 cm^{-1}, C≡N stretch: 2328.51, 2301.96, 2257.80 cm^{-1}. Anal. Calc. for C46 H21 Cu6 F48 N19 O4: C, 25.13; H, 0.96; N, 12.11; found: C, 25.44; H, 1.21; N, 12.79.

An acetonitrile molecule (C2 H3 N) is present in the unit cell of the crystal structure and is included in the empirical formula of the Cu(II) blue crystal product. The synthesis for the Cu(II) blue crystals were reproduced multiple times, thus allowing for the approximations of the durations for the aforementioned observations: the change in the physical color of the solution and the growth of the crystals.
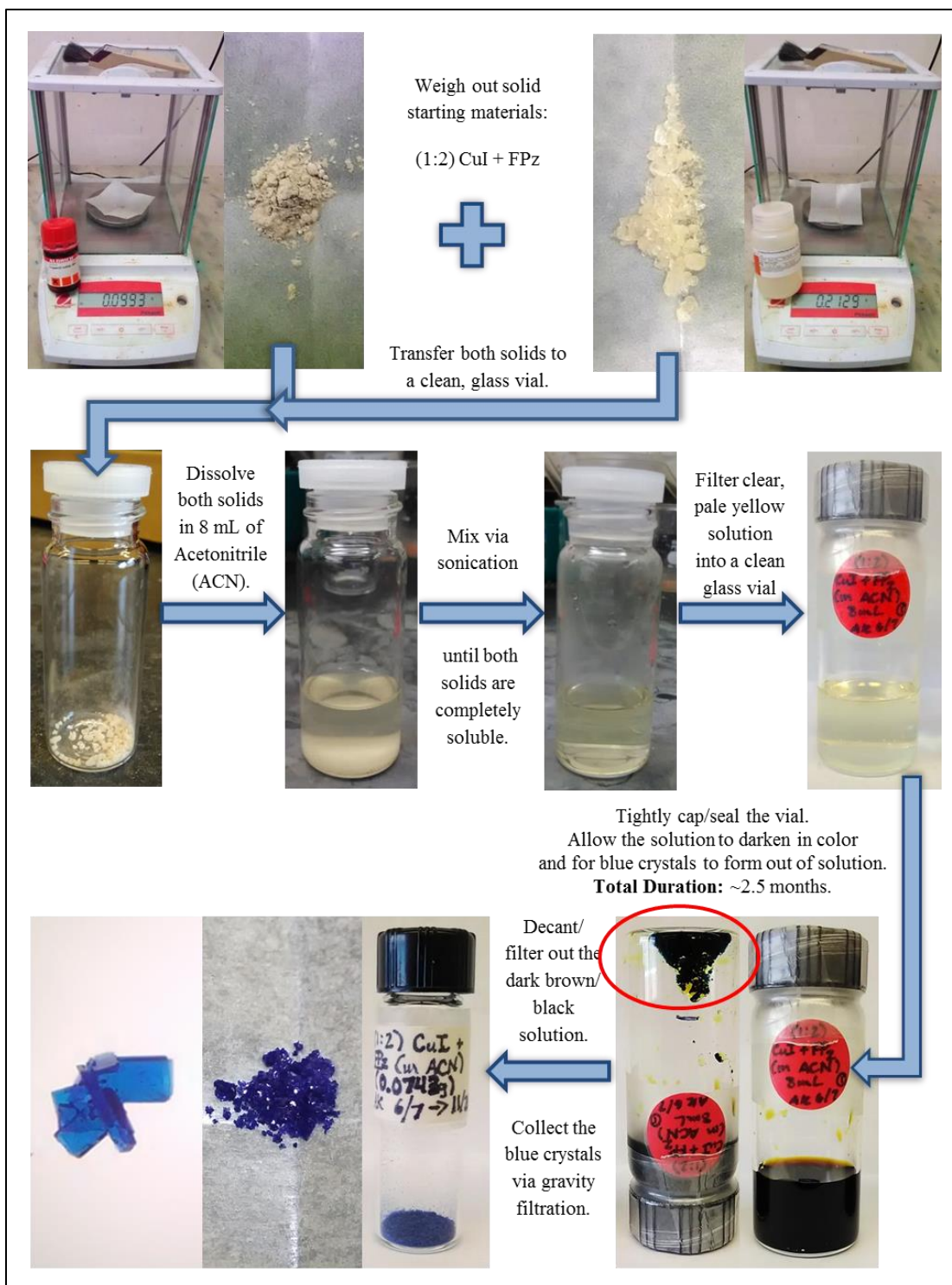
Figure 37. Solvent-mediated synthesis of $\{Cu_3[3,5\text{-}(CF_3)_2Pz]_4(ACN)(OH)_2\}_2 \cdot ACN$ blue crystals.

2.2.8.2 Solvent-mediated Syntheses of (1:1), (1:1.5), and (1:2) CuI + FPzH (in ACN)

Solvent-mediated syntheses for Cu(I) product were attempted multiple times using the same starting materials: CuI, [3,5-(CF$_3$)$_2$Pz]H, and ACN, using Schlenk technique, with and without heating, and while varying the molar ratios of Cu(I) to [3,5-(CF$_3$)$_2$Pz]H: (1:1), (1:1.5), and (1:2). Upon adding CuI to [3,5-(CF$_3$)$_2$Pz]H in ACN, an immediate change was observed, from a clear, colorless solution to a clear, pale yellow solution. The reaction mixture was typically allowed to stir for 2-4 hours under room temperature, resulting in a clear, yellow solution. Afterward, the solvent was removed under vaccum, yielding in a lavender colored powder (solid) with no luminesence. The resulting powder was washed with diethyl ether in order to remove excess ligand. FT-IR spectra were obtained before and after the aformentioned diethyl ether washes, resulting in the complete loss of the [3,5-(CF$_3$)$_2$Pz]H ligand (a lack of peaks associated with the ligand) following the washes.

Solvent-mediated syntheses for the 1:1 molar ratio of Cu(I) to [3,5-(CF$_3$)$_2$Pz]H were repeated in a similar manner, however, with heating under reflux at 60°C. After stiring for 0.5 hours, an off-white precipitate formed out of the yellow solution, which resulted in the precipitation of fine, off-white crystalline. The crystalline precipitate was collected and washed with diethyl ether. The FT-IR spectrum for the washed crystalline was obtained, revealing the complete absence of the [3,5-(CF$_3$)$_2$Pz]H ligand. The same solvent-mediated synthesis with heat was preformed, however, allowing the mixture to stir for one week. After three days, a change in the physical color of the solution was observed from clear, yellow to clear, green-brown.

A solvent-mediated synthesis at room temperature for the 1:1 molar ratio of Cu(I) to [3,5-(CF$_3$)$_2$Pz]H was performed, allowing the reaction mixture to stir for 5 weeks until the reaction mixture became orange in color. Afterward the solvent was removed under vaccum, resulting in a lavender colored powder (solid) with strong, orange photoluminescence under Short Wave UV (254 nm). A small amount of the luminescent solid was placed on a glass slide and a few drops of diethyl ether was added onto the solid, washing off the orange luminescence. On the same glass slide, another small amount of the luminescent solid was added and was allowed to sit on a lab bench/counter for one week undistrubed, resulting in the loss of the orange luminescence.

2.2.8.3 Solventless Synthesis of (1:1) CuI + FPzH

A solventless synthesis of the 1:1 molar ratio of Cu(I) to [3,5-(CF$_3$)$_2$Pz]H was attempted via mechanically grinding with heat (up to 50°C); however, the [3,5-(CF$_3$)$_2$Pz]H completely sublimed, leaving behind only CuI. The progress of the reaction was difficult to monitor via the disappearance/appearance of photoluminescence (checked using a handheld UV lamp). The resulting powder was tan (same as the CuI starting materials) in physical color and did not exhibit photoluminescence under Short Wave UV (λex = 254 nm) nor Long Wave UV (λex = 365 nm). Upon further heating, the CuI exhibited weak, red photoluminescence under Short Wave UV (λex = 254 nm) and Long Wave UV (λex = 365 nm).

2.2.9 Synthesis of Compound 9: {[CuI(PVP)] · 1.5 H_2O}_∞

CuI + 4 (PVP)_n (single VP units) + 1.5 H_2O

ACN ↓ DCM
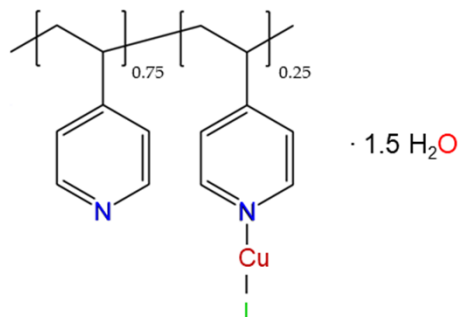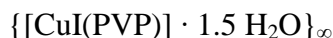
{[CuI(PVP)] · 1.5 H_2O}_∞

2.2.9.1 Solvent-mediated Synthesis of {[CuI(PVP)] · 1.5 H_2O}_∞

Under constant N_2 atmosphere, CuI (0.1000 g, 0.5251 mmol) was dissolved in 5 mL of ACN (bubbled with N_2). In a small glass vial, PVP (0.0555 g, 0.567 mmol) was dissolved in 4 mL of DCM (bubbled with N_2). Using a disposable pasture pipette, the solution of PVP in DCM was transferred to the solution of CuI in ACN, resulting in an immediate color change, from clear, pale yellow and colorless solutions to cloudy/milky, pale yellow (formation of pale yellow precipitate). The resulting reaction mixture was allowed to stir for 24 hours in order to allow the starting materials to completely react. Afterward, additional PVP (0.1605 g, 1.527 mmol) was added to the reaction mixture, resulting in an immediate color change from pale yellow to yellow (more yellow in color). The resulting reaction mixture was allowed to stir for another 24 hours in order to allow the starting material to completely react. The yellow reaction mixture was filtered, collecting the yellow precipitate (product) on the filter. Furthermore, the yellow filter product was washed with several 1 mL portions of both ACN and DCM for excess CuI and/or PVP. The filter product was placed under vacuum for 2.5 hours in order to completely remove traces of solvent, yielding the dry product: yellow, solid (yield 66%).

Mp: 40.00-235°C (loss/removal of water), 235-270°C (change in color from yellow to brown), 275-290°C (dec.). IR: =C-H stretch (aromatic): 3027.00, 821.61 cm^{-1}, C=C stretch (aromatic): 1651.56 cm^{-1}, C=N stretch (aromatic): 1598.29, 1556.87, 1494.93 cm^{-1}, C-C stretch (aromatic): 1416.45 cm^{-1}, C-N stretch (aromatic): 1220.23 cm^{-1}, C-H stretch (alkyl sp3): 2925.17, 2855.61 cm^{-1}, O-H stretch: 3377.12 cm^{-1}. Anal. Calc. for C56 H62 Cu2 I2 N8 O3 (MW = 1276.05 g/mol): C, 52.71; H, 4.90; N, 8.78; N, 8.78; found: C, 52.76; H, 4.98; N, 8.82.

The yellow, solid product was checked under a handheld UV lamp for photoluminescence under Short Wave UV (λ_{ex} = 254 nm) and Long Wave UV (λ_{ex} = 365 nm). Yellow photoluminescence was observed under 254 nm (medium-strong yellow luminescence) and 365 nm (strong, yellow luminescence). The yellow, solid product was partially soluble in pyridine.

CHAPTER III

CHARACTERIZATION OF STRUCTURAL, PHYSICAL AND PHOTOPHYSICAL
PROPERTIES FOR MIXED-LIGAND COPPER(I/II) AND SILVER(I) COMPLEXES
AND METALLOPOLYMERS WITH PYRAZOLATE- AND PHENANTHROLINE-
BASED LIGANDS AND POLY(4-VINYL PYRIDINE)

This chapter will focus on the characterization of the various copper(I/II) and silver(I) complexes and metallopolymers with regard to their structural, physical, and photophysical properties. Section 3.1: *Methods of Characterizations,* describes the various analytical instrumentations utilized in obtaining experimental data pertaining to the aforementioned properties, as well as their respective experimental parameters. Section 3.2: *Results and Discussion,* examines the experimental data and discusses the structural, physical, and photophysical properties in detail with regard to each respective metal-ligand system.

3.1 Methods of Characterizations

All products were thoroughly characterized with regard to their structural, physical, and photophysical properties using: single crystal X-ray diffraction, elemental analysis, FT-IR spectroscopy, thermogravimetric analysis (TGA), photoluminescence (PL) spectroscopy, and UV-Vis absorption spectroscopy.

3.1.1 X-ray Crystallographic Data

Single crystal X-ray diffraction experiments were performed by UNT's crystallographer, Dr. Vladimir Nesterov. Crystal structure determinations for compounds 1−8 were carried out using a Bruker SMART APEX2 CCD-based X-ray diffractometer equipped with a low temperature device and Mo-target X-ray tube (wavelength = 0.71073 Å). Some follow-up/verification measurements were carried out on a more recently-commissioned Rigaku XtaLAB Synergy-S Diffractometer equipped with dual Mo and Cu PhotonJet-S microfocus X-ray sources, a HyPix-6000HE Hybrid Photon Counting detector, and an Oxford Cryostream 800 liquid nitrogen cooling system. For compounds 1-7, measurements were taken at 100(10) K. For compound 8, measurements were taken at 275(30) K. Data collection, indexing, and initial cell refinements were carried out using APEX2, and frame integration and final cell refinements were done using SAINT. An absorption correction was applied using the program SADABS. All non-hydrogen atoms were refined anisotropically. The hydrogen atoms were placed in idealized positions and were refined as riding atoms. Structure solution, refinement, graphic and generation of publication materials were performed by using SHELXTL software.

3.1.2 Elemental Analysis Data

CHN elemental analysis was performed using a PerkinElmer 2400 Series II CHNS/O Elemental Analyzer.

3.1.3 FT-IR Spectroscopy

Infrared (IR) spectra were recorded using a Thermo Scientific Nicolet iS50 Fourier-Transform Infrared (FTIR) spectrometer with a built-in diamond ATR and/or a Thermo Scientific Nicolet 380 FTIR spectrometer with a SMART iTX Accessory.

3.1.4 Thermogravimetric analysis (TGA)

Thermogravimetric analysis (TGA) was performed using a TA Instruments Q500 TGA analyzer, heating at a ramp rate of 2°C/min. TGA data were analyzed using TA Instruments Universal Analysis 2000 (Version 4.5A) software. Melting point data were obtained using: a digital Optimelt, heating at a ramp rate of 2°C/min, and/or a TA Instruments DSC Q20 Differential Scanning Calorimeter (DSC), heating at a ramp rate of 10°C/min. DSC data were analyzed using TA Instruments Universal Analysis 2000 (Version 4.5A) software.

3.1.5 Spectroscopic Measurements

UV-Visible (UV-Vis) absorption spectra were recorded using a Thermo Scientific Evolution 300 UV-Vis spectrophotometer, equipped with a xenon lamp. All scans were performed using a bandwidth of 1.0 nm. Steady-state photoluminescence spectra were acquired with a PTI QuantaMaster model QM-3/2006SE scanning spectrofluorometer, equipped with: a 75-W xenon lamp, emission and excitation monochromators, excitation correction unit, and a photomultiplier tube (PMT) detector. The emission spectra were corrected for the detector wavelength-dependent response. The excitation spectra were

also corrected for the wavelength-dependent lamp intensity. Lifetime data were acquired using a high speed pulsed xenon lamp source interfaced to the PTI instrument along with an autocalibrated "QuadraScopic" monochromator for excitation wavelength selection.

3.2 Results and Discussion

3.2.1 Compound 1: {Cu$_2$[3,5-(CF$_3$)$_2$Pz]$_2$(4,7-phen)}$_2$

3.2.1.1 X-ray Crystallographic Data

In this section, the X-ray crystallographic data for {Cu$_2$[3,5-(CF$_3$)$_2$Pz]$_2$(4,7-phen)}$_2$ (see Tables 1A-B) are discussed. {Cu$_2$[3,5-(CF$_3$)$_2$Pz]$_2$(4,7-phen)}$_2$ single crystals were obtained using solvent-mediated powder. Table 1A shows that {Cu$_2$[3,5-(CF$_3$)$_2$Pz]$_2$(4,7-phen)}$_2$ crystallizes in the triclinic crystal system with the space group P-1 with Z = 1 and the unit cell dimensions: a = 8.2838(6) Å, b = 12.8010(7) Å, c = 13.3054(8) Å, α = 113.533(5)°, β = 99.037(5)°, and γ = 102.948(5)°. {Cu$_2$[3,5-(CF$_3$)$_2$Pz]$_2$(4,7-phen)}$_2$ has the empirical formula C44 H20 Cu4 F24 N12 (MW = 1426.88 g/mol).

As shown in Figure 38A, the asymmetric unit cell of {Cu$_2$[3,5-(CF$_3$)$_2$Pz]$_2$(4,7-phen)}$_2$ exhibits a Cu(I) dimer, with two Cu(I) centers: Cu1 and Cu2, respectively, doubly bridged via the two [3,5-(CF$_3$)$_2$Pz]$^-$ ligands (via N1 and N4, and via N2 and N3, respectively); moreover, the Cu(I) center, Cu2, is coordinated with the 4,7-phen ligand via N5. As shown in Figure 38B, the symmetric unit cell exhibits two Cu(I) dimers, doubly bridged via the two 4,7-phen ligands, with Cu1 coordinated with N6A, and Cu1A coordinated with N6, thereby forming a dimer-of-dimers structure. Overall, the Cu(I)

complex exhibits a heteroleptic, tetrameric structure with two pyrazolate-bridged dimers bridged via two 4,7-phen ligands.

Figure 38C shows the packing structure of $\{Cu_2[3,5\text{-}(CF_3)_2Pz]_2(4,7\text{-phen})\}_2$. The bond lengths (Å) and angles (°) are shown in Table 1B. The full-matrix least-squares refinement method was used on F^2, resulting in a goodness-of-fit value of 1.038 with R1 = 3.86 % and wR2 = 8.16% for all data.

Table 1. **(A)** X-ray Crystallographic Data for $\{Cu_2[3,5-(CF_3)_2Pz]_2(4,7\text{-phen})\}_2$; **(B)** Bond lengths [Å] and angles [°] for $\{Cu_2[3,5-(CF_3)_2Pz]_2(4,7\text{-phen})\}_2$.

Empirical formula	C44 H20 Cu4 F24 N12
Formula weight	1426.88
Temperature	100.00(10) K
Wavelength	0.71073 Å
Crystal system	Triclinic
Space group	P-1
Unit cell dimensions	a = 8.2838(6) Å α = 113.533(5)°.
	b = 12.8010(7) Å β = 99.037(5)°.
	c = 13.3054(8) Å γ = 102.948(5)°.
Volume	1211.74(14) Å3
Z	1
Density (calculated)	1.955 Mg/m3
Absorption coefficient	1.874 mm-1
F(000)	700
Crystal size	0.1 x 0.04 x 0.02 mm3
Theta range for data collection	1.829 to 27.103°.
Index ranges	-10<=h<=10, -16<=k<=15, -17<=l<=16
Reflections collected	18177
Independent reflections	5328 [R(int) = 0.0325]
Completeness to theta = 25.242°	99.90%
Absorption correction	Semi-empirical from equivalents
Max. and min. transmission	1.00000 and 0.84707
Refinement method	Full-matrix least-squares on F^2
Data / restraints / parameters	5328 / 0 / 379
Goodness-of-fit on F2	1.038
Final R indices [I>2sigma(I)]	R1 = 0.0307, wR2 = 0.0774
R indices (all data)	R1 = 0.0386, wR2 = 0.0816
Extinction coefficient	n/a
Largest diff. peak and hole	0.706 and -0.526 e.Å-3

(A)

Bond Lengths [Å] (*blue*)		&	Angles [°] (red)		
Cu(1)-N(1)	1.9553(18)	C(20)-H(20)	0.93	C(8)-C(7)-H(7)	128.4
Cu(1)-N(4)	1.9954(19)	C(20)-C(21)	1.343(3)	N(4)-C(8)-C(7)	111.2(2)
Cu(1)-N(6)#1	1.9840(18)	C(21)-H(21)	0.93	N(4)-C(8)-C(10)	120.7(2)
Cu(2)-N(2)	1.9508(18)	C(21)-C(22)	1.431(3)	C(7)-C(8)-C(10)	128.1(2)
Cu(2)-N(3)	1.9765(19)	N(1)-Cu(1)-N(4)	115.54(7)	F(7)-C(9)-F(8)	105.4(2)
Cu(2)-N(5)	1.9737(18)	N(1)-Cu(1)-N(6)#1	127.83(8)	F(7)-C(9)-C(6)	112.4(2)
F(1)-C(4)	1.337(3)	N(6)#1-Cu(1)-N(4)	116.63(8)	F(8)-C(9)-C(6)	112.7(2)
F(2)-C(4)	1.350(3)	N(2)-Cu(2)-N(3)	113.30(7)	F(9)-C(9)-F(7)	107.4(2)
F(3)-C(4)	1.342(3)	N(2)-Cu(2)-N(5)	126.45(8)	F(9)-C(9)-F(8)	107.1(2)
F(4)-C(5)	1.342(3)	N(5)-Cu(2)-N(3)	119.85(7)	F(9)-C(9)-C(6)	111.4(2)
F(5)-C(5)	1.330(3)	N(2)-N(1)-Cu(1)	119.67(14)	F(10)-C(10)-F(12)	106.3(2)
F(6)-C(5)	1.349(3)	C(1)-N(1)-Cu(1)	132.78(15)	F(10)-C(10)-C(8)	113.39(19)
F(7)-C(9)	1.339(3)	C(1)-N(1)-N(2)	106.99(17)	F(11)-C(10)-F(10)	105.58(19)
F(8)-C(9)	1.347(3)	N(1)-N(2)-Cu(2)	119.73(14)	F(11)-C(10)-F(12)	106.49(19)
F(9)-C(9)	1.329(3)	C(3)-N(2)-Cu(2)	132.72(15)	F(11)-C(10)-C(8)	113.4(2)
F(10)-C(10)	1.345(3)	C(3)-N(2)-N(1)	107.55(17)	F(12)-C(10)-C(8)	111.19(19)
F(11)-C(10)	1.341(3)	N(4)-N(3)-Cu(2)	118.99(14)	N(5)-C(11)-H(11)	118.4
F(12)-C(10)	1.345(3)	C(6)-N(3)-Cu(2)	133.56(15)	N(5)-C(11)-C(12)	123.1(2)
N(1)-N(2)	1.357(2)	C(6)-N(3)-N(4)	107.37(18)	C(12)-C(11)-H(11)	118.4
N(1)-C(1)	1.350(3)	N(3)-N(4)-Cu(1)	119.01(14)	C(11)-C(12)-H(12)	120.5
N(2)-C(3)	1.344(3)	C(8)-N(4)-Cu(1)	133.51(15)	C(13)-C(12)-C(11)	119.1(2)
N(3)-N(4)	1.364(2)	C(8)-N(4)-N(3)	107.16(18)	C(13)-C(12)-H(12)	120.5
N(3)-C(6)	1.346(3)	C(11)-N(5)-Cu(2)	121.51(15)	C(12)-C(13)-H(13)	120.2
N(4)-C(8)	1.346(3)	C(11)-N(5)-C(22)	118.26(18)	C(12)-C(13)-C(14)	119.7(2)
N(5)-C(11)	1.329(3)	C(22)-N(5)-Cu(2)	120.18(14)	C(14)-C(13)-H(13)	120.2
N(5)-C(22)	1.362(3)	C(18)-N(6)-Cu(1)#1	120.82(15)	C(13)-C(14)-C(15)	123.65(19)
N(6)-C(18)	1.338(3)	C(18)-N(6)-C(19)	117.82(18)	C(13)-C(14)-C(22)	117.5(2)
N(6)-C(19)	1.365(3)	C(19)-N(6)-Cu(1)#1	121.21(14)	C(22)-C(14)-C(15)	118.83(19)
C(1)-C(2)	1.382(3)	N(1)-C(1)-C(2)	111.47(19)	C(16)-C(15)-C(14)	123.23(19)
C(1)-C(4)	1.486(3)	N(1)-C(1)-C(4)	120.95(19)	C(16)-C(15)-C(19)	117.3(2)
C(2)-H(2)	0.93	C(2)-C(1)-C(4)	127.6(2)	C(19)-C(15)-C(14)	119.44(19)
C(2)-C(3)	1.382(3)	C(1)-C(2)-H(2)	128.7	C(15)-C(16)-H(16)	120
C(3)-C(5)	1.487(3)	C(1)-C(2)-C(3)	102.59(19)	C(17)-C(16)-C(15)	120.0(2)
C(6)-C(7)	1.381(3)	C(3)-C(2)-H(2)	128.7	C(17)-C(16)-H(16)	120
C(6)-C(9)	1.483(3)	N(2)-C(3)-C(2)	111.40(19)	C(16)-C(17)-H(17)	120.4
C(7)-H(7)	0.93	N(2)-C(3)-C(5)	119.95(19)	C(16)-C(17)-C(18)	119.2(2)
C(7)-C(8)	1.378(3)	C(2)-C(3)-C(5)	128.6(2)	C(18)-C(17)-H(17)	120.4
C(8)-C(10)	1.481(3)	F(1)-C(4)-F(2)	106.64(18)	N(6)-C(18)-C(17)	123.1(2)
C(11)-H(11)	0.93	F(1)-C(4)-F(3)	107.23(18)	N(6)-C(18)-H(18)	118.4
C(11)-C(12)	1.399(3)	F(1)-C(4)-C(1)	111.17(18)	C(17)-C(18)-H(18)	118.4
C(12)-H(12)	0.93	F(2)-C(4)-C(1)	112.75(18)	N(6)-C(19)-C(15)	122.45(19)
C(12)-C(13)	1.369(3)	F(3)-C(4)-F(2)	105.64(18)	N(6)-C(19)-C(20)	117.73(18)
C(13)-H(13)	0.93	F(3)-C(4)-C(1)	112.99(18)	C(15)-C(19)-C(20)	119.82(19)
C(13)-C(14)	1.407(3)	F(4)-C(5)-F(6)	106.28(18)	C(19)-C(20)-H(20)	119.6
C(14)-C(15)	1.449(3)	F(4)-C(5)-C(3)	111.13(18)	C(21)-C(20)-C(19)	120.84(19)
C(14)-C(22)	1.412(3)	F(5)-C(5)-F(4)	107.07(18)	C(21)-C(20)-H(20)	119.6
C(15)-C(16)	1.406(3)	F(5)-C(5)-F(6)	106.24(18)	C(20)-C(21)-H(21)	119.3
C(15)-C(19)	1.406(3)	F(5)-C(5)-C(3)	113.63(19)	C(20)-C(21)-C(22)	121.31(19)
C(16)-H(16)	0.93	F(6)-C(5)-C(3)	112.05(18)	C(22)-C(21)-H(21)	119.3

C(16)-C(17)	1.361(3)	N(3)-C(6)-C(7)	111.0(2)	N(5)-C(22)-C(14)	122.30(19)
C(17)-H(17)	0.93	N(3)-C(6)-C(9)	120.0(2)	N(5)-C(22)-C(21)	117.94(18)
C(17)-C(18)	1.389(3)	C(7)-C(6)-C(9)	129.0(2)	C(14)-C(22)-C(21)	119.76(19)
C(18)-H(18)	0.93	C(6)-C(7)-H(7)	128.4		
C(19)-C(20)	1.433(3)	C(8)-C(7)-C(6)	103.2(2)		
Symmetry transformations used to generate equivalent atoms:					
#1 -x+1,-y+1,-z+1					

(B)
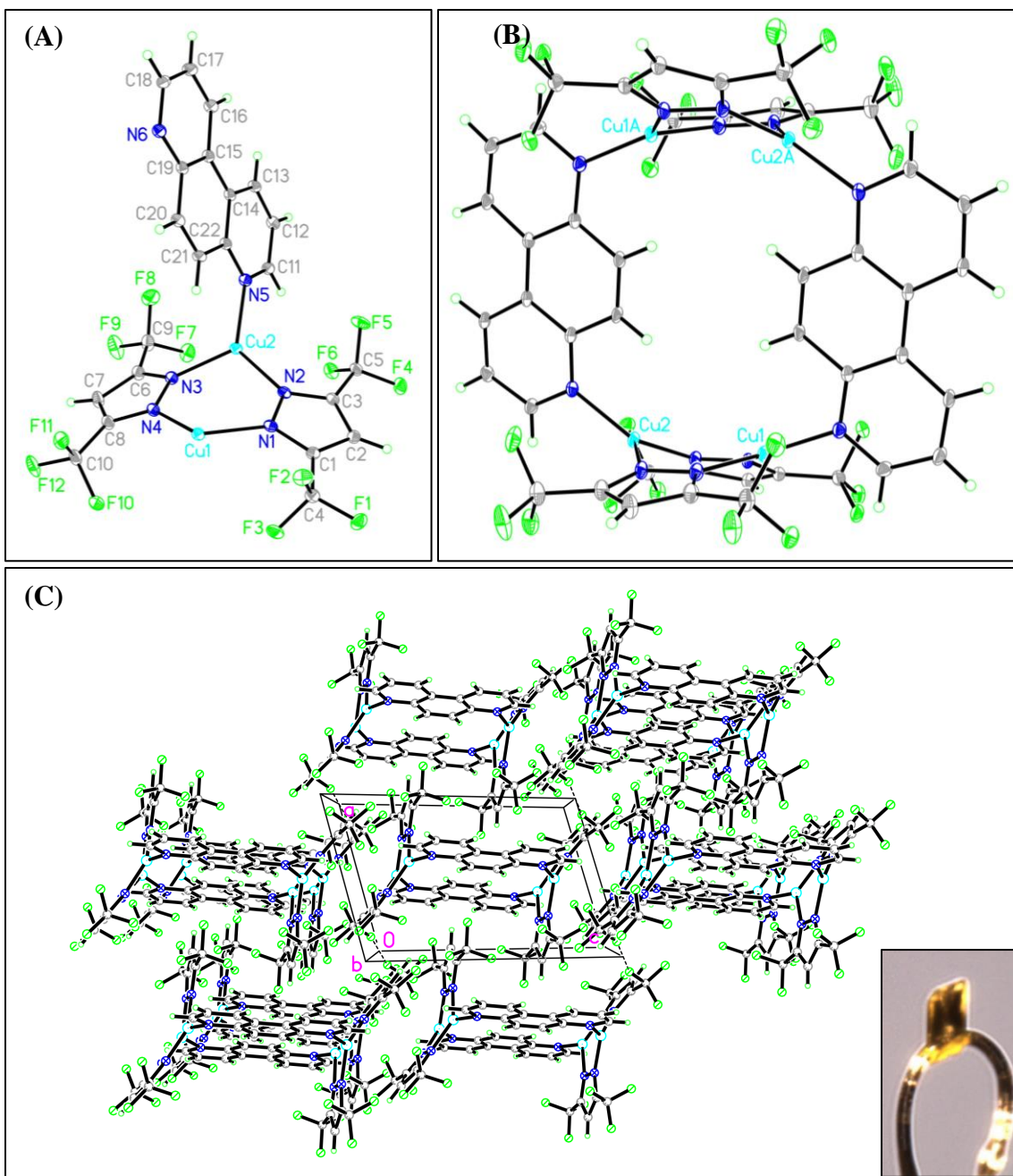
Figure 38. Crystal Structure of {Cu$_2$[3,5-(CF$_3$)$_2$Pz]$_2$(4,7-phen)}$_2$: **(A)** Asymmetric Unit Cell, **(B)** Symmetric Unit Cell, and **(C)** Packing.

3.2.1.2 Elemental Analysis Data

In this section, the elemental analysis data are discussed, comparing the experimentally found data with the theoretical Anal. Calc., shown in Table 2. The theoretical percentages of carbon (C), hydrogen (H), and nitrogen (N) were analytically calculated (Anal. Calc.) based on the empirical formula C44 H20 Cu4 F24 N12 (MW = 1426.88 g/mol): C, 37.04; H, 1.41; N, 11.78. The experimentally found data for solvent-mediated (C, 37.37; H, 1.46; N, 11.57) and solventless powder (C, 36.98; H, 1.41; N, 11.45) are similar to one another and match with the theoretical Anal. Calc. within ±0.3 for C, H, and N. This comparison confirms that same $\{Cu_2[3,5\text{-}(CF_3)_2Pz]_2(4,7\text{-phen})\}_2$ product was synthesize via both solvent-mediated and solventless syntheses. The experimentally found data for crystals (C, 37.37; H, 1.46; N, 11.57) relatively match that of the theoretical Anal. Calc. within ±0.76 for C, ±0.01 for H, and ±0.60 for N.

Table 2. Elemental analysis data for {$Cu_2[3,5-(CF_3)_2Pz]_2(4,7-phen)$}$_2$ solvent-mediated powder, solventless powder, and crystals: theoretical Anal. Calc. versus experimentally found data.

Elemental Analysis				
{$Cu_2[3,5-(CF_3)_2Pz]_2(4,7-phen)$}$_2$ = C44 H20 Cu4 F24 N12				
		Solvent-Mediated Powder	Solventless Powder	Crystals
Element	Theoretical Anal. Calc.	Experimentally Found	Experimentally Found	Experimentally Found
C	37.04%	37.37%	36.98%	36.28%
H	1.41%	1.46%	1.41%	1.42%
N	11.78%	11.57%	11.45%	11.18%
Cu	17.81%			

3.2.1.3 Characterization using FT-IR Spectroscopy

In this section, the IR spectra for{$Cu_2[3,5-(CF_3)_2Pz]_2(4,7-phen)$}$_2$ solvent-mediated powder, solventless powder, and crystals, as shown in Figure 39, are discussed. The IR spectra for solvent-mediated powder, solventless powder, and crystals are relatively identical to one another and feature the functional groups characteristic of both the [3,5-(CF_3)_2Pz]^- and 4,7-phen ligands: =C-H stretch (aromatic), C=C stretch (aromatic), C=N stretch (aromatic), C-C stretch (aromatic), C-N stretch (aromatic), and C-F stretch.
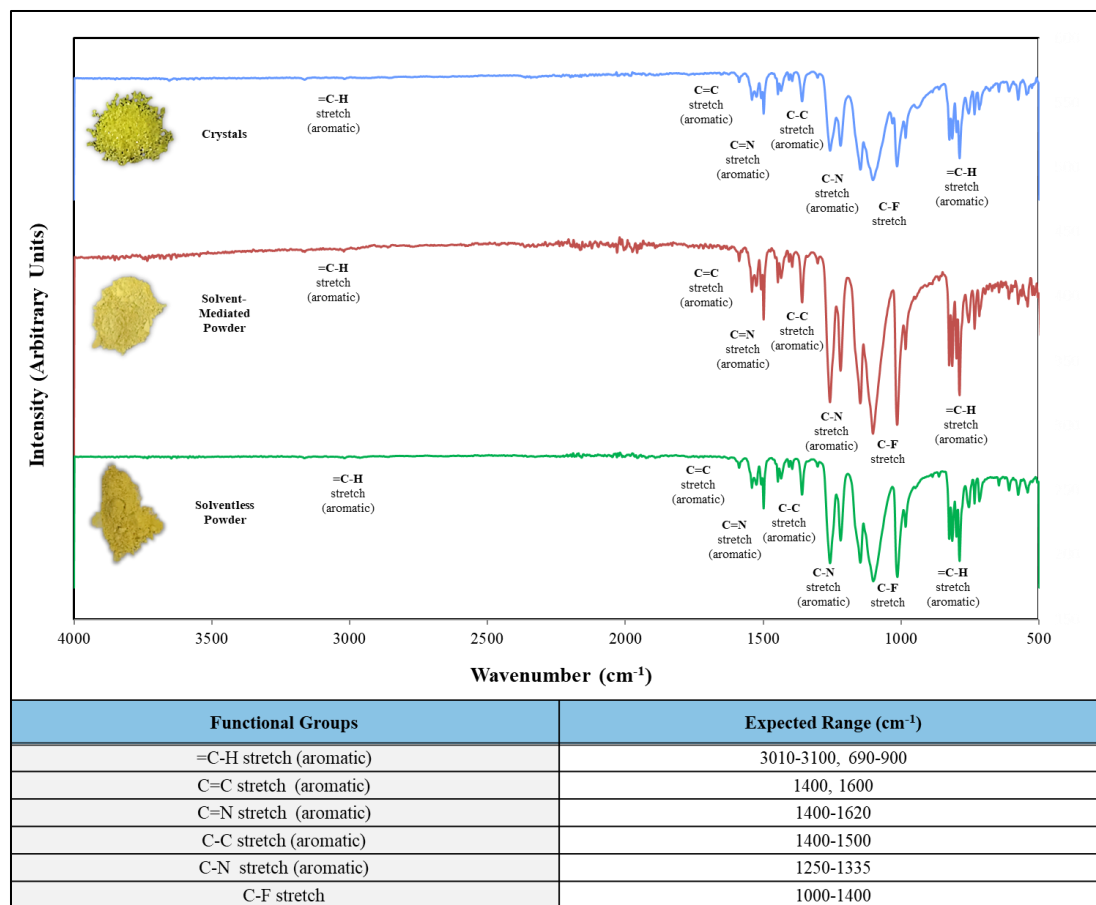
Figure 39. Stacked FT-IR spectra for $\{Cu_2[3,5\text{-}(CF_3)_2Pz]_2(4,7\text{-phen})\}_2$ crystals (*top*), solvent-mediated powder (*middle*), solventless powder (*bottom*).

3.2.1.4 Characterization using TGA Analyses

In this section, the TGA analyses for $\{Cu_2[3,5\text{-}(CF_3)_2Pz]_2(4,7\text{-phen})\}_2$ solvent-mediated powder, solventless powder, and crystals, as shown in Figures 40-42, are discussed. The TGA analyses of solvent-mediated powder, solventless powder, and crystals are relatively similar to one another with regard to percent weight loss, onset temperature, and inflection points. The solvent-mediated powder, solventless powder, and crystals, respectively, show a significant weight loss of 95.44%, 98.02%, and

96.49%, respectively, with onset temperatures (the temperatures at which weight loss begins) of 228.76°C, 227.98°C, and 222.64°C, respectively. Furthermore, the 1st derivative peaks show the greatest rate of change on the weight loss curves at 254.25°C, 254.96°C, and 256.04°C, respectively.

With regard to the emperical formula C44 H20 Cu4 F24 N12 (MW = 1426.88 g/mol), the theoretical percentage of copper is 17.81%; however, weight loss of 95.44%. 98.02%, and 96.49% was observed, which was primarily due to the sublimation of the $[3,5-(CF_3)_2Pz]^-$ and 4,7-phen ligands (total theoretical percentage of C, H, N and F of 82.19%). The remaining weight following the aforementioned weight loss should theoretically be the remaining copper.

The differences in onset/offset temperatures and 1st derivative peaks may be attributed to the differences in sample weights for the solvent-mediated powder, solventless powder, and crystals: 6.8800 mg, 9.2810 mg, and 4.7810 mg, respectively.
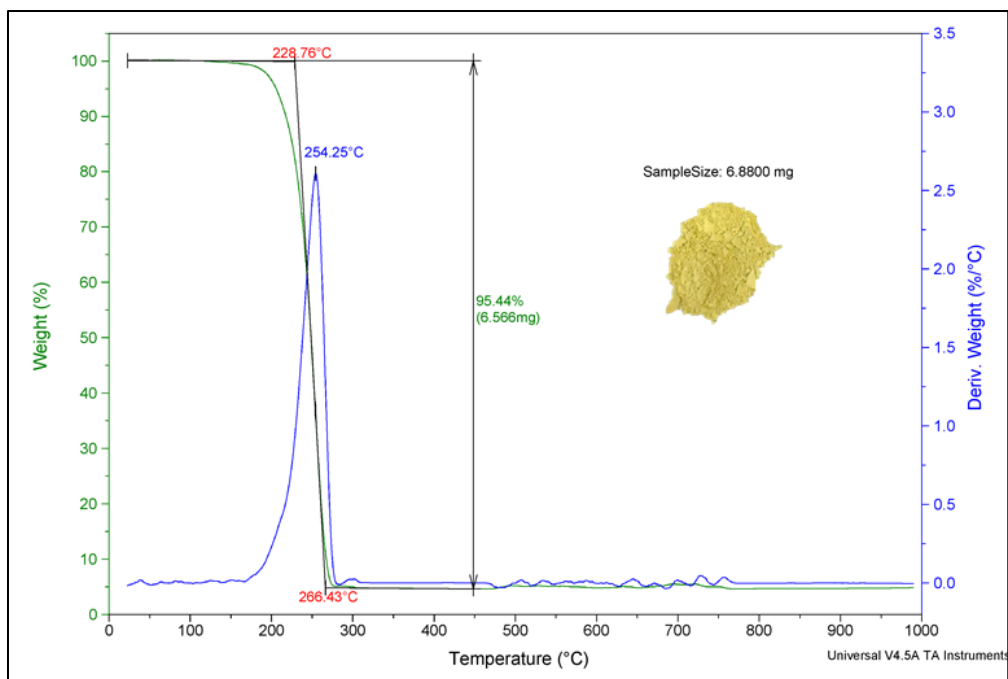
Figure 40. TGA analysis for {Cu$_2$[3,5-(CF$_3$)$_2$Pz]$_2$(4,7-phen)}$_2$ solvent-mediated powder.
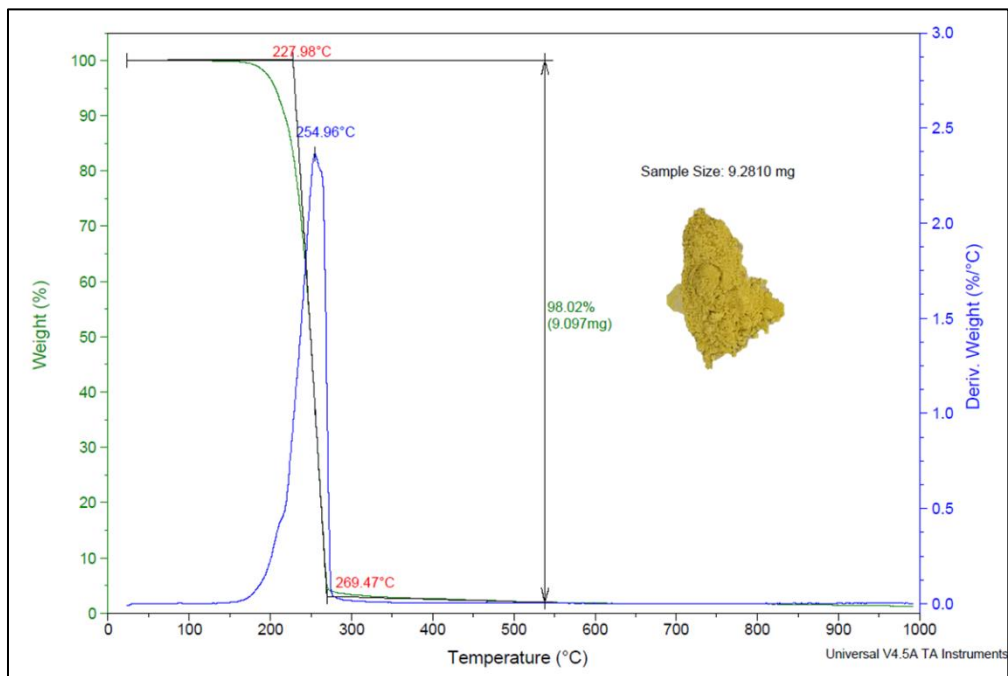
Figure 41. TGA analysis for {Cu$_2$[3,5-(CF$_3$)$_2$Pz]$_2$(4,7-phen)}$_2$ solventless powder.
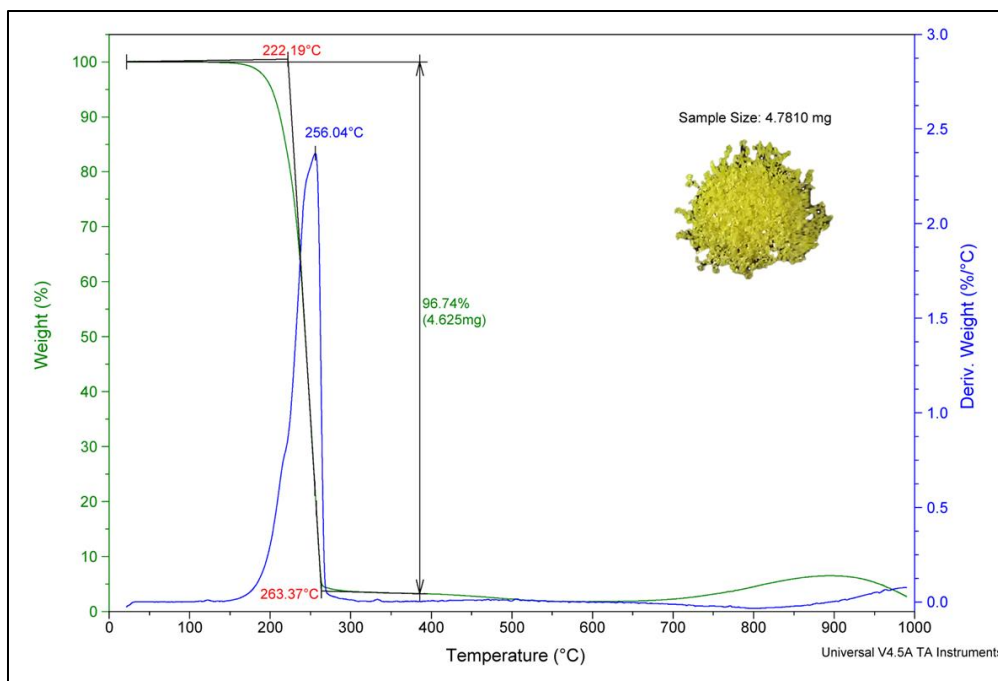
Figure 42. TGA analysis for $\{Cu_2[3,5-(CF_3)_2Pz]_2(4,7\text{-phen})\}_2$ crystals.

3.2.1.5 Characterization using Photoluminescence and UV-Vis Absorption Spectroscopy

In this section, the photoluminescence and UV-Vis absorption spectroscopy of $\{Cu_2[3,5-(CF_3)_2Pz]_2(4,7\text{-phen})\}_2$ solvent-mediated powder are discussed.

The solvent-mediated powder was transfered to a clean, quartz tube, and its photoluminescence was checked under a handheld UV lamp under Short Wave UV ($\lambda_{ex} = 254$ nm) and Long Wave UV ($\lambda_{ex} = 365$ nm), at room temperature (RT) and cryogenic temperature (77K). As shown in Figures 43 and 44 at RT, a yellow luminescence was observed under 254 nm (medium-weak, yellow luminescence) and 365 nm (medium-strong, yellow luminescence); meanwhile, at 77K, the yellow luminescence became

significantly more intense (more bright) under 254 nm (strong, yellow luminescence) and 365 nm (very strong, yellow luminescence).

As shown in Figures 45 and 46, at RT, the photoluminescence of the $\{Cu_2[3,5\text{-}(CF_3)_2Pz]_2(4,7\text{-}phen)\}_2$ solvent-mediated powder (suspended in cyclohexane) was measured using an excitation wavelength of $\lambda_{ex} = 348$ nm, producing an emission band with a maximum emission peak at $\lambda_{em} = 565$ nm. A photoluminescence decay curve for the emission at $\lambda_{em} = 565$ nm was fitted with a Chi2 value of 1.027, a Durbin Watson value of 1.254, and a Z value of -0.1198. The photoluminescence observed at RT is characterized as phosphorescence (10^{-5} s to 10 s) based on the lifetime (τ) of 54.36 μs.

As shown in Figures 45-47, at 77K, the photoluminescence of the $\{Cu_2[3,5\text{-}(CF_3)_2Pz]_2(4,7\text{-}phen)\}_2$ solvent-mediated powder (solid) was measured using an excitation wavelength of $\lambda_{ex} = 318$ nm, producing an emission band with a maximum emission peak at $\lambda_{em} = 567$ nm. A photoluminescence decay curve for the emission at $\lambda_{em} = 565$ nm was fitted with a Chi2 value of 1.085, a Durbin Watson value of 1.624, and a Z value of -0.007597. The photoluminescence observed at 77 K is characterized as phosphorescence (10^{-5} s to 10 s) based on the lifetimes (τ) of 93.67 μs.
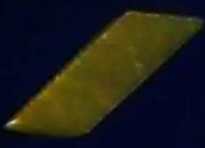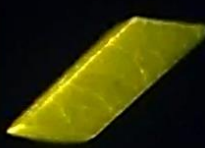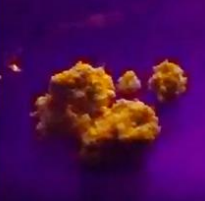
	Physical Color	254 nm	365 nm
Crystals			
Solvent-mediated Powder			
Solventless Powder			

Figure 43. Photoluminescence of {Cu$_2$[3,5-(CF$_3$)$_2$Pz]$_2$(4,7-phen)}$_2$ crystals (*top*), solvent-mediated powder (*middle*), and solventless powder (*bottom*) under Short Wave UV (λ_{ex} = 254 nm) and Long Wave UV (λ_{ex} = 365 nm), at room temperature (RT).
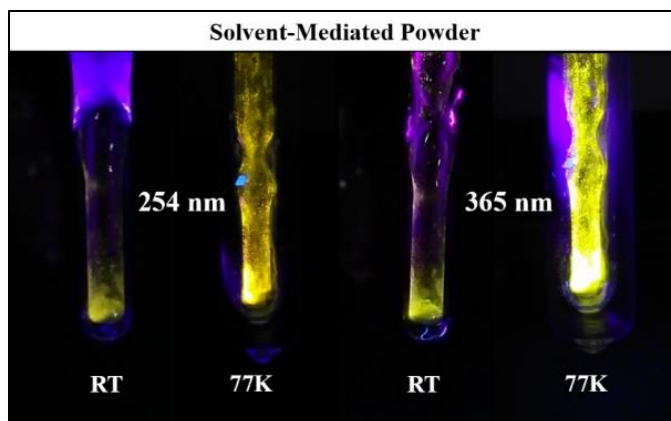
Figure 44. Photoluminescence of $\{Cu_2[3,5\text{-}(CF_3)_2Pz]_2(4,7\text{-phen})\}_2$ solvent-mediated powder in a quartz tube under Short Wave UV (λ_{ex} = 254 nm) and Long Wave UV (λ_{ex} = 365 nm), at room temperature (RT) vs. cryogenic temperature (77K).
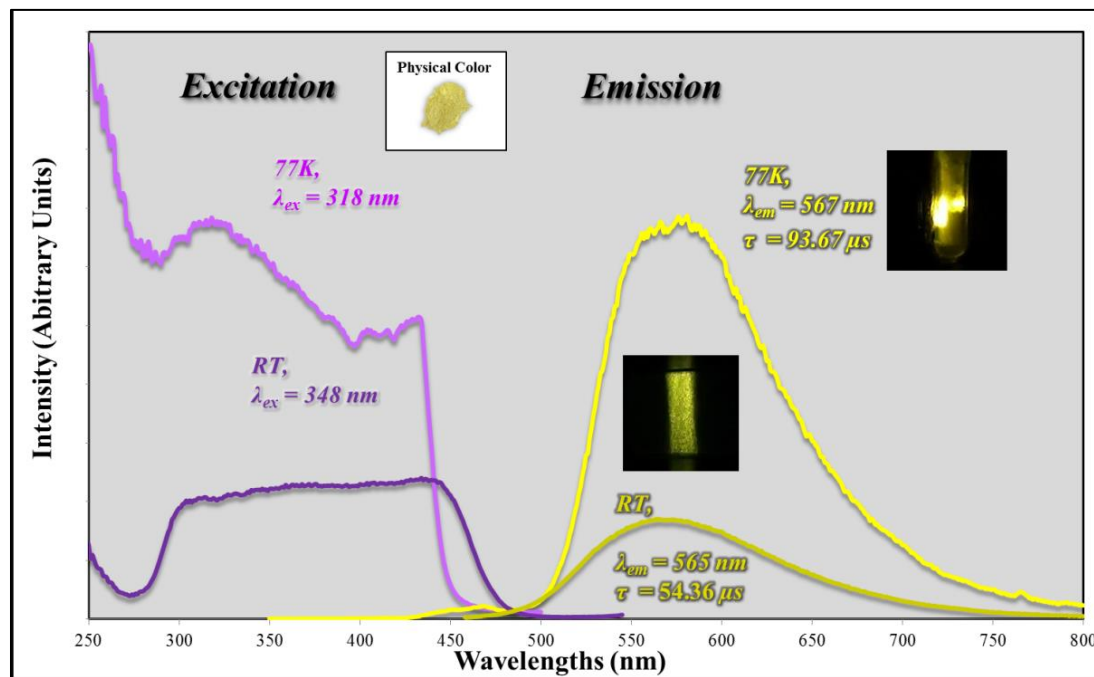
Figure 45. Photoluminescence spectra for $\{Cu_2[3,5\text{-}(CF_3)_2Pz]_2(4,7\text{-phen})\}_2$ solvent-mediated powder, at room temperature (RT) vs. cryogenic temperature (77K).
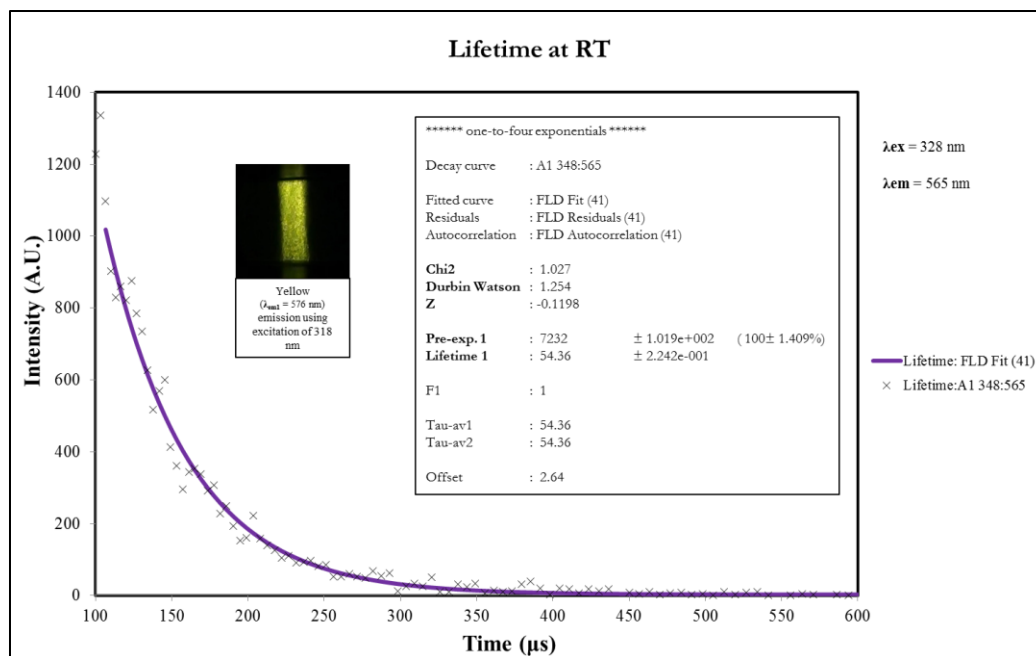
Figure 46. Photoluminescence Lifetime decay curve for $\{Cu_2[3,5\text{-}(CF_3)_2Pz]_2(4,7\text{-phen})\}_2$ solvent-mediated powder (suspended in cyclohexane), at room temperature (RT).
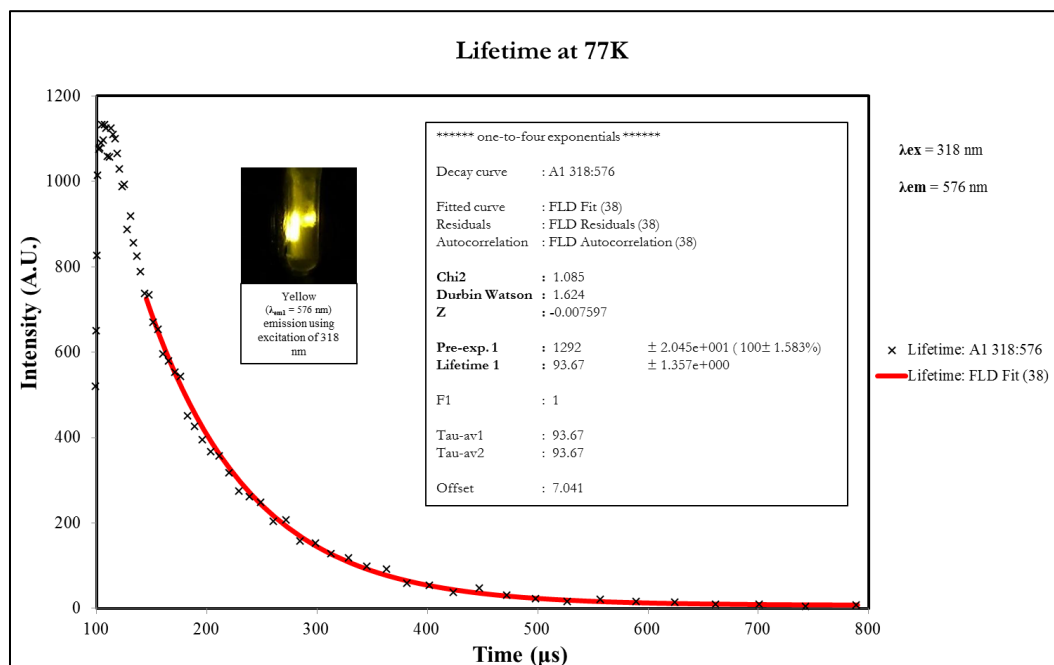
Figure 47. Photoluminescence lifetime decay curve for $\{Cu_2[3,5\text{-}(CF_3)_2Pz]_2(4,7\text{-phen})\}_2$ solvent-mediated powder, at cryogenic temperature (77K).

The UV-Vis absorption spectra for $\{Cu_2[3,5\text{-}(CF_3)_2Pz]_2(4,7\text{-phen})\}_2$ solvent-mediated powder, shown in Figure 48, were obtained using three dilutions in dichloromethane (DCM) (UV cutoff wavelength = 235 nm): 1×10^{-3} M, 1×10^{-4} M, and 1×10^{-5} M. A red shift was observed as the concentration increased, shifting more toward the visible region, as well as $\pi\text{-}\pi^*$ transition with an extinction coefficient (ε_{271}) of 5000 $L\cdot mol^{-1}\cdot cm^{-1}$ (λ_{max2} = 271 nm: A = 0.5, C = 1×10^{-4} M).
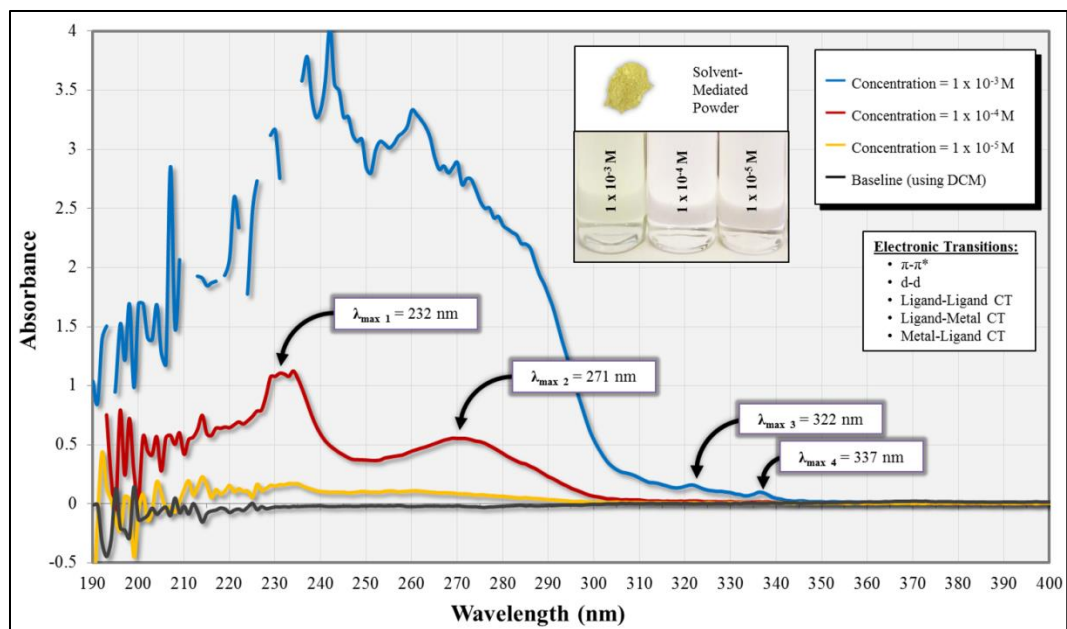
(A)
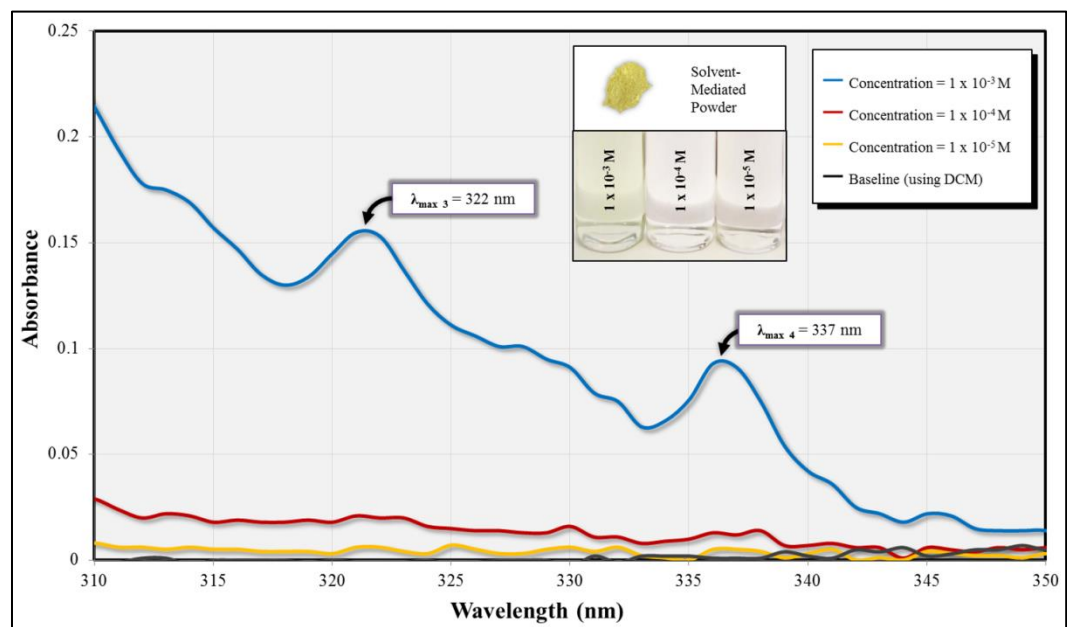
(B)

Figure 48. UV-Vis Spectra for {Cu$_2$[3,5-(CF$_3$)$_2$Pz]$_2$(4,7-phen)}$_2$ Solvent-Mediated Powder in DCM Solutions (UV Cutoff Wavelength = 235 nm): (A) Full-View = 190-400 nm; (B) Zoomed-In = 310-350 nm.

3.2.2 Compound 2: {Ag$_5$[3,5-(CF$_3$)$_2$Pz]$_5$(4,7-phen)$_4$}$_\infty$

3.2.2.1 X-ray Crystallographic Data

In this section, the X-ray crystallographic data (shown in Tables 3A-B) are discussed. {Ag$_5$[3,5-(CF$_3$)$_2$Pz]$_5$(4,7-phen)$_4$}$_\infty$ single crystals were obtained using solvent-mediated powder (synthesized using dichloromethane, DCM). Table 3A shows that {Ag$_5$[3,5-(CF$_3$)$_2$Pz]$_5$(4,7-phen)$_4$}$_\infty$ crystallizes in the triclinic crystal system with the space group *P*-1 with Z = 2 and the unit cell dimensions: a = 12.9838(2) Å, b = 15.2012(2) Å, c = 21.2451(3) Å, α = 74.3630(10)°, β = 89.7040(10)°, and γ = 84.2850(10)°. {Ag$_5$[3,5-(CF$_3$)$_2$Pz]$_5$(4,7-phen)$_4$}$_\infty$ has the empirical formula C77 H47 Ag5 F30 N18 O (MW = 2349.67 g/mol), which accounts for the presence of a diethyl ether molecule (C4 H10 O) in the asymmetric unit cell.

As shown in Figures 49A-C, the asymmetric and symmetric unit cell, as well as the crystal packing, of {Ag$_5$[3,5-(CF$_3$)$_2$Pz]$_5$(4,7-phen)$_4$}$_\infty$ exhibits 3- and 4-coordinated Ag(I) centers with Ag2 and Ag3, and Ag1 and Ag4, respectively, doubly bridged via two [3,5-(CF$_3$)$_2$Pz]$^-$ ligands, and Ag1 and Ag4 singly bridged via one [3,5-(CF$_3$)$_2$Pz]$^-$ ligand; moreover, Ag1 and Ag2, Ag3 and Ag5, and Ag3 and Ag4, respectively, are bridged via 4,7-phen ligands. The two 4-coordinated Ag(I) centers: Ag1 and Ag3, differ from one another in that Ag1 is coordinated with three [3,5-(CF$_3$)$_2$Pz]$^-$ ligands (via N1, N14, and N16) and one 4,7-phen ligand (via N3), meanwhile Ag3 is coordinated with two [3,5-(CF$_3$)$_2$Pz]$^-$ ligands (via N6 and N8) and two 4,7-phen ligands (via N9 and N11). Figure 49B shows the symmetric unit cell with two asymmetric units with their respective diethyl ether molecules.

The packing structure, shown in Figure 49C, shows that $\{Ag_5[3,5-(CF_3)_2Pz]_5(4,7-phen)_4\}_\infty$ is a coordination polymer with the 3- and 4-coordinated Ag(I) centers: Ag2 and Ag3, respectively, linked with the next adjacent 4- and 3-coordinated Ag(I) centers: Ag1 and Ag5, respectively, via two 4,7-phen-bridging ligands (via N3 and N4, and N11 and N12, respectively). Furthermore, the aforementioned 4,7-phen ligands (linking Ag1 with Ag2 and Ag3 with Ag5) exhibit [Ag2Ar2] π-π stacked pairing.

The bond lengths (Å) and angles (°) are shown in Table 3B. The full-matrix least-squares refinement method was used on F^2, resulting in a goodness-of-fit value of 1.118 with R1 = 5.86 % and wR2 = 11.97% for all data.

Table 3. (A) X-ray Crystallographic Data for {Ag₅[3,5-(CF₃)₂Pz]₅(4,7-phen)₄}∞; **(B)** Bond lengths [Å] and angles [°] for {Ag₅[3,5-(CF₃)₂Pz]₅(4,7-phen)₄}∞.

Empirical formula	C77 H47 Ag5 F30 N18 O
Formula weight	2349.67
Temperature	100.01(10) K
Wavelength	0.71073 Å
Crystal system	Triclinic
Space group	P-1
Unit cell dimensions	a = 12.9838(2) Å α = 74.3630(10)°. b = 15.2012(2) Å β = 89.7040(10)°. c = 21.2451(3) Å γ = 84.2850(10)°.
Volume	4016.84(10) Å^3
Z	2
Density (calculated)	1.943 Mg/m^3
Absorption coefficient	1.327 mm^{-1}
F(000)	2296
Crystal size	0.09 x 0.04 x 0.03 mm^3
Theta range for data collection	1.846 to 27.103°.
Index ranges	-16<=h<=16, -19<=k<=19, -27<=l<=27
Reflections collected	90873
Independent reflections	17685 [R(int) = 0.0447]
Completeness to theta = 25.242°	99.9 %
Absorption correction	Semi-empirical from equivalents
Max. and min. transmission	1.00000 and 0.87648
Refinement method	Full-matrix least-squares on F^2
Data / restraints / parameters	17685 / 70 / 1184
Goodness-of-fit on F^2	1.118
Final R indices [I>2sigma(I)]	R1 = 0.0480, wR2 = 0.1141
R indices (all data)	R1 = 0.0586, wR2 = 0.1197
Extinction coefficient	n/a
Largest diff. peak and hole	1.825 and -1.428 e.Å^{-3}

(A)

Bond Lengths [Å] (*blue*) & Angles [°] (*red*)					
Ag(1)-N(1)	2.366(4)	C(72)-C(73)	1.438(8)	F(17)-C(27)-F(16)	106.5(5)
Ag(1)-N(3)	2.307(4)	O(1S)-C(1S)	1.5068	F(17)-C(27)-F(18)	105.7(5)
Ag(1)-N(14)	2.368(4)	O(1S)-C(3S)	1.4644	F(17)-C(27)-C(25)	113.1(5)
Ag(1)-N(16)	2.357(4)	C(1S)-H(1SA)	0.97	F(18)-C(27)-F(16)	106.2(5)
Ag(2)-N(4)#1	2.230(4)	C(1S)-H(1SB)	0.97	F(18)-C(27)-C(25)	112.8(6)
Ag(2)-N(5)	2.236(4)	C(1S)-C(2S)	1.563	N(9)-C(28)-H(28)	118
Ag(2)-N(7)	2.258(4)	C(2S)-H(2SA)	0.96	N(9)-C(28)-C(29)	124.0(5)
Ag(3)-N(6)	2.356(4)	C(2S)-H(2SB)	0.96	C(29)-C(28)-H(28)	118
Ag(3)-N(8)	2.341(4)	C(2S)-H(2SC)	0.96	C(28)-C(29)-H(29)	120.3
Ag(3)-N(9)	2.324(4)	C(3S)-H(3SA)	0.97	C(30)-C(29)-C(28)	119.4(5)
Ag(3)-N(11)#1	2.517(4)	C(3S)-H(3SB)	0.97	C(30)-C(29)-H(29)	120.3
Ag(4)-N(10)	2.228(4)	C(3S)-C(4S)	1.669	C(29)-C(30)-H(30)	120.6
Ag(4)-N(13)	2.305(4)	C(4S)-H(4SA)	0.96	C(29)-C(30)-C(31)	118.8(5)
Ag(4)-N(15)	2.274(4)	C(4S)-H(4SB)	0.96	C(31)-C(30)-H(30)	120.6
Ag(5)-N(2)	2.220(4)	C(4S)-H(4SC)	0.96	C(30)-C(31)-C(32)	122.9(4)
Ag(5)-N(12)	2.454(5)	N(1)-Ag(1)-N(14)	102.46(14)	C(39)-C(31)-C(30)	118.1(4)
Ag(5)-N(17)	2.253(4)	N(3)-Ag(1)-N(1)	116.20(14)	C(39)-C(31)-C(32)	119.0(4)
F(1)-C(4)	1.355(6)	N(3)-Ag(1)-N(14)	118.25(15)	C(33)-C(32)-C(31)	123.3(5)
F(2)-C(4)	1.336(6)	N(3)-Ag(1)-N(16)	128.83(14)	C(36)-C(32)-C(31)	119.1(4)
F(3)-C(4)	1.338(6)	N(16)-Ag(1)-N(1)	97.59(14)	C(36)-C(32)-C(33)	117.6(4)
F(4)-C(5)	1.349(5)	N(16)-Ag(1)-N(14)	87.54(15)	C(32)-C(33)-H(33)	120.5
F(5)-C(5)	1.379(5)	N(4)#1-Ag(2)-N(5)	133.54(15)	C(34)-C(33)-C(32)	119.0(5)
F(6)-C(5)	1.337(5)	N(4)#1-Ag(2)-N(7)	127.48(16)	C(34)-C(33)-H(33)	120.5
F(7)-C(21)	1.347(6)	N(5)-Ag(2)-N(7)	98.98(16)	C(33)-C(34)-H(34)	120.1
F(8)-C(21)	1.348(6)	N(6)-Ag(3)-N(11)#1	100.97(14)	C(33)-C(34)-C(35)	119.8(5)
F(9)-C(21)	1.334(6)	N(8)-Ag(3)-N(6)	98.38(15)	C(35)-C(34)-H(34)	120.1
F(10)-C(22)	1.339(7)	N(8)-Ag(3)-N(11)#1	91.26(15)	N(10)-C(35)-C(34)	123.4(5)
F(11)-C(22)	1.337(7)	N(9)-Ag(3)-N(6)	120.23(15)	N(10)-C(35)-H(35)	118.3
F(12)-C(22)	1.304(7)	N(9)-Ag(3)-N(8)	125.70(15)	C(34)-C(35)-H(35)	118.3
F(13)-C(26)	1.354(7)	N(9)-Ag(3)-N(11)#1	114.38(14)	N(10)-C(36)-C(32)	122.6(4)
F(14)-C(26)	1.334(7)	N(10)-Ag(4)-N(13)	137.32(15)	N(10)-C(36)-C(37)	117.2(4)
F(15)-C(26)	1.315(7)	N(10)-Ag(4)-N(15)	127.34(15)	C(32)-C(36)-C(37)	120.2(4)
F(16)-C(27)	1.342(7)	N(15)-Ag(4)-N(13)	93.10(15)	C(36)-C(37)-H(37)	119.7
F(17)-C(27)	1.335(7)	N(2)-Ag(5)-N(12)	104.63(15)	C(38)-C(37)-C(36)	120.7(5)
F(18)-C(27)	1.342(8)	N(2)-Ag(5)-N(17)	153.16(16)	C(38)-C(37)-H(37)	119.7
F(19)-C(55)	1.335(8)	N(17)-Ag(5)-N(12)	99.82(16)	C(37)-C(38)-H(38)	119.5
F(20)-C(55)	1.326(7)	N(2)-N(1)-Ag(1)	119.7(3)	C(37)-C(38)-C(39)	121.1(4)
F(21)-C(55)	1.326(7)	C(1)-N(1)-Ag(1)	133.0(3)	C(39)-C(38)-H(38)	119.5
F(22)-C(56)	1.336(6)	C(1)-N(1)-N(2)	106.7(4)	N(9)-C(39)-C(31)	122.5(5)
F(23)-C(56)	1.348(7)	N(1)-N(2)-Ag(5)	117.9(3)	N(9)-C(39)-C(38)	117.7(4)
F(24)-C(56)	1.350(6)	C(3)-N(2)-Ag(5)	133.5(3)	C(31)-C(39)-C(38)	119.9(4)
F(25)-C(60)	1.341(6)	C(3)-N(2)-N(1)	108.2(4)	N(11)-C(40)-H(40)	118.4
F(26)-C(60)	1.354(7)	C(6)-N(3)-Ag(1)	118.7(3)	N(11)-C(40)-C(41)	123.2(5)
F(27)-C(60)	1.342(6)	C(6)-N(3)-C(17)	116.5(4)	C(41)-C(40)-H(40)	118.4
F(28)-C(61)	1.431(6)	C(17)-N(3)-Ag(1)	124.7(3)	C(40)-C(41)-H(41)	120.3
F(29)-C(61)	1.338(6)	C(13)-N(4)-Ag(2)#2	118.3(3)	C(42)-C(41)-C(40)	119.4(5)
F(30)-C(61)	1.351(6)	C(13)-N(4)-C(14)	118.4(4)	C(42)-C(41)-H(41)	120.3
N(1)-N(2)	1.368(6)	C(14)-N(4)-Ag(2)#2	123.3(3)	C(41)-C(42)-H(42)	120.2
N(1)-C(1)	1.351(6)	N(6)-N(5)-Ag(2)	118.5(3)	C(41)-C(42)-C(43)	119.6(5)
N(2)-C(3)	1.357(6)	C(18)-N(5)-Ag(2)	133.3(3)	C(43)-C(42)-H(42)	120.2
N(3)-C(6)	1.331(6)	C(18)-N(5)-N(6)	107.5(4)	C(42)-C(43)-C(44)	123.7(5)

N(3)-C(17)	1.370(6)	N(5)-N(6)-Ag(3)	115.9(3)	C(42)-C(43)-C(51)	117.7(5)
N(4)-C(13)	1.315(7)	C(20)-N(6)-Ag(3)	136.3(3)	C(51)-C(43)-C(44)	118.6(5)
N(4)-C(14)	1.370(6)	C(20)-N(6)-N(5)	107.0(4)	C(45)-C(44)-C(43)	123.5(5)
N(5)-N(6)	1.364(6)	N(8)-N(7)-Ag(2)	118.0(3)	C(48)-C(44)-C(43)	119.3(5)
N(5)-C(18)	1.346(6)	C(23)-N(7)-Ag(2)	133.5(3)	C(48)-C(44)-C(45)	117.2(5)
N(6)-C(20)	1.335(7)	C(23)-N(7)-N(8)	108.0(4)	C(44)-C(45)-H(45)	120.5
N(7)-N(8)	1.350(6)	N(7)-N(8)-Ag(3)	116.5(3)	C(46)-C(45)-C(44)	118.9(6)
N(7)-C(23)	1.346(6)	C(25)-N(8)-Ag(3)	134.0(4)	C(46)-C(45)-H(45)	120.5
N(8)-C(25)	1.342(7)	C(25)-N(8)-N(7)	107.1(4)	C(45)-C(46)-H(46)	120.1
N(9)-C(28)	1.326(7)	C(28)-N(9)-Ag(3)	118.0(3)	C(45)-C(46)-C(47)	119.8(5)
N(9)-C(39)	1.372(6)	C(28)-N(9)-C(39)	117.3(4)	C(47)-C(46)-H(46)	120.1
N(10)-C(35)	1.331(6)	C(39)-N(9)-Ag(3)	124.6(3)	N(12)-C(47)-C(46)	123.5(5)
N(10)-C(36)	1.375(6)	C(35)-N(10)-Ag(4)	120.3(3)	N(12)-C(47)-H(47)	118.2
N(11)-C(40)	1.328(7)	C(35)-N(10)-C(36)	117.5(4)	C(46)-C(47)-H(47)	118.2
N(11)-C(51)	1.376(7)	C(36)-N(10)-Ag(4)	122.0(3)	N(12)-C(48)-C(44)	123.5(5)
N(12)-C(47)	1.333(8)	C(40)-N(11)-Ag(3)#2	117.2(3)	N(12)-C(48)-C(49)	116.3(5)
N(12)-C(48)	1.368(7)	C(40)-N(11)-C(51)	117.8(5)	C(44)-C(48)-C(49)	120.1(5)
N(13)-N(14)	1.361(6)	C(51)-N(11)-Ag(3)#2	125.0(3)	C(48)-C(49)-H(49)	119.5
N(13)-C(52)	1.353(7)	C(47)-N(12)-Ag(5)	118.8(4)	C(50)-C(49)-C(48)	121.0(5)
N(14)-C(54)	1.346(6)	C(47)-N(12)-C(48)	117.0(5)	C(50)-C(49)-H(49)	119.5
N(15)-N(16)	1.348(6)	C(48)-N(12)-Ag(5)	124.1(4)	C(49)-C(50)-H(50)	119.7
N(15)-C(57)	1.344(6)	N(14)-N(13)-Ag(4)	115.3(3)	C(49)-C(50)-C(51)	120.5(5)
N(16)-C(59)	1.354(6)	C(52)-N(13)-Ag(4)	120.8(3)	C(51)-C(50)-H(50)	119.7
N(17)-C(62)	1.326(7)	C(52)-N(13)-N(14)	107.3(4)	N(11)-C(51)-C(43)	122.2(5)
N(17)-C(73)	1.360(7)	N(13)-N(14)-Ag(1)	116.0(3)	N(11)-C(51)-C(50)	117.4(5)
N(18)-C(69)	1.318(7)	C(54)-N(14)-Ag(1)	130.7(4)	C(43)-C(51)-C(50)	120.4(5)
N(18)-C(70)	1.362(7)	C(54)-N(14)-N(13)	107.2(4)	N(13)-C(52)-C(53)	111.2(5)
C(1)-C(2)	1.381(7)	N(16)-N(15)-Ag(4)	118.0(3)	N(13)-C(52)-C(55)	121.4(5)
C(1)-C(4)	1.488(7)	C(57)-N(15)-Ag(4)	133.2(4)	C(53)-C(52)-C(55)	127.4(5)
C(2)-H(2)	0.93	C(57)-N(15)-N(16)	108.0(4)	C(52)-C(53)-H(53)	128.6
C(2)-C(3)	1.395(7)	N(15)-N(16)-Ag(1)	115.8(3)	C(52)-C(53)-C(54)	102.7(5)
C(3)-C(5)	1.421(5)	N(15)-N(16)-C(59)	107.9(4)	C(54)-C(53)-H(53)	128.6
C(5)-F(4A)	1.353(7)	C(59)-N(16)-Ag(1)	134.1(3)	N(14)-C(54)-C(53)	111.6(5)
C(5)-F(5A)	1.354(7)	C(62)-N(17)-Ag(5)	119.1(3)	N(14)-C(54)-C(56)	120.0(5)
C(5)-F(6A)	1.398(7)	C(62)-N(17)-C(73)	118.1(4)	C(53)-C(54)-C(56)	128.3(5)
C(6)-H(6)	0.93	C(73)-N(17)-Ag(5)	122.3(3)	F(19)-C(55)-C(52)	113.5(5)
C(6)-C(7)	1.389(7)	C(69)-N(18)-C(70)	117.4(5)	F(20)-C(55)-F(19)	105.0(6)
C(7)-H(7)	0.93	N(1)-C(1)-C(2)	111.6(4)	F(20)-C(55)-C(52)	113.3(5)
C(7)-C(8)	1.368(7)	N(1)-C(1)-C(4)	120.5(4)	F(21)-C(55)-F(19)	106.0(6)
C(8)-H(8)	0.93	C(2)-C(1)-C(4)	127.8(5)	F(21)-C(55)-F(20)	105.5(5)
C(8)-C(9)	1.409(7)	C(1)-C(2)-H(2)	128.2	F(21)-C(55)-C(52)	112.8(5)
C(9)-C(10)	1.449(7)	C(1)-C(2)-C(3)	103.6(4)	F(22)-C(56)-F(23)	106.5(5)
C(9)-C(17)	1.404(7)	C(3)-C(2)-H(2)	128.2	F(22)-C(56)-F(24)	106.6(4)
C(10)-C(11)	1.411(7)	N(2)-C(3)-C(2)	109.9(4)	F(22)-C(56)-C(54)	111.7(5)
C(10)-C(14)	1.415(7)	N(2)-C(3)-C(5)	122.3(5)	F(23)-C(56)-F(24)	105.1(5)
C(11)-H(11)	0.93	C(2)-C(3)-C(5)	127.7(5)	F(23)-C(56)-C(54)	113.6(4)
C(11)-C(12)	1.367(7)	F(1)-C(4)-C(1)	112.5(4)	F(24)-C(56)-C(54)	112.8(5)
C(12)-H(12)	0.93	F(2)-C(4)-F(1)	105.3(4)	N(15)-C(57)-C(58)	110.6(5)
C(12)-C(13)	1.401(7)	F(2)-C(4)-F(3)	106.9(4)	N(15)-C(57)-C(60)	120.7(5)
C(13)-H(13)	0.93	F(2)-C(4)-C(1)	114.0(4)	C(58)-C(57)-C(60)	128.7(5)
C(14)-C(15)	1.426(7)	F(3)-C(4)-F(1)	106.5(4)	C(57)-C(58)-H(58)	128.2
C(15)-H(15)	0.93	F(3)-C(4)-C(1)	111.2(4)	C(57)-C(58)-C(59)	103.7(4)
C(15)-C(16)	1.355(7)	F(4)-C(5)-F(5)	102.0(5)	C(59)-C(58)-H(58)	128.2

C(16)-H(16)	0.93	F(4)-C(5)-C(3)	116.1(4)	N(16)-C(59)-C(58)	109.9(4)
C(16)-C(17)	1.440(7)	F(5)-C(5)-C(3)	111.9(4)	N(16)-C(59)-C(61)	121.1(5)
C(18)-C(19)	1.381(8)	F(6)-C(5)-F(4)	107.3(5)	C(58)-C(59)-C(61)	128.8(5)
C(18)-C(21)	1.479(7)	F(6)-C(5)-F(5)	103.1(4)	F(25)-C(60)-F(26)	105.0(5)
C(19)-H(19)	0.93	F(6)-C(5)-C(3)	114.9(4)	F(25)-C(60)-F(27)	106.8(5)
C(19)-C(20)	1.389(7)	F(4A)-C(5)-C(3)	118.2(11)	F(25)-C(60)-C(57)	114.1(5)
C(20)-C(22)	1.479(7)	F(4A)-C(5)-F(5A)	106.9(9)	F(26)-C(60)-C(57)	113.2(5)
C(23)-C(24)	1.388(7)	F(4A)-C(5)-F(6A)	100.6(9)	F(27)-C(60)-F(26)	105.4(4)
C(23)-C(26)	1.484(7)	F(5A)-C(5)-C(3)	119.0(8)	F(27)-C(60)-C(57)	111.6(5)
C(24)-H(24)	0.93	F(5A)-C(5)-F(6A)	100.2(8)	F(29)-C(61)-F(28)	101.7(5)
C(24)-C(25)	1.389(8)	F(6A)-C(5)-C(3)	108.9(7)	F(29)-C(61)-F(30)	110.3(7)
C(25)-C(27)	1.483(8)	N(3)-C(6)-H(6)	117.8	F(29)-C(61)-C(59)	116.7(5)
C(28)-H(28)	0.93	N(3)-C(6)-C(7)	124.4(5)	F(30)-C(61)-F(28)	97.8(6)
C(28)-C(29)	1.393(7)	C(7)-C(6)-H(6)	117.8	F(30)-C(61)-C(59)	115.6(7)
C(29)-H(29)	0.93	C(6)-C(7)-H(7)	120.4	C(59)-C(61)-F(28)	112.2(5)
C(29)-C(30)	1.374(7)	C(8)-C(7)-C(6)	119.1(5)	C(59)-C(61)-F(28A)	110.5(6)
C(30)-H(30)	0.93	C(8)-C(7)-H(7)	120.4	F(29A)-C(61)-C(59)	123.6(6)
C(30)-C(31)	1.410(7)	C(7)-C(8)-H(8)	120.4	F(29A)-C(61)-F(28A)	104.1(6)
C(31)-C(32)	1.456(7)	C(7)-C(8)-C(9)	119.2(5)	F(29A)-C(61)-F(30A)	106.4(9)
C(31)-C(39)	1.409(7)	C(9)-C(8)-H(8)	120.4	F(30A)-C(61)-C(59)	113.6(10)
C(32)-C(33)	1.415(7)	C(8)-C(9)-C(10)	122.7(5)	F(30A)-C(61)-F(28A)	94.4(11)
C(32)-C(36)	1.403(7)	C(17)-C(9)-C(8)	117.6(4)	N(17)-C(62)-H(62)	118.5
C(33)-H(33)	0.93	C(17)-C(9)-C(10)	119.7(4)	N(17)-C(62)-C(63)	123.0(5)
C(33)-C(34)	1.371(7)	C(11)-C(10)-C(9)	123.4(5)	C(63)-C(62)-H(62)	118.5
C(34)-H(34)	0.93	C(11)-C(10)-C(14)	117.7(5)	C(62)-C(63)-H(63)	120.3
C(34)-C(35)	1.388(7)	C(14)-C(10)-C(9)	118.9(4)	C(64)-C(63)-C(62)	119.4(5)
C(35)-H(35)	0.93	C(10)-C(11)-H(11)	120.2	C(64)-C(63)-H(63)	120.3
C(36)-C(37)	1.427(7)	C(12)-C(11)-C(10)	119.6(5)	C(63)-C(64)-H(64)	120.2
C(37)-H(37)	0.93	C(12)-C(11)-H(11)	120.2	C(63)-C(64)-C(65)	119.5(5)
C(37)-C(38)	1.359(7)	C(11)-C(12)-H(12)	120.6	C(65)-C(64)-H(64)	120.2
C(38)-H(38)	0.93	C(11)-C(12)-C(13)	118.9(5)	C(64)-C(65)-C(66)	123.7(5)
C(38)-C(39)	1.425(7)	C(13)-C(12)-H(12)	120.6	C(64)-C(65)-C(73)	117.3(5)
C(40)-H(40)	0.93	N(4)-C(13)-C(12)	123.7(5)	C(73)-C(65)-C(66)	118.9(5)
C(40)-C(41)	1.398(8)	N(4)-C(13)-H(13)	118.2	C(67)-C(66)-C(65)	123.7(5)
C(41)-H(41)	0.93	C(12)-C(13)-H(13)	118.2	C(67)-C(66)-C(70)	116.9(5)
C(41)-C(42)	1.373(8)	N(4)-C(14)-C(10)	121.7(5)	C(70)-C(66)-C(65)	119.4(5)
C(42)-H(42)	0.93	N(4)-C(14)-C(15)	118.4(4)	C(66)-C(67)-H(67)	120.2
C(42)-C(43)	1.397(8)	C(10)-C(14)-C(15)	119.9(4)	C(68)-C(67)-C(66)	119.6(5)
C(43)-C(44)	1.457(8)	C(14)-C(15)-H(15)	119.4	C(68)-C(67)-H(67)	120.2
C(43)-C(51)	1.417(7)	C(16)-C(15)-C(14)	121.1(5)	C(67)-C(68)-H(68)	120.4
C(44)-C(45)	1.420(7)	C(16)-C(15)-H(15)	119.4	C(67)-C(68)-C(69)	119.2(5)
C(44)-C(48)	1.399(8)	C(15)-C(16)-H(16)	119.6	C(69)-C(68)-H(68)	120.4
C(45)-H(45)	0.93	C(15)-C(16)-C(17)	120.8(5)	N(18)-C(69)-C(68)	123.5(5)
C(45)-C(46)	1.368(9)	C(17)-C(16)-H(16)	119.6	N(18)-C(69)-H(69)	118.3
C(46)-H(46)	0.93	N(3)-C(17)-C(9)	123.1(4)	C(68)-C(69)-H(69)	118.3
C(46)-C(47)	1.389(9)	N(3)-C(17)-C(16)	117.3(4)	N(18)-C(70)-C(66)	123.4(5)
C(47)-H(47)	0.93	C(9)-C(17)-C(16)	119.6(4)	N(18)-C(70)-C(71)	117.1(5)
C(48)-C(49)	1.435(8)	N(5)-C(18)-C(19)	111.2(4)	C(66)-C(70)-C(71)	119.5(5)
C(49)-H(49)	0.93	N(5)-C(18)-C(21)	120.2(5)	C(70)-C(71)-H(71)	119.2
C(49)-C(50)	1.354(8)	C(19)-C(18)-C(21)	128.6(5)	C(72)-C(71)-C(70)	121.6(5)
C(50)-H(50)	0.93	C(18)-C(19)-H(19)	128.8	C(72)-C(71)-H(71)	119.2
C(50)-C(51)	1.425(8)	C(18)-C(19)-C(20)	102.5(5)	C(71)-C(72)-H(72)	119.5
C(52)-C(53)	1.383(8)	C(20)-C(19)-H(19)	128.8	C(71)-C(72)-C(73)	121.1(5)

C(52)-C(55)	1.478(8)	N(6)-C(20)-C(19)	111.8(5)	C(73)-C(72)-H(72)	119.5
C(53)-H(53)	0.93	N(6)-C(20)-C(22)	120.4(5)	N(17)-C(73)-C(65)	122.6(5)
C(53)-C(54)	1.383(8)	C(19)-C(20)-C(22)	127.8(5)	N(17)-C(73)-C(72)	117.8(5)
C(54)-C(56)	1.487(8)	F(7)-C(21)-F(8)	104.8(4)	C(65)-C(73)-C(72)	119.5(5)
C(57)-C(58)	1.382(8)	F(7)-C(21)-C(18)	112.9(4)	C(3S)-O(1S)-C(1S)	101.8
C(57)-C(60)	1.472(8)	F(8)-C(21)-C(18)	113.0(4)	O(1S)-C(1S)-H(1SA)	110.5
C(58)-H(58)	0.93	F(9)-C(21)-F(7)	107.0(4)	O(1S)-C(1S)-H(1SB)	110.5
C(58)-C(59)	1.390(8)	F(9)-C(21)-F(8)	106.4(4)	O(1S)-C(1S)-C(2S)	106.1
C(59)-C(61)	1.414(5)	F(9)-C(21)-C(18)	112.2(4)	H(1SA)-C(1S)-H(1SB)	108.7
C(61)-F(28A)	1.414(7)	F(10)-C(22)-C(20)	112.7(5)	C(2S)-C(1S)-H(1SA)	110.5
C(61)-F(29A)	1.347(6)	F(11)-C(22)-F(10)	103.3(5)	C(2S)-C(1S)-H(1SB)	110.5
C(61)-F(30A)	1.371(7)	F(11)-C(22)-C(20)	112.1(5)	C(1S)-C(2S)-H(2SA)	109.5
C(62)-H(62)	0.93	F(12)-C(22)-F(10)	107.3(5)	C(1S)-C(2S)-H(2SB)	109.5
C(62)-C(63)	1.401(8)	F(12)-C(22)-F(11)	107.9(5)	C(1S)-C(2S)-H(2SC)	109.5
C(63)-H(63)	0.93	F(12)-C(22)-C(20)	113.0(5)	H(2SA)-C(2S)-H(2SB)	109.5
C(63)-C(64)	1.364(8)	N(7)-C(23)-C(24)	111.0(5)	H(2SA)-C(2S)-H(2SC)	109.5
C(64)-H(64)	0.93	N(7)-C(23)-C(26)	120.9(5)	H(2SB)-C(2S)-H(2SC)	109.5
C(64)-C(65)	1.408(7)	C(24)-C(23)-C(26)	128.0(5)	O(1S)-C(3S)-H(3SA)	112.4
C(65)-C(66)	1.458(7)	C(23)-C(24)-H(24)	128.9	O(1S)-C(3S)-H(3SB)	112.4
C(65)-C(73)	1.412(7)	C(23)-C(24)-C(25)	102.1(5)	O(1S)-C(3S)-C(4S)	96.8
C(66)-C(67)	1.402(7)	C(25)-C(24)-H(24)	128.9	H(3SA)-C(3S)-H(3SB)	110
C(66)-C(70)	1.407(7)	N(8)-C(25)-C(24)	111.8(5)	C(4S)-C(3S)-H(3SA)	112.4
C(67)-H(67)	0.93	N(8)-C(25)-C(27)	121.1(5)	C(4S)-C(3S)-H(3SB)	112.4
C(67)-C(68)	1.370(8)	C(24)-C(25)-C(27)	127.0(5)	C(3S)-C(4S)-H(4SA)	109.5
C(68)-H(68)	0.93	F(13)-C(26)-C(23)	112.6(5)	C(3S)-C(4S)-H(4SB)	109.5
C(68)-C(69)	1.395(8)	F(14)-C(26)-F(13)	103.4(4)	C(3S)-C(4S)-H(4SC)	109.5
C(69)-H(69)	0.93	F(14)-C(26)-C(23)	112.6(5)	H(4SA)-C(4S)-H(4SB)	109.5
C(70)-C(71)	1.430(7)	F(15)-C(26)-F(13)	106.2(5)	H(4SA)-C(4S)-H(4SC)	109.5
C(71)-H(71)	0.93	F(15)-C(26)-F(14)	108.8(5)	H(4SB)-C(4S)-H(4SC)	109.5
C(71)-C(72)	1.342(8)	F(15)-C(26)-C(23)	112.6(5)		
C(72)-H(72)	0.93	F(16)-C(27)-C(25)	112.0(5)		

Symmetry transformations used to generate equivalent atoms:
#1 x-1,y,z   #2 x+1,y,z

(B)
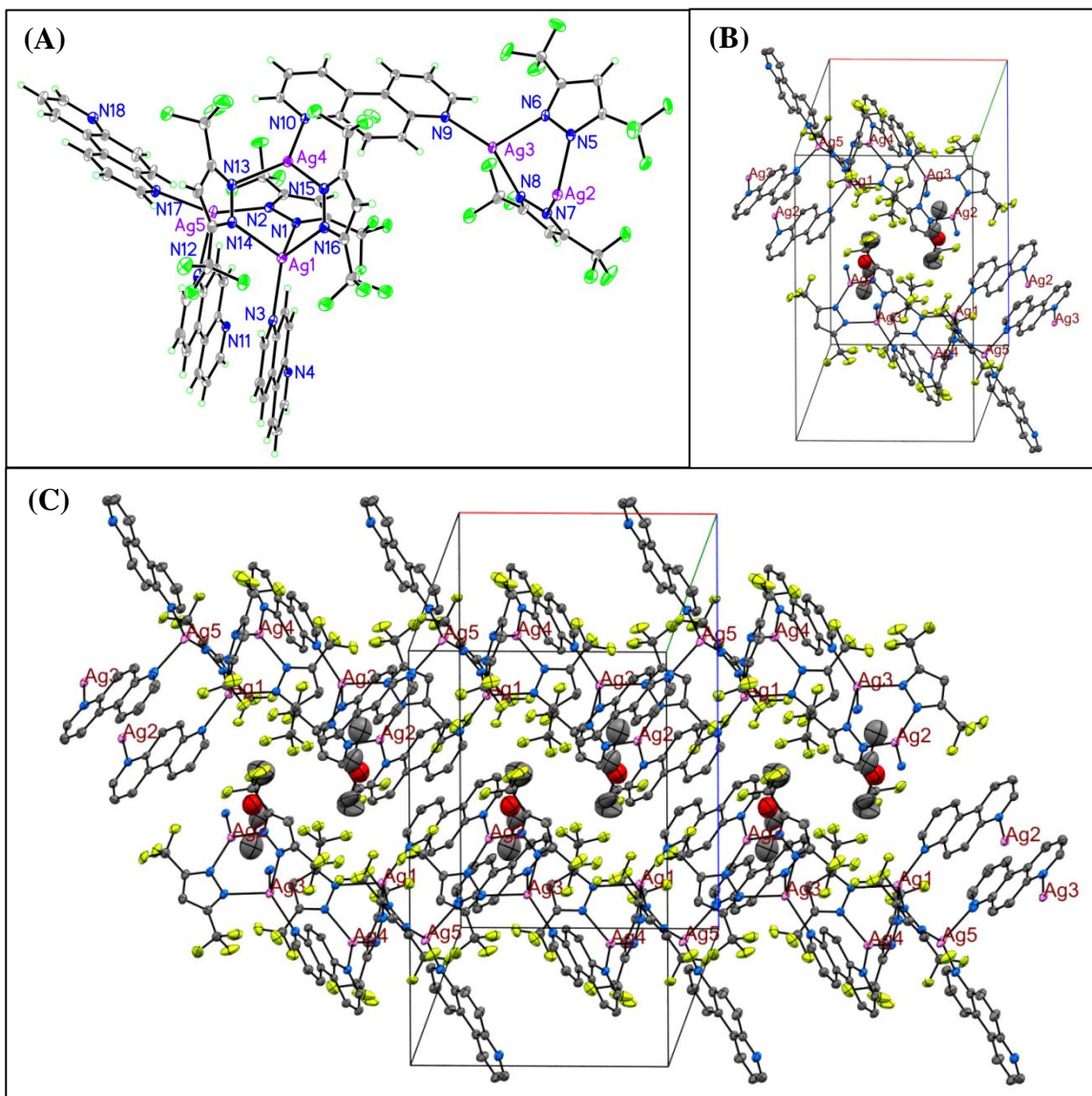
Figure 49. Crystal Structure of {Ag$_5$[3,5-(CF$_3$)$_2$Pz]$_5$(4,7-phen)$_4$}$_\infty$: **(A)** Asymmetric Unit Cell, **(B)** Symmetric Unit Cell, and **(C)** Packing.

3.2.2.2 Elemental Analysis Data

In this section, the elemental analysis data for $\{Ag_5[3,5\text{-}(CF_3)_2Pz]_5(4,7\text{-phen})_4\}_\infty$ are discussed, comparing the experimentally found data with the theoretical Anal. Calc. (see Table 4).

For the crystals (containing diethyl ether), the theoretical percentages of carbon (C), hydrogen (H), and nitrogen (N) were analytically calculated (Anal. Calc.) based on the empirical formula C77 H47 Ag5 F30 N18 O (MW = 2349.67 g/mol): C, 39.36; H, 2.02; N, 10.73. The experimentally found data for the crystals (C, 39.09; H, 1.98; N, 10.38) matched with the theoretical Anal. Calc. within ±0.27 for C, ±0.04 for H, and ±0.35 for N. The empirical formula for crystals accounts for the presence of a diethyl ether molecule (C4 H10 O).

For the solvent-mediated powder (free from solvent traces), synthesized using dichloromethane (DCM), the theoretical percentages of carbon (C), hydrogen (H), and nitrogen (N) were analytically calculated (Anal. Calc.) based on the empirical formula C73 H37 Ag5 F30 N18 (MW = 2275.49 g/mol): C, 38.53; H, 1.64; N, 11.08. The empirical formula for the solvent-mediated powder, solid product accounts for the absence of solvent traces. The experimentally found data for the solvent-mediated powder (C, 38.32; H, 1.56; N, 10.80) matched with the theoretical Anal. Calc. (free from solvent traces) within ±0.21 for C, ±0.08 for H, and ±0.28 for N.

For the solvent-mediated powder (containing toluene traces), synthesized using toluene, the theoretical percentages of carbon (C), hydrogen (H), and nitrogen (N) were analytically calculated (Anal. Calc.) based on the empirical formula C80 H45 Ag5 F30

N18 (MW = 2367.63 g/mol): C, 40.58; H, 1.92; N, 10.65. The empirical formula for the solvent-mediated powder, solid product accounts for the presence of a toluene molecule (C7 H8). The experimentally found data for the solvent-mediated powder with toluene traces (C, 40.35; H, 1.90; N, 10.49) matched with the theoretical Anal. Calc. (with toluene traces) within ± 0.23 for C, ± 0.02 for H, and ± 0.16 for N.

In comparison between the crystals and both solvent-mediated powders, the same $\{Ag_5[3,5-(CF_3)_2Pz]_5(4,7-phen)_4\}_\infty$ product was synthesized/crystallized, while accounting for the presence/absence of the respective solvent molecules.

Table 4. Elemental analysis data for $\{Ag_5[3,5\text{-}(CF_3)_2Pz]_5(4,7\text{-phen})_4\}_\infty$ crystals with diethyl ether and solvent-mediated powder synthesized using dichloromethane (DCM), and solvent-mediated powder synthesized using toluene: theoretical Anal. Calc. versus experimentally found data. The theoretical Anal. Calc. was adjusted in order to account for the presence of diethyl ether (1*), the absence of solvent traces (2*), and the presence of toluene (3*).

Elemental Analysis			
$Ag_5[3,5\text{-}(CF_3)_2Pz]_5(4,7\text{-phen})_4\}_\infty$			
	1* Crystals with diethyl ether	2* Solvent-Mediated Powder (in DCM)	3* Solvent-Mediated Powder (in Toluene)
1* $Ag_5[3,5\text{-}(CF_3)_2Pz]_5(4,7\text{-phen})_4\}_\infty$ + Diethyl ether = C77 H47 Ag5 F30 N18 O			
Element	Theoretical Anal. Calc. 1*	Experimentally Found	Experimentally Found	Experimentally Found
C	39.36%	39.09%	38.32%	40.35%
H	2.02%	1.98%	1.56%	1.90%
N	10.73%	10.38%	10.80%	10.49%
Ag	22.95%			
2* $Ag_5[3,5\text{-}(CF_3)_2Pz]_5(4,7\text{-phen})_4\}_\infty$ *(no solvent traces)* = C73 H37 Ag5 F30 N18			
Element	Theoretical Anal. Calc. 2*	Experimentally Found	Experimentally Found	Experimentally Found
C	38.53%	39.09%	38.32%	40.35%
H	1.64%	1.98%	1.56%	1.90%
N	11.08%	10.38%	10.80%	10.49%
Ag	23.70%			
3* $Ag_5[3,5\text{-}(CF_3)_2Pz]_5(4,7\text{-phen})_4\}_\infty$ + Toluene = C80 H45 Ag5 F30 N18			
Element	Theoretical Anal. Calc. 3*	Experimentally Found	Experimentally Found	Experimentally Found
C	40.58%	39.09%	38.32%	40.35%
H	1.92%	1.98%	1.56%	1.90%
N	10.65%	10.38%	10.80%	10.49%
Ag	22.78%			

3.2.2.3 Characterization using FT-IR Spectroscopy

In this section, the IR spectra for $\{Ag_5[3,5\text{-}(CF_3)_2Pz]_5(4,7\text{-phen})_4\}_\infty$ crystals (with diethyl ether), solvent-mediated powder synthesized using dichloromethane (DCM), and solvent-mediated powder synthesized using toluene, shown in Figure 50, are discussed. The IR spectra for the crystals and both solvent-mediated powders are relatively similar to one another and feature the functional groups characteristic of both the $[3,5\text{-}(CF_3)_2Pz]^-$ and 4,7-phen ligands: =C-H stretch (aromatic), C=C stretch (aromatic), C=N stretch (aromatic), C-C stretch (aromatic), C-N stretch (aromatic), and C-F stretch. The IR spectrum for the crystals shows peaks characteristic of the functional groups for diethyl ether: C-H (sp^3): 2957.83, 2922.78, 2850.76 cm^{-1} and C-O stretch: 1138.93 cm^{-1}, which are not present in the IR spectrum for the solvent-mediated powder (absent of solvent traces). The IR spectrum for the solvent-mediated powder synthesized using toluene shows a peak characteristic of a functional group for toluene: C-H bending "oop": 738, which is not present in the IR spectrum for solvent-mediated powder synthesized using DCM (absent of solvent traces).

Functional Groups	Expected Range (cm^{-1})
=C-H stretch (aromatic)	3010-3100, 690-900
C=C stretch (aromatic)	1400, 1600
C=N stretch (aromatic)	1400-1620
C-C stretch (aromatic)	1400-1500
C-N stretch (aromatic)	1250-1335
C-F stretch	1000-1400
C-H stretch (C-CH$_3$)	2850-2960
C-O stretch	1000-1300
C-H bending "oop"	675-900
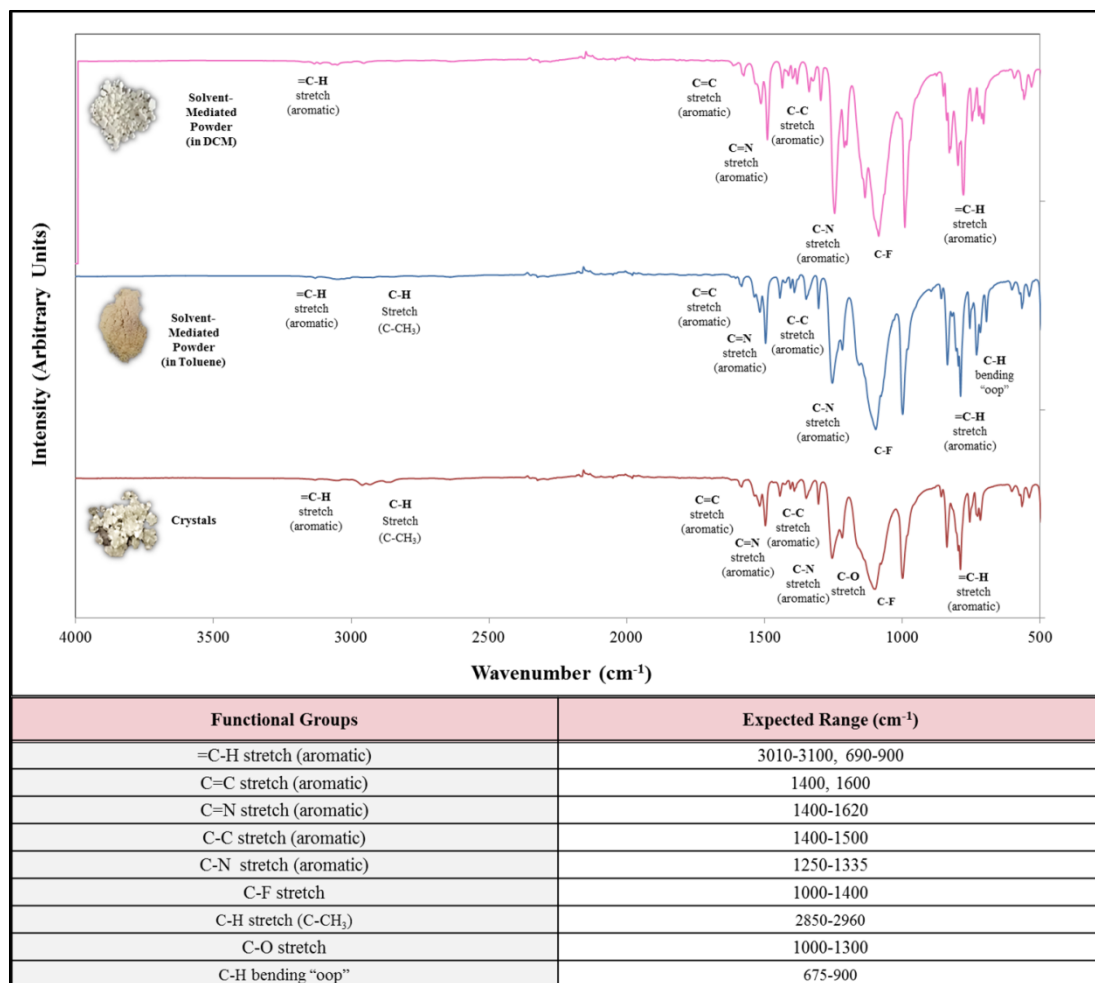
Figure 50. Stacked FT-IR spectra for $\{Ag_5[3,5\text{-}(CF_3)_2Pz]_5(4,7\text{-phen})_4\}_\infty$ solvent-mediated powder synthesized using dichloromethane (DCM) (*top*), solvent-mediated powder synthesized using toluene (*middle*), crystals with diethyl ether (*bottom*).

3.2.2.4 Characterization using TGA and DSC Analyses

In this section, the TGA analyses (and DSC analysis) for the $\{Ag_5[3,5\text{-}(CF_3)_2Pz]_5(4,7\text{-phen})_4\}_\infty$ crystals with diethyl ether, solvent-mediated powder synthesized using dichloromethane (DCM), and solvent-mediated powder synthesized using toluene, shown in Figures 51-54, are discussed.

The TGA analyses for the crystals and both of the solvent-mediated powders are relatively similar to one another with regard to percent weight loss, onset temperature, and inflection points. As shown in Figures 51-53, TGA analysis for crystals with diethyl ether, solvent-mediated powder synthesized using DCM, and solvent-mediated powder synthesized using toluene, respectively, show a significant weight loss of 93.22%, 93.07%, and 90.83%, respectively, with onset temperatures (the temperatures at which weight loss begins) of 247.68°C, 239.62°C, and 258.61°C, respectively, and offset temperatures (the temperatures at which weight loss ends) of 285.49°C, 284.66°C, and 298.10°C, respectively. Furthermore, the 1st derivative peaks show the greatest rate of change on the weight loss curves at 277.30°C, 274.18°C, and 288.57°C, respectively.

The TGA analysis for the crystals, shown in Figure 51, shows a weight loss of 3.494% between 115.76°C and 134.96°C (with a 1st derivative peak at 129.23°C), which is attributed to the removal of the solvent traces of diethyl ether. With regard to the molecular weight (MW) of 2349.6 g/mol (empirical formula: C77 H47 Ag5 F30 N18 O) for the crystals with diethyl ether traces, the diethyl ether molecule (MW = 74.12 g/mol) accounts for 3.155% of the total molecular weight, which is relatively close to the aforementioned 3.494% weight loss. In contrast, the TGA analyses for the solvent-mediated powder synthesized using DCM, shown in Figure 52, does not show any weight loss prior to its onset temperature of 239.62°C, which confirms the absence of solvent traces. The TGA analysis for the solvent-mediated powder synthesized using toluene, shown in Figure 53, shows a weight loss of 1.297% between 100.11°C and 129.92°C (with a 1st derivative peak at 117.60°C), which is attributed to the removal of the solvent

traces of toluene. With regard to the molecular weight of 2367.63 g/mol (empirical formula: C80 H45 Ag5 F30 N18) for the solvent-mediated powder synthesized using toluene, the toluene molecule (MW = 92.14 g/mol) accounts for 3.891% of the total molecular weight, which is greater than the aforementioned 1.297% weight loss. The difference in percentage of toluene present may possibly be attributed to the partial evaporation of toluene from the solventless powder prior to running TGA for the sample.

With regard to the crystals and its emperical formula of C77 H47 Ag5 F30 N18 O (MW = 2349.67 g/mol): C, 39.36; H, 2.02; N, 10.73, the theoretical percentage of silver is 22.95%; however, the total weight loss of 96.72% (Solvent: 3.494% + Solid: 93.22%) was observed, which was primarily due to the sublimation of the $[3,5\text{-}(CF_3)_2Pz]^-$ and 4,7-phen ligands and solvent traces (total theoretical percentage of C, H, N, F, and O of 77.05%). The remaining weight following the aforementioned weight loss should theoretically be the remaining silver.

With regard to the solvent-mediated powder synthesized using DCM and its emperical formula of C73 H37 Ag5 F30 N18 (MW = 2275.49 g/mol): C, 38.53; H, 1.64; N, 11.08, the theoretical percentage of silver is 23.70%; however, the weight loss of 93.22% was observed, which was primarily due to the sublimation of the $[3,5\text{-}(CF_3)_2Pz]^-$ and 4,7-phen ligands (total theoretical percentage of C, H, N and F of 76.30%). The remaining weight following the aforementioned weight loss should theoretically be the remaining silver.

With regard to the solvent-mediated powder synthesized using toluene and its emperical formula of C80 H45 Ag5 F30 N18 (MW = 2367.63 g/mol): C, 40.58; H, 1.92;

N, 10.65, the theoretical percentage of silver is 22.78%; however, the total weight loss of 92.12% (Solvent: 1.297% + Solid: 90.83%) was observed, which was primarily due to the sublimation of the $[3,5\text{-}(CF_3)_2Pz]^-$ and 4,7-phen ligands and solvent traces (total theoretical percentage of C, H, N and F of 77.22%). The remaining weight following the aforementioned weight loss should theoretically be the remaining silver.

The differences in onset/offset temperatures and 1st derivative peaks may be attributed to the differences in sample weights for the crystals with diethyl ether, solvent-mediated powder synthesized using DCM, and solvent-mediated powder synthesized using toluene: 9.9890 mg, 6.7840 mg and 9.9090 mg, respectively, and/or the presence/absence of solvent traces.

Figure 54 shows the DSC analysis for $\{Ag_5[3,5\text{-}(CF_3)_2Pz]_5(4,7\text{-phen})_4\}_\infty$ crystals with diethyl ether. Two endothermic events were observed. A major (sharp) peak maximum is observed at 124.81°C (onset temperature = 120.85°C), which is characteristic of melting and is similar to the observed melting point of the solvent-mediated powder synthesized using DCM (125.3-127.2°C). A minor peak maximum is observed at 144.35°C (onset temperature = ~141.2°C), which may be related to the 3.494% weight loss observed between 115.76°C and 134.96°C in the TGA analysis for the crystals (see Figure 51).
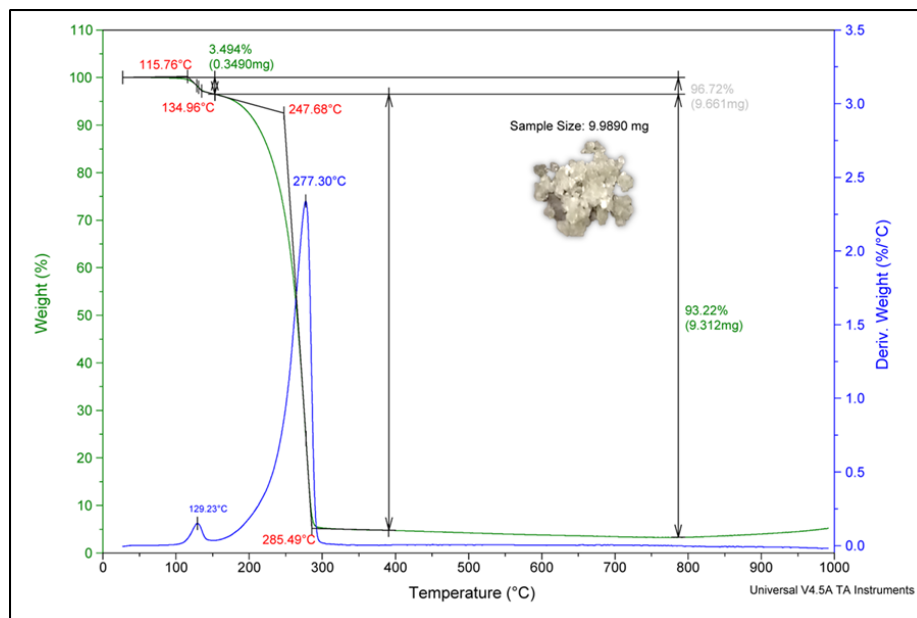
Figure 51. TGA analysis for $\{Ag_5[3,5\text{-}(CF_3)_2Pz]_5(4,7\text{-phen})_4\}_\infty$ crystals with diethyl ether.
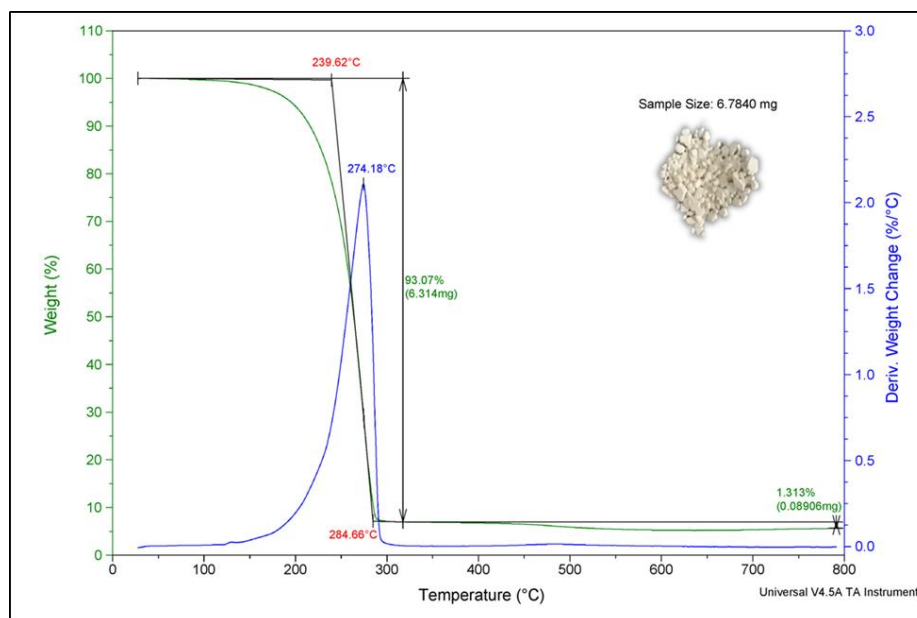
Figure 52. TGA analysis for $\{Ag_5[3,5\text{-}(CF_3)_2Pz]_5(4,7\text{-phen})_4\}_\infty$ solvent-mediated powder synthesized using DCM.
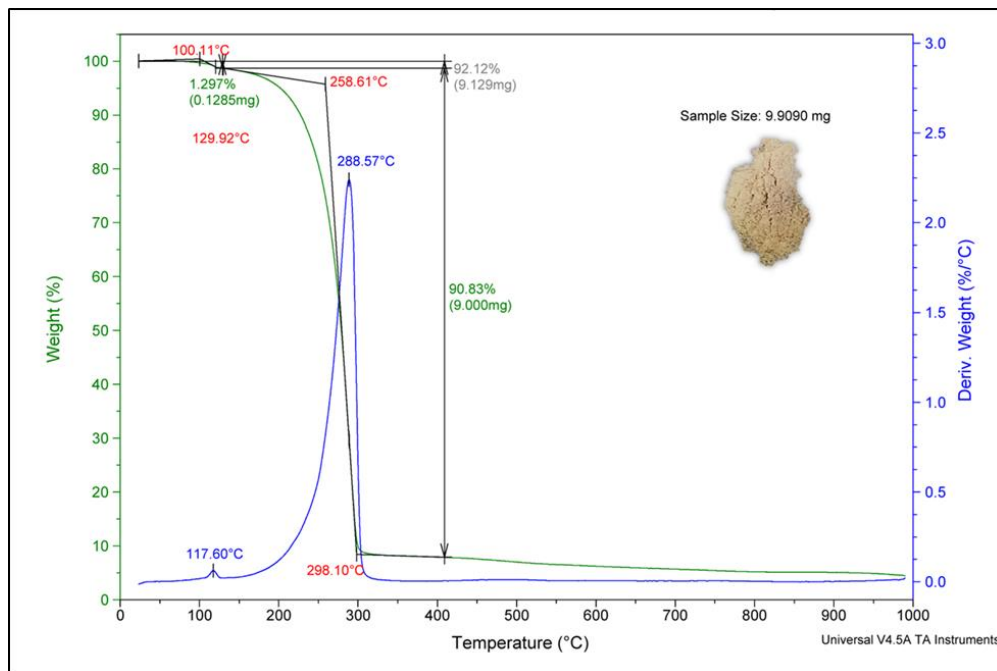
Figure 53. TGA analysis for $\{Ag_5[3,5\text{-}(CF_3)_2Pz]_5(4,7\text{-phen})_4\}_\infty$ solvent-mediated powder synthesized using toluene.
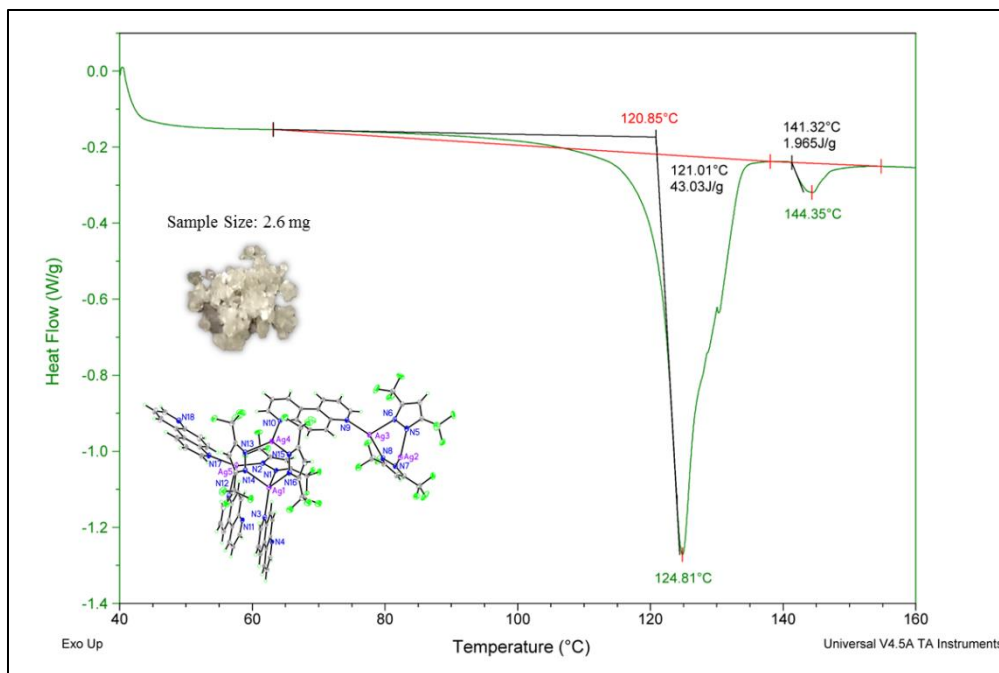
Figure 54. DSC analysis of $\{Ag_5[3,5\text{-}(CF_3)_2Pz]_5(4,7\text{-phen})_4\}_\infty$ crystals.

3.2.2.5 Characterization using UV-Vis Absorption Spectroscopy

In this section, the UV-Vis absorption spectroscopy of $\{Ag_5[3,5\text{-}(CF_3)_2Pz]_5(4,7\text{-}phen)_4\}_\infty$ solvent-mediated powder (synthesized using dichloromethane, DCM) is discussed. The UV-Vis absorption spectra for $\{Ag_5[3,5\text{-}(CF_3)_2Pz]_5(4,7\text{-}phen)_4\}_\infty$, shown in Figure 55, were obtained using four dilutions in methanol (UV cutoff wavelength = 205 nm): 1×10^{-3} M, 1×10^{-4} M, 1×10^{-5} M, and 1×10^{-6} M. A red shift was observed as the concentration increased, shifting more toward the visible region, as well as $\pi\text{-}\pi^*$ transition with an extinction coefficient (ε_{273}) of 100,000 $L\cdot mol^{-1}\cdot cm^{-1}$ $(\lambda_{max2} = 273$ nm: A = 1.0, C = 1×10^{-4} M).
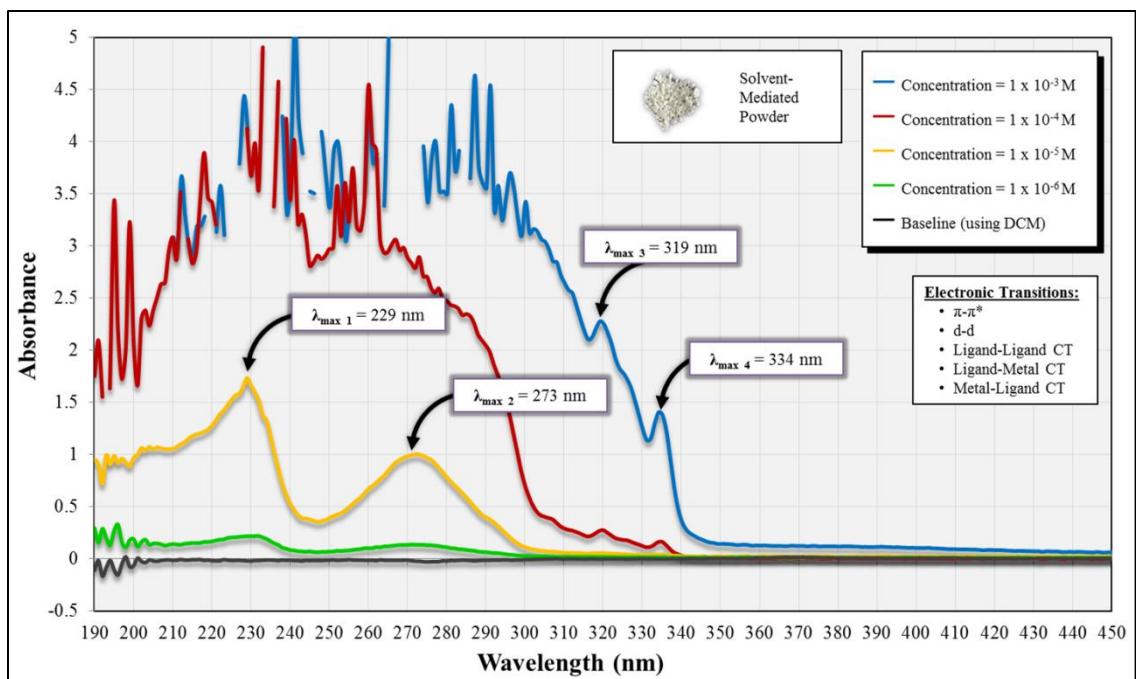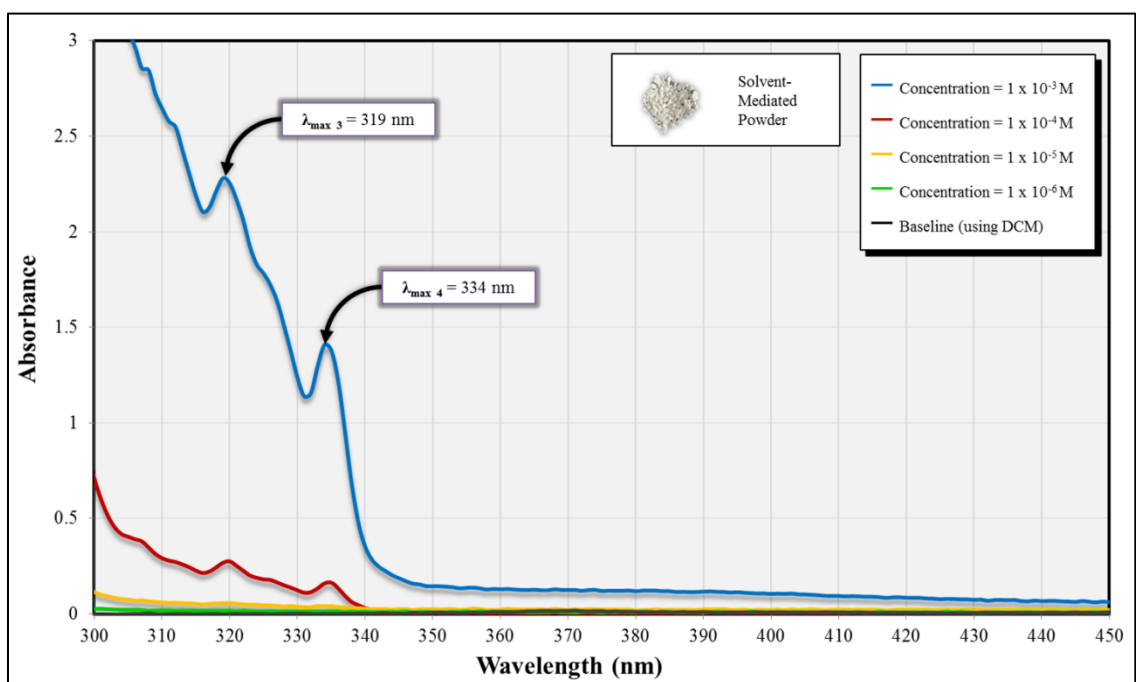
Figure 55. UV-Vis Spectra for $\{Ag_5[3,5\text{-}(CF_3)_2Pz]_5(4,7\text{-phen})_4\}_\infty$ solvent-mediated powder (synthesized using DCM) in methanol solutions (UV cutoff wavelength = 205 nm): **(A)** Full-View = 190-450 nm; **(B)** Zoomed-In = 300-450 nm.

3.2.3 Compound 3: {Cu[3,5-(CF$_3$)$_2$Pz](1,7-phen)}$_2$

3.2.3.1 X-ray Crystallographic Data

In this section, the X-ray crystallographic data for {Cu[3,5-(CF$_3$)$_2$Pz](1,7-phen)}$_2$ (shown in Tables 5A-B) are discussed. {Cu[3,5-(CF$_3$)$_2$Pz](1,7-phen)}$_2$ single crystals were obtained using solvent-mediated powder. Table 5A shows that {Cu[3,5-(CF$_3$)$_2$Pz](1,7-phen)}$_2$ crystallizes in the monoclinic crystal system with the space group P 1 2$_1$/n 1 with Z = 2 and the unit cell dimensions: a = 9.9749(3) Å, b = 6.0080(2) Å, c = 27.5128(7) Å, α = 90°, β = 95.975(2)°, and γ = 90°. {Cu[3,5-(CF$_3$)$_2$Pz](1,7-phen)}$_2$ has the empirical formula C34 H18 Cu2 F12 N8 (MW = 893.64 g/mol).

As shown in Figure 56A, the symmetric unit cell of {Cu[3,5-(CF$_3$)$_2$Pz](1,7-phen)}$_2$ exhibits a Cu(I) dimeric structure, with two 3-coordinated Cu(I) centers: Cu1 and Cu1A, respectively, doubly bridged via the two [3,5-(CF$_3$)$_2$Pz]$^-$ ligands (via N1 and N2, and via N1A and N2A, respectively); moreover, both Cu(I) centers, Cu1 and Cu1A, respectively, are coordinated with 1,7-phen ligands via N3 and N3A, respectively. Although each respective 1,7-phen ligand contain two potential N binding sites (via N3 and N4, and N3A and N4A, respectively), the two Cu(I) centers only coordinate via N3 and N3A. N4 and N4A of the 1,7-phen ligands are not coordinated to either Cu(I) center. Overall, {Cu[3,5-(CF$_3$)$_2$Pz](1,7-phen)}$_2$ exhibits a heteroleptic, dinuclear complex with two double bridging [3,5-(CF$_3$)$_2$Pz]$^-$ ligands and two monodentate 1,7-phen ligands, which essentially serve as end caps.

Figure 56B shows the packing structure of $\{Cu[3,5-(CF_3)_2Pz](1,7\text{-phen})\}_2$. Table 5B shows the bond lengths (Å) and angles (°). The full-matrix least-squares refinement method was used on F^2, resulting in a goodness-of-fit value of 1.162 with R1 = 5.71 % and wR2 = 13.14% for all data.

Table 5. (A) X-ray Crystallographic Data for {Cu[3,5-$(CF_3)_2$Pz](1,7-phen)}$_2$; **(B)** Bond lengths [Å] and angles [°] for {Cu[3,5-$(CF_3)_2$Pz](1,7-phen)}$_2$.

Empirical formula	C34 H18 Cu2 F12 N8
Formula weight	893.64
Temperature	100.00(10) K
Wavelength	0.71073 Å
Crystal system	Monoclinic
Space group	P 1 21/n 1
Unit cell dimensions	a = 9.9749(3) Å α = 90°. b = 6.0080(2) Å β = 95.975(2)°. c = 27.5128(7) Å γ = 90°.
Volume	1639.86(8) Å^3
Z	2
Density (calculated)	1.810 Mg/m^3
Absorption coefficient	1.407 mm^{-1}
F(000)	888
Crystal size	0.08 x 0.04 x 0.03 mm^3
Theta range for data collection	2.109 to 27.102°.
Index ranges	-12<=h<=12, -7<=k<=7, -35<=l<=35
Reflections collected	24885
Independent reflections	3603 [R(int) = 0.0647]
Completeness to theta = 25.242°	100.0 %
Absorption correction	Semi-empirical from equivalents
Max. and min. transmission	1.00000 and 0.67796
Refinement method	Full-matrix least-squares on F^2
Data / restraints / parameters	3603 / 0 / 253
Goodness-of-fit on F^2	1.162
Final R indices [I>2sigma(I)]	R1 = 0.0494, wR2 = 0.1268
R indices (all data)	R1 = 0.0571, wR2 = 0.1314
Extinction coefficient	n/a
Largest diff. peak and hole	1.316 and -0.670 e.Å^{-3}

(A)

Bond Lengths [Å] (*blue*)		&	Angles [°] (*red*)	
Cu(1)-N(1)	1.967(3)	C(15)-H(15)	0.93	F(6)-C(5)-C(3)	112.8(3)
Cu(1)-N(2)#1	1.975(3)	C(15)-C(16)	1.348(4)	N(3)-C(6)-H(6)	118.1
Cu(1)-N(3)	1.997(3)	C(16)-H(16)	0.93	N(3)-C(6)-C(7)	123.9(3)
F(1)-C(4)	1.342(4)	C(16)-C(17)	1.427(4)	C(7)-C(6)-H(6)	118.1
F(2)-C(4)	1.348(4)	N(1)-Cu(1)-N(2)#1	117.34(10)	C(6)-C(7)-H(7)	120.7
F(3)-C(4)	1.339(4)	N(1)-Cu(1)-N(3)	119.83(11)	C(8)-C(7)-C(6)	118.7(3)
F(4)-C(5)	1.339(4)	N(2)#1-Cu(1)-N(3)	121.78(10)	C(8)-C(7)-H(7)	120.7
F(5)-C(5)	1.337(4)	N(2)-N(1)-Cu(1)	119.2(2)	C(7)-C(8)-H(8)	120.4
F(6)-C(5)	1.350(4)	C(1)-N(1)-Cu(1)	133.3(2)	C(7)-C(8)-C(9)	119.3(3)
N(1)-N(2)	1.371(3)	C(1)-N(1)-N(2)	107.1(2)	C(9)-C(8)-H(8)	120.4
N(1)-C(1)	1.338(4)	N(1)-N(2)-Cu(1)#1	121.95(19)	C(8)-C(9)-C(10)	123.3(3)
N(2)-C(3)	1.344(4)	C(3)-N(2)-Cu(1)#1	130.4(2)	C(8)-C(9)-C(17)	118.5(3)
N(3)-C(6)	1.318(4)	C(3)-N(2)-N(1)	107.2(2)	C(17)-C(9)-C(10)	118.2(3)
N(3)-C(17)	1.372(4)	C(6)-N(3)-Cu(1)	124.0(2)	N(4)-C(10)-C(9)	117.3(3)
N(4)-C(10)	1.361(4)	C(6)-N(3)-C(17)	118.3(3)	N(4)-C(10)-C(14)	122.9(3)
N(4)-C(11)	1.333(4)	C(17)-N(3)-Cu(1)	117.2(2)	C(14)-C(10)-C(9)	119.8(3)
C(1)-C(2)	1.384(4)	C(11)-N(4)-C(10)	116.6(3)	N(4)-C(11)-H(11)	117.6
C(1)-C(4)	1.489(4)	N(1)-C(1)-C(2)	111.7(3)	N(4)-C(11)-C(12)	124.8(3)
C(2)-H(2)	0.93	N(1)-C(1)-C(4)	121.5(3)	C(12)-C(11)-H(11)	117.6
C(2)-C(3)	1.383(4)	C(2)-C(1)-C(4)	126.8(3)	C(11)-C(12)-H(12)	120.8
C(3)-C(5)	1.489(4)	C(1)-C(2)-H(2)	128.7	C(13)-C(12)-C(11)	118.4(3)
C(6)-H(6)	0.93	C(3)-C(2)-C(1)	102.7(3)	C(13)-C(12)-H(12)	120.8
C(6)-C(7)	1.403(4)	C(3)-C(2)-H(2)	128.7	C(12)-C(13)-H(13)	120.5
C(7)-H(7)	0.93	N(2)-C(3)-C(2)	111.4(3)	C(12)-C(13)-C(14)	119.1(3)
C(7)-C(8)	1.376(4)	N(2)-C(3)-C(5)	120.6(3)	C(14)-C(13)-H(13)	120.5
C(8)-H(8)	0.93	C(2)-C(3)-C(5)	128.0(3)	C(10)-C(14)-C(13)	118.1(3)
C(8)-C(9)	1.403(5)	F(1)-C(4)-F(2)	105.8(2)	C(10)-C(14)-C(15)	119.7(3)
C(9)-C(10)	1.454(4)	F(1)-C(4)-C(1)	113.1(3)	C(13)-C(14)-C(15)	122.1(3)
C(9)-C(17)	1.416(4)	F(2)-C(4)-C(1)	112.7(3)	C(14)-C(15)-H(15)	119.6
C(10)-C(14)	1.403(5)	F(3)-C(4)-F(1)	107.1(3)	C(16)-C(15)-C(14)	120.8(3)
C(11)-H(11)	0.93	F(3)-C(4)-F(2)	106.6(3)	C(16)-C(15)-H(15)	119.6
C(11)-C(12)	1.397(5)	F(3)-C(4)-C(1)	111.0(3)	C(15)-C(16)-H(16)	119.4
C(12)-H(12)	0.93	F(4)-C(5)-F(6)	106.6(2)	C(15)-C(16)-C(17)	121.1(3)
C(12)-C(13)	1.371(5)	F(4)-C(5)-C(3)	111.2(3)	C(17)-C(16)-H(16)	119.4
C(13)-H(13)	0.93	F(5)-C(5)-F(4)	106.8(3)	N(3)-C(17)-C(9)	121.3(3)
C(13)-C(14)	1.412(4)	F(5)-C(5)-F(6)	106.3(3)	N(3)-C(17)-C(16)	118.4(3)
C(14)-C(15)	1.436(4)	F(5)-C(5)-C(3)	112.8(2)	C(9)-C(17)-C(16)	120.2(3)
Symmetry transformations used to generate equivalent atoms:					
#1 -x+1,-y+1,-z+1					

(B)

Figure 56. Crystal Structure of {Cu[3,5-(CF$_3$)$_2$Pz](1,7-phen)}$_2$: **(A)** Symmetric Unit Cell and **(B)** Packing.

3.2.3.2 Elemental Analysis Data

In this section, the elemental analysis data are discussed, comparing the experimentally found data with the theoretical Anal. Calc. (see Table 6). The theoretical percentages of carbon (C), hydrogen (H), and nitrogen (N) were analytically calculated (Anal. Calc.) based on the empirical formula C34 H18 Cu2 F12 N8 (MW = 893.64g/mol): C, 45.70; H, 2.03; N, 12.54. The experimentally found data for the solvent-mediated powder (C, 45.79; H, 1.77; N, 12.31) relatively match that of the theoretical Anal. Calc. within ±0.09 for C, ±0.26 for H, and ±0.23 for N. The experimentally found data for the crude solventless powder (C, 47.44; H, 2.00; N, 12.33) is similar to the theoretical Anal. Calc., particularly for H and N (within ±0.03 and ±0.21, respectively); however, it differs significantly for C (within ±1.74). The experimentally found data for crystals (C, 45.84; H, 2.00; N, 12.46 relatively match that of the theoretical Anal. Calc. within ±0.14 for C, ±0.03 for H, and ±0.08 for N. The elemental analysis data for $\{Cu[3,5-(CF_3)_2Pz](1,7-phen)\}_2$ solvent-mediated powder and crystals are very similar and confirms that they are the same product. The elemental analysis data for $\{Cu[3,5-(CF_3)_2Pz](1,7-phen)\}_2$ solventless powder (crude) shows that impurities are present, which are attributed to the presence of excess 1,7-phen ligand with $\{Cu[3,5-(CF_3)_2Pz](1,7-phen)\}_2$ in a 1:4 molar ratio (approximately).

Table 6. Elemental analysis data for {Cu[3,5-(CF$_3$)$_2$Pz](1,7-phen)}$_2$ solvent-mediated powder, solventless powder, and crystals: theoretical Anal. Calc. versus experimentally found data.

Elemental Analysis				
{Cu[3,5-(CF$_3$)$_2$Pz](1,7-phen)}$_2$ = C34 H18 Cu2 F12 N8				
		Solvent-Mediated	Solventless	Crystals
Element	Theoretical Anal. Calc.	Experimentally Found	Experimentally Found	Experimentally Found
C	45.70%	45.79%	47.44%	45.84%
H	2.03%	1.77%	2.00%	2.00%
N	12.54%	12.31%	12.33%	12.46%
Cu	14.22%			

3.2.3.3 Characterization using FT-IR Spectroscopy

In this section, the IR spectra for {Cu[3,5-(CF$_3$)$_2$Pz](1,7-phen)}$_2$ solvent-mediated powder, solventless powder, and crystals, as shown in Figure 57, are discussed. The IR spectra for solvent-mediated powder, solventless powder, and crystals are relatively identical to one another and feature the functional groups characteristic of both the [3,5-(CF$_3$)$_2$Pz]$^-$ and 4,7-phen ligands: =C-H stretch (aromatic), C=C stretch (aromatic), C=N stretch (aromatic), C-C stretch (aromatic), C-N stretch (aromatic), and C-F stretch.

Functional Groups	Expected Range (cm^{-1})
=C-H stretch (aromatic)	3010-3100, 690-900
C=C stretch (aromatic)	1400, 1600
C=N stretch (aromatic)	1400-1620
C-C stretch (aromatic)	1400-1500
C-N stretch (aromatic)	1250-1335
C-F stretch	1000-1400
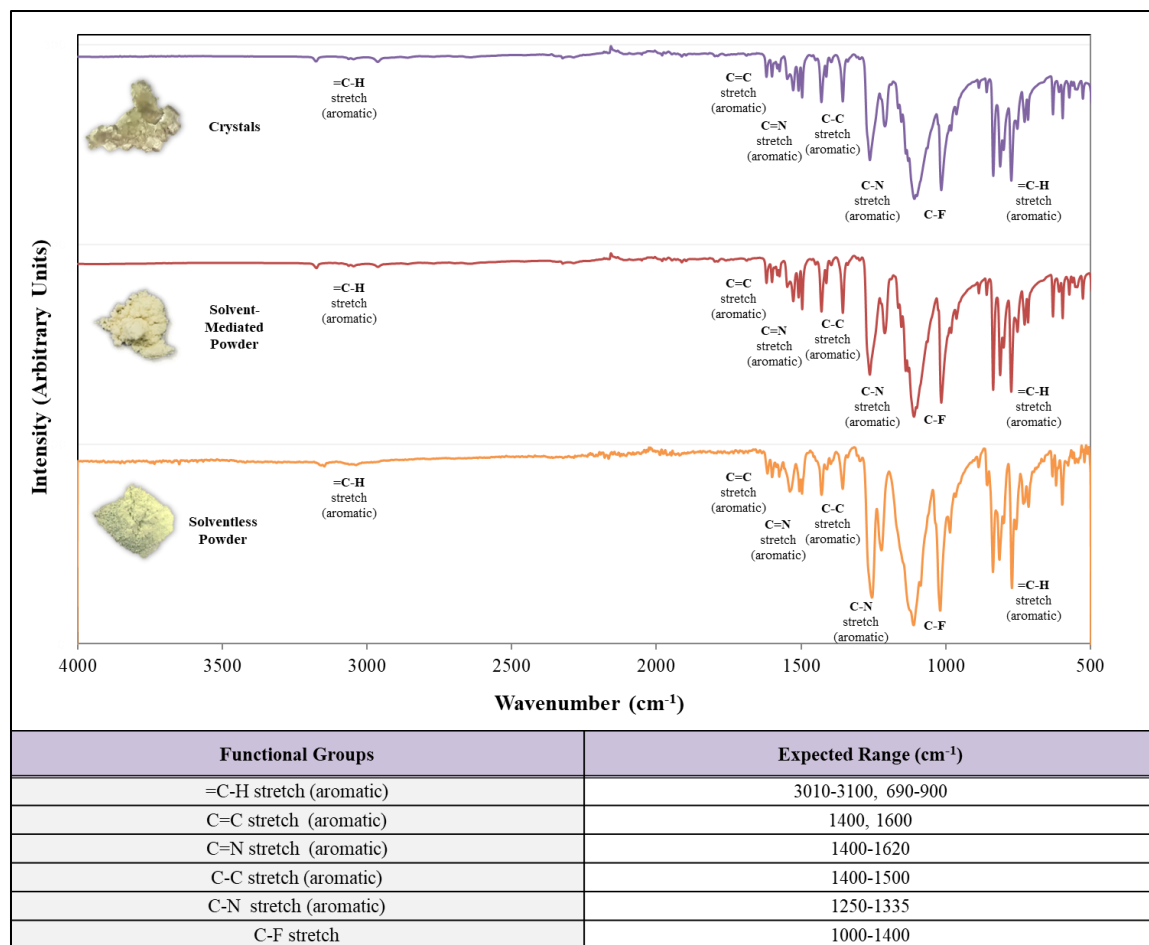
Figure 57. Stacked FT-IR spectra for {Cu[3,5-(CF$_3$)$_2$Pz](1,7-phen)}$_2$ crystals (*top*), solvent-mediated powder (*middle*), solventless powder (*bottom*).

3.2.3.4 Characterization using TGA Analyses

In this section, the TGA analyses for {Cu[3,5-(CF$_3$)$_2$Pz](1,7-phen)}$_2$ solvent-mediated powder and solventless powder, shown in Figures 58 and 59, respectively, are discussed.

The TGA analyses of solvent-mediated powder and solventless powder are relatively similar to one another with regard to onset temperatures and inflection points; however, they differ significantly in the percent weight loss (for the first weight drops)

122

and the total weight loss. The solvent-mediated powder and solventless powder, respectively, show significant weight losses of 97.34%, and 88.92%, respectively, for the first weight drop, followed by 1.442% and 2.507%, respectively, for the second weight drop, resulting in total weight losses of 98.78% and 91.42%, respectively. For the first weight drops, onset temperatures (the temperatures at which weight loss begins) of 230.70°C and 233.67°C, respectively, and 1st derivative peaks (greatest rate of change on the weight loss curves) of 261.53% and 262.71%, respectively, were observed. The slight difference in onset temperatures and 1st derivative peaks (inflection points) may be attributed to the differences in sample size for the solvent-mediated powder and solventless powder: 11.6550 mg and 11.8980 mg, respectively, in that as the sample size increases, an increase (shift) in temperature occurs.

With regard to the emperical formula C34 H18 Cu2 F12 N8 (MW = 893.64 g/mol), the theoretical percentage of copper is 14.22%; however, the total weight losses of 98.36%, and 91.42%, respectively, were observed, which were primarily due to the sublimation of the $[3,5\text{-}(CF_3)_2Pz]^-$ and 1,7-phen ligands (total theoretical percentage of C, H, N and F of 85.78%). The remaining weight percentages, 1.64% and 8.58%, respectively, following the aforementioned weight losses (after heating up to 800°C) should theoretically be copper.

In comparison between the solvent-mediated powder and solventless powder, respectively, the solventless powder retains an additional weight percentage of 8.42% after the first (significant) weight drop, despite having a similar onset temperature and inflection point as the solvent-mediated powder. Moreover, after the second weight drop,

the solventless powder retains an additional weight percentage of 6.94%. The additional weight percentages are impurities most likely related to the presence of excess 1,7-phenanthroline ligand (sublimes between 194°C and 237°C).
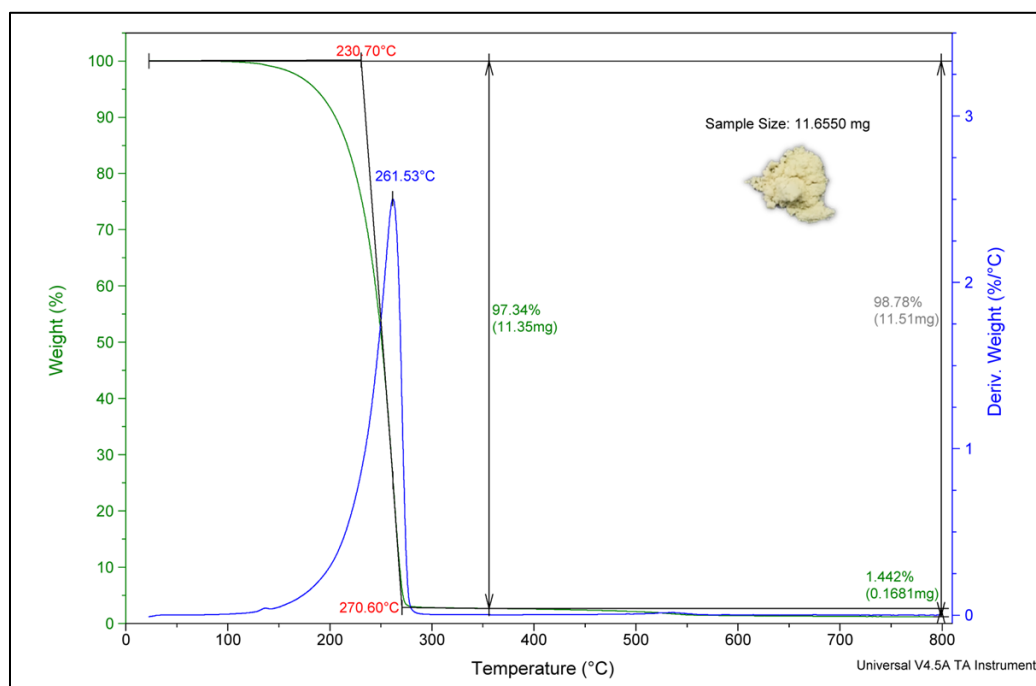
Figure 58. TGA analysis for {Cu[3,5-$(CF_3)_2$Pz](1,7-phen)}$_2$ solvent-mediated powder.
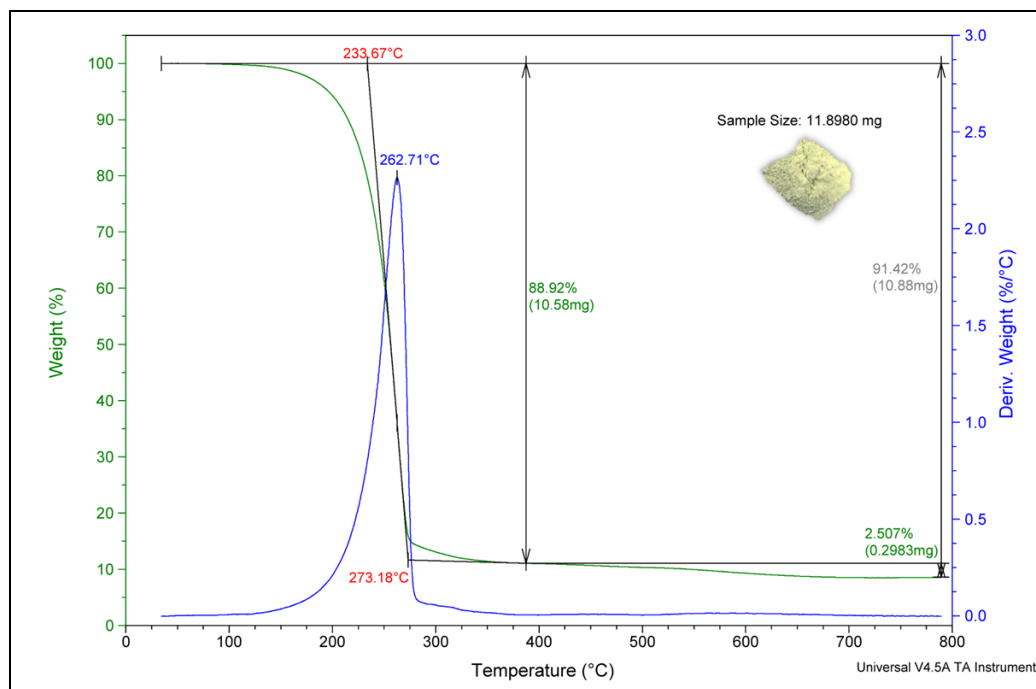
Figure 59. TGA analysis for {Cu[3,5-(CF$_3$)$_2$Pz](1,7-phen)}$_2$ solventless powder.

3.2.3.5 Characterization using Photoluminescence and UV-Vis Absorption Spectroscopy

In this section, the photoluminescence and UV-Vis absorption spectroscopy of {Cu[3,5-(CF$_3$)$_2$Pz](1,7-phen)}$_2$ solvent-mediated powder are discussed.

As shown in Figure 60, the solvent-mediated powder, solventless powder, and crystals were checked under a handheld UV lamp for photoluminescence, under Short Wave UV (λ_{ex} = 254 nm) and Long Wave UV (λ_{ex} = 365 nm), at room temperature (RT). At RT, yellow photoluminescence was observed under 254 nm and 365 nm for solvent-mediated powder, solventless powder, and crystals; however, the solventless power exhibited strong, yellow photoluminescence, while the solvent-mediated powder and crystals exhibited weak, yellow photoluminescence. As shown in Figure 61, at 77K, the

125

yellow photoluminescence for both solvent-mediated powder, solventless powder became significantly more intense (more bright), especially under 365 nm. Solventless powder exhibited the most intense photoluminescence under 254 nm and 365 nm and was used to measure photoluminescence and lifetime decay.

As shown in Figures 62 and 63, at RT, the photoluminescence of the $\{Cu[3,5-(CF_3)_2Pz](1,7\text{-}phen)\}_2$ solventless powder (solid) was measured using an excitation wavelength of $\lambda_{ex} = 321$ nm, producing an emission band with a maximum emission peak at $\lambda_{em} = 568$ nm. A photoluminescence decay curve for the emission at $\lambda_{em} = 568$ nm was fitted with a Chi2 value of 1.014, a Durbin Watson value of 1.787, and a Z value of -0.0406. The photoluminescence observed at RT is characterized as fluorescence ($<10^{-5}$ s) based on the lifetimes (τ) of 7.529 µs.

As shown in Figures 62-64, at 77K, the photoluminescence of the $\{Cu[3,5-(CF_3)_2Pz](1,7\text{-}phen)\}_2$ solventless powder (solid) was measured using an excitation wavelength of $\lambda_{ex} = 343$ nm, producing an emission band with a maximum emission peak at $\lambda_{em} = 572$ nm. A photoluminescence decay curve for the emission at $\lambda_{em} = 572$ nm was fitted with a Chi2 value of 1.044, a Durbin Watson value of 1.769, and a Z value of 6.333×10^{-5} (0.00006333). The photoluminescence observed at 77 K is characterized as phosphorescence ($>10^{-5}$ s) based on the lifetimes (τ) of 25.54 µs.
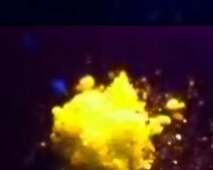
Figure 60. Photoluminescence of {Cu[3,5-(CF$_3$)$_2$Pz](1,7-phen)}$_2$ crystals (*top*), solvent-mediated powder (*middle*), and solventless powder (*bottom*) under Short Wave UV (λ_{ex} = 254 nm) and Long Wave UV (λ_{ex} = 365 nm), at room temperature (RT).
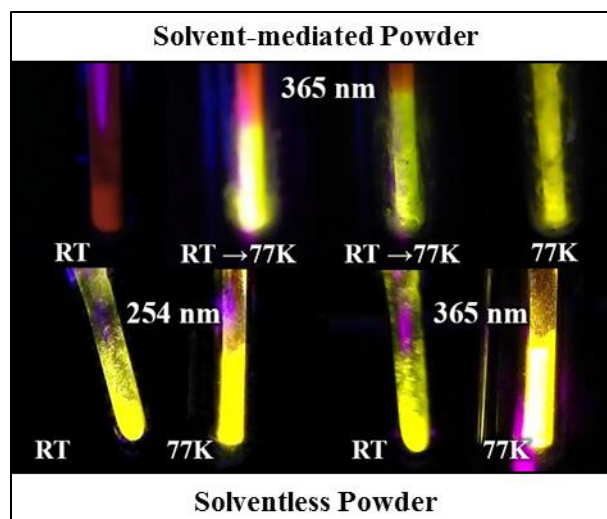
Figure 61. Photoluminescence of {Cu[3,5-(CF$_3$)$_2$Pz](1,7-phen)}$_2$ solvent-mediated powder (*top*) and solventless powder (*bottom*) under Short Wave UV (λ_{ex} = 254 nm) and Long Wave UV (λ_{ex} = 365 nm), at room temperature (RT) vs. cryogenic temperature (77K).
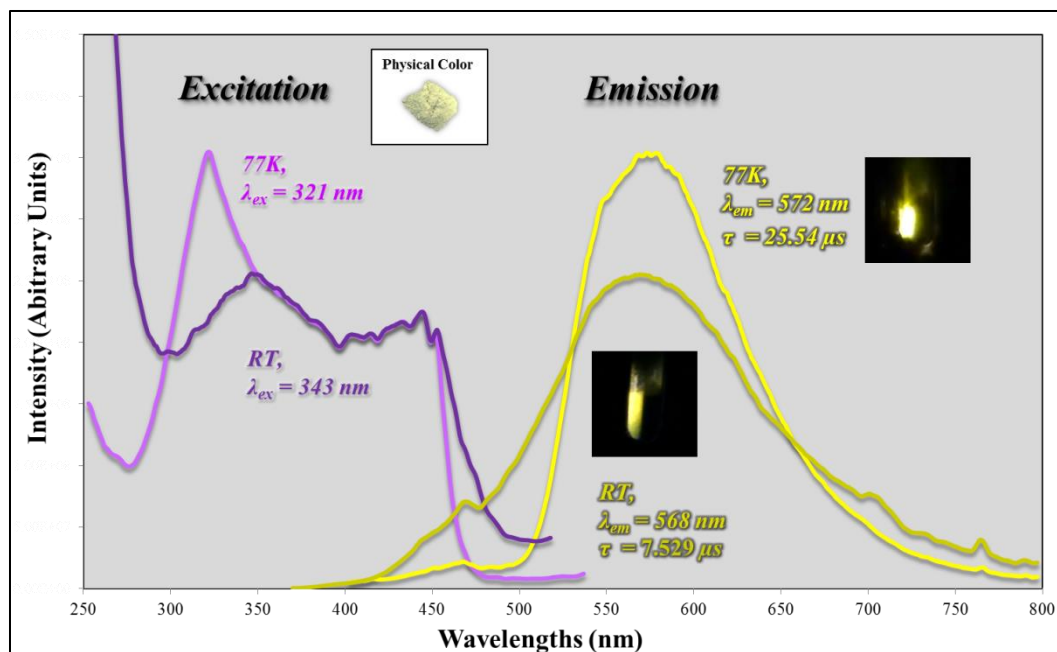
Figure 62. Photoluminescence spectra for $\{Cu[3,5-(CF_3)_2Pz](1,7\text{-phen})\}_2$, solventless powder, at room temperature (RT) vs. cryogenic temperature (77K).
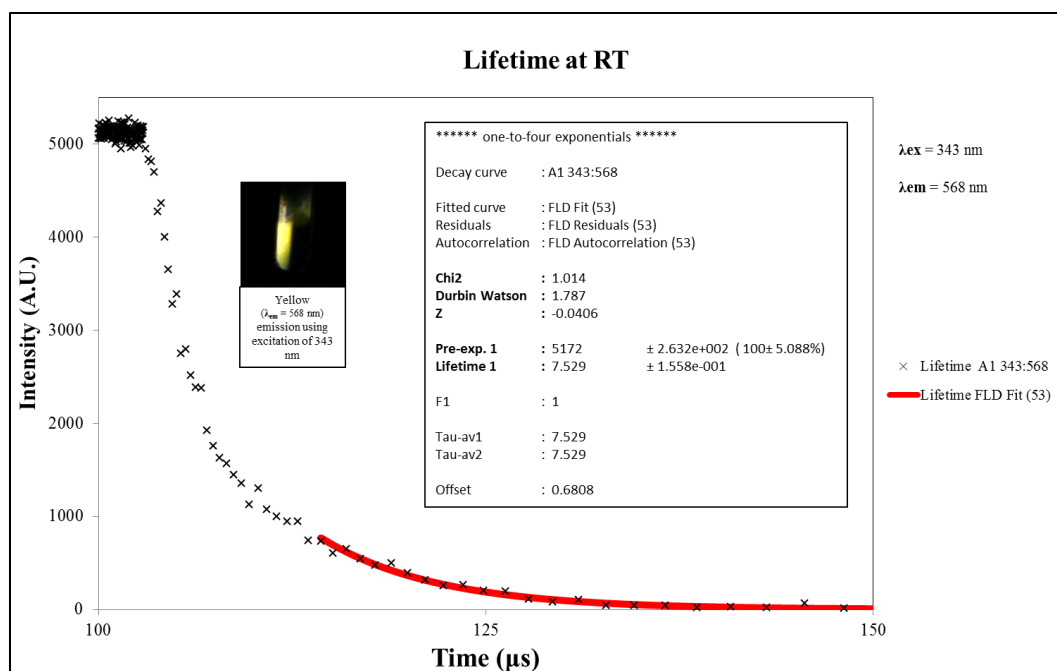
Figure 63. Photoluminescence lifetime decay curve for $\{Cu[3,5-(CF_3)_2Pz](1,7\text{-phen})\}_2$ solventless powder, at room temperature (RT).
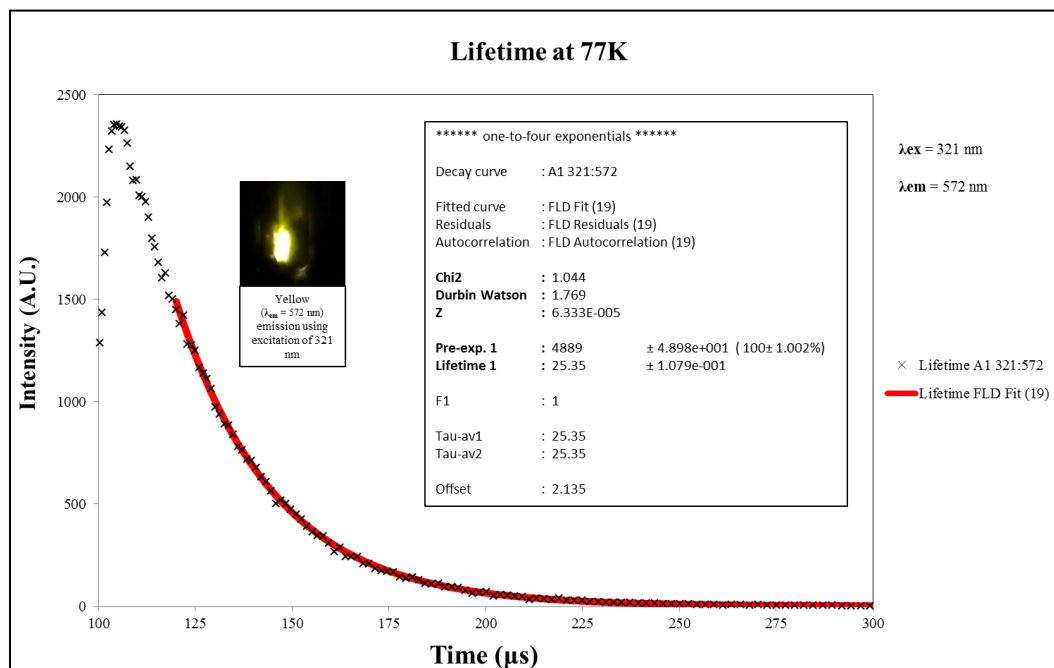
Figure 64. Photoluminescence lifetime decay curve for $\{Cu[3,5\text{-}(CF_3)_2Pz](1,7\text{-phen})\}_2$ solventless powder, at cryogenic temperature (77K).

The UV-Vis absorption spectra for $\{Cu[3,5\text{-}(CF_3)_2Pz](1,7\text{-phen})\}_2$, shown in Figure 65, were obtained using three dilutions in hexane (UV cutoff wavelength = 195 nm): 1×10^{-3} M, 1×10^{-4} M, and 1×10^{-5} M. A red shift was observed as the concentration increased, shifting more toward the visible region (up to 450 nm), as well as $\pi\text{-}\pi^*$ transition with an extinction coefficient (ε_{267}) of 38917 L·mol^{-1}·cm^{-1} (λ_{max2} = 267 nm: A = 0.934, C = 2.4×10^{-5} M).
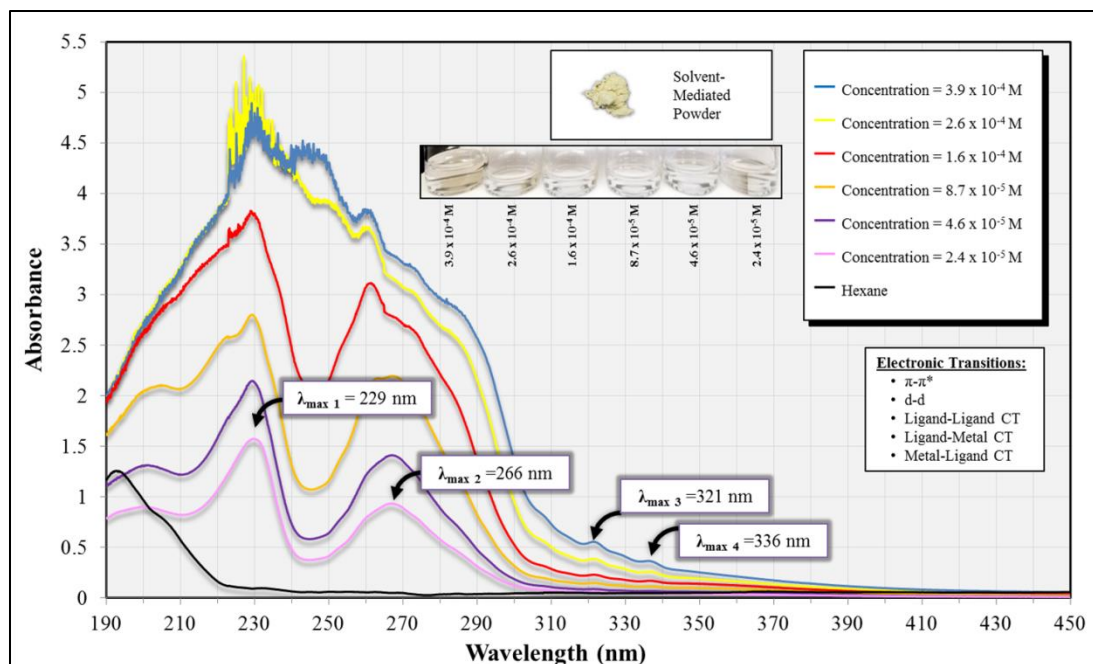
(A)
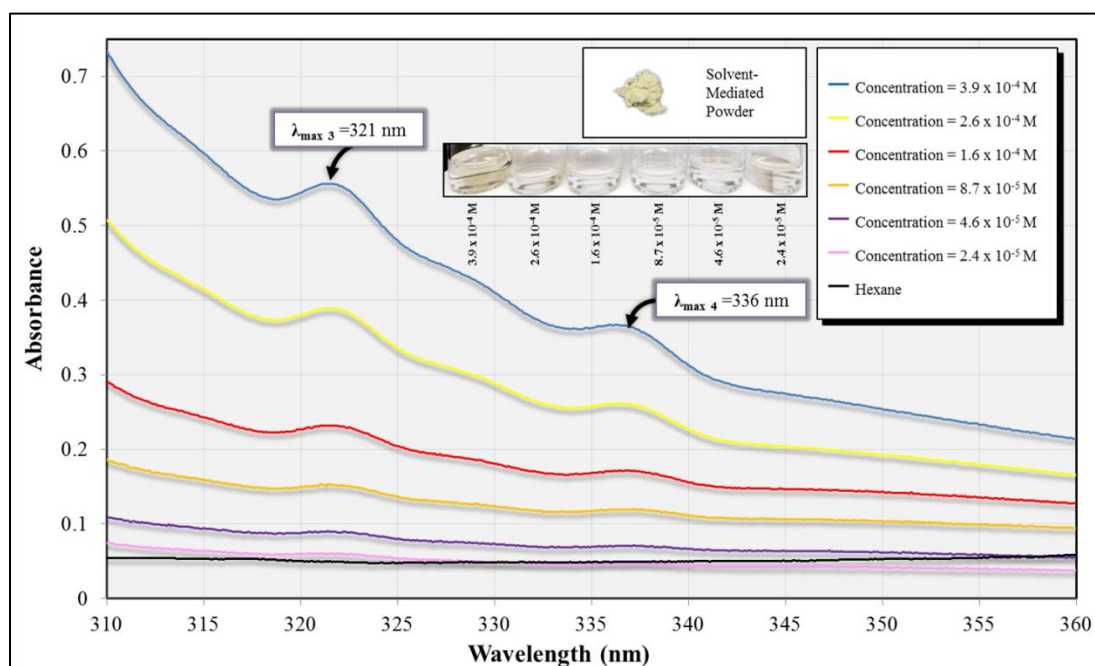
(B)

Figure 65. UV-Vis Spectra for $\{Cu[3,5-(CF_3)_2Pz](1,7-phen)\}_2$ solvent-mediated powder in hexane solutions (UV cutoff wavelength = 210 nm): **(A)** Full-View = 190-450 nm; **(B)** Zoomed-In = 310-360 nm.

3.2.4.1 X-ray Crystallographic Data

In this section, the X-ray crystallographic data for Ag$_2$[3,5-(CF$_3$)$_2$Pz]$_2$(1,7-phen)$_3$ (see Tables 7A-B) are discussed. Ag$_2$[3,5-(CF$_3$)$_2$Pz]$_2$(1,7-phen)$_3$ single crystals were obtained using solvent-mediated powder (synthesized using hexane). Table 7A shows that Ag$_2$[3,5-(CF$_3$)$_2$Pz]$_2$(1,7-phen)$_3$ crystallizes in the triclinic crystal system with the space group *P*-1 with Z = 2 and the unit cell dimensions: a = 10.23310(10) Å, b = 14.5834(3) Å, c = 14.8482(3) Å, α = 97.358(2)°, β = 97.1520(10)°, and γ = 104.9420(10)°. Ag$_2$[3,5-(CF$_3$)$_2$Pz]$_2$(1,7-phen)$_3$ has the empirical formula C46 H26 Ag2 F12 N10 (MW = 1162.51 g/mol).

As shown in Figure 66A, the asymmetric unit cell of Ag$_2$[3,5-(CF$_3$)$_2$Pz]$_2$(1,7-phen)$_3$ exhibits a Ag(I) dimeric structure with 3- and 4-coordinated Ag(I) centers: Ag1 and Ag2, respectively, doubly bridged via the two [3,5-(CF$_3$)$_2$Pz]$^-$ ligands (via N1 and N2, and via N3 and N4, respectively). Moreover, the 3-coordinated Ag(I) center, Ag1, is coordinated with one 1,7-phen ligand via N7; meanwhile, the 4-coordinated Ag(I) center, Ag2, is coordinated with two 1,7-phen ligands via N5 and N9. Although each respective 1,7-phen ligand contains two potential N binding sites (via N5 and N6, N7 and N8, and N9 and N10, respectively), the two Ag(I) centers only coordinate via N5, N7, and N9, N6, N8, and N10 of the 1,7-phen ligands are not coordinated to either Ag(I) center.

Figure 66B-D show the packing structure of $Ag_2[3,5-(CF_3)_2Pz]_2(1,7-phen)_3$, which exhibits $[Ag2Ar2]$ π-π stacked pairs, as well as an End-Ar π-π stacked pair. Table 7B shows the bond lengths (Å) and angles (°). The full-matrix least-squares refinement method was used on F^2, resulting in a goodness-of-fit value of 1.057 with R1 = 2.08 % and wR2 = 5.19% for all data.

Table 7. (A) X-ray Crystallographic Data for $Ag_2[3,5-(CF_3)_2Pz]_2(1,7\text{-phen})_3$; **(B)** Bond lengths [Å] and angles [°] for $Ag_2[3,5-(CF_3)_2Pz]_2(1,7\text{-phen})_3$.

Empirical formula	C46 H26 Ag2 F12 N10
Formula weight	1162.51
Temperature	100.00(10) K
Wavelength	0.71073 Å
Crystal system	Triclinic
Space group	P-1
Unit cell dimensions	a = 10.23310(10) Å α = 97.358(2)°. b = 14.5834(3) Å β = 97.1520(10)°. c = 14.8482(3) Å γ = 104.9420(10)°.
Volume	2094.41(7) Å^3
Z	2
Density (calculated)	1.843 Mg/m^3
Absorption coefficient	1.039 mm^{-1}
F(000)	1148
Crystal size	0.09 x 0.03 x 0.02 mm^3
Theta range for data collection	2.088 to 27.101°.
Index ranges	-13<=h<=13, -18<=k<=18, -19<=l<=19
Reflections collected	91279
Independent reflections	9227 [R(int) = 0.0326]
Completeness to theta = 25.242°	100.0 %
Absorption correction	Semi-empirical from equivalents
Max. and min. transmission	1.00000 and 0.91617
Refinement method	Full-matrix least-squares on F^2
Data / restraints / parameters	9227 / 0 / 631
Goodness-of-fit on F^2	1.057
Final R indices [I>2sigma(I)]	R1 = 0.0191, wR2 = 0.0511
R indices (all data)	R1 = 0.0208, wR2 = 0.0519
Extinction coefficient	n/a
Largest diff. peak and hole	0.549 and -0.301 e.Å^{-3}

(A)

Bond Lengths [Å] (blue)		& Angles [°] (red)		
Ag(1)-N(2)	2.2633(12)	C(40)-C(41)	1.405(2)	N(6)-C(15)-C(14)	117.65(13)
Ag(1)-N(4)	2.2485(13)	C(41)-H(41)	0.93	N(6)-C(15)-C(19)	123.01(14)
Ag(1)-N(7)	2.2175(13)	C(41)-C(42)	1.372(2)	C(19)-C(15)-C(14)	119.34(13)
Ag(2)-N(1)	2.3381(12)	C(42)-H(42)	0.93	N(6)-C(16)-H(16)	117.7
Ag(2)-N(3)	2.3147(12)	C(42)-C(43)	1.414(2)	N(6)-C(16)-C(17)	124.62(15)
Ag(2)-N(5)	2.4971(13)	C(43)-C(44)	1.432(2)	C(17)-C(16)-H(16)	117.7
Ag(2)-N(9)	2.3139(13)	C(44)-H(44)	0.93	C(16)-C(17)-H(17)	120.8
F(1)-C(4)	1.3466(18)	C(44)-C(45)	1.361(2)	C(18)-C(17)-C(16)	118.47(14)
F(2)-C(4)	1.3322(17)	C(45)-H(45)	0.93	C(18)-C(17)-H(17)	120.8
F(3)-C(4)	1.3471(18)	C(45)-C(46)	1.433(2)	C(17)-C(18)-H(18)	120.4
F(4)-C(5)	1.3398(19)	N(4)-Ag(1)-N(2)	104.86(5)	C(17)-C(18)-C(19)	119.30(15)
F(5)-C(5)	1.3374(19)	N(7)-Ag(1)-N(2)	124.90(5)	C(19)-C(18)-H(18)	120.4
F(6)-C(5)	1.337(2)	N(7)-Ag(1)-N(4)	129.64(5)	C(15)-C(19)-C(20)	119.76(13)
F(7)-C(9)	1.3333(19)	N(1)-Ag(2)-N(5)	93.26(4)	C(18)-C(19)-C(15)	117.78(14)
F(8)-C(9)	1.337(2)	N(3)-Ag(2)-N(1)	106.94(4)	C(18)-C(19)-C(20)	122.46(14)
F(9)-C(9)	1.347(2)	N(3)-Ag(2)-N(5)	99.01(4)	C(19)-C(20)-H(20)	119.4
F(10)-C(10)	1.3377(19)	N(9)-Ag(2)-N(1)	123.94(4)	C(21)-C(20)-C(19)	121.12(14)
F(11)-C(10)	1.3348(19)	N(9)-Ag(2)-N(3)	124.79(4)	C(21)-C(20)-H(20)	119.4
F(12)-C(10)	1.3419(19)	N(9)-Ag(2)-N(5)	98.11(4)	C(20)-C(21)-H(21)	119.8
N(1)-N(2)	1.3572(17)	N(2)-N(1)-Ag(2)	115.07(9)	C(20)-C(21)-C(22)	120.49(14)
N(1)-C(1)	1.3493(19)	C(1)-N(1)-Ag(2)	136.34(10)	C(22)-C(21)-H(21)	119.8
N(2)-C(3)	1.3490(19)	C(1)-N(1)-N(2)	107.03(12)	N(5)-C(22)-C(14)	121.92(13)
N(3)-N(4)	1.3582(17)	N(1)-N(2)-Ag(1)	118.38(9)	N(5)-C(22)-C(21)	117.90(13)
N(3)-C(6)	1.3456(19)	C(3)-N(2)-Ag(1)	132.88(10)	C(14)-C(22)-C(21)	120.18(13)
N(4)-C(8)	1.340(2)	C(3)-N(2)-N(1)	107.72(12)	N(7)-C(23)-H(23)	118.3
N(5)-C(11)	1.328(2)	N(4)-N(3)-Ag(2)	116.78(9)	N(7)-C(23)-C(24)	123.35(14)
N(5)-C(22)	1.3698(19)	C(6)-N(3)-Ag(2)	136.29(10)	C(24)-C(23)-H(23)	118.3
N(6)-C(15)	1.361(2)	C(6)-N(3)-N(4)	106.91(12)	C(23)-C(24)-H(24)	120.4
N(6)-C(16)	1.327(2)	N(3)-N(4)-Ag(1)	116.03(9)	C(25)-C(24)-C(23)	119.30(14)
N(7)-C(23)	1.334(2)	C(8)-N(4)-Ag(1)	133.59(10)	C(25)-C(24)-H(24)	120.4
N(7)-C(34)	1.3691(19)	C(8)-N(4)-N(3)	107.92(12)	C(24)-C(25)-H(25)	120.5
N(8)-C(27)	1.358(2)	C(11)-N(5)-Ag(2)	118.11(10)	C(24)-C(25)-C(26)	118.92(14)
N(8)-C(28)	1.330(2)	C(11)-N(5)-C(22)	117.73(13)	C(26)-C(25)-H(25)	120.5
N(9)-C(35)	1.330(2)	C(22)-N(5)-Ag(2)	124.16(10)	C(25)-C(26)-C(27)	122.00(14)
N(9)-C(46)	1.3763(19)	C(16)-N(6)-C(15)	116.83(14)	C(25)-C(26)-C(34)	118.75(14)
N(10)-C(39)	1.356(2)	C(23)-N(7)-Ag(1)	118.72(10)	C(34)-C(26)-C(27)	119.24(13)
N(10)-C(40)	1.329(2)	C(23)-N(7)-C(34)	118.17(13)	N(8)-C(27)-C(26)	117.03(14)
C(1)-C(2)	1.384(2)	C(34)-N(7)-Ag(1)	122.44(10)	N(8)-C(27)-C(31)	123.43(14)
C(1)-C(4)	1.485(2)	C(28)-N(8)-C(27)	116.71(14)	C(31)-C(27)-C(26)	119.53(13)
C(2)-H(2)	0.93	C(35)-N(9)-Ag(2)	114.22(10)	N(8)-C(28)-H(28)	117.9
C(2)-C(3)	1.385(2)	C(35)-N(9)-C(46)	117.64(13)	N(8)-C(28)-C(29)	124.27(15)
C(3)-C(5)	1.482(2)	C(46)-N(9)-Ag(2)	128.02(10)	C(29)-C(28)-H(28)	117.9
C(6)-C(7)	1.387(2)	C(40)-N(10)-C(39)	117.06(13)	C(28)-C(29)-H(29)	120.5
C(6)-C(9)	1.486(2)	N(1)-C(1)-C(2)	111.50(13)	C(30)-C(29)-C(28)	119.06(15)
C(7)-H(7)	0.93	N(1)-C(1)-C(4)	122.29(13)	C(30)-C(29)-H(29)	120.5
C(7)-C(8)	1.388(2)	C(2)-C(1)-C(4)	126.14(13)	C(29)-C(30)-H(30)	120.6
C(8)-C(10)	1.488(2)	C(1)-C(2)-H(2)	128.6	C(29)-C(30)-C(31)	118.83(15)
C(11)-H(11)	0.93	C(1)-C(2)-C(3)	102.71(13)	C(31)-C(30)-H(30)	120.6
C(11)-C(12)	1.404(2)	C(3)-C(2)-H(2)	128.6	C(27)-C(31)-C(30)	117.70(14)
C(12)-H(12)	0.93	N(2)-C(3)-C(2)	111.03(13)	C(27)-C(31)-C(32)	119.44(14)
C(12)-C(13)	1.374(2)	N(2)-C(3)-C(5)	120.43(13)	C(30)-C(31)-C(32)	122.85(14)
C(13)-H(13)	0.93	C(2)-C(3)-C(5)	128.53(14)	C(31)-C(32)-H(32)	119.4

C(13)-C(14)	1.406(2)	F(1)-C(4)-F(3)	105.46(12)	C(33)-C(32)-C(31)	121.29(14)
C(14)-C(15)	1.448(2)	F(1)-C(4)-C(1)	112.08(12)	C(33)-C(32)-H(32)	119.4
C(14)-C(22)	1.415(2)	F(2)-C(4)-F(1)	106.92(12)	C(32)-C(33)-H(33)	119.6
C(15)-C(19)	1.411(2)	F(2)-C(4)-F(3)	107.32(12)	C(32)-C(33)-C(34)	120.78(14)
C(16)-H(16)	0.93	F(2)-C(4)-C(1)	113.54(12)	C(34)-C(33)-H(33)	119.6
C(16)-C(17)	1.401(2)	F(3)-C(4)-C(1)	111.05(12)	N(7)-C(34)-C(26)	121.47(13)
C(17)-H(17)	0.93	F(4)-C(5)-C(3)	111.68(13)	N(7)-C(34)-C(33)	118.82(13)
C(17)-C(18)	1.372(2)	F(5)-C(5)-F(4)	106.50(14)	C(26)-C(34)-C(33)	119.71(13)
C(18)-H(18)	0.93	F(5)-C(5)-F(6)	106.12(14)	N(9)-C(35)-H(35)	118
C(18)-C(19)	1.408(2)	F(5)-C(5)-C(3)	112.60(13)	N(9)-C(35)-C(36)	123.96(14)
C(19)-C(20)	1.436(2)	F(6)-C(5)-F(4)	106.06(13)	C(36)-C(35)-H(35)	118
C(20)-H(20)	0.93	F(6)-C(5)-C(3)	113.36(14)	C(35)-C(36)-H(36)	120.5
C(20)-C(21)	1.359(2)	N(3)-C(6)-C(7)	111.60(13)	C(37)-C(36)-C(35)	119.04(14)
C(21)-H(21)	0.93	N(3)-C(6)-C(9)	120.75(14)	C(37)-C(36)-H(36)	120.5
C(21)-C(22)	1.432(2)	C(7)-C(6)-C(9)	127.55(14)	C(36)-C(37)-H(37)	120.5
C(23)-H(23)	0.93	C(6)-C(7)-H(7)	128.8	C(36)-C(37)-C(38)	118.92(14)
C(23)-C(24)	1.399(2)	C(6)-C(7)-C(8)	102.36(13)	C(38)-C(37)-H(37)	120.5
C(24)-H(24)	0.93	C(8)-C(7)-H(7)	128.8	C(37)-C(38)-C(39)	121.72(14)
C(24)-C(25)	1.372(2)	N(4)-C(8)-C(7)	111.21(13)	C(37)-C(38)-C(46)	118.88(13)
C(25)-H(25)	0.93	N(4)-C(8)-C(10)	121.07(14)	C(46)-C(38)-C(39)	119.39(13)
C(25)-C(26)	1.406(2)	C(7)-C(8)-C(10)	127.70(14)	N(10)-C(39)-C(38)	117.37(13)
C(26)-C(27)	1.450(2)	F(7)-C(9)-F(8)	107.62(14)	N(10)-C(39)-C(43)	123.37(14)
C(26)-C(34)	1.414(2)	F(7)-C(9)-F(9)	106.10(14)	C(43)-C(39)-C(38)	119.25(13)
C(27)-C(31)	1.410(2)	F(7)-C(9)-C(6)	112.78(13)	N(10)-C(40)-H(40)	118
C(28)-H(28)	0.93	F(8)-C(9)-F(9)	105.92(14)	N(10)-C(40)-C(41)	124.01(15)
C(28)-C(29)	1.400(2)	F(8)-C(9)-C(6)	111.78(14)	C(41)-C(40)-H(40)	118
C(29)-H(29)	0.93	F(9)-C(9)-C(6)	112.20(14)	C(40)-C(41)-H(41)	120.5
C(29)-C(30)	1.372(2)	F(10)-C(10)-F(12)	106.95(14)	C(42)-C(41)-C(40)	118.96(15)
C(30)-H(30)	0.93	F(10)-C(10)-C(8)	112.46(13)	C(42)-C(41)-H(41)	120.5
C(30)-C(31)	1.412(2)	F(11)-C(10)-F(10)	106.57(14)	C(41)-C(42)-H(42)	120.5
C(31)-C(32)	1.435(2)	F(11)-C(10)-F(12)	106.13(13)	C(41)-C(42)-C(43)	118.94(14)
C(32)-H(32)	0.93	F(11)-C(10)-C(8)	113.56(13)	C(43)-C(42)-H(42)	120.5
C(32)-C(33)	1.356(2)	F(12)-C(10)-C(8)	110.73(13)	C(39)-C(43)-C(42)	117.65(14)
C(33)-H(33)	0.93	N(5)-C(11)-H(11)	118.1	C(39)-C(43)-C(44)	119.59(14)
C(33)-C(34)	1.435(2)	N(5)-C(11)-C(12)	123.72(14)	C(42)-C(43)-C(44)	122.76(14)
C(35)-H(35)	0.93	C(12)-C(11)-H(11)	118.1	C(43)-C(44)-H(44)	119.3
C(35)-C(36)	1.401(2)	C(11)-C(12)-H(12)	120.4	C(45)-C(44)-C(43)	121.36(14)
C(36)-H(36)	0.93	C(13)-C(12)-C(11)	119.26(14)	C(45)-C(44)-H(44)	119.3
C(36)-C(37)	1.371(2)	C(13)-C(12)-H(12)	120.4	C(44)-C(45)-H(45)	119.8
C(37)-H(37)	0.93	C(12)-C(13)-H(13)	120.6	C(44)-C(45)-C(46)	120.49(14)
C(37)-C(38)	1.407(2)	C(12)-C(13)-C(14)	118.72(14)	C(46)-C(45)-H(45)	119.8
C(38)-C(39)	1.452(2)	C(14)-C(13)-H(13)	120.6	N(9)-C(46)-C(38)	121.56(13)
C(38)-C(46)	1.410(2)	C(13)-C(14)-C(15)	122.25(13)	N(9)-C(46)-C(45)	118.54(13)
C(39)-C(43)	1.410(2)	C(13)-C(14)-C(22)	118.65(13)	C(38)-C(46)-C(45)	119.90(13)
C(40)-H(40)	0.93	C(22)-C(14)-C(15)	119.10(13)		
Symmetry transformations used to generate equivalent atoms:					

(B)
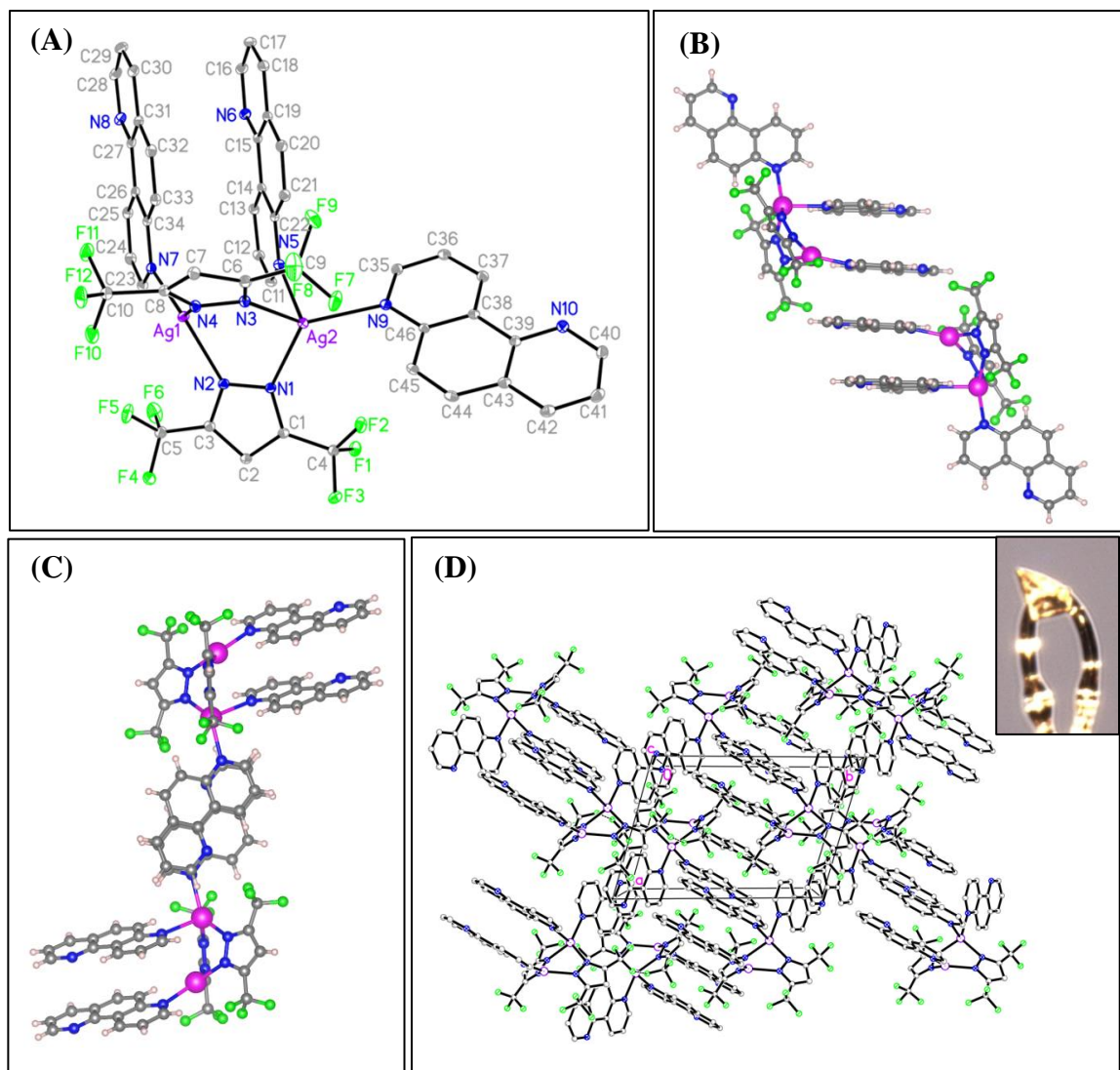
Figure 66. Crystal Structure of Ag$_2$[3,5-(CF$_3$)$_2$Pz]$_2$(1,7-phen)$_3$: **(A)** Asymmetric Unit Cell and **(B-D)** Packing.

3.2.4.2 Elemental Analysis Data

In this section, the elemental analysis data for $Ag_2[3,5-(CF_3)_2Pz]_2(1,7-phen)_n$, (n = 2 or 3) are discussed, comparing the experimentally found data with the theoretical Anal. Calc. values, shown in Table 8.

With regard to the $Ag_2[3,5-(CF_3)_2Pz]_2(1,7-phen)_3$ crystals (1*), the theoretical percentages of carbon (C), hydrogen (H), and nitrogen (N) were analytically calculated (Anal. Calc.) based on the empirical formula C46 H26 Ag2 F12 N10 (MW = 1162.51 g/mol): C, 47.53; H, 2.25; N, 12.05. The experimentally found data for the crystals (C, 47.20; H, 2.16; N, 11.84) relatively match that of the theoretical Anal. Calc. values within ±0.33 for C, ±0.09 for H, and ±0.21 for N.

With regard to the solvent-mediated powders, the empirical formula was adjusted in order to account for the presence of two of the three 1,7-phen ligands in the molecular structure, with the resulting structure resembling the Ag(I) analogue of {Cu[3,5-$(CF_3)_2Pz](1,7-phen)$}$_2$. The theoretical percentages of carbon (C), hydrogen (H), and nitrogen (N) were analytically calculated based on the empirical formula C34 H18 Ag2 F12 N8 (MW = 982.28 g/mol): C, 41.57; H, 1.85; N, 11.41. The experimentally found data for the solvent-mediated powder synthesized using hexane (C, 40.34; H, 1.78; N, 11.10) somewhat match that of the theoretical Anal. Calc. values within ±1.23 for C, ±0.07 for H, and ±0.31 for N. The experimentally found data for the crude (unwashed) solvent-mediated powder synthesized using benzene (C, 42.03; H, 1.67; N, 11.18)

relatively match that of the theoretical Anal. Calc. values within a difference of ±0.46 for C, ±0.18 for H, and ±0.23 for N.

The elemental analysis data for the crystals and the solvent-mediated powders are dramatically different, suggesting that the crystals and the solvent-mediated powders are different in their overall molecular structure with the crystals resembling $Ag_2[3,5-(CF_3)_2Pz]_2(1,7-phen)_3$ and the solvent-mediated powders resembling $Ag_2[3,5-(CF_3)_2Pz]_2(1,7-phen)_3 = \{Ag[3,5-(CF_3)_2Pz](1,7-phen)\}_2$. The elemental analysis data for both solvent-mediated powders shows that impurities are present; however, the data suggests that the crude (unwashed) solvent-mediated powder synthesized using benzene contains less impurities compared to that of the solvent-mediated powder synthesized using hexane.

With regard to the $Ag_3[3,5-(CF_3)_2Pz]_3(1,7-phen)$ crystals (3*), the theoretical percentages of carbon (C), hydrogen (H), and nitrogen (N) were analytically calculated (Anal. Calc.) based on the empirical formula C27 H11 Ag3 F18 N8 (MW = 1113.01 /mol): C, 29.14; H, 1.00; N, 10.07. The experimentally found data for the crystals (29.31; H, 0.92; N, 10.08) match that of the theoretical Anal. Calc. values within ±0.17 for C, ±0.08 for H, and ±0.01 for N.

Table 8. Elemental analysis data for $Ag_2[3,5-(CF_3)_2Pz]_2[(1,7-phen)]_n$ (n = 2 or 3) crystals and solvent-mediated powder and $Ag_3[3,5-(CF_3)_2Pz]_3(1,7-phen)$ crystals: theoretical Anal. Calc. versus experimentally found data.

Elemental Analysis					
$Ag_2[3,5-(CF_3)_2Pz]_2[(1,7-phen)]_n$, ($n$ = 2 or 3) & $Ag_3[3,5-(CF_3)_2Pz]_3(1,7-phen)$					
	1* Crystals	2* Solvent-Mediated Powder (in Hexane) *filtered*	2* Solvent-Mediated Powder (in Benzene) *unwashed*	3* Crystals	
1* $Ag_2[3,5-(CF_3)_2Pz]_2(1,7-phen)_3$ = C46 H26 Ag2 F12 N10 (MW = 1162.51 g/mol)					
Element	**Theoretical Anal. Calc. 1***	**Experimentally Found**	**Experimentally Found**	**Experimentally Found**	**Experimentally Found**
C	47.53%	47.20%	40.34%	42.03%	29.52%
H	2.25%	2.16%	1.78%	1.67%	0.95%
N	12.05%	11.84%	11.10%	11.18%	10.13%
Ag	18.56%				
2* $Ag_2[3,5-(CF_3)_2Pz]_2(1,7-phen)_2$ = C34 H18 Ag2 F12 N8 (MW = 982.28 g/mol)					
Element	**Theoretical Anal. Calc. 2***	**Experimentally Found**	**Experimentally Found**	**Experimentally Found**	**Experimentally Found**
C	41.57%	47.20%	40.34%	42.03%	29.52%
H	1.85%	2.16%	1.78%	1.67%	0.95%
N	11.41%	11.84%	11.10%	11.18%	10.13%
Ag	21.96%				
3* $Ag_3[3,5-(CF_3)_2Pz]_3(1,7-phen)$ = C27 H11 Ag3 F18 N8 (MW = 1113.01 g/mol)					
Element	**Theoretical Anal. Calc. 3***	**Experimentally Found**	**Experimentally Found**	**Experimentally Found**	**Experimentally Found**
C	29.14%	47.20%	40.34%	42.03%	29.52%
H	1.00%	2.16%	1.78%	1.67%	0.95%
N	10.07%	11.84%	11.10%	11.18%	10.13%
Ag	29.08%				

3.2.4.3 Characterization using FT-IR Spectroscopy

In this section, the IR spectra for $Ag_2[3,5-(CF_3)_2Pz]_2(1,7-phen)_3$ crystals, $\{Ag[3,5-(CF_3)_2Pz](1,7-phen)\}_2$ solvent-mediated powder synthesized using hexane, and $\{Ag[3,5-(CF_3)_2Pz](1,7-phen)\}_2$ solvent-mediated powder (crude) synthesized using benzene, as shown in Figure 67, are discussed. The IR spectra for the crystals and solvent-mediated powders are relatively identical to one another and feature the functional groups characteristic of both the $[3,5-(CF_3)_2Pz]^-$ and 4,7-phen ligands: =C-H stretch (aromatic), C=C stretch (aromatic), C=N stretch (aromatic), C-C stretch (aromatic), C-N stretch (aromatic), and C-F stretch. Minor shifts in observed peaks and intensities are observed in the fingerprint region between 1000 cm^{-1} and 1300 cm^{-1}.

Functional Groups	Expected Range (cm^{-1})
=C-H stretch (aromatic)	3010-3100, 690-900
C=C stretch (aromatic)	1400, 1600
C=N stretch (aromatic)	1400-1620
C-C stretch (aromatic)	1400-1500
C-N stretch (aromatic)	1250-1335
C-F stretch	1000-1400
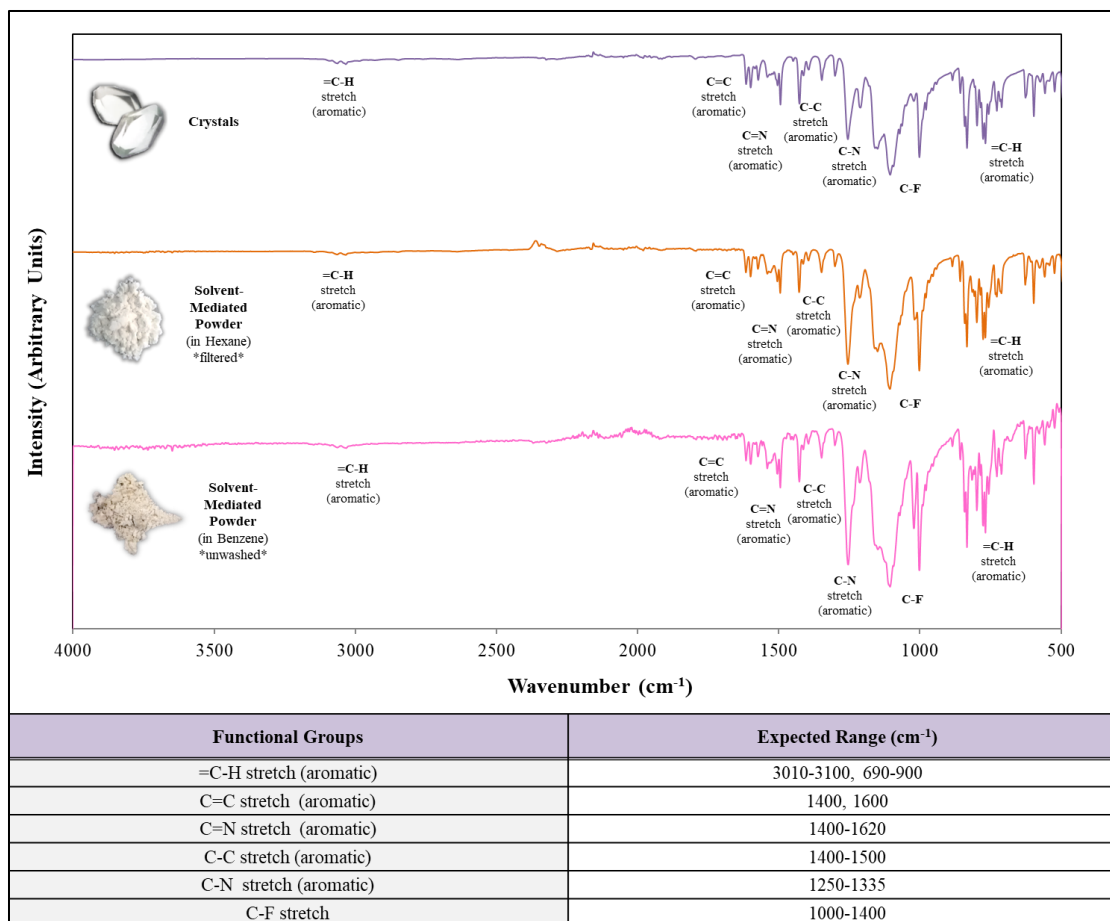
Figure 67. Stacked FT-IR spectra for Ag$_2$[3,5-(CF$_3$)$_2$Pz]$_2$(1,7-phen)$_3$ crystals (*top*), {Ag[3,5-(CF$_3$)$_2$Pz](1,7-phen)}$_2$ solvent-mediated powder synthesized using hexane (*middle*), and {Ag[3,5-(CF$_3$)$_2$Pz](1,7-phen)}$_2$ solvent-mediated powder (crude) synthesized using benzene (*bottom*).

141

3.2.4.4 Characterization using TGA Analyses

In this section, the TGA analyses of the $Ag_2[3,5-(CF_3)_2Pz]_2(1,7-phen)_3$ crystals and $\{Ag[3,5-(CF_3)_2Pz](1,7-phen)\}_2$ solvent-mediated powders, shown in Figures 68-70, respectively, are discussed.

The TGA analyses of the $Ag_2[3,5-(CF_3)_2Pz]_2(1,7-phen)_3$ crystals and $\{Ag[3,5-(CF_3)_2Pz](1,7-phen)\}_2$ solvent-mediated powders are relatively similar to one another with regard to the percent weight losses; however, they differ significantly from one another with regard to onset temperatures and inflection points. The crystals, solvent-mediated powder synthesized using hexane, and solvent-mediated powder (crude) synthesized using benzene, respectively, show significant weight losses of 99.40%, 95.70%, and 99.01%, respectively. Moreover, the onset temperatures (the temperatures at which weight loss begins) of 219.84°C, 242.39°C °C, and 247.30°C, respectively, and 1st derivative peaks (greatest rate of change on the weight loss curves) of 257.09°C, 270.76°C, and 284.97°C, respectively, were observed. The slight difference in onset temperatures and 1st derivative peaks (inflection points) between the solvent-mediated powder synthesized using hexane and crude (unwashed) solvent-mediated powder synthesized using benzene may be attributed to the differences in sample size: 10.0170 mg and 12.3730 mg, respectively, in that as the sample size increases, an increase (shift) in temperature occurs.

With regard to the $Ag_2[3,5-(CF_3)_2Pz]_2(1,7-phen)_3$ crystals and the emperical formula C46 H26 Ag2 F12 N10 (MW = 1162.51 g/mol), the theoretical percentage of silver is 18.56%; however, the total weight loss of 99.40% was observed, which is

primarily due to the sublimation of the $[3,5\text{-}(CF_3)_2Pz]^-$ and 1,7-phen ligands (total theoretical percentage of C, H, N and F of 81.44%). The remaining weight percentage: 0.60%, following the aforementioned weight losses should theoretically be silver.

With regard to the $\{Ag[3,5\text{-}(CF_3)_2Pz](1,7\text{-phen})\}_2$ solvent-mediated powders and the emperical formula C34 H18 Ag2 F12 N8 (MW = 982.28 g/mol), the theoretical percentage of silver is 21.96%; however, the total weight losses of 95.70%, and 99.01%, respectively, were observed, which were primarily due to the sublimation of the $[3,5\text{-}(CF_3)_2Pz]^-$ and 1,7-phen ligands (total theoretical percentage of C, H, N and F of 78.04%). The remaining weight percentages, 4.30% and 0.99%, respectively, following the aforementioned weight losses should theoretically be silver.

In comparison between the solvent-mediated powder synthesized using hexane and crude (unwashed) solvent-mediated powder synthesized using benzene, the former retained an additional weight percentage of 3.31% following the weight drop, which is due to the presence of impurities.
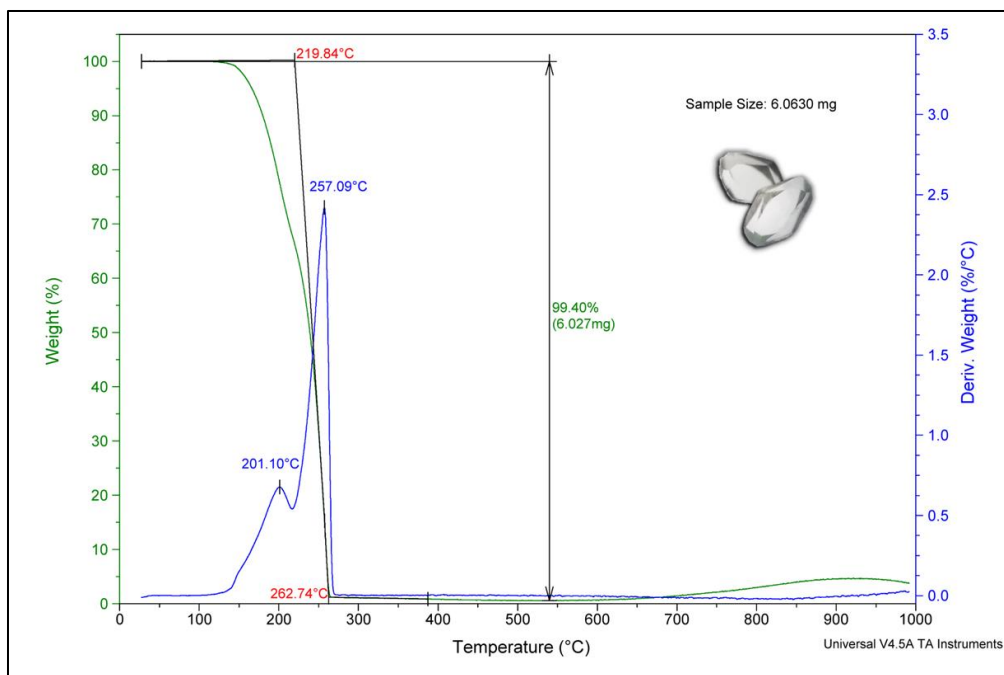
Figure 68. TGA analysis for Ag$_2$[3,5-(CF$_3$)$_2$Pz]$_2$(1,7-phen)$_3$ crystals.
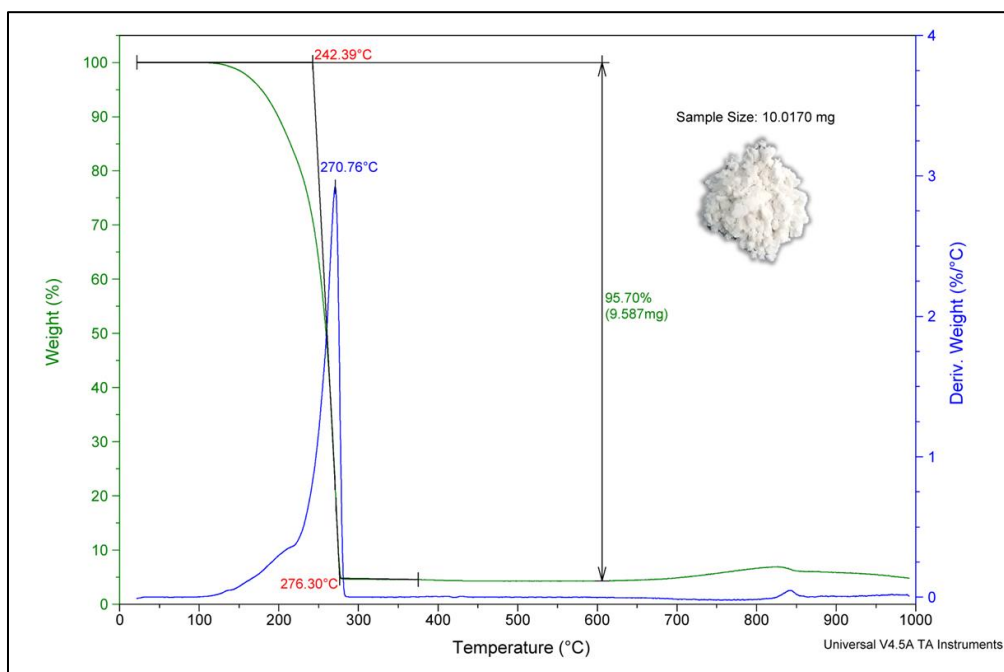
Figure 69. TGA analysis for {Ag[3,5-(CF$_3$)$_2$Pz](1,7-phen)}$_2$ solvent-mediated powder synthesized using hexane**.**
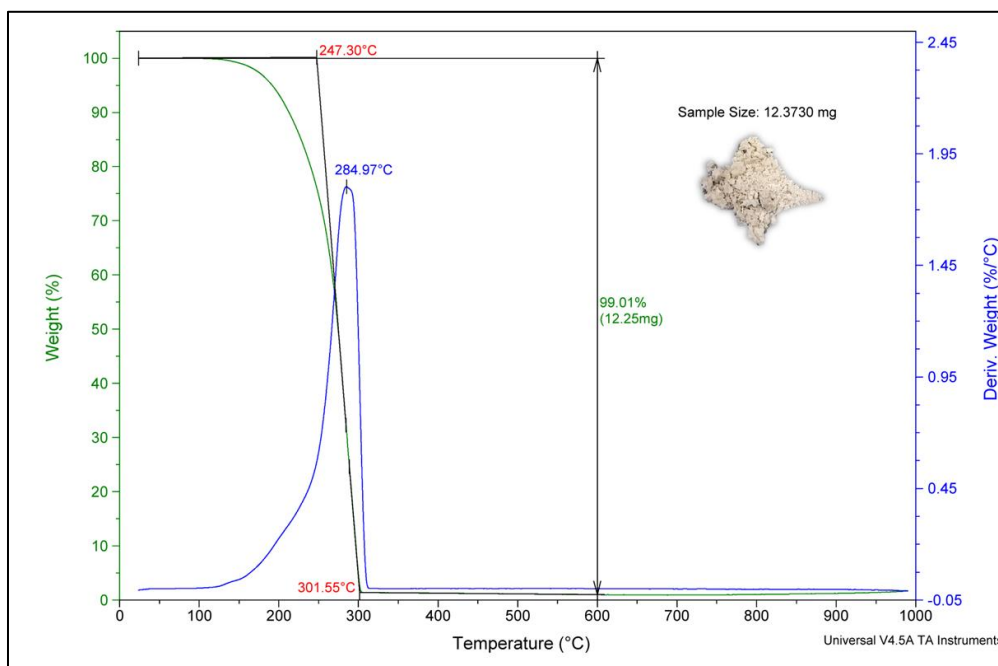
Figure 70. TGA analysis for {Ag[3,5-(CF$_3$)$_2$Pz](1,7-phen)}$_2$ solvent-mediated powder (crude) synthesized using benzene.

3.2.4.5 Characterization using Photoluminescence and UV-Vis Absorption Spectroscopy

In this section, the photoluminescence and UV-Vis absorption spectroscopy of {Ag[3,5-(CF$_3$)$_2$Pz](1,7-phen)}$_2$ solvent-mediated powder synthesized using hexane are discussed.

The solvent-mediated powder does not exhibit photoluminescence at room temperature. The white solid was transferred to a clean, quartz tube, and its photoluminescence was checked under a handheld UV lamp under Short Wave UV (λex = 254 nm) and Long Wave UV (λex = 365 nm), at 77K. At 77K, the solvent-mediated

145

powder exhibited green photoluminescence only under 365 nm (medium-strong, green luminescence).

As shown in Figures 71 and 72, at 77K, the photoluminescence of $\{Ag[3,5-(CF_3)_2Pz](1,7\text{-phen})\}_2$ solvent-mediated powder (solid) was measured using the excitation wavelength of $\lambda_{ex} = 328$nm, producing an emission band, with a maximum peak at $\lambda_{em} = 535$ nm and a shoulder peak (minor) at $\lambda_{em} = 465$ nm. A photoluminescence decay curve for the emission at $\lambda_{em} = 535$ nm peak was fitted with a Chi2 value of 0.9516, a Durbin Watson value of 1.563, and a Z value of -0.08823. The 77K emission lifetime (τ) of 9.666 µs was observed, which is characterized as fluorescence (Lifetime $< 10^{-5}$ s).

The UV-Vis absorption spectra for $\{Ag[3,5-(CF_3)_2Pz](1,7\text{-phen})\}_2$ solvent-mediated powder, shown in Figure 73, were obtained using three dilutions in cyclohexane (UV cutoff wavelength = 210 nm): 1×10^{-3} M, 1×10^{-4} M, and 1×10^{-5} M. A red shift was observed as the concentration increased, shifting more toward the visible region (up to 360 nm), as well as $\pi\text{-}\pi^*$ transition with an extinction coefficient (ε_{267}) of 64100 L·mol^{-1}·cm^{-1} ($\lambda_{max2} = 267$ nm: A = 0.641, C = 1×10^{-5} M).
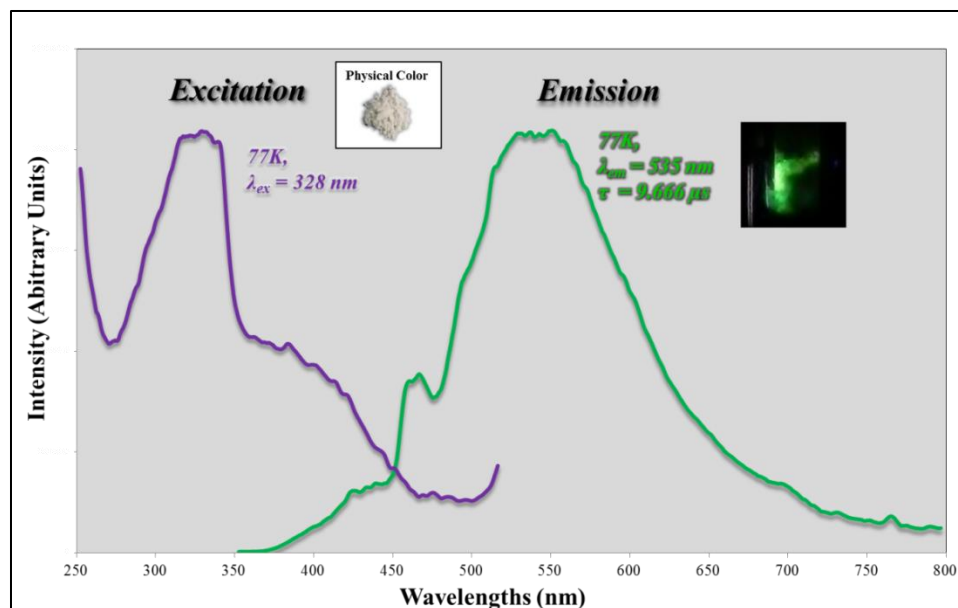
Figure 71. Photoluminescence spectra for $\{Ag[3,5\text{-}(CF_3)_2Pz](1,7\text{-}phen)\}_2$ solvent-mediated powder (synthesized using hexane), at cryogenic temperature (77K).
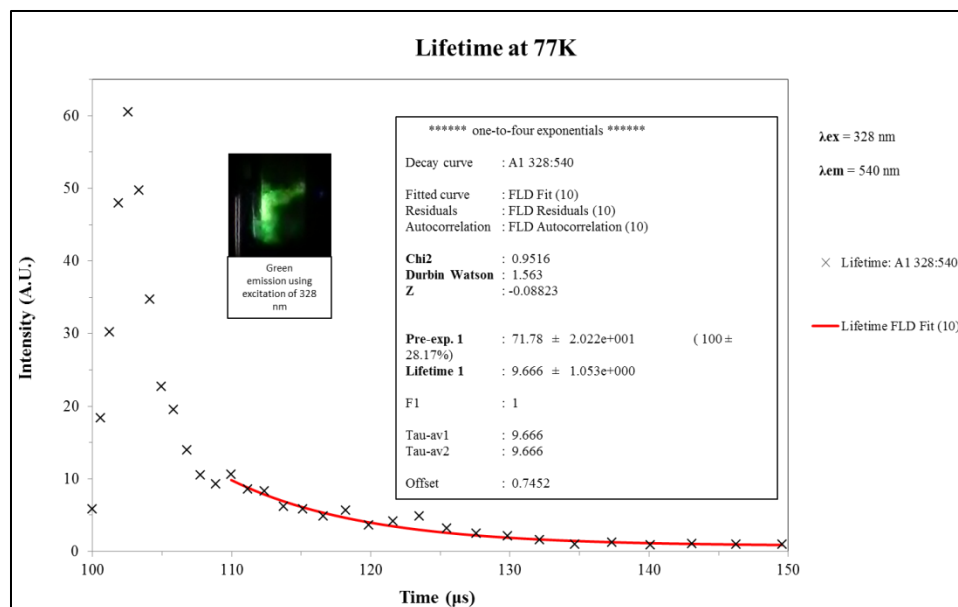
Figure 72. Photoluminescence lifetime decay curve for $\{Ag[3,5\text{-}(CF_3)_2Pz](1,7\text{-}phen)\}_2$ solvent-mediated powder (synthesized using hexane), at cryogenic temperature (77K).
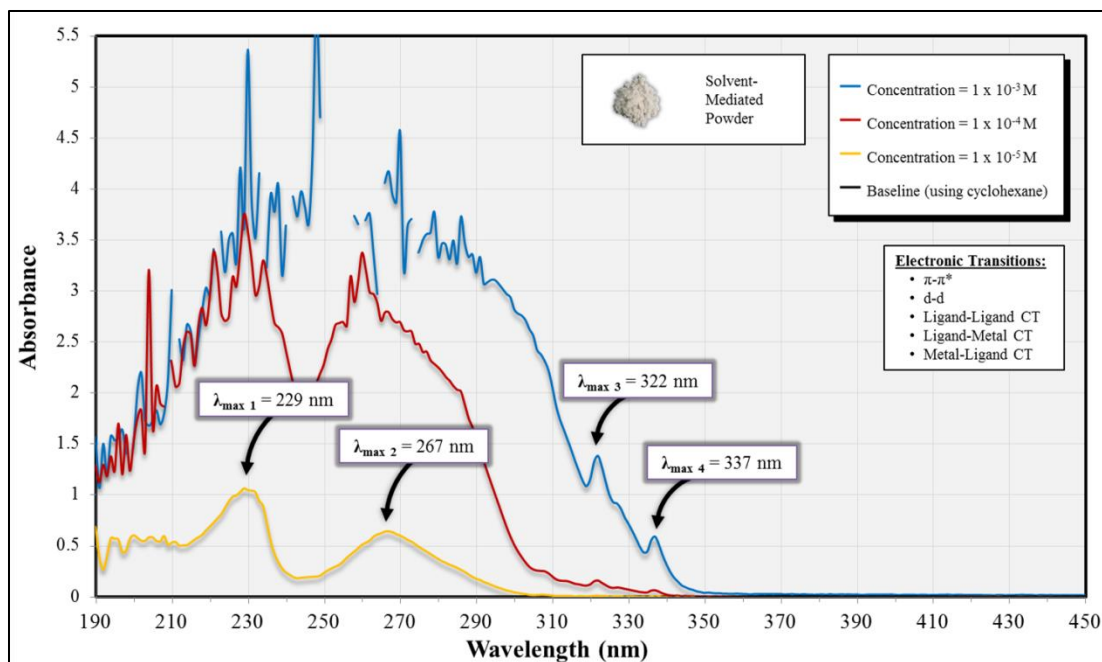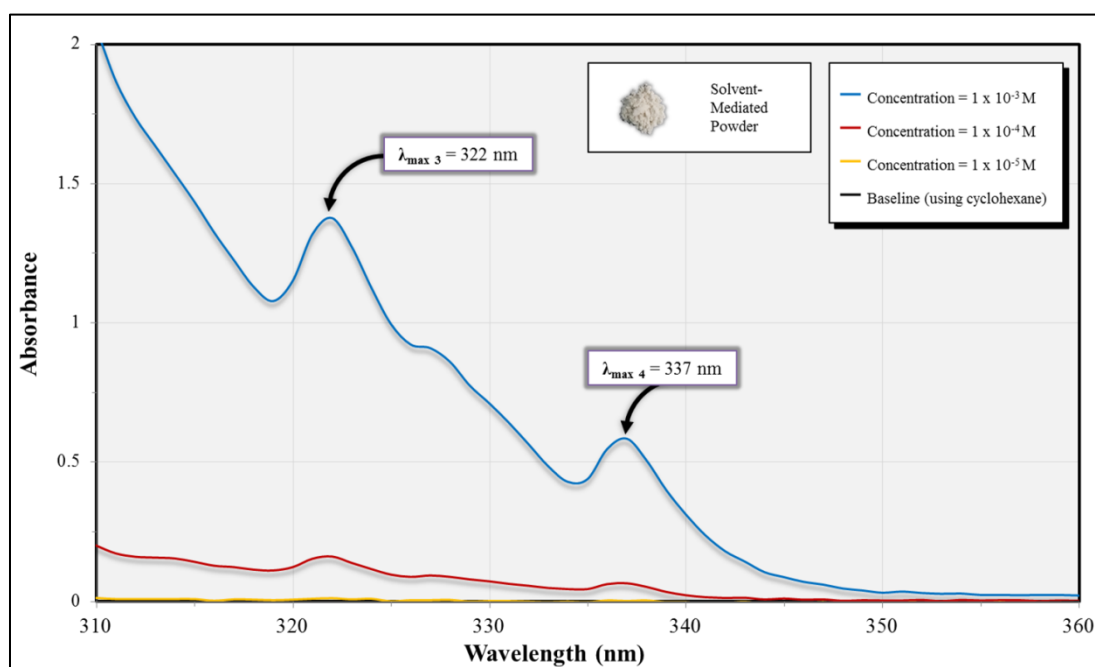
Figure 73. UV-Vis Spectra for {Ag[3,5-(CF$_3$)$_2$Pz](1,7-phen)}$_2$ solvent-mediated powder (synthesized using hexane) in cyclohexane solutions (UV cutoff wavelength = 210 nm): **(A)** Full-View = 190-450 nm; **(B)** Zoomed-In = 300-450 nm.

3.2.5 Compound 5: {Cu[3,5-(CF$_3$)$_2$Pz](dmp)}$_2$

3.2.5.1 X-ray Crystallographic Data

In this section, the X-ray crystallographic data for {Cu[3,5-(CF$_3$)$_2$Pz](dmp)}$_2$ (shown in Tables 9A-B) are discussed. {Cu[3,5-(CF$_3$)$_2$Pz](dmp)}$_2$ single crystals were obtained using solventless powder (as well as solvent-mediated powder). Table 9A shows that {Cu[3,5-(CF$_3$)$_2$Pz](dmp)}$_2$ crystallizes in the triclinic crystal system with the space group *P*-1 with Z = 1 and the unit cell dimensions: a = 8.9519(3) Å, b = 9.7326(4) Å, c = 11.8462(4) Å, α = 78.654(3)°, β = 67.899(4)°, and γ = 77.957(3)°. {Cu[3,5-(CF$_3$)$_2$Pz](dmp)}$_2$ has the empirical formula C38 H26 Cu2 F12 N8 (MW = 949.75 g/mol).

As shown in Figure 74A, the asymmetric unit cell shows the Cu(I) center: Cu1, coordinates with the [3,5-(CF$_3$)$_2$Pz]$^-$ ligand (via N1) and the dmp ligand (via N3 and N4). As shown in Figure 74B, the symmetric unit cell of {Cu[3,5-(CF$_3$)$_2$Pz](dmp)}$_2$ exhibits a Cu(I) dimeric structure with two 4-coordinated Cu(I) centers: Cu1 and Cu1A, respectively, doubly bridged via two [3,5-(CF$_3$)$_2$Pz]$^-$ ligands (via N1 and N2, and N1A and N2A, respectively). Moreover, each respective Cu(I) center is coordinated (via bidentate chelating) with their respective dmp ligands (via N3 and N4, and N3A and N4A, respectively). Overall, {Cu[3,5-(CF$_3$)$_2$Pz](dmp)}$_2$ exhibits a heteroleptic, dinuclear complex with two double bridging [3,5-(CF$_3$)$_2$Pz]$^-$ ligands and two bidentate chelating dmp ligands, which essentially serve as end caps.

Figure 74C shows the packing structure of {Cu[3,5-(CF$_3$)$_2$Pz](dmp)}$_2$. The bond lengths (Å) and angles (°) are shown in Table 9B. The full-matrix least-squares

refinement method was used on F^2, resulting in a goodness-of-fit value of 1.058 with R1

= 3.59 % and wR2 = 9.73% for all data.

Table 9. (A) X-ray Crystallographic Data for {Cu[3,5-$(CF_3)_2$Pz](dmp)}$_2$;
(B) Bond lengths [Å] and angles [°] for {Cu[3,5-$(CF_3)_2$Pz](dmp)}$_2$.

Empirical formula	C38 H26 Cu2 F12 N8
Formula weight	949.75
Temperature	100.01(10) K
Wavelength	0.71073 Å
Crystal system	Triclinic
Space group	P-1
Unit cell dimensions	a = 8.9519(3) Å α = 78.654(3)°.
	b = 9.7326(4) Å β = 67.899(4)°.
	c = 11.8462(4) Å γ = 77.957(3)°.
Volume	927.23(6) Å^3
Z	1
Density (calculated)	1.701 Mg/m^3
Absorption coefficient	1.250 mm^{-1}
F(000)	476
Crystal size	0.09 x 0.05 x 0.03 mm^3
Theta range for data collection	2.158 to 27.102°.
Index ranges	-11<=h<=11, -12<=k<=12, -15<=l<=15
Reflections collected	12973
Independent reflections	4055 [R(int) = 0.0297]
Completeness to theta = 25.242°	99.9 %
Absorption correction	Semi-empirical from equivalents
Max. and min. transmission	1.00000 and 0.85851
Refinement method	Full-matrix least-squares on F^2
Data / restraints / parameters	4055 / 0 / 273
Goodness-of-fit on F^2	1.058
Final R indices [I>2sigma(I)]	R1 = 0.0333, wR2 = 0.0956
R indices (all data)	R1 = 0.0359, wR2 = 0.0973
Extinction coefficient	n/a
Largest diff. peak and hole	0.860 and -0.599 e.Å^{-3}

(A)

Bond Lengths [Å] (blue) & Angles [°] (red)					
Cu(1)-N(1)	2.0031(16)	C(19)-H(19A)	0.96	C(6)-C(7)-H(7)	120
Cu(1)-N(2)#1	2.0057(15)	C(19)-H(19B)	0.96	C(8)-C(7)-C(6)	119.9(2)
Cu(1)-N(3)	2.1083(16)	C(19)-H(19C)	0.96	C(8)-C(7)-H(7)	120
Cu(1)-N(4)	2.0760(16)	N(1)-Cu(1)-N(2)#1	114.75(6)	C(7)-C(8)-H(8)	120.2
F(1)-C(4)	1.344(3)	N(1)-Cu(1)-N(3)	111.21(6)	C(7)-C(8)-C(9)	119.68(19)
F(2)-C(4)	1.339(3)	N(1)-Cu(1)-N(4)	118.17(6)	C(9)-C(8)-H(8)	120.2
F(3)-C(4)	1.342(2)	N(2)#1-Cu(1)-N(3)	110.80(6)	C(8)-C(9)-C(10)	123.54(19)
F(4)-C(5)	1.342(2)	N(2)#1-Cu(1)-N(4)	116.54(6)	C(8)-C(9)-C(17)	116.88(18)
F(5)-C(5)	1.343(2)	N(4)-Cu(1)-N(3)	79.87(6)	C(17)-C(9)-C(10)	119.57(19)
F(6)-C(5)	1.338(2)	N(2)-N(1)-Cu(1)	121.83(12)	C(9)-C(10)-H(10)	119.6
N(1)-N(2)	1.366(2)	C(1)-N(1)-Cu(1)	130.66(13)	C(11)-C(10)-C(9)	120.75(18)
N(1)-C(1)	1.351(2)	C(1)-N(1)-N(2)	106.89(15)	C(11)-C(10)-H(10)	119.6
N(2)-C(3)	1.348(2)	N(1)-N(2)-Cu(1)#1	122.07(12)	C(10)-C(11)-H(11)	119.5
N(3)-C(6)	1.328(3)	C(3)-N(2)-Cu(1)#1	130.24(13)	C(10)-C(11)-C(12)	120.93(18)
N(3)-C(17)	1.361(2)	C(3)-N(2)-N(1)	107.38(15)	C(12)-C(11)-H(11)	119.5
N(4)-C(15)	1.337(3)	C(6)-N(3)-Cu(1)	128.96(13)	C(13)-C(12)-C(11)	123.28(18)
N(4)-C(16)	1.364(2)	C(6)-N(3)-C(17)	118.61(16)	C(16)-C(12)-C(11)	119.75(19)
C(1)-C(2)	1.383(3)	C(17)-N(3)-Cu(1)	112.44(12)	C(16)-C(12)-C(13)	116.97(18)
C(1)-C(4)	1.484(3)	C(15)-N(4)-Cu(1)	128.20(13)	C(12)-C(13)-H(13)	120.2
C(2)-H(2)	0.93	C(15)-N(4)-C(16)	118.36(16)	C(14)-C(13)-C(12)	119.53(18)
C(2)-C(3)	1.389(3)	C(16)-N(4)-Cu(1)	113.37(12)	C(14)-C(13)-H(13)	120.2
C(3)-C(5)	1.488(3)	N(1)-C(1)-C(2)	111.83(16)	C(13)-C(14)-H(14)	120
C(6)-C(7)	1.412(3)	N(1)-C(1)-C(4)	121.53(17)	C(13)-C(14)-C(15)	120.08(19)
C(6)-C(18)	1.503(3)	C(2)-C(1)-C(4)	126.63(18)	C(15)-C(14)-H(14)	120
C(7)-H(7)	0.93	C(1)-C(2)-H(2)	128.8	N(4)-C(15)-C(14)	121.64(18)
C(7)-C(8)	1.371(3)	C(1)-C(2)-C(3)	102.44(16)	N(4)-C(15)-C(19)	117.27(18)
C(8)-H(8)	0.93	C(3)-C(2)-H(2)	128.8	C(14)-C(15)-C(19)	121.09(19)
C(8)-C(9)	1.405(3)	N(2)-C(3)-C(2)	111.46(16)	N(4)-C(16)-C(12)	123.41(18)
C(9)-C(10)	1.437(3)	N(2)-C(3)-C(5)	122.17(16)	N(4)-C(16)-C(17)	117.15(16)
C(9)-C(17)	1.407(3)	C(2)-C(3)-C(5)	126.36(17)	C(12)-C(16)-C(17)	119.44(17)
C(10)-H(10)	0.93	F(1)-C(4)-C(1)	113.07(17)	N(3)-C(17)-C(9)	123.32(17)
C(10)-C(11)	1.357(3)	F(2)-C(4)-F(1)	105.79(17)	N(3)-C(17)-C(16)	117.13(16)
C(11)-H(11)	0.93	F(2)-C(4)-F(3)	106.29(17)	C(9)-C(17)-C(16)	119.55(17)
C(11)-C(12)	1.432(3)	F(2)-C(4)-C(1)	113.81(17)	C(6)-C(18)-H(18A)	109.5
C(12)-C(13)	1.408(3)	F(3)-C(4)-F(1)	106.26(17)	C(6)-C(18)-H(18B)	109.5
C(12)-C(16)	1.406(3)	F(3)-C(4)-C(1)	111.07(17)	C(6)-C(18)-H(18C)	109.5
C(13)-H(13)	0.93	F(4)-C(5)-F(5)	106.21(15)	H(18A)-C(18)-H(18B)	109.5
C(13)-C(14)	1.373(3)	F(4)-C(5)-C(3)	113.29(17)	H(18A)-C(18)-H(18C)	109.5
C(14)-H(14)	0.93	F(5)-C(5)-C(3)	112.88(16)	H(18B)-C(18)-H(18C)	109.5
C(14)-C(15)	1.408(3)	F(6)-C(5)-F(4)	106.73(16)	C(15)-C(19)-H(19A)	109.5
C(15)-C(19)	1.498(3)	F(6)-C(5)-F(5)	106.98(17)	C(15)-C(19)-H(19B)	109.5
C(16)-C(17)	1.443(3)	F(6)-C(5)-C(3)	110.34(16)	C(15)-C(19)-H(19C)	109.5
C(18)-H(18A)	0.96	N(3)-C(6)-C(7)	121.60(19)	H(19A)-C(19)-H(19B)	109.5
C(18)-H(18B)	0.96	N(3)-C(6)-C(18)	117.06(18)	H(19A)-C(19)-H(19C)	109.5
C(18)-H(18C)	0.96	C(7)-C(6)-C(18)	121.34(19)	H(19B)-C(19)-H(19C)	109.5
Symmetry transformations used to generate equivalent atoms:					
#1 -x+1,-y+1,-z+1					

(B)
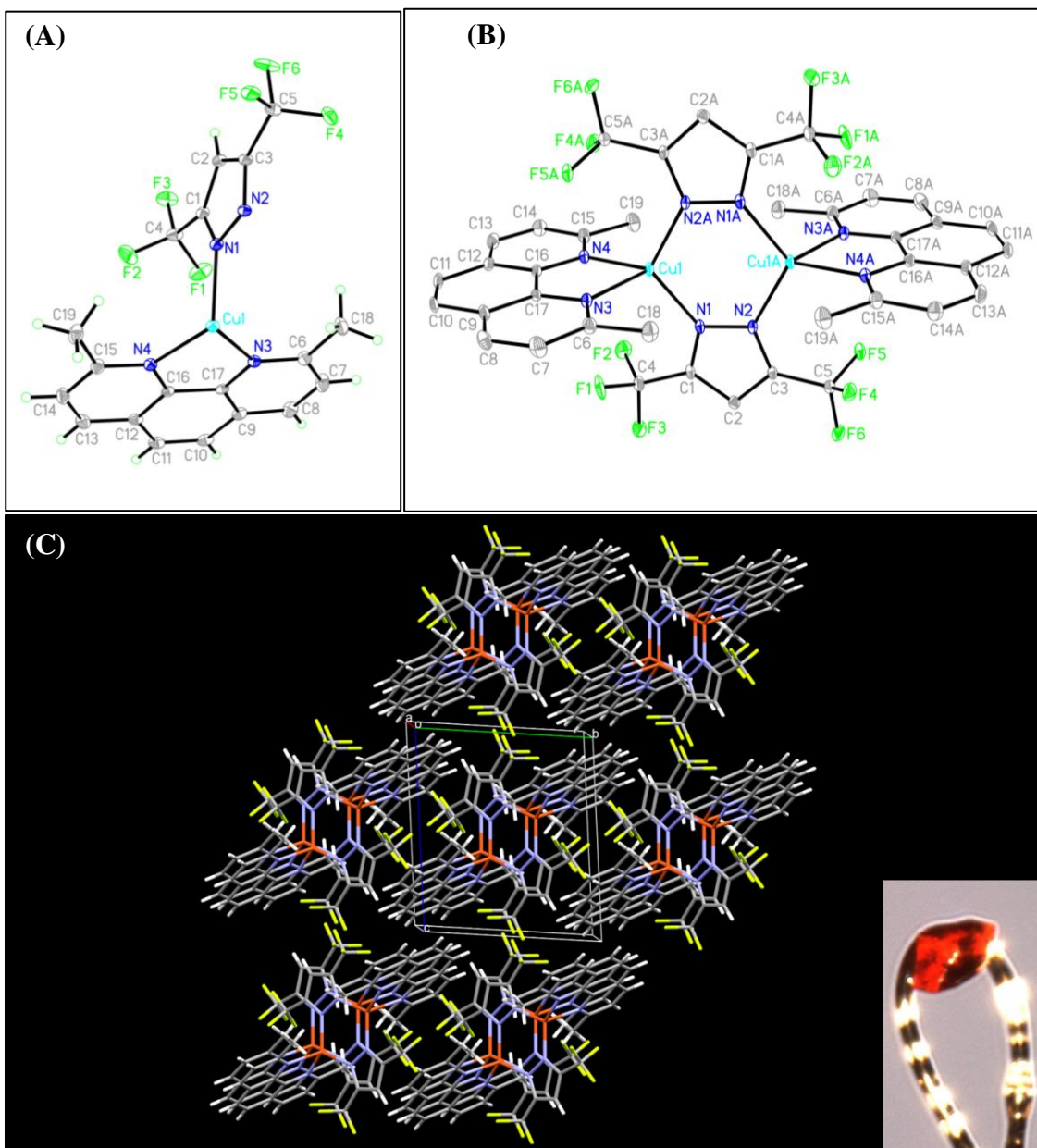
Figure 74. Crystal Structure of {Cu[3,5-(CF$_3$)$_2$Pz](dmp)}$_2$: **(A)** Asymmetric Unit Cell, **(B)** Symmetric Unit Cell, and **(C)** Packing.

3.2.5.2 Elemental Analysis Data

In this section, the elemental analysis data are discussed, comparing the experimentally found data with the theoretical Anal. Calc. (see Table 10). The theoretical percentages of carbon (C), hydrogen (H), and nitrogen (N) were analytically calculated (Anal. Calc.) based on the empirical formula C38 H26 Cu2 F12 N8 (MW = 949.75 g/mol): C, 48.06; H, 2.76; N, 11.80. The experimentally found data for solvent-mediated (C, 47.99; H, 2.76; N, 11.65) and solventless powder (C, 48.03; H, 2.68; N, 11.61) are similar to one another and match with the theoretical Anal. Calc. within ±0.3 for C, H, and N. This comparison confirms that same {Cu[3,5-(CF$_3$)$_2$Pz](dmp)}$_2$ product was synthesized via both solvent-mediated and solventless syntheses. The experimentally found data for crystals (C, 48.06; H, 2.72; N, 11.69) match that of the theoretical Anal. Calc. within ±0.00 for C, ±0.04 for H, and ± 0.11 for N.

Table 10. Elemental analysis data for {Cu[3,5-(CF$_3$)$_2$Pz](dmp)}$_2$ solvent-mediated powder, solventless powder, and crystals: theoretical Anal. Calc. versus experimentally found data.

Elemental Analysis				
Empirical Formula: C38 H26 Cu2 F12 N8 (MW = 949.75 g/mol)				
		Solvent-Mediated	Solventless	Crystals
Element	**Theoretical Anal. Calc.**	**Experimentally Found**	**Experimentally Found**	**Experimentally Found**
C	48.06%	47.99%	48.03%	48.06%
H	2.76%	2.76%	2.68%	2.72%
N	11.80%	11.65%	11.61%	11.69%
Cu	13.38%			

3.2.5.3 Characterization using FT-IR Spectroscopy

In this section, the IR spectra for $\{Cu[3,5-(CF_3)_2Pz](dmp)\}_2$ solvent-mediated powder, solventless powder, and crystals, as shown in Figure 75, are discussed. The IR spectra for solvent-mediated powder, solventless powder, and crystals are relatively identical to one another and feature the functional groups characteristic of both the $[3,5-(CF_3)_2Pz]^-$ and dmp ligands: =C-H stretch (aromatic), C=C stretch (aromatic), C=N stretch (aromatic), C-C stretch (aromatic), C-N stretch (aromatic), C-F stretch, and C-H stretch (C-CH$_3$).

Functional Groups	Expected Range (cm^{-1})
=C-H stretch (aromatic)	3010-3100, 690-900
C=C stretch (aromatic)	1400, 1600
C=N stretch (aromatic)	1400-1620
C-C stretch (aromatic)	1400-1500
C-N stretch (aromatic)	1250-1335
C-F stretch	1000-1400
C-H stretch (C-CH$_3$)	2862-2882, 2652-2972
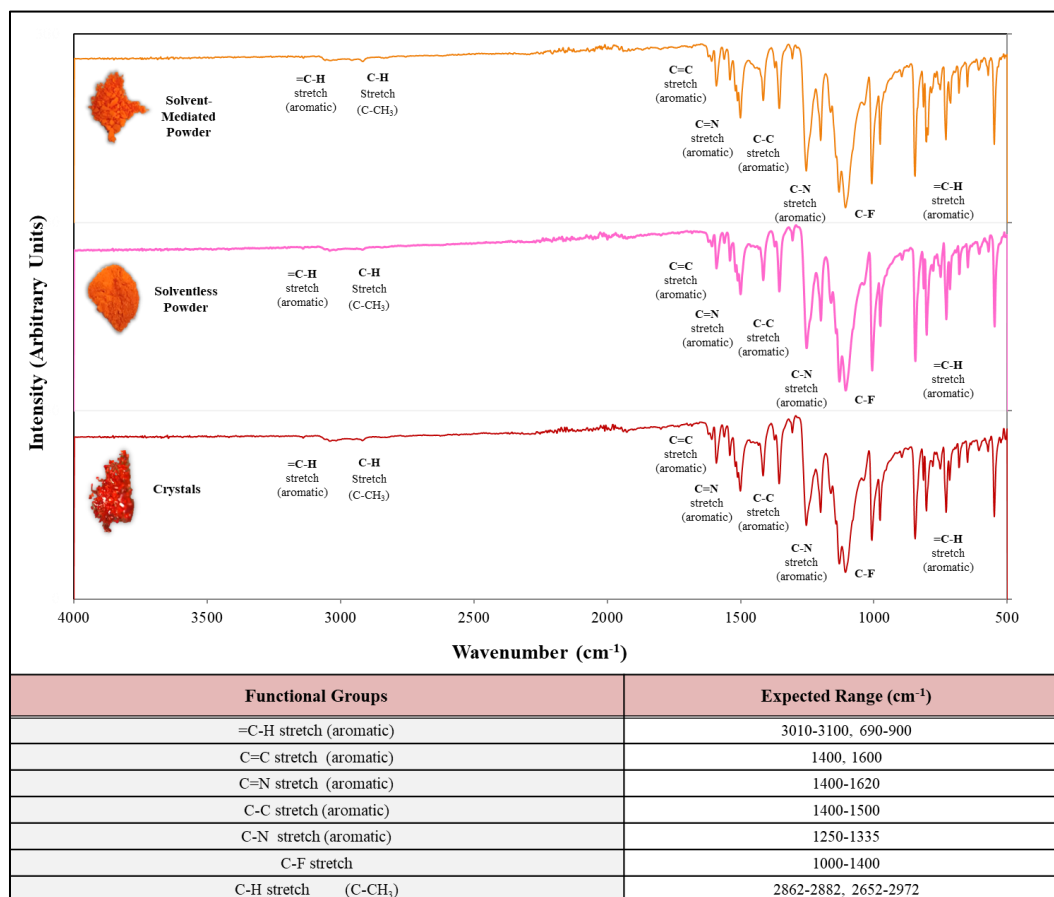
Figure 75. Stacked FT-IR spectra for $\{Cu[3,5-(CF_3)_2Pz](dmp)\}_2$ solvent-mediated powder (*top*), solventless powder (*middle*), and crystals (*bottom*).

3.2.5.4 Characterization using TGA and DSC Analyses

In this section, the TGA analyses (and DSC analysis) for $\{Cu[3,5-(CF_3)_2Pz](dmp)\}_2$ crystals, solventless powder, and solvent-mediated powder, as shown in Figures 76-79, are discussed.

The TGA analyses of crystals, solventless powder, and solvent-mediated powder, shown in Figures 76-78, respectively, are relatively similar to one another with regard to total percent weight loss, onset temperatures, and inflection points; however, they differ significantly in the percent weight loss for the first and second weight drop. The crystals, solventless powder, and solvent-mediated powder, respectively, show significant weight losses of 61.34%, 54.90%, and 44.15%, respectively, for the first weight drop, followed by 16.39%, 17.42%, and 35.76%, respectively, for the second weight drop, resulting in total weight losses of 77.73%, 72.31%, and 79.90%, respectively. For the first weight drop, onset temperatures (the temperatures at which weight loss begins) of 292.88°C, 296.51°C, and 304.02°C, respectively, and 1st derivative peaks (greatest rate of change on the weight loss curves) of 316.28°C, 324.14°C, 335.35°C, respectively, were observed. The differences in onset temperatures and 1st derivative peaks (inflection points) may be attributed to the differences in sample for the crystals, solventless powder, and solvent-mediated powder: 3.9580 mg, 6.1730 mg, 10.2700 mg, respectively, in that as the sample size increases, an increase (shift) in temperature occurs.

With regard to the emperical formula C38 H26 Cu2 F12 N8 (MW = 949.75 g/mol), the theoretical percentage of copper is 13.38%; however, the total weight losses of 77.73%, 72.31%, and 79.90%, respectively, were observed, which was primarily due

to the sublimation of the $[3,5\text{-}(CF_3)_2Pz]^-$ and dmp ligands (total theoretical percentage of C, H, N and F of 86.62%). The remaining weight percentages, 22.27%, 27.69%, and 20.10%, respectively, following the aforementioned weight losses (after heating up to 1000°C) should theoretically be copper (primarily) and possibly impurities related to the dmp ligand rather than $[3,5\text{-}(CF_3)_2Pz]^-$ ligand (completely sublimes by 150°C). The differences in weight loss with regard to the crystals, solventless powder, and solvent-mediated powder may be related to the presence of more than one polymorph.

Figure 79 shows the DSC analysis for $\{Cu[3,5\text{-}(CF_3)_2Pz](dmp)\}_2$ solvent-mediated powder. A sharp peak maximum is observed at 265.40°C (melting point), with an onset temperature of 264.32°C. The TGA analysis for the solvent-mediated powder, shown in Figure 78, shows that the sample begins to decompose before 304.02°C (the on-set temperature for weight loss). Therefore, the sample was not heated beyond 272°C (using DSC) as a precaution in order to avoid heating the sample to decomposition, which can destroy/damage the sensor of the DSC instrument.
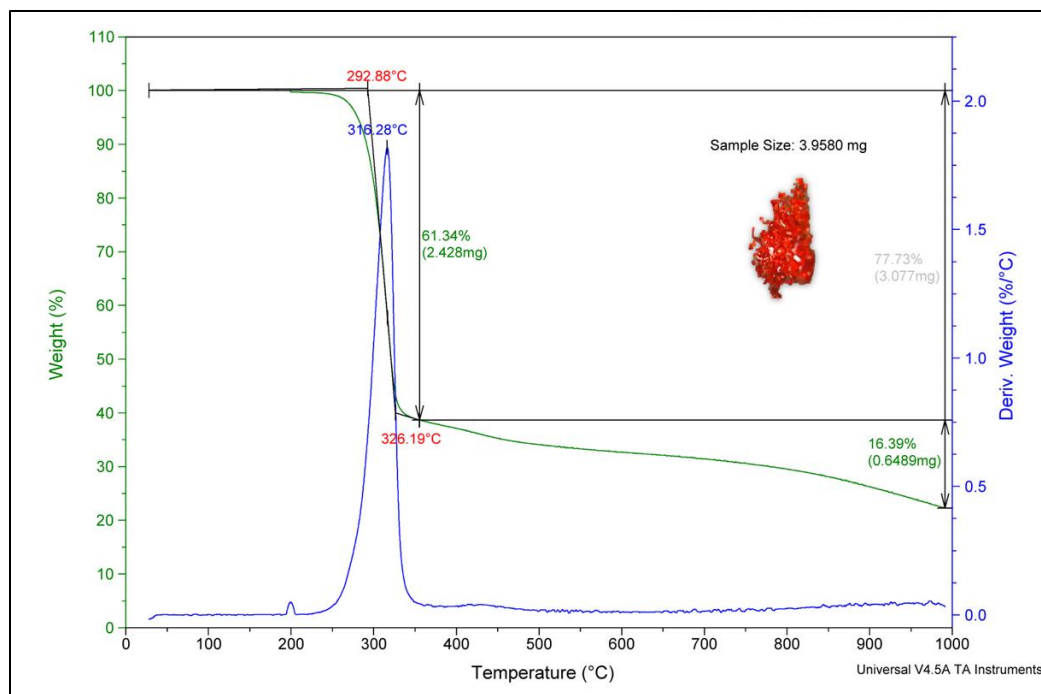
Figure 76. TGA analysis for {Cu[3,5-(CF$_3$)$_2$Pz](dmp)}$_2$ crystals.
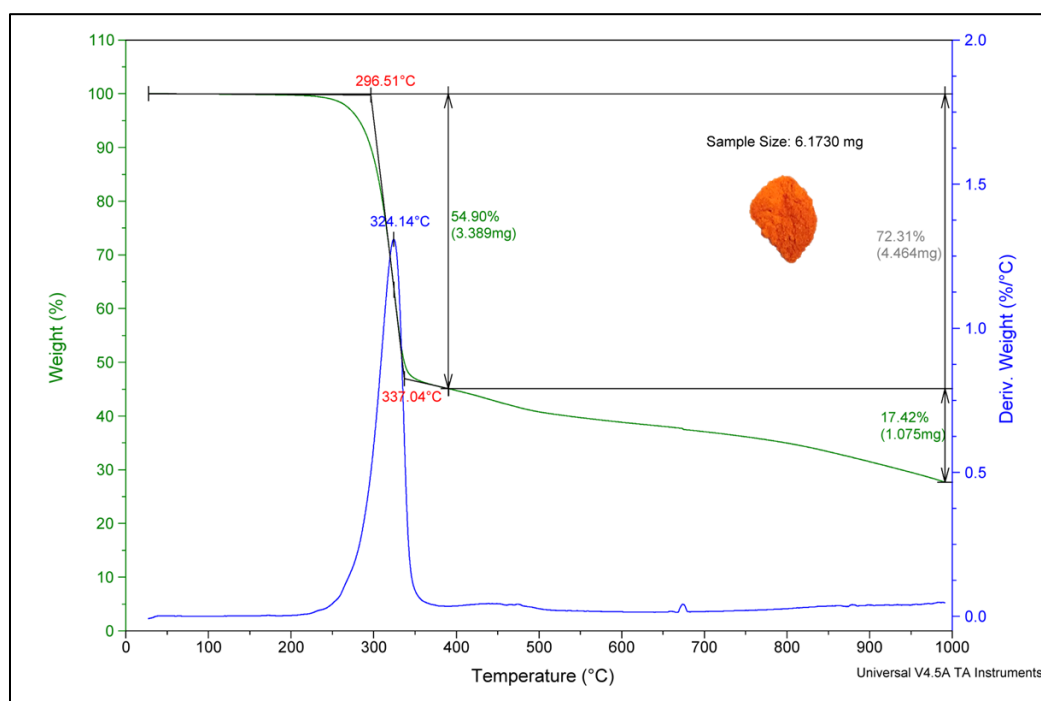
Figure 77. TGA analysis for {Cu[3,5-(CF$_3$)$_2$Pz](dmp)}$_2$ solventless powder.
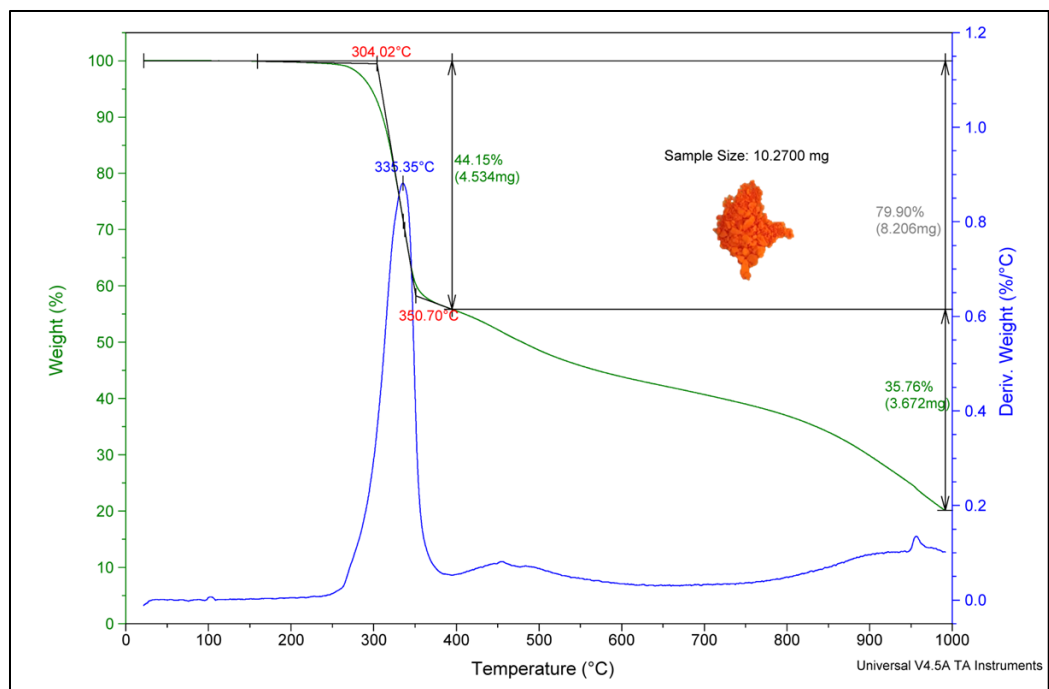
Figure 78. TGA analysis for {Cu[3,5-$(CF_3)_2$Pz](dmp)}$_2$ solvent-mediated powder.
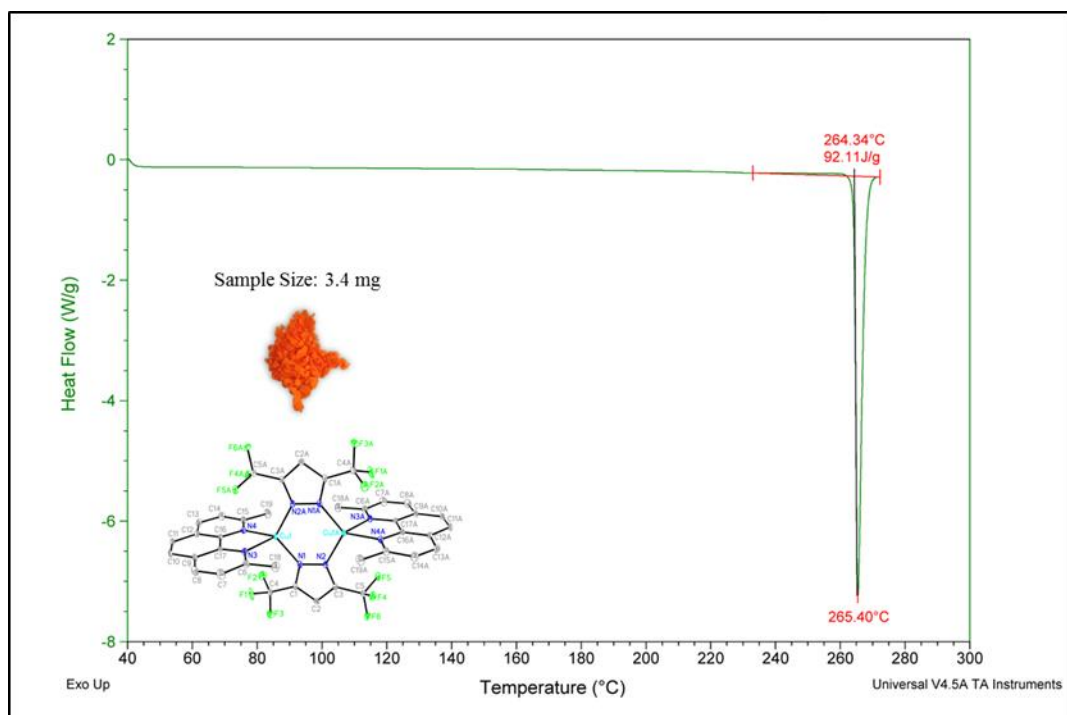
Figure 79. DSC analysis for {Cu[3,5-$(CF_3)_2$Pz](dmp)}$_2$ solvent-mediated powder.

3.2.5.5 Characterization using Photoluminescence and UV-Vis Absorption Spectroscopy

In this section, the photoluminescence and UV-Vis absorption spectroscopy of {Cu[3,5-$(CF_3)_2$Pz](dmp)}$_2$ solvent-mediated powder are discussed.

As show in Figure 80, the photoluminescence of the solvent-mediated powder and solventless powder were checked under a handheld UV lamp for luminescence, under Short Wave UV (λ_{ex} = 254 nm) and Long Wave UV (λ_{ex} = 365 nm), at room temperature (RT). Medium-weak, red photoluminescence was observed under both 254 nm and 365 nm. The red photoluminescence of the solvent-mediated powder (in a quarts NMR tube) was checked under 77K; however, an observable change (i.e. photoluminescence enhancement or quenching) was not observed.

As shown in Figure 81, at RT, the photoluminescence of the {Cu[3,5-$(CF_3)_2$Pz](dmp)}$_2$ solvent-mediated powder (solid) was measured using excitation wavelengths of λ_{ex} = 250 nm and λ_{ex} = 270 nm, respectively, producing noisy emission bands with a maximum emission peaks at λ_{em} = 683 nm and λ_{em} = 689 nm, respectively. A suitable photoluminescence decay curve was not obtained, using either of the aforementioned excitation and emission wavelengths, due to the weak emission intensity of the sample and noisy spectra. In addition, the photoluminescence was measured using an excitation wavelength of λ_{ex} = 470 nm, however an emission spectrum similar to that under the excitation wavelength of λ_{ex} = 270 nm was produced.

The UV-Vis absorption spectra for {Cu[3,5-$(CF_3)_2$Pz](dmp)}$_2$, shown in Figure 82, were obtained using three dilutions in dichloromethane (UV cutoff wavelength = 235 nm): 1 x 10^{-3} M, 1 x 10^{-4} M, and 1 x 10^{-5} M. A red shift was observed as the

concentration increased, shifting into the visible region (up to 650 nm), as well as π-π* transition with an extinction coefficient (ε_{273}) of 50,000 L·mol^{-1}·cm^{-1} (λ_{max2} = 273 nm: A = 0.5, C = 1 x 10^{-5} M).
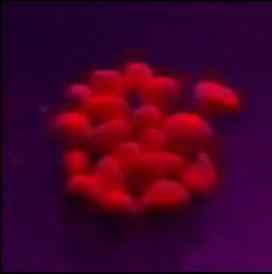
Figure 80. Photoluminescence of {Cu[3,5-(CF$_3$)$_2$Pz](dmp)}$_2$ crystals (top), solvent-mediated powder (*middle*), and solventless powder (*bottom*) under Short Wave UV (λ_{ex} = 254 nm) and Long Wave UV (λ_{ex} = 365 nm), at room temperature (RT).
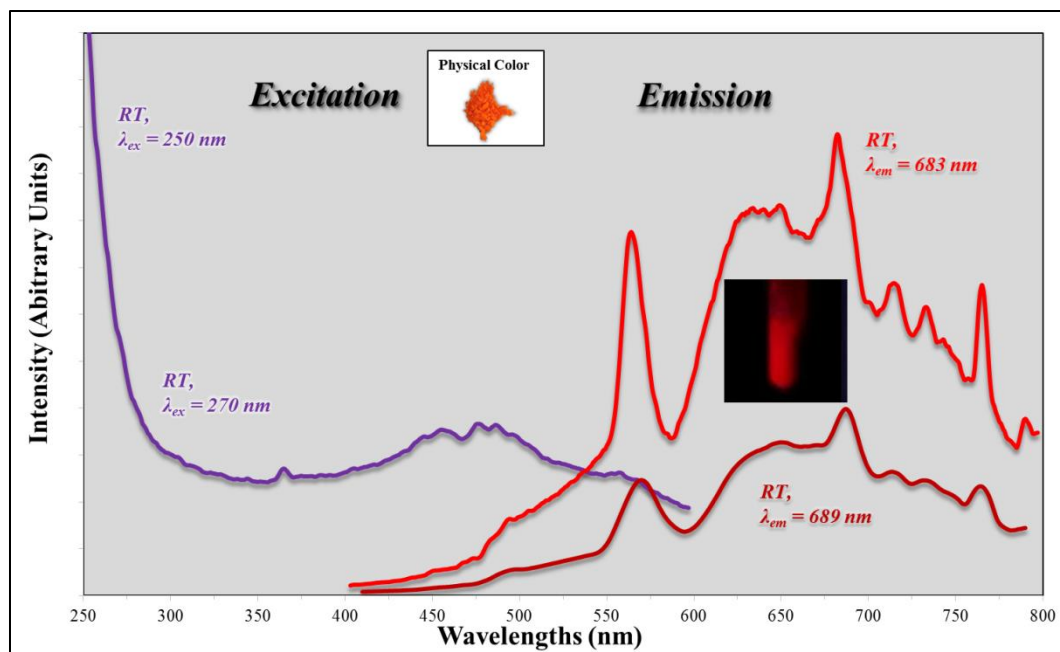
Figure 81. Photoluminescence spectra for {Cu[3,5-(CF$_3$)$_2$Pz](dmp)} solvent-mediated powder, at room temperature (RT).
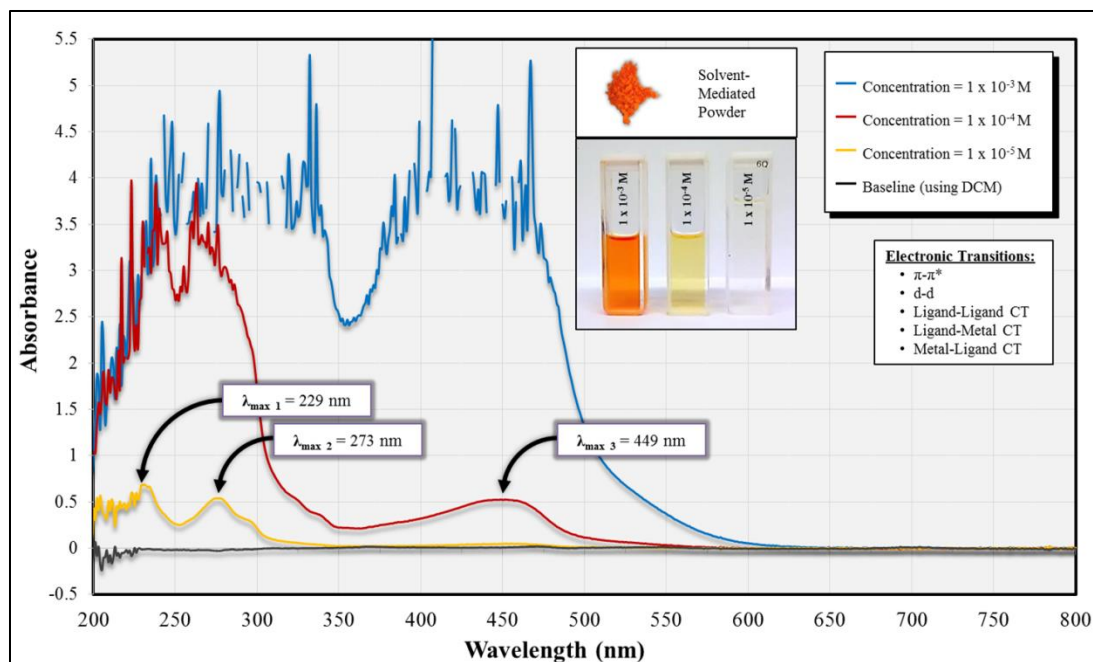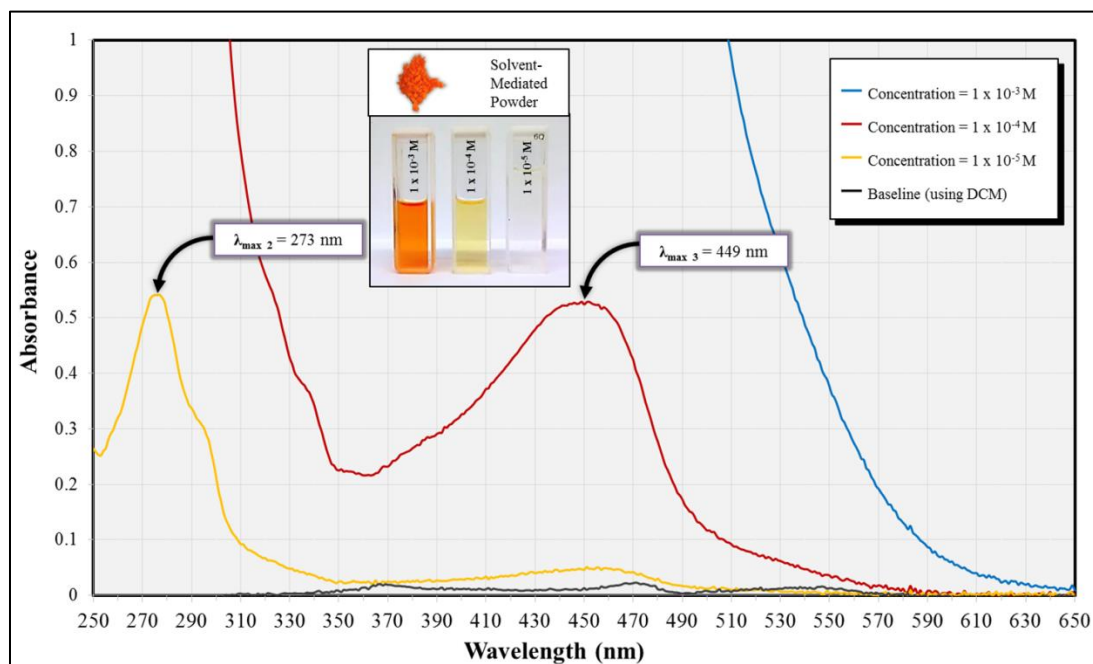
Figure 82. UV-Vis Spectra for {Cu[3,5-(CF₃)₂Pz](dmp)}₂ solvent-mediated powder in DCM solutions (UV cutoff wavelength = 235 nm): **(A)** Full-View =200-800 nm; **(B)** Zoomed-In = 350-650 nm.

3.2.6 Compound 7: [Cu(Lactate)(dmp)]$_2$

3.2.6.1 X-ray Crystallographic Data

In this section, the X-ray crystallographic data for [Cu(Lactate)(dmp)]$_2$ (shown in Tables 11A-B) are discussed. [Cu(Lactate)(dmp)]$_2$ single crystals were obtained using {Cu[3,5-(CF$_3$)$_2$Pz](dmp)}$_2$ solvent-mediated powder. Table 11A shows that [Cu(Lactate)(dmp)]$_2$ crystallizes in the triclinic crystal system with the space group *P*-1 with Z = 1 and the unit cell dimensions: a = 10.2318(4) Å, b = 10.7381(4) Å, c = 12.1324(4) Å, α = 77.890(3)°, β = 77.413(3)°, and γ = 69.836(3)°. [Cu(Lactate)(dmp)]$_2$ has the empirical formula C38 H36 Cl12 Cu2 N4 O6 (MW = 1197.19 g/mol), which accounts for the presence of four chloroform molecules (C H Cl3) in the symmetric unit cell.

As shown in Figure 83A, the asymmetric unit cell shows that the Cu(II) center: Cu1, coordinates (via bidentate chelating) with both the deprotonated lactate (CH$_3$CH(O$^-$)COO$^-$) ligand (via O1 and O3) and the dmp ligand (via N1 and N2). As shown in Figure 83B, the symmetric unit cell of [Cu(Lactate)(dmp)]$_2$ exhibits a Cu(II) dimeric structure with two 5-coordinated Cu(II) centers: Cu1 and Cu1A, respectively, doubly bridged via two deprotonated lactate ligands (via O3 and O3A). Moreover, each respective Cu(II) center is coordinated (via bidentate chelating) with their respective dmp ligands (via N1 and N2, and N1A and N2A, respectively). Overall, [Cu(Lactate)(dmp)]$_2$ exhibits a heteroleptic, dinuclear complex with two double bridging deprotonated lactate ligands and two bidentate chelating dmp ligands, which essentially serve as end caps. The

deprotonated lactate ligands act as both a bidentate chelating ligands (via O1 and O3, and O1A and O3A, respectively) and monodentate bridging ligands (via O3 and O3A).

Figure 83C shows the packing structure of $[Cu(Lactate)(dmp)]_2$. The bond lengths (Å) and angles (°) are shown in Table 11B. The full-matrix least-squares refinement method was used on F^2, resulting in a goodness-of-fit value of 1.029 with R1 = 4.03 % and wR2 = 9.14% for all data.

Table 11. (A) X-ray Crystallographic Data for [Cu(Lactate)(dmp)]$_2$; **(B)** Bond lengths [Å] and angles [°] for [Cu(Lactate)(dmp)]$_2$.

Empirical formula	C38 H36 Cl12 Cu2 N4 O6
Formula weight	1197.19
Temperature	100.00(10) K
Wavelength	0.71073 Å
Crystal system	Triclinic
Space group	P-1
Unit cell dimensions	a = 10.2318(4) Å α = 77.890(3)°.
	b = 10.7381(4) Å β = 77.413(3)°.
	c = 12.1324(4) Å γ = 69.836(3)°.
Volume	1207.95(8) Å^3
Z	1
Density (calculated)	1.646 Mg/m^3
Absorption coefficient	1.592 mm^{-1}
F(000)	602
Crystal size	0.1 x 0.051 x 0.03 mm^3
Theta range for data collection	2.043 to 27.100°.
Index ranges	-13<=h<=11, -13<=k<=13, -15<=l<=15
Reflections collected	15968
Independent reflections	5254 [R(int) = 0.0293]
Completeness to theta = 25.242°	100.0 %
Absorption correction	Semi-empirical from equivalents
Max. and min. transmission	1.00000 and 0.91635
Refinement method	Full-matrix least-squares on F^2
Data / restraints / parameters	5254 / 66 / 346
Goodness-of-fit on F^2	1.029
Final R indices [I>2sigma(I)]	R1 = 0.0359, wR2 = 0.0889
R indices (all data)	R1 = 0.0403, wR2 = 0.0914
Extinction coefficient	n/a
Largest diff. peak and hole	0.599 and -0.787 e.Å^{-3}

(A)

Bond Lengths [Å] (*blue*) & Angles [°] (*red*)				
Cu(1)-Cu(1)#1	3.0023(5)	Cl(6A)-C(2A)	1.569(12)	C(1)-C(13)-H(13A)	109.5
Cu(1)-O(1)	1.9626(15)	C(2A)-H(2A)	0.98	C(1)-C(13)-H(13B)	109.5
Cu(1)-O(3)	1.9210(15)	C(2A)-H(2AA)	0.98	C(1)-C(13)-H(13C)	109.5
Cu(1)-O(3)#1	1.9804(15)	O(1)-Cu(1)-Cu(1)#1	119.97(5)	H(13A)-C(13)-H(13B)	109.5
Cu(1)-N(1)	2.2894(18)	O(1)-Cu(1)-O(3)#1	148.79(7)	H(13A)-C(13)-H(13C)	109.5
Cu(1)-N(2)	2.0059(18)	O(1)-Cu(1)-N(1)	108.59(6)	H(13B)-C(13)-H(13C)	109.5
O(1)-C(15)	1.286(3)	O(1)-Cu(1)-N(2)	97.21(7)	C(10)-C(14)-H(14A)	109.5
O(2)-C(15)	1.239(3)	O(3)-Cu(1)-Cu(1)#1	40.42(4)	C(10)-C(14)-H(14B)	109.5
O(3)-C(16)	1.391(4)	O(3)#1-Cu(1)-Cu(1)#1	38.97(4)	C(10)-C(14)-H(14C)	109.5
O(3)-C(16A)	1.515(13)	O(3)-Cu(1)-O(1)	84.21(6)	H(14A)-C(14)-H(14B)	109.5
N(1)-C(1)	1.330(3)	O(3)-Cu(1)-O(3)#1	79.39(7)	H(14A)-C(14)-H(14C)	109.5
N(1)-C(12)	1.366(3)	O(3)-Cu(1)-N(1)	109.23(7)	H(14B)-C(14)-H(14C)	109.5
N(2)-C(10)	1.336(3)	O(3)#1-Cu(1)-N(1)	101.85(6)	O(1)-C(15)-C(16)	116.7(2)
N(2)-C(11)	1.360(3)	O(3)-Cu(1)-N(2)	171.55(7)	O(1)-C(15)-C(16A)	116.4(6)
C(1)-C(2)	1.413(3)	O(3)#1-Cu(1)-N(2)	95.49(7)	O(2)-C(15)-O(1)	123.8(2)
C(1)-C(13)	1.499(3)	N(1)-Cu(1)-Cu(1)#1	110.25(5)	O(2)-C(15)-C(16)	119.2(2)
C(2)-H(2)	0.93	N(2)-Cu(1)-Cu(1)#1	134.11(5)	O(2)-C(15)-C(16A)	117.6(6)
C(2)-C(3)	1.366(4)	N(2)-Cu(1)-N(1)	78.29(7)	O(3)-C(16)-C(15)	108.8(2)
C(3)-H(3)	0.93	C(15)-O(1)-Cu(1)	113.62(14)	O(3)-C(16)-H(16)	109.4
C(3)-C(4)	1.408(3)	Cu(1)-O(3)-Cu(1)#1	100.61(7)	O(3)-C(16)-C(17)	111.4(3)
C(4)-C(5)	1.434(3)	C(16)-O(3)-Cu(1)#1	127.97(18)	C(15)-C(16)-H(16)	109.4
C(4)-C(12)	1.408(3)	C(16)-O(3)-Cu(1)	114.90(17)	C(17)-C(16)-C(15)	108.4(3)
C(5)-H(5)	0.93	C(16A)-O(3)-Cu(1)	111.2(5)	C(17)-C(16)-H(16)	109.4
C(5)-C(6)	1.354(4)	C(1)-N(1)-Cu(1)	133.78(15)	O(3)-C(16A)-H(16A)	107.3
C(6)-H(6)	0.93	C(1)-N(1)-C(12)	118.46(19)	C(15)-C(16A)-O(3)	107.1(9)
C(6)-C(7)	1.430(4)	C(12)-N(1)-Cu(1)	107.69(14)	C(15)-C(16A)-H(16A)	107.3
C(7)-C(8)	1.409(4)	C(10)-N(2)-Cu(1)	123.21(15)	C(17A)-C(16A)-O(3)	115.3(9)
C(7)-C(11)	1.414(3)	C(10)-N(2)-C(11)	119.69(19)	C(17A)-C(16A)-C(15)	112.1(11)
C(8)-H(8)	0.93	C(11)-N(2)-Cu(1)	116.68(14)	C(17A)-C(16A)-H(16A)	107.3
C(8)-C(9)	1.369(4)	N(1)-C(1)-C(2)	121.6(2)	C(16)-C(17)-H(17A)	109.5
C(9)-H(9)	0.93	N(1)-C(1)-C(13)	118.1(2)	C(16)-C(17)-H(17B)	109.5
C(9)-C(10)	1.411(3)	C(2)-C(1)-C(13)	120.2(2)	C(16)-C(17)-H(17C)	109.5
C(10)-C(14)	1.498(3)	C(1)-C(2)-H(2)	119.9	H(17A)-C(17)-H(17B)	109.5
C(11)-C(12)	1.440(3)	C(3)-C(2)-C(1)	120.1(2)	H(17A)-C(17)-H(17C)	109.5
C(13)-H(13A)	0.96	C(3)-C(2)-H(2)	119.9	H(17B)-C(17)-H(17C)	109.5
C(13)-H(13B)	0.96	C(2)-C(3)-H(3)	120.2	C(16A)-C(17A)-H(17D)	109.5
C(13)-H(13C)	0.96	C(2)-C(3)-C(4)	119.6(2)	C(16A)-C(17A)-H(17E)	109.5
C(14)-H(14A)	0.96	C(4)-C(3)-H(3)	120.2	C(16A)-C(17A)-H(17F)	109.5
C(14)-H(14B)	0.96	C(3)-C(4)-C(5)	123.1(2)	H(17D)-C(17A)-H(17E)	109.5
C(14)-H(14C)	0.96	C(12)-C(4)-C(3)	117.0(2)	H(17D)-C(17A)-H(17F)	109.5
C(15)-C(16)	1.567(4)	C(12)-C(4)-C(5)	119.9(2)	H(17E)-C(17A)-H(17F)	109.5
C(15)-C(16A)	1.477(14)	C(4)-C(5)-H(5)	119.6	Cl(1)-C(1A)-H(1A)	109
C(16)-H(16)	0.98	C(6)-C(5)-C(4)	120.9(2)	Cl(1A)-C(1A)-H(1AA)	108.4

C(16)-C(17)	1.535(5)	C(6)-C(5)-H(5)	119.6	Cl(2)-C(1A)-Cl(1)	107.8(2)
C(16A)-H(16A)	0.98	C(5)-C(6)-H(6)	119.6	Cl(2)-C(1A)-H(1A)	109
C(16A)-C(17A)	1.428(18)	C(5)-C(6)-C(7)	120.7(2)	Cl(2A)-C(1A)-Cl(1A)	110.0(4)
C(17)-H(17A)	0.96	C(7)-C(6)-H(6)	119.6	Cl(2A)-C(1A)-Cl(3A)	114.2(4)
C(17)-H(17B)	0.96	C(8)-C(7)-C(6)	123.2(2)	Cl(2A)-C(1A)-H(1AA)	108.4
C(17)-H(17C)	0.96	C(8)-C(7)-C(11)	117.1(2)	Cl(3)-C(1A)-Cl(1)	111.8(3)
C(17A)-H(17D)	0.96	C(11)-C(7)-C(6)	119.7(2)	Cl(3)-C(1A)-Cl(2)	110.1(2)
C(17A)-H(17E)	0.96	C(7)-C(8)-H(8)	120	Cl(3)-C(1A)-H(1A)	109
C(17A)-H(17F)	0.96	C(9)-C(8)-C(7)	119.9(2)	Cl(3A)-C(1A)-Cl(1A)	107.3(4)
Cl(1)-C(1A)	1.810(5)	C(9)-C(8)-H(8)	120	Cl(3A)-C(1A)-H(1AA)	108.4
Cl(1A)-C(1A)	1.792(8)	C(8)-C(9)-H(9)	120	Cl(4)-C(2A)-H(2A)	108.6
Cl(2)-C(1A)	1.771(4)	C(8)-C(9)-C(10)	119.9(2)	Cl(4A)-C(2A)-Cl(5A)	101.9(5)
Cl(2A)-C(1A)	1.652(8)	C(10)-C(9)-H(9)	120	Cl(4A)-C(2A)-Cl(6A)	113.2(7)
Cl(3)-C(1A)	1.731(5)	N(2)-C(10)-C(9)	121.0(2)	Cl(4A)-C(2A)-H(2AA)	111
Cl(3A)-C(1A)	1.741(7)	N(2)-C(10)-C(14)	118.0(2)	Cl(5)-C(2A)-Cl(4)	109.86(19)
C(1A)-H(1A)	0.98	C(9)-C(10)-C(14)	121.0(2)	Cl(5)-C(2A)-H(2A)	108.6
C(1A)-H(1AA)	0.98	N(2)-C(11)-C(7)	122.2(2)	Cl(5A)-C(2A)-H(2AA)	111
Cl(4)-C(2A)	1.800(5)	N(2)-C(11)-C(12)	118.15(19)	Cl(6)-C(2A)-Cl(4)	108.1(3)
Cl(4A)-C(2A)	1.437(10)	C(7)-C(11)-C(12)	119.6(2)	Cl(6)-C(2A)-Cl(5)	113.0(2)
Cl(5)-C(2A)	1.796(4)	N(1)-C(12)-C(4)	123.2(2)	Cl(6)-C(2A)-H(2A)	108.6
Cl(5A)-C(2A)	1.832(7)	N(1)-C(12)-C(11)	117.84(19)	Cl(6A)-C(2A)-Cl(5A)	108.4(5)
Cl(6)-C(2A)	1.727(4)	C(4)-C(12)-C(11)	119.0(2)	Cl(6A)-C(2A)-H(2AA)	111

Symmetry transformations used to generate equivalent atoms:
#1 -x,-y+1,-z+1

(B)
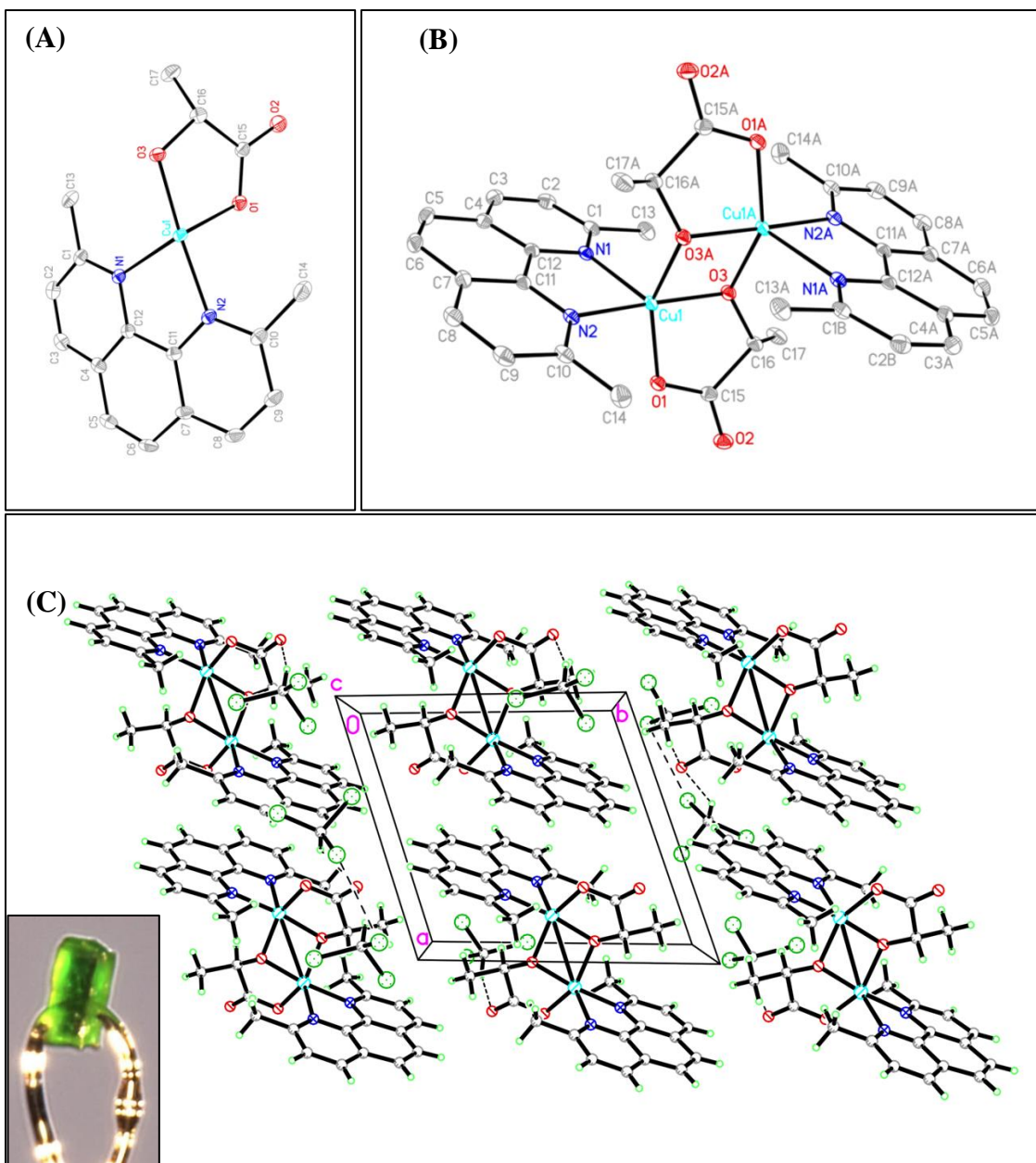
Figure 83. Crystal Structure of [Cu(Lactate)(dmp)]₂: **(A)** Asymmetric Unit Cell, **(B)** Symmetric Unit Cell, and **(C)** Packing.

3.2.6.2 Elemental Analysis Data
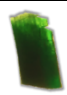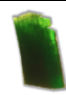
In this section, the elemental analysis data for [Cu(Lactate)(dmp)]$_2$ crystals, shown in Table 12, are discussed, comparing the experimentally found data with the theoretical Anal. Calc.

The theoretical percentages of carbon (C), hydrogen (H), and nitrogen (N) were analytically calculated (Anal. Calc.) based on the "adjusted" empirical formula C137 H129 Cl3 Cu8 N16 O24 (MW = 2998.31 g/mol): C, 54.88; H, 4.34; N, 7.47. The "adjusted" empirical formula for the crystals accounts for presence of one chloroform molecule (C H Cl3) for every four units of [Cu(Lactate)(dmp)]$_2$. As shown in Table 12, two sets of experimentally found data were obtained for two samples of [Cu(Lactate)(dmp)]$_2$ green crystal, with the "first" sample (*left*) containing less impurities and the "second" sample (*right*) containing more impurities. The "first" set of experimentally found data for the green crystals (C, 54.55; H, 4.08; N, 7.88) relatively match that of the theoretical Anal. Calc. within ±0.33 for C, ±0.26 for H, and ±0.41 for N. The "second" set of experimentally found data for the green crystals (C, 50.93; H, 3.77; N, 7.53) somewhat match that of the theoretical Anal. Calc. within ±3.95 for C, ±0.57 for H, and ±0.35 for N. However, the significant difference in %C suggests the presence of impurities in the "second" (*right*) sample, possibly related to the presence of {Cu[3,5-(CF$_3$)$_2$Pz](dmp)}$_2$. The elemental data showed that the "first" set of experimentally found data contained less impurities compared to the "second" set of experimentally found data.

The theoretical percentages of carbon (C), hydrogen (H), and nitrogen (N) were analytically calculated (Anal. Calc.) based on the "original" empirical formula C38 H36

Cl12 Cu2 N4 O6 (MW = 1197.19 g/mol): C, 38.12; H, 3.03; N, 4.68. The "first" set of experimentally found data for the green crystals (C, 54.55; H, 4.08; N, 7.88) does not match that of the theoretical Anal. Calc. and differs within ±16.43 for C, ±1.05 for H, and ±3.20 for N. The "original" empirical formula accounts for presence of four chloroform molecule (C H Cl3) for every unit of [Cu(Lactate)(dmp)]$_2$; however, it is worth noting that the green crystals are very unstable out of solution, which prompted the "adjustment" of the "original" empirical formula to reflect the presence of chloroform with [Cu(Lactate)(dmp)]$_2$ in a 1:4 molar ratio, rather than a 4:1 molar ratio.

Table 12. Elemental analysis data for [Cu(Lactate)(dmp)]$_2$ crystals: theoretical Anal. Calc. versus experimentally found data.

Elemental Analysis			
[Cu(Lactate)(dmp)]$_2$ = C34 H32 Cu2 N4 O6			
		Crystals *(w/ less impurities)*	**Crystals** *(w/ more impurities)*
4 [Cu(Lactate)(dmp)]$_2$ + Chloroform = 4(C34 H32 Cu2 N4 O6), (C H Cl3)			
Element	**Theoretical Anal. Calc.**	**Experimentally Found**	**Experimentally Found**
C	54.88%	54.55%	50.93%
H	4.34%	4.08%	3.77%
N	7.47%	7.88%	7.53%
Cu	16.96%		
[Cu(Lactate)(dmp)]$_2$ + 4 Chloroform = (C34 H32 Cu2 N4 O6), 4 (C H Cl3)			
Element	**Theoretical Anal. Calc.**	**Experimentally Found**	**Experimentally Found**
C	38.12%	54.55%	54.55%
H	3.03%	4.08%	4.08%
N	4.68%	7.88%	7.88%
Cu	10.62%		

3.2.6.3 Characterization using FT-IR Spectroscopy

In this section, the IR spectrum for [Cu(Lactate)(dmp)]$_2$ crystals, as shown in Figure 84, is discussed. The IR spectrum features the functional groups characteristic of both the deprotonated lactate and the dmp ligands: =C-H stretch (aromatic), C=C stretch (aromatic), C=N stretch (aromatic), C-C stretch (aromatic), C-N stretch (aromatic), C-F stretch, C-H stretch (C-CH$_3$), C=O stretch (COO$^-$), and C-O stretch (COO$^-$).

Functional Groups	Expected Range (cm^{-1})
=C-H stretch (aromatic)	3010-3100, 690-900
C=C stretch (aromatic)	1400, 1600
C=N stretch (aromatic)	1400-1620
C-C stretch (aromatic)	1400-1500
C-N stretch (aromatic)	1250-1335
C-H stretch (C-CH$_3$)	2862-2882, 2652-2972
C=O stretch (COO$^-$)	1600
C-O stretch (COO$^-$)	1300, 1100
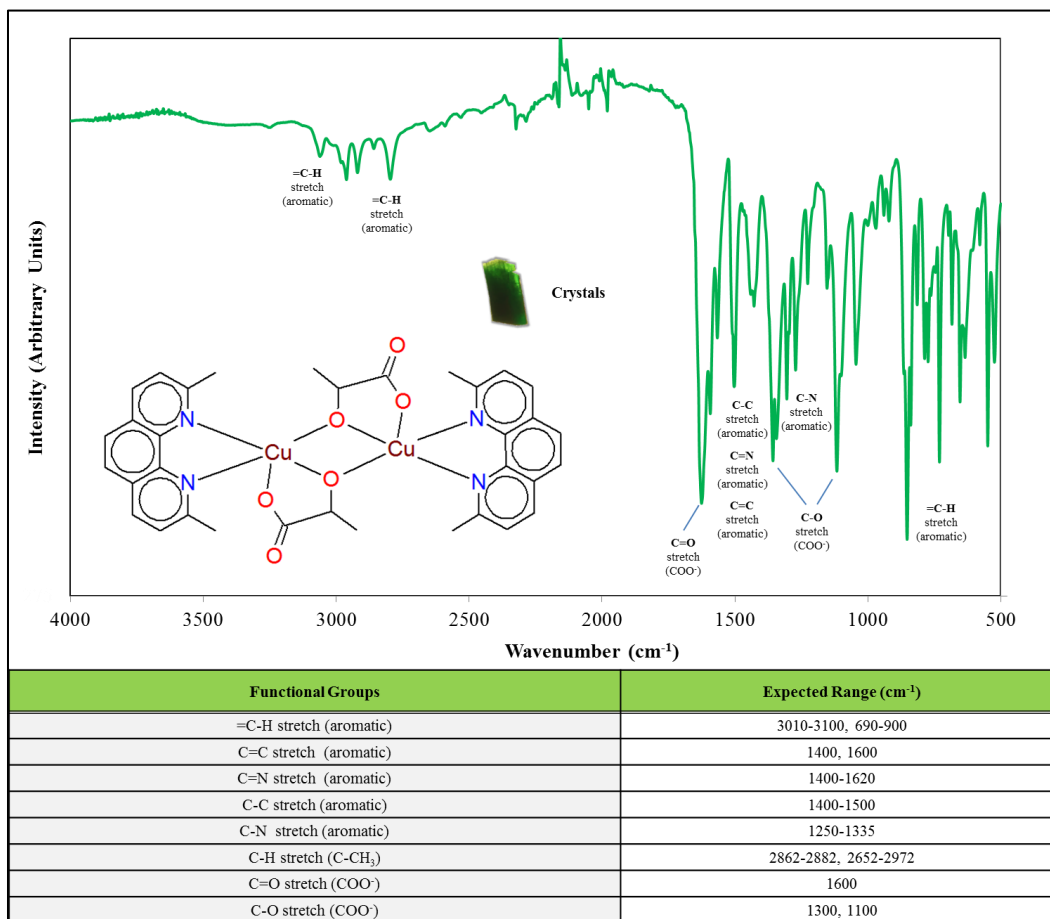
Figure 84. FT-IR spectrum for [Cu(Lactate)(dmp)]$_2$ crystals.

3.2.7 Compound 6: {Ag[3,5-(CF$_3$)$_2$Pz](dmp)}$_2$

3.2.7.1 X-ray Crystallographic Data

In this section, the X-ray crystallographic data for {Ag[3,5-(CF$_3$)$_2$Pz](dmp)}$_2$ (shown in Tables 13A-B) are discussed. {Ag[3,5-(CF$_3$)$_2$Pz](dmp)}$_2$ single crystals were obtained using solvent-mediated powder. Table 13A shows that {Ag[3,5-(CF$_3$)$_2$Pz](dmp)}$_2$ crystallizes in the triclinic crystal system with the space group *P*-1 with Z = 1 and the unit cell dimensions: a = 8.3485(3) Å, b = 10.3770(3) Å, c = 11.8547(4) Å, α = 97.062(2)°, β = 106.059(3)°, and γ = 100.705(2)°. {Ag[3,5-(CF$_3$)$_2$Pz](dmp)}$_2$ has the empirical formula C38 H26 Ag2 F12 N8 (MW = 1038.41 g/mol).

As shown in Figure 85A, the asymmetric unit cell shows that the Ag(I) center: Ag1, coordinates with the [3,5-(CF$_3$)$_2$Pz]$^-$ ligand (via N1) and the dmp ligand (via N3 and N4). As shown in Figure 85B, the symmetric unit cell of {Ag[3,5-(CF$_3$)$_2$Pz](dmp)}$_2$ exhibits a Ag(I) dimeric structure with two 4-coordinated Ag(I) centers: Ag1 and Ag1A, respectively, doubly bridged via two [3,5-(CF$_3$)$_2$Pz]$^-$ ligands (via N1 and N2, and N1A and N2A, respectively). Moreover, each respective Ag(I) center is coordinated (via bidentate chelating) with their respective dmp ligands (via N3 and N4, and N3A and N4A, respectively). Overall, {Ag[3,5-(CF$_3$)$_2$Pz](dmp)}$_2$ exhibits a heteroleptic, dinuclear complex with two double bridging [3,5-(CF$_3$)$_2$Pz]$^-$ ligands and two bidentate chelating dmp ligands, which essentially serve as end caps.

Figure 85C shows the packing structure of $\{Ag[3,5-(CF_3)_2Pz](dmp)\}_2$. The bond lengths (Å) and angles (°) are shown in Table 13B. The full-matrix least-squares refinement method was used on F^2, resulting in a goodness-of-fit value of 1.043 with R1 = 3.00 % and wR2 = 7.25% for all data.

Table 13. (A) X-ray Crystallographic Data for {Ag[3,5-(CF$_3$)$_2$Pz](dmp)}$_2$;
(B) Bond lengths [Å] and angles [°] for {Ag[3,5-(CF$_3$)$_2$Pz](dmp)}$_2$.

Empirical formula	C38 H26 Ag2 F12 N8
Formula weight	1038.41
Temperature	100.01(10) K
Wavelength	0.71073 Å
Crystal system	Triclinic
Space group	P-1
Unit cell dimensions	a = 8.3485(3) Å $\quad$ α= 97.062(2)°. b = 10.3770(3) Å $\quad$ β= 106.059(3)°. c = 11.8547(4) Å $\quad$ γ = 100.705(2)°.
Volume	953.08(6) Å^3
Z	1
Density (calculated)	1.809 Mg/m^3
Absorption coefficient	1.128 mm^{-1}
F(000)	512
Crystal size	0.1 x 0.05 x 0.03 mm^3
Theta range for data collection	2.032 to 27.100°.
Index ranges	-10<=h<=10, -13<=k<=12, -14<=l<=15
Reflections collected	14815
Independent reflections	4169 [R(int) = 0.0314]
Completeness to theta = 25.242°	99.9 %
Absorption correction	Semi-empirical from equivalents
Max. and min. transmission	1.00000 and 0.90026
Refinement method	Full-matrix least-squares on F^2
Data / restraints / parameters	4169 / 0 / 273
Goodness-of-fit on F^2	1.043
Final R indices [I>2sigma(I)]	R1 = 0.0274, wR2 = 0.0706
R indices (all data)	R1 = 0.0300, wR2 = 0.0725
Extinction coefficient	n/a
Largest diff. peak and hole	1.254 and -0.565 e.Å^{-3}

(A)

Bond Lengths [Å] (*blue*) & Angles [°] (red)					
Ag(1)-N(1)	2.2447(19)	C(19)-H(19A)	0.96	C(6)-C(7)-H(7)	120.3
Ag(1)-N(2)#1	2.2686(18)	C(19)-H(19B)	0.96	C(8)-C(7)-C(6)	119.5(2)
Ag(1)-N(3)	2.3693(19)	C(19)-H(19C)	0.96	C(8)-C(7)-H(7)	120.3
Ag(1)-N(4)	2.3816(19)	N(1)-Ag(1)-N(2)#1	118.08(7)	C(7)-C(8)-H(8)	119.7
F(1)-C(4)	1.341(3)	N(1)-Ag(1)-N(3)	117.60(7)	C(7)-C(8)-C(9)	120.5(2)
F(2)-C(4)	1.345(3)	N(1)-Ag(1)-N(4)	116.77(7)	C(9)-C(8)-H(8)	119.7
F(3)-C(4)	1.338(3)	N(2)#1-Ag(1)-N(3)	117.05(6)	C(8)-C(9)-C(10)	123.1(2)
F(4)-C(5)	1.307(3)	N(2)#1-Ag(1)-N(4)	106.79(7)	C(17)-C(9)-C(8)	116.9(2)
F(5)-C(5)	1.338(3)	N(3)-Ag(1)-N(4)	70.72(6)	C(17)-C(9)-C(10)	120.0(2)
F(6)-C(5)	1.330(3)	N(2)-N(1)-Ag(1)	119.64(14)	C(9)-C(10)-H(10)	119.6
N(1)-N(2)	1.360(2)	C(1)-N(1)-Ag(1)	132.67(15)	C(11)-C(10)-C(9)	120.7(2)
N(1)-C(1)	1.348(3)	C(1)-N(1)-N(2)	107.41(18)	C(11)-C(10)-H(10)	119.6
N(2)-C(3)	1.352(3)	N(1)-N(2)-Ag(1)#1	121.16(14)	C(10)-C(11)-H(11)	119.5
N(3)-C(6)	1.326(3)	C(3)-N(2)-Ag(1)#1	131.25(15)	C(10)-C(11)-C(12)	121.0(2)
N(3)-C(17)	1.368(3)	C(3)-N(2)-N(1)	107.08(18)	C(12)-C(11)-H(11)	119.5
N(4)-C(15)	1.332(3)	C(6)-N(3)-Ag(1)	124.19(15)	C(13)-C(12)-C(11)	122.9(2)
N(4)-C(16)	1.359(3)	C(6)-N(3)-C(17)	119.34(19)	C(13)-C(12)-C(16)	117.2(2)
C(1)-C(2)	1.384(3)	C(17)-N(3)-Ag(1)	116.47(14)	C(16)-C(12)-C(11)	119.9(2)
C(1)-C(4)	1.487(3)	C(15)-N(4)-Ag(1)	124.98(15)	C(12)-C(13)-H(13)	120.1
C(2)-H(2)	0.93	C(15)-N(4)-C(16)	119.0(2)	C(14)-C(13)-C(12)	119.9(2)
C(2)-C(3)	1.385(3)	C(16)-N(4)-Ag(1)	115.98(14)	C(14)-C(13)-H(13)	120.1
C(3)-C(5)	1.492(3)	N(1)-C(1)-C(2)	111.48(19)	C(13)-C(14)-H(14)	120.1
C(6)-C(7)	1.418(3)	N(1)-C(1)-C(4)	120.5(2)	C(13)-C(14)-C(15)	119.8(2)
C(6)-C(18)	1.496(3)	C(2)-C(1)-C(4)	128.1(2)	C(15)-C(14)-H(14)	120.1
C(7)-H(7)	0.93	C(1)-C(2)-H(2)	128.7	N(4)-C(15)-C(14)	121.7(2)
C(7)-C(8)	1.357(4)	C(1)-C(2)-C(3)	102.5(2)	N(4)-C(15)-C(19)	117.1(2)
C(8)-H(8)	0.93	C(3)-C(2)-H(2)	128.7	C(14)-C(15)-C(19)	121.2(2)
C(8)-C(9)	1.409(4)	N(2)-C(3)-C(2)	111.48(19)	N(4)-C(16)-C(12)	122.5(2)
C(9)-C(10)	1.432(3)	N(2)-C(3)-C(5)	120.2(2)	N(4)-C(16)-C(17)	118.81(19)
C(9)-C(17)	1.403(3)	C(2)-C(3)-C(5)	128.3(2)	C(12)-C(16)-C(17)	118.7(2)
C(10)-H(10)	0.93	F(1)-C(4)-F(2)	105.94(19)	N(3)-C(17)-C(9)	122.4(2)
C(10)-C(11)	1.349(4)	F(1)-C(4)-C(1)	113.27(19)	N(3)-C(17)-C(16)	118.00(19)
C(11)-H(11)	0.93	F(2)-C(4)-C(1)	112.8(2)	C(9)-C(17)-C(16)	119.6(2)
C(11)-C(12)	1.436(3)	F(3)-C(4)-F(1)	106.47(19)	C(6)-C(18)-H(18A)	109.5
C(12)-C(13)	1.405(4)	F(3)-C(4)-F(2)	106.56(19)	C(6)-C(18)-H(18B)	109.5
C(12)-C(16)	1.409(3)	F(3)-C(4)-C(1)	111.36(19)	C(6)-C(18)-H(18C)	109.5
C(13)-H(13)	0.93	F(4)-C(5)-F(5)	108.7(2)	H(18A)-C(18)-H(18B)	109.5
C(13)-C(14)	1.365(4)	F(4)-C(5)-F(6)	107.0(2)	H(18A)-C(18)-H(18C)	109.5
C(14)-H(14)	0.93	F(4)-C(5)-C(3)	111.1(2)	H(18B)-C(18)-H(18C)	109.5
C(14)-C(15)	1.404(4)	F(5)-C(5)-C(3)	112.4(2)	C(15)-C(19)-H(19A)	109.5
C(15)-C(19)	1.503(3)	F(6)-C(5)-F(5)	104.4(2)	C(15)-C(19)-H(19B)	109.5
C(16)-C(17)	1.452(3)	F(6)-C(5)-C(3)	112.8(2)	C(15)-C(19)-H(19C)	109.5
C(18)-H(18A)	0.96	N(3)-C(6)-C(7)	121.4(2)	H(19A)-C(19)-H(19B)	109.5
C(18)-H(18B)	0.96	N(3)-C(6)-C(18)	118.0(2)	H(19A)-C(19)-H(19C)	109.5
C(18)-H(18C)	0.96	C(7)-C(6)-C(18)	120.6(2)	H(19B)-C(19)-H(19C)	109.5
Symmetry transformations used to generate equivalent atoms:					
#1 -x+1,-y+1,-z+1					

(B)

175
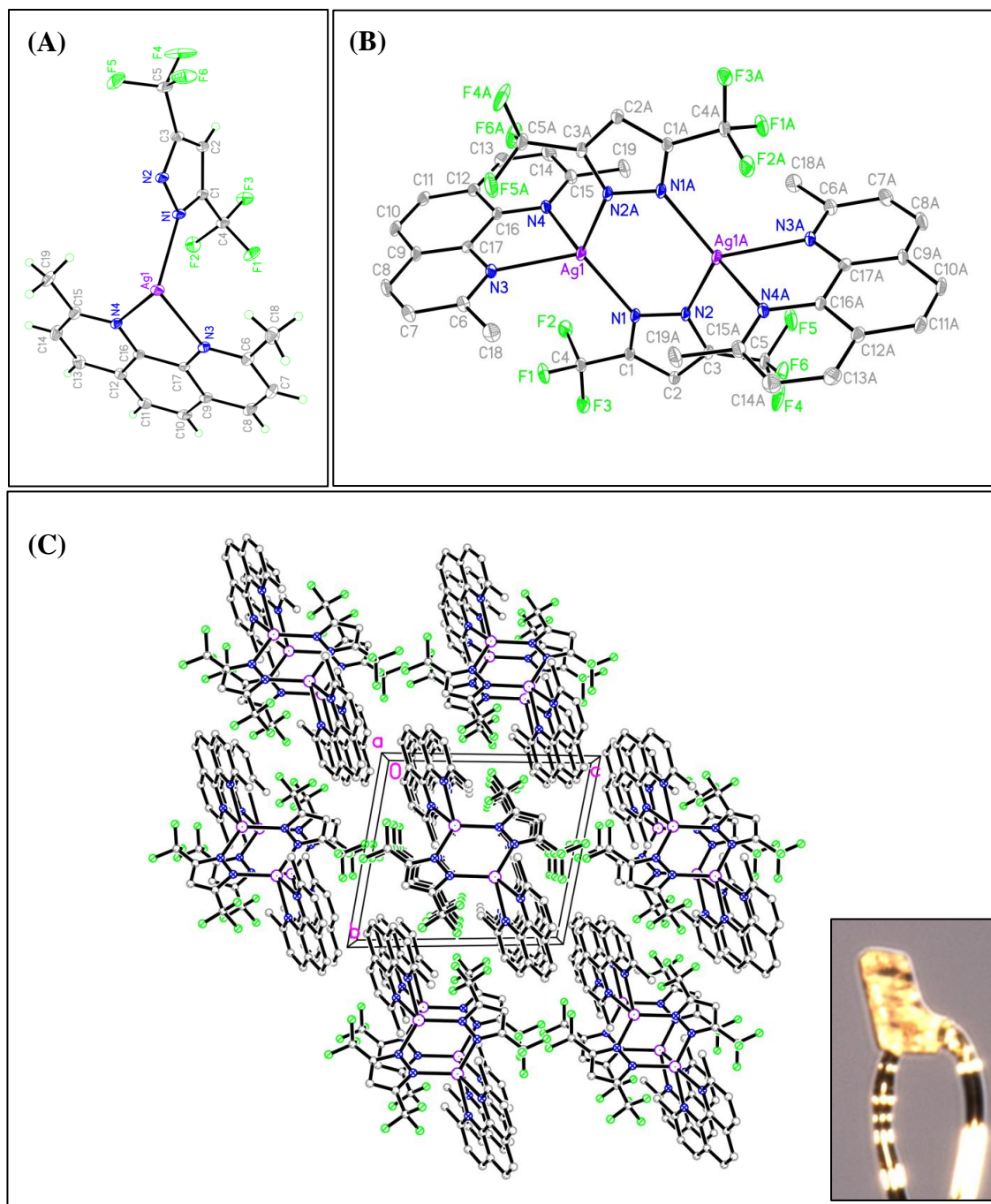
Figure 85. Crystal Structure of {Ag[3,5-(CF$_3$)$_2$Pz](dmp)}$_2$: **(A)** Asymmetric Unit Cell, **(B)** Symmetric Unit Cell, and **(C)** Packing.

3.2.7.2 Elemental Analysis Data

In this section, the elemental analysis data are discussed, comparing the experimentally found data with the theoretical Anal. Calc., shown in Table 14. The theoretical percentages of carbon (C), hydrogen (H), and nitrogen (N) were analytically calculated (Anal. Calc.) based on the empirical formula C38 H26 Ag2 F12 N8 (MW = 1038.41 g/mol): C, 43.95; H, 2.52; N, 10.79. The experimentally found data for the solvent-mediated powder (C, 43.94; H, 2.48; N, 10.69) match that of the theoretical Anal. Calc. within ±0.01 for C, ±0.04 for H, and ±0.10 for N. The experimentally found data for crystals (C, 48.03; H, 2.68; N, 11.61) match that of the theoretical Anal. Calc. within ±0.02 for C, ±0.07 for H, and ±0.02 for N. This comparison confirms that the solvent-mediated powder and crystals are the same {Ag [3,5-$(CF_3)_2$Pz](dmp)}$_2$ product.

Table 14. Elemental analysis data for {Ag[3,5-$(CF_3)_2$Pz](dmp)}$_2$ solvent-mediated powder and crystals: theoretical Anal. Calc. versus experimentally found data.

Elemental Analysis			
Empirical Formula: C38 H26 Ag2 F12 N8 (MW = 1038.41 g/mol)			
		Solvent-Mediated	Crystals
Element	**Theoretical Anal. Calc.**	**Experimentally Found**	**Experimentally Found**
C	43.95%	43.94%	43.93%
H	2.52%	2.48%	2.45%
N	10.79%	10.69%	10.77%
Ag	20.78%		

3.2.7.3 Characterization using FT-IR Spectroscopy

In this section, the IR spectra for$\{Ag[3,5\text{-}(CF_3)_2Pz](dmp)\}_2$ solvent-mediated powder, solventless powder, and crystals, as shown in Figure 86, are discussed. The IR spectra for solvent-mediated powder, solventless powder, and crystals are relatively identical to one another and feature the functional groups characteristic of both the $[3,5\text{-}(CF_3)_2Pz]^-$ and dmp ligands: =C-H stretch (aromatic), C=C stretch (aromatic), C=N stretch (aromatic), C-C stretch (aromatic), C-N stretch (aromatic), C-F stretch, and C-H stretch (C-CH_3).

Functional Groups	Expected Range (cm^{-1})
=C-H stretch (aromatic)	3010-3100, 690-900
C=C stretch (aromatic)	1400, 1600
C=N stretch (aromatic)	1400-1620
C-C stretch (aromatic)	1400-1500
C-N stretch (aromatic)	1250-1335
C-F stretch	1000-1400
C-H stretch (C-CH_3)	2862-2882, 2652-2972
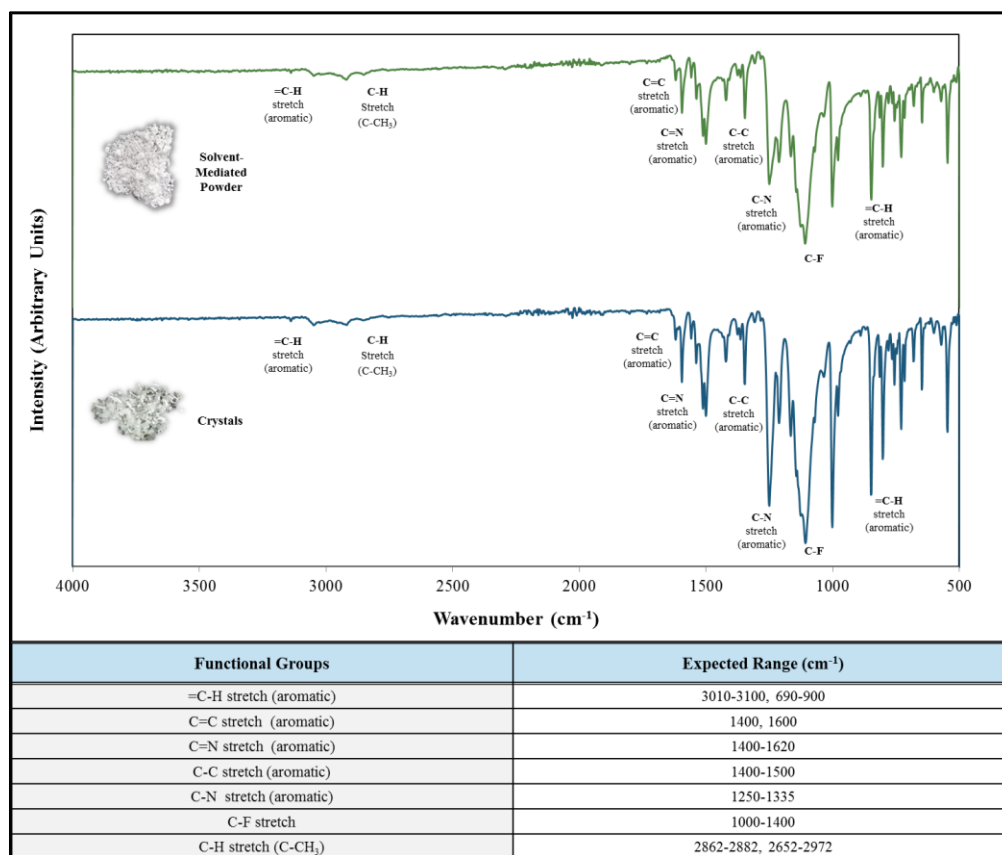
Figure 86. Stacked FT-IR spectra for $\{Ag[3,5\text{-}(CF_3)_2Pz](dmp)\}_2$ solvent-mediated powder (*top*) and crystals (*bottom*).

3.2.7.4 Characterization using TGA and DSC Analyses

In this section, the TGA analyses (and DSC analysis) for {Ag[3,5-$(CF_3)_2$Pz](dmp)}$_2$ crystals and solvent-mediated powder, as shown in Figures 87-89, are discussed.

The TGA analyses of crystals and solvent-mediated powder, shown in Figures 87 and 88, respectively, are relatively similar to one another with regard to percent weight loss, onset temperatures, and inflection points. The crystals and solvent-mediated powder, respectively, show significant weight losses of 60.62% and 58.36%, respectively, for the first weight drop, followed by 18.08% and 11.39%, respectively, for the second weight drop, resulting in total weight losses of 78.70% and 69.75%, respectively. For the first weight drop, onset temperatures (the temperatures at which weight loss begins) of 260.24°C and 258.04°C, respectively, and 1st derivative peaks (greatest rate of change on the weight loss curves) of 276.10°C and 282.5°C, respectively, were observed. The differences in onset temperatures and 1st derivative peaks (inflection points) may be attributed to the differences in sample for the crystals, solventless powder, and solvent-mediated powder: 5.5880 mg, 9.4180 mg, respectively, in that as the sample size increases, an increase (shift) in temperature occurs.

With regard to the emperical formula C38 H26 Ag2 F12 N8 (MW = 1038.41g/mol), the theoretical percentage of silver is 20.78%; however, the total weight losses of 78.70%, and 69.75%, respectively, were observed, which was primarily due to the sublimation of the [3,5-$(CF_3)_2$Pz]$^-$ and dmp ligands (total theoretical percentage of C, H, N and F of 79.22%). The remaining weight percentages, 21.30%, and 30.25%,

respectively, following the aforementioned weight losses (after heating up to 1000°C) should theoretically be silver (primarily) and possibly dmp rather than $[3,5-(CF_3)_2Pz]^-$ (completely sublimes by 150°C). With regard to the crystals, the theoretical percentage of silver is 20.78%, which is relatively close to the remaining weight percentages of 21.30%.

Figure 89 shows the DSC analysis for $\{Ag[3,5-(CF_3)_2Pz](dmp)\}_2$ solvent-mediated powder. A sharp peak maximum is observed at 254.60°C (melting point), with an onset temperature of 252.54°C. The TGA analysis for the solvent-mediated powder, shown in Figure 88 shows that the sample begins to decompose before 258.04°C (the on-set temperature for weight loss). Therefore, the sample was not heated beyond 256°C (using DSC) as a precaution in order to avoid heating the sample to decomposition, which can destroy/damage the sensor of the DSC instrument.
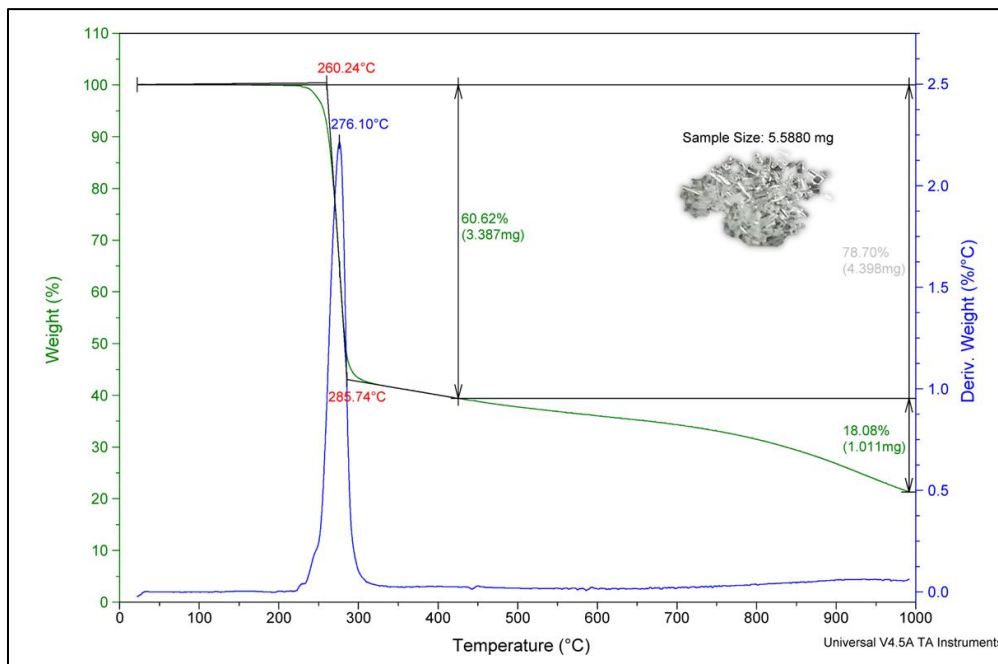
Figure 87. TGA analysis for $\{Ag[3,5-(CF_3)_2Pz](dmp)\}_2$ crystals.
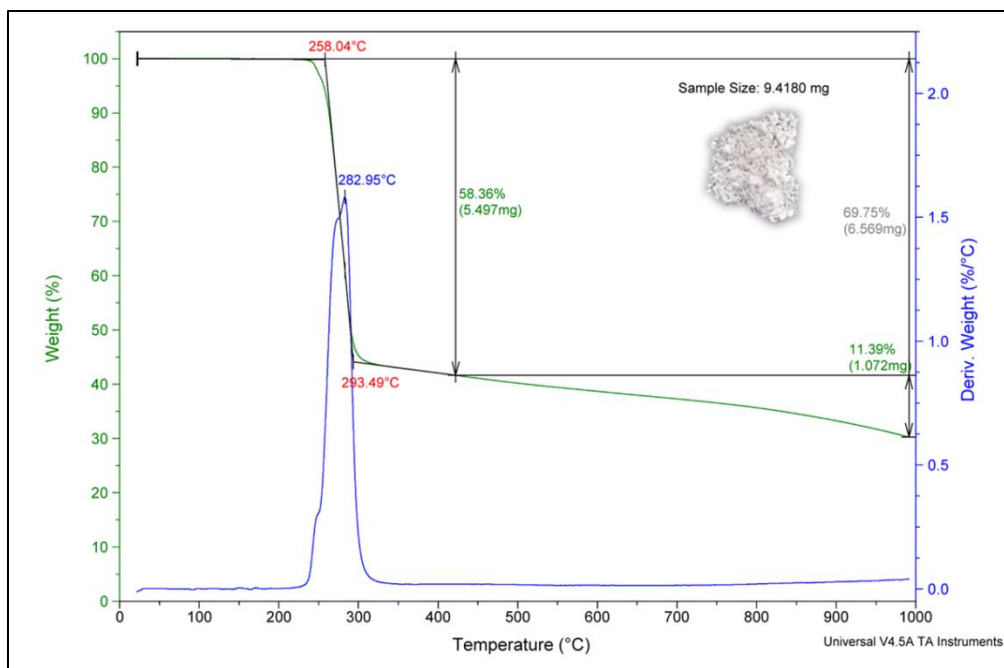
Figure 88. TGA analysis for {Ag[3,5-(CF$_3$)$_2$Pz](dmp)}$_2$ solvent-mediated powder.
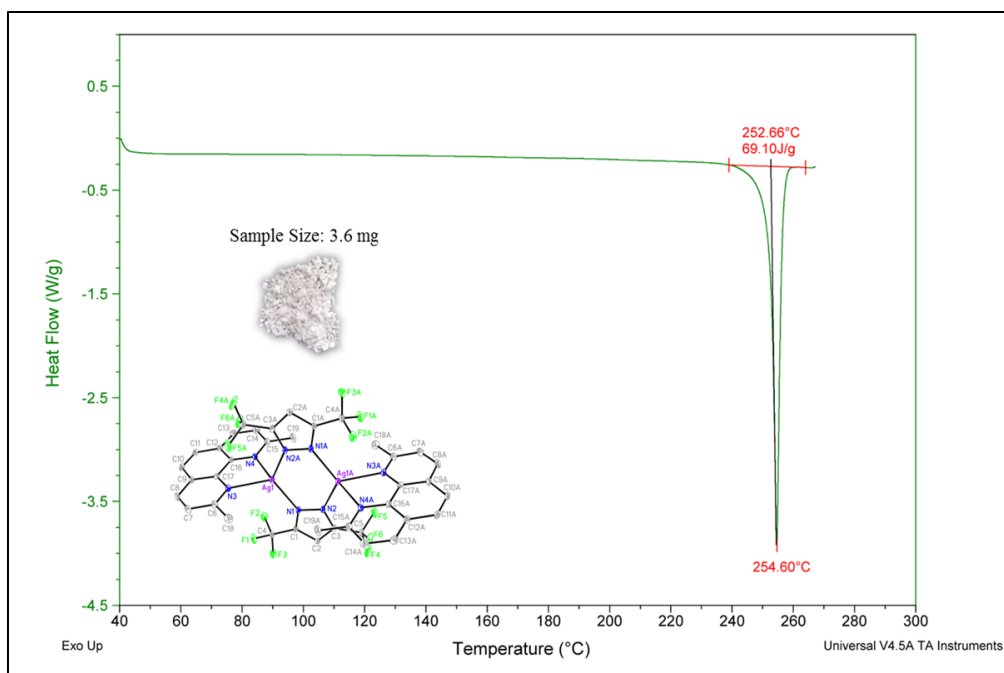
Figure 89. DSC analysis for {Ag[3,5-(CF$_3$)$_2$Pz](dmp)}$_2$ solvent-mediated powder.

3.2.7.5 Characterization using Photoluminescence and UV-Vis Absorption Spectroscopy

In this section, the photoluminescence and UV-Vis absorption spectroscopy of $\{Ag[3,5-(CF_3)_2Pz](dmp)\}_2$ solvent-mediated powder are discussed.

As shown in Figure 90, the solvent-mediated powder does not exhibit photoluminescence at room temperature (RT). The white solid was transfered to a clean, quartz tube, and its photoluminescence was checked under a handheld UV lamp, under Short Wave UV (λ_{ex} = 254 nm) and Long Wave UV (λ_{ex} = 365 nm), at cryogenic temperature (77K). At 77K, green photoluminescence was observed under 254 nm (medium-strong, green luminescence) and 365 nm (Strong, green luminescence).

As shown in Figures 91-93, at 77K, the photoluminescence of the $\{Ag[3,5-(CF_3)_2Pz](dmp)\}_2$ solvent-mediated powder (solid) was measured using an excitation wavelength of λ_{ex} = 338nm, producing an emission band with emission peaks at λ_{em} = 497 nm (minor, shoulder peak) and λ_{em} = 529 nm (major peak), respectively. A photoluminescence decay curve for the emission at λ_{em} = 497 nm was fitted with a Chi2 value of 1.000, a Durbin Watson value of 1.996, and a Z value of -0.4837. The photoluminescence observed at 77 K, for λ_{em} = 497 nm, was characterized as phosphorescence (10^{-5} s to 10 s) based on the lifetime (τ) of 11.55 μs. A photoluminescence decay curve for the emission at λ_{em} = 529 nm was fitted with a Chi2 value of 1.026, a Durbin Watson value of 1.458, and a Z value of -0.01585. The photoluminescence observed at 77 K, for λ_{em} = 529 nm, was characterized as phosphorescence (10^{-5} s to 10 s) based on the lifetime (τ) of 12.32 μs.

The UV-Vis absorption spectra for $\{Ag[3,5\text{-}(CF_3)_2Pz](dmp)\}_2$, shown in Figure 94, were obtained using three dilutions in isopropanol (isopropyl alcohol) (UV cutoff wavelength = 210 nm): 1×10^{-3} M, 1×10^{-4} M, and 1×10^{-5} M. A red shift was observed as the concentration increased, shifting toward the visible region (up to 390 nm), as well as $\pi\text{-}\pi^*$ transition with an extinction coefficient (ε_{273}) of 50,000 $L\cdot mol^{-1}\cdot cm^{-1}$ ($\lambda_{max2} = 273$ nm: A = 0.5, C = 1×10^{-5} M).
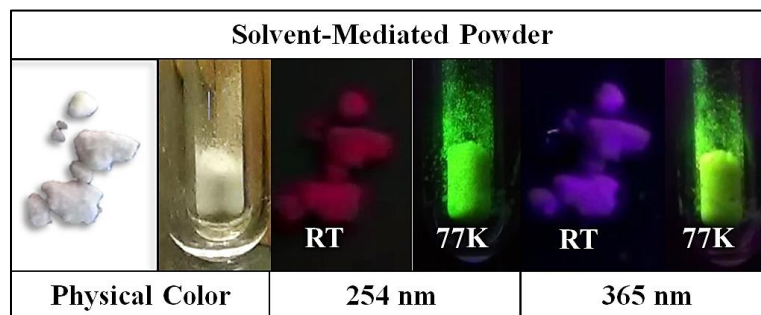
Figure 90. Photoluminescence of $\{Ag[3,5\text{-}(CF_3)_2Pz](dmp)\}_2$ solvent-mediated powder (solid) under Short Wave UV ($\lambda_{ex} = 254$ nm) and Long Wave UV ($\lambda_{ex} = 365$ nm), at room temperature (RT) vs. cryogenic temperature (77K).
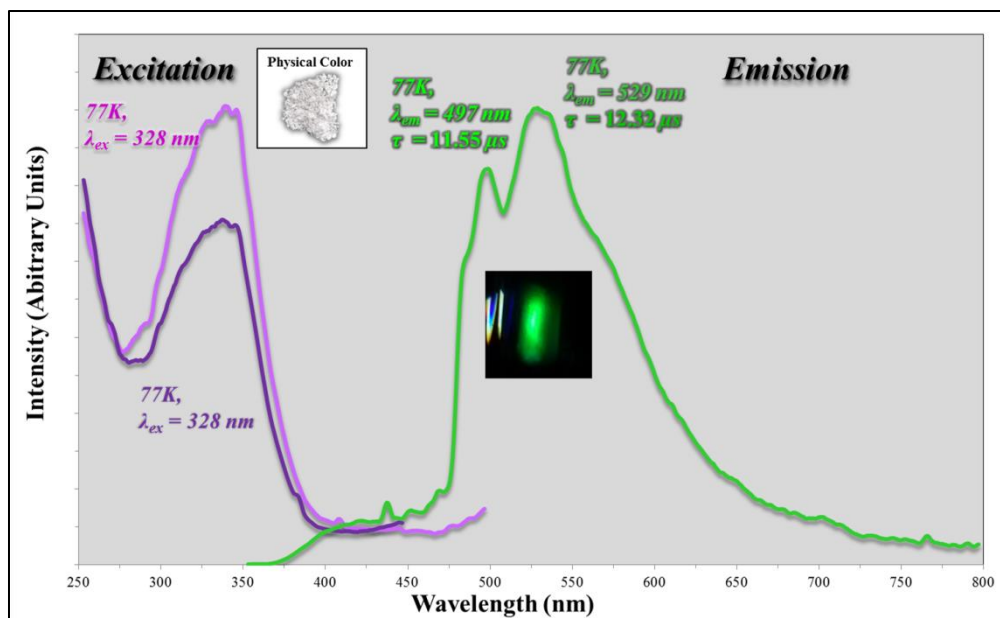
Figure 91. Photoluminescence spectra for {Ag[3,5-(CF$_3$)$_2$Pz](dmp)}$_2$ solvent-mediated powder, cryogenic temperature (77K).
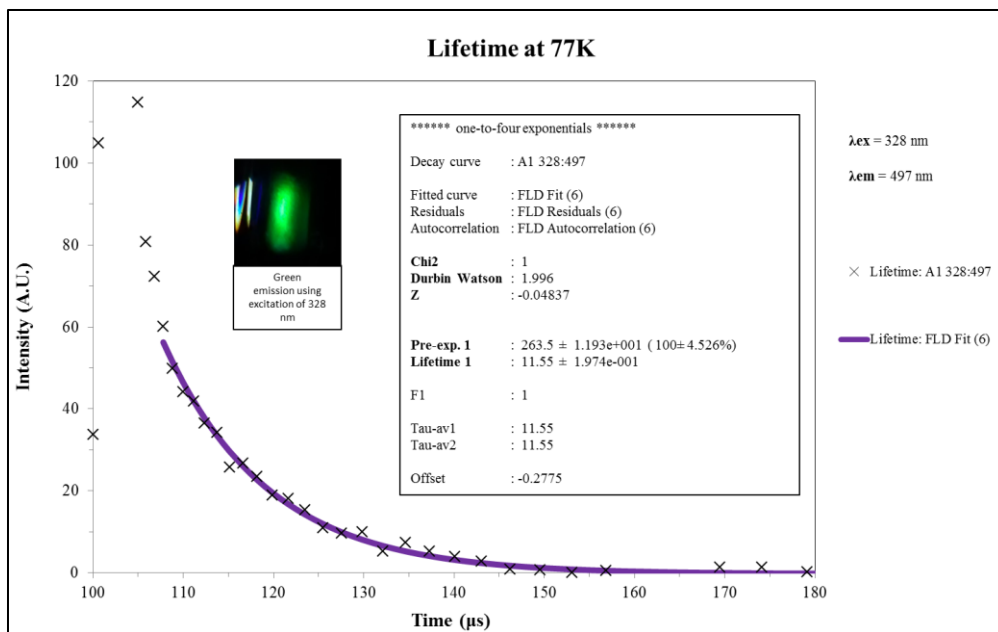
Figure 92. Lifetime Decay Curve for {Ag[3,5-(CF$_3$)$_2$Pz](dmp)}$_2$ Solvent-Mediated Powder, cryogenic temperature (77K), for λ_{em} = 497 nm with λ_{ex} = 328 nm.
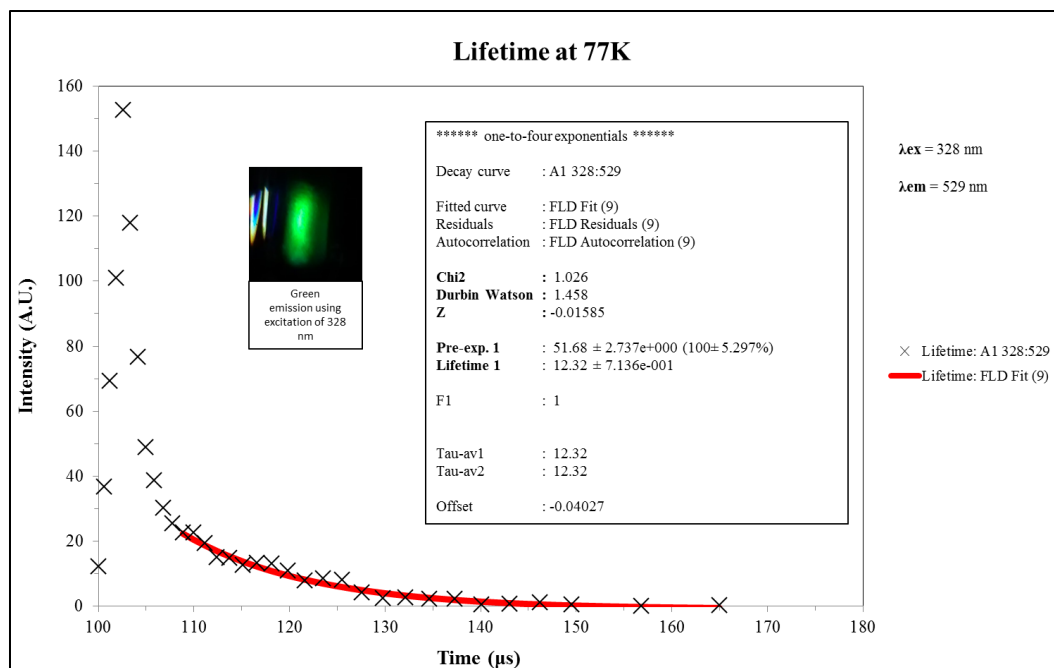
Figure 93. Lifetime Decay Curve for {Ag[3,5-$(CF_3)_2$Pz](dmp)}$_2$ Solvent-Mediated Powder, cryogenic temperature (77K), for λ_{em} = 529 nm with λ_{ex} = 328 nm.
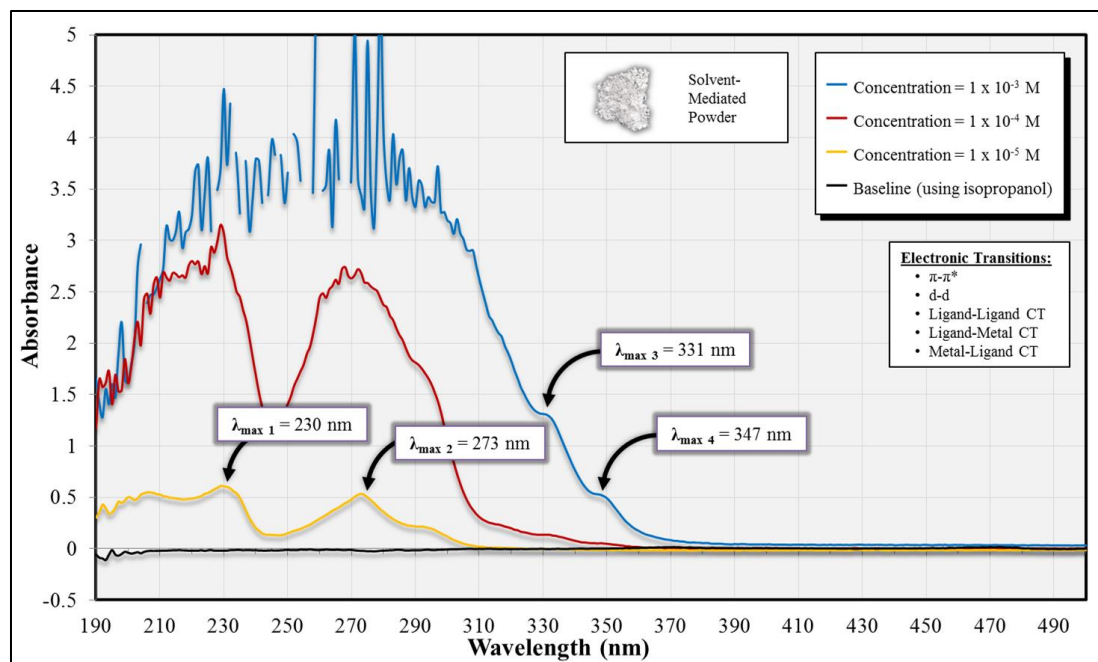
(A)
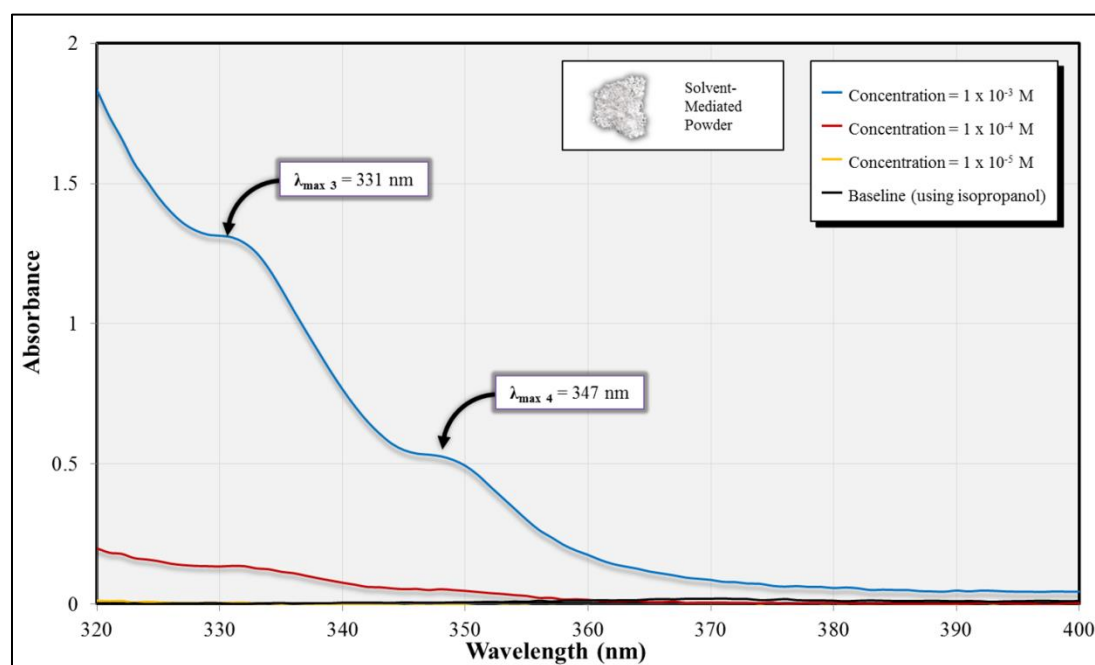
(B)

Figure 94. UV-Vis Spectra of $\{Ag[3,5-(CF_3)_2Pz](dmp)\}_2$ solvent-mediated powder in isopropanol (isopropyl alcohol) solutions (UV cutoff wavelength = 210 nm): (A) Full-View = 190-500 nm; (B) Zoomed-In = 320-400 nm.

3.2.8 Compound 8: {Cu$_3$[3,5-(CF$_3$)$_2$Pz]$_4$(ACN)(OH)$_2$}$_2$ · ACN

3.2.8.1 X-ray Crystallographic Data

In this section, the X-ray crystallographic data for {Cu$_3$[3,5-(CF$_3$)$_2$Pz]$_4$(ACN)(OH)$_2$}$_2$ · ACN (shown in Tables 15A-B) are discussed. {Cu$_3$[3,5-(CF$_3$)$_2$Pz]$_4$(ACN)(OH)$_2$}$_2$ · ACN single crystals were obtained directly from a solvent-mediated synthesis. Table 15A shows that {Cu$_3$[3,5-(CF$_3$)$_2$Pz]$_4$(ACN)(OH)$_2$}$_2$ · ACN crystallizes in the triclinic crystal system with the space group *P*-1 with Z = 2 and the unit cell dimensions: a = 13.0587(2) Å, b = 13.0955(2) Å, c = 23.4403(3) Å, α = 80.5200(10)°, β = 84.8790(10)°, and γ = 60.208(2)°. {Cu$_3$[3,5-(CF$_3$)$_2$Pz]$_4$(ACN)(OH)$_2$}$_2$ · ACN has the empirical formula C46 H21 Cu6 F48 N19 O4 (MW = 2197.06 g/mol), which accounts for the presence of an acetonitrile (ACN) molecule (C2 H3 N) in the symmetric unit cell.

As shown in Figure 95A, the symmetric unit cell of {Cu$_3$[3,5-(CF$_3$)$_2$Pz]$_4$(ACN)(OH)$_2$}$_2$ · ACN exhibits a Cu(II) hexameric structure with two 4-coordinated Cu(II) centers: Cu2 and Cu2A, and four 5-coordinated Cu(II) centers: Cu1, Cu3, Cu1A, and Cu3A, respectively. The aforementioned structure, herein described as a hexameric, copper(II) complex, is composed of two trimeric units, each possessing a trinuclear Cu3O(H) core. Furthermore, each Cu3O(H) core is composed of three Cu(II) centers: Cu1, Cu2, and Cu3, and Cu1A, Cu2A, and Cu3A, respectively, which are bridged via a single hydroxo (OH⁻) ligand (via O1 and O1B, respectively). The two Cu3O(H) cores are doubly bridged via two hydroxo ligands (via O2 and O2B). Both respective Cu3O(H) cores contain a single ACN ligand, which is coordinated with the

respective 4-coordinated Cu(II) center (Cu2 and Cu2A). Cu1 and Cu2 (Cu1A and Cu2 are singly bridged via one [3,5-$(CF_3)_2$Pz]$^-$ ligand. Cu1 and Cu2 (Cu1A and Cu2A) are singly bridged via one [3,5-$(CF_3)_2$Pz]$^-$ ligand. Similarly Cu3 and Cu2 (Cu3A and Cu2A) are singly bridged via one [3,5-$(CF_3)_2$Pz]$^-$ ligand. Cu1 and Cu3 (Cu1A and Cu3A) are doubly bridged via two [3,5-$(CF_3)_2$Pz]$^-$ ligands.

Figure 95B shows the packing structure of {Cu$_3$[3,5-$(CF_3)_2$Pz]$_4$(ACN)(OH)$_2$}$_2$. The bond lengths (Å) and angles (°) are shown in Table 15B. The full-matrix least-squares refinement method was used on F^2, resulting in a goodness-of-fit value of 1.255 with R1 = 6.64 % and wR2 = 12.30% for all data.

Table 15. **(A)** X-ray Crystallographic Data for $\{Cu_3[3,5\text{-}(CF_3)_2Pz]_4(ACN)(OH)_2\}_2 \cdot$ ACN; **(B)** Bond lengths [Å] and angles [°] for $\{Cu_3[3,5\text{-}(CF_3)_2Pz]_4(ACN)(OH)_2\}_2 \cdot$ ACN.

Empirical formula	C46 H21 Cu6 F48 N19 O4
Formula weight	2197.06
Temperature	127(30) K
Wavelength	0.71073 Å
Crystal system	Triclinic
Space group	P-1
Unit cell dimensions	a = 13.0587(2) Å α = 80.5200(10)°. b = 13.0955(2) Å β = 84.8790(10)°. c = 23.4403(3) Å γ = 60.208(2)°.
Volume	3431.11(11) Å^3
Z	2
Density (calculated)	2.127 Mg/m^3
Absorption coefficient	2.017 mm^{-1}
F(000)	2136
Crystal size	0.09 x 0.04 x 0.02 mm^3
Theta range for data collection	1.797 to 27.103°.
Index ranges	-16<=h<=16, -14<=k<=16, -29<=l<=30
Reflections collected	56171
Independent reflections	15057 [R(int) = 0.0376]
Completeness to theta = 25.242°	99.9 %
Absorption correction	Semi-empirical from equivalents
Max. and min. transmission	1.00000 and 0.71182
Refinement method	Full-matrix least-squares on F^2
Data / restraints / parameters	15057 / 63 / 1137
Goodness-of-fit on F^2	1.255
Final R indices [I>2sigma(I)]	R1 = 0.0583, wR2 = 0.1204
R indices (all data)	R1 = 0.0664, wR2 = 0.1230
Extinction coefficient	n/a
Largest diff. peak and hole	1.173 and -1.135 e.Å^{-3}

(A)

Bond Lengths [Å] (*blue*) & Angles [°] (red)					
Cu(1)-O(1)	2.165(3)	C(2S)-H(2SA)	0.96	N(7A)-C(16A)-C(19A)	121.5(5)
Cu(1)-O(2)	1.942(3)	C(2S)-H(2SB)	0.96	C(17A)-C(16A)-C(19A)	127.4(5)
Cu(1)-N(1)	2.006(4)	C(2S)-H(2SC)	0.96	C(16A)-C(17A)-H(17A)	128.5
Cu(1)-N(3)	2.078(4)	O(2)-Cu(1)-O(1)	96.45(13)	C(18A)-C(17A)-C(16A)	103.1(4)
Cu(1)-N(8)#1	2.033(4)	O(2)-Cu(1)-N(1)	95.05(14)	C(18A)-C(17A)-H(17A)	128.5
Cu(2)-O(1)	1.898(3)	O(2)-Cu(1)-N(3)	174.11(15)	N(8A)-C(18A)-C(17A)	111.3(5)
Cu(2)-N(2)	1.992(4)	O(2)-Cu(1)-N(8)#1	90.96(15)	N(8A)-C(18A)-C(20A)	121.5(5)
Cu(2)-N(5)	1.995(4)	N(1)-Cu(1)-O(1)	86.75(14)	C(17A)-C(18A)-C(20A)	127.3(5)
Cu(2)-N(9)	1.988(4)	N(1)-Cu(1)-N(3)	90.36(15)	F(19A)-C(19A)-C(16A)	110.4(4)
Cu(3)-O(1)#1	2.134(3)	N(1)-Cu(1)-N(8)#1	170.34(16)	F(20A)-C(19A)-F(19A)	106.0(4)
Cu(3)-O(2)	1.957(3)	N(3)-Cu(1)-O(1)	81.50(14)	F(20A)-C(19A)-C(16A)	112.8(4)
Cu(3)-N(4)#1	2.109(4)	N(8)#1-Cu(1)-O(1)	100.10(14)	F(21A)-C(19A)-F(19A)	107.5(4)
Cu(3)-N(6)#1	2.000(4)	N(8)#1-Cu(1)-N(3)	83.99(15)	F(21A)-C(19A)-F(20A)	106.8(5)
Cu(3)-N(7)	2.015(4)	O(1)-Cu(2)-N(2)	89.26(15)	F(21A)-C(19A)-C(16A)	113.0(4)
Cu(4)-O(1A)	2.151(3)	O(1)-Cu(2)-N(5)	90.07(15)	F(22A)-C(20A)-F(23A)	106.0(4)
Cu(4)-O(2A)	1.956(3)	O(1)-Cu(2)-N(9)	156.64(16)	F(22A)-C(20A)-C(18A)	111.1(4)
Cu(4)-N(1A)	2.005(4)	N(2)-Cu(2)-N(5)	170.17(17)	F(23A)-C(20A)-C(18A)	111.9(5)
Cu(4)-N(5A)	2.009(4)	N(9)-Cu(2)-N(2)	93.21(17)	F(24A)-C(20A)-F(22A)	108.3(5)
Cu(4)-N(7A)	2.090(4)	N(9)-Cu(2)-N(5)	91.30(17)	F(24A)-C(20A)-F(23A)	105.9(5)
Cu(5)-O(1A)	1.892(3)	O(2)-Cu(3)-O(1)#1	97.25(13)	F(24A)-C(20A)-C(18A)	113.3(5)
Cu(5)-N(2A)	1.994(4)	O(2)-Cu(3)-N(4)#1	175.58(14)	N(9A)-C(21A)-C(22A)	178.1(7)
Cu(5)-N(3A)	2.004(4)	O(2)-Cu(3)-N(6)#1	94.00(15)	C(21A)-C(22A)-H(22A)	109.5
Cu(5)-N(9A)	1.982(4)	O(2)-Cu(3)-N(7)	92.96(15)	C(21A)-C(22A)-H(22B)	109.5
Cu(6)-O(1A)#2	2.142(3)	N(4)#1-Cu(3)-O(1)#1	80.66(14)	C(21A)-C(22A)-H(22C)	109.5
Cu(6)-O(2A)	1.960(3)	N(6)#1-Cu(3)-O(1)#1	86.90(14)	H(22A)-C(22A)-H(22B)	109.5
Cu(6)-N(4A)#2	2.008(4)	N(6)#1-Cu(3)-N(4)#1	89.79(15)	H(22A)-C(22A)-H(22C)	109.5
Cu(6)-	2.018(4)	N(6)#1-Cu(3)-N(7)	168.39(16)	H(22B)-C(22A)-	109.5

				H(22C)	
N(6A)#2					
Cu(6)-N(8A)#2	2.085(4)	N(7)-Cu(3)-O(1)#1	101.42(14)	Cu(1)-O(1)-H(1)	112(4)
F(1A)-C(4A)	1.273(14)	N(7)-Cu(3)-N(4)#1	83.68(16)	Cu(2)-O(1)-Cu(1)	105.01(15)
F(2A)-C(4A)	1.332(12)	O(2A)-Cu(4)-O(1A)	96.35(13)	Cu(2)-O(1)-Cu(3)#1	105.86(14)
F(3A)-C(4A)	1.425(11)	O(2A)-Cu(4)-N(1A)	94.33(15)	Cu(2)-O(1)-H(1)	120(4)
F(4A)-C(5A)	1.333(6)	O(2A)-Cu(4)-N(5A)	91.11(15)	Cu(3)#1-O(1)-Cu(1)	97.11(13)
F(5A)-C(5A)	1.338(6)	O(2A)-Cu(4)-N(7A)	174.65(15)	Cu(3)#1-O(1)-H(1)	114(4)
F(6A)-C(5A)	1.347(6)	N(1A)-Cu(4)-O(1A)	88.00(14)	Cu(1)-O(2)-Cu(3)	136.37(18)
F(7A)-C(9A)	1.337(6)	N(1A)-Cu(4)-N(5A)	169.57(16)	Cu(1)-O(2)-H(2)	118(5)
F(8A)-C(9A)	1.343(6)	N(1A)-Cu(4)-N(7A)	90.12(15)	Cu(3)-O(2)-H(2)	101(5)
F(9A)-C(9A)	1.333(6)	N(5A)-Cu(4)-O(1A)	100.26(14)	N(2)-N(1)-Cu(1)	116.8(3)
F(10A)-C(10A)	1.338(6)	N(5A)-Cu(4)-N(7A)	84.97(15)	C(1)-N(1)-Cu(1)	136.9(3)
F(11A)-C(10A)	1.333(6)	N(7A)-Cu(4)-O(1A)	80.81(14)	C(1)-N(1)-N(2)	106.1(4)
F(12A)-C(10A)	1.329(6)	O(1A)-Cu(5)-N(2A)	89.56(15)	N(1)-N(2)-Cu(2)	118.4(3)
F(13A)-C(14A)	1.313(6)	O(1A)-Cu(5)-N(3A)	89.65(15)	C(3)-N(2)-Cu(2)	133.0(3)
F(14A)-C(14A)	1.310(6)	O(1A)-Cu(5)-N(9A)	159.10(16)	C(3)-N(2)-N(1)	108.5(4)
F(15A)-C(14A)	1.333(6)	N(2A)-Cu(5)-N(3A)	169.87(16)	N(4)-N(3)-Cu(1)	116.1(3)
F(16A)-C(15A)	1.309(6)	N(9A)-Cu(5)-N(2A)	92.17(17)	C(6)-N(3)-Cu(1)	135.7(3)
F(17A)-C(15A)	1.313(6)	N(9A)-Cu(5)-N(3A)	92.17(17)	C(6)-N(3)-N(4)	108.0(4)
F(18A)-C(15A)	1.314(6)	O(2A)-Cu(6)-O(1A)#2	96.09(13)	N(3)-N(4)-Cu(3)#1	116.7(3)
F(19A)-C(19A)	1.347(6)	O(2A)-Cu(6)-N(4A)#2	94.39(14)	C(8)-N(4)-Cu(3)#1	135.5(3)
F(20A)-C(19A)	1.337(6)	O(2A)-Cu(6)-N(6A)#2	92.51(15)	C(8)-N(4)-N(3)	107.4(4)
F(21A)-C(19A)	1.328(7)	O(2A)-Cu(6)-N(8A)#2	175.38(15)	N(6)-N(5)-Cu(2)	118.1(3)
F(22A)-C(20A)	1.335(6)	N(4A)#2-Cu(6)-O(1A)#2	86.73(14)	C(11)-N(5)-Cu(2)	134.7(3)
F(23A)-C(20A)	1.354(7)	N(4A)#2-Cu(6)-N(6A)#2	169.32(16)	C(11)-N(5)-N(6)	107.2(4)
F(24A)-C(20A)	1.330(7)	N(4A)#2-Cu(6)-N(8A)#2	89.56(15)	N(5)-N(6)-Cu(3)#1	117.4(3)
O(1A)-H(1A)	0.867(10)	N(6A)#2-Cu(6)-O(1A)#2	100.64(14)	C(13)-N(6)-Cu(3)#1	134.6(3)
O(2A)-H(2A)	0.867(10)	N(6A)#2-Cu(6)-N(8A)#2	83.92(15)	C(13)-N(6)-N(5)	108.0(4)
N(1A)-N(2A)	1.358(5)	N(8A)#2-Cu(6)-O(1A)#2	81.73(14)	N(8)-N(7)-Cu(3)	117.6(3)
N(1A)-C(1A)	1.345(6)	Cu(4)-O(1A)-H(1A)	106(6)	C(16)-N(7)-Cu(3)	134.6(3)
N(2A)-C(3A)	1.356(6)	Cu(5)-O(1A)-Cu(4)	104.52(14)	C(16)-N(7)-N(8)	107.8(4)
N(3A)-N(4A)	1.358(5)	Cu(5)-O(1A)-Cu(6)#2	106.06(15)	N(7)-N(8)-Cu(1)#1	117.5(3)
N(3A)-C(6A)	1.349(6)	Cu(5)-O(1A)-H(1A)	128(6)	C(18)-N(8)-Cu(1)#1	134.4(3)
N(4A)-C(8A)	1.357(6)	Cu(6)#2-O(1A)-Cu(4)	97.14(13)	C(18)-N(8)-N(7)	108.1(4)
N(5A)-N(6A)	1.353(5)	Cu(6)#2-O(1A)-	111(6)	C(21)-N(9)-Cu(2)	171.9(4)

		H(1A)			
N(5A)-C(11A)	1.339(6)	Cu(4)-O(2A)-Cu(6)	136.64(17)	N(1)-C(1)-C(2)	111.4(4)
N(6A)-C(13A)	1.359(6)	Cu(4)-O(2A)-H(2A)	114(5)	N(1)-C(1)-C(4)	121.8(4)
N(7A)-N(8A)	1.366(5)	Cu(6)-O(2A)-H(2A)	108(5)	C(2)-C(1)-C(4)	126.7(4)
N(7A)-C(16A)	1.355(6)	N(2A)-N(1A)-Cu(4)	115.6(3)	C(1)-C(2)-H(2B)	128.2
N(8A)-C(18A)	1.341(6)	C(1A)-N(1A)-Cu(4)	136.8(3)	C(1)-C(2)-C(3)	103.5(4)
N(9A)-C(21A)	1.135(7)	C(1A)-N(1A)-N(2A)	107.4(4)	C(3)-C(2)-H(2B)	128.2
C(1A)-C(2A)	1.384(7)	N(1A)-N(2A)-Cu(5)	118.9(3)	N(2)-C(3)-C(2)	110.4(4)
C(1A)-C(4A)	1.474(7)	C(3A)-N(2A)-Cu(5)	133.7(3)	N(2)-C(3)-C(5)	121.2(4)
C(2A)-H(2AA)	0.93	C(3A)-N(2A)-N(1A)	107.2(4)	C(2)-C(3)-C(5)	128.3(5)
C(2A)-C(3A)	1.367(7)	N(4A)-N(3A)-Cu(5)	117.7(3)	F(1)-C(4)-F(3)	105.2(4)
C(3A)-C(5A)	1.489(7)	C(6A)-N(3A)-Cu(5)	133.9(3)	F(1)-C(4)-C(1)	113.3(4)
C(4A)-F(1B)	1.294(9)	C(6A)-N(3A)-N(4A)	108.4(4)	F(2)-C(4)-F(1)	109.0(5)
C(4A)-F(2B)	1.303(7)	N(3A)-N(4A)-Cu(6)#2	117.6(3)	F(2)-C(4)-F(3)	106.7(5)
C(4A)-F(3B)	1.409(9)	C(8A)-N(4A)-Cu(6)#2	136.2(3)	F(2)-C(4)-C(1)	111.3(4)
C(6A)-C(7A)	1.374(7)	C(8A)-N(4A)-N(3A)	106.0(4)	F(3)-C(4)-C(1)	111.0(4)
C(6A)-C(9A)	1.491(7)	N(6A)-N(5A)-Cu(4)	118.1(3)	F(4)-C(5)-F(5)	106.5(4)
C(7A)-H(7A)	0.93	C(11A)-N(5A)-Cu(4)	133.7(3)	F(4)-C(5)-F(6)	107.5(5)
C(7A)-C(8A)	1.379(7)	C(11A)-N(5A)-N(6A)	108.2(4)	F(4)-C(5)-C(3)	112.3(4)
C(8A)-C(10A)	1.495(7)	N(5A)-N(6A)-Cu(6)#2	117.1(3)	F(5)-C(5)-F(6)	105.9(4)
C(11A)-C(12A)	1.393(7)	N(5A)-N(6A)-C(13A)	107.2(4)	F(5)-C(5)-C(3)	113.1(5)
C(11A)-C(14A)	1.491(7)	C(13A)-N(6A)-Cu(6)#2	135.7(3)	F(6)-C(5)-C(3)	111.1(4)
C(12A)-H(12A)	0.93	N(8A)-N(7A)-Cu(4)	116.1(3)	N(3)-C(6)-C(7)	110.8(5)
C(12A)-C(13A)	1.377(7)	C(16A)-N(7A)-Cu(4)	136.5(3)	N(3)-C(6)-C(9)	122.4(4)
C(13A)-C(15A)	1.487(7)	C(16A)-N(7A)-N(8A)	106.7(4)	C(7)-C(6)-C(9)	126.9(5)
C(16A)-C(17A)	1.385(7)	N(7A)-N(8A)-Cu(6)#2	116.5(3)	C(6)-C(7)-H(7)	128.4
C(16A)-C(19A)	1.486(7)	C(18A)-N(8A)-Cu(6)#2	135.5(3)	C(8)-C(7)-C(6)	103.2(4)
C(17A)-H(17A)	0.93	C(18A)-N(8A)-N(7A)	107.8(4)	C(8)-C(7)-H(7)	128.4
C(17A)-C(18A)	1.381(7)	C(21A)-N(9A)-Cu(5)	177.7(4)	N(4)-C(8)-C(7)	110.7(4)
C(18A)-C(20A)	1.491(7)	N(1A)-C(1A)-C(2A)	110.9(4)	N(4)-C(8)-C(10)	121.7(5)
C(21A)-C(22A)	1.462(9)	N(1A)-C(1A)-C(4A)	122.4(4)	C(7)-C(8)-C(10)	127.5(5)
C(22A)-H(22A)	0.96	C(2A)-C(1A)-C(4A)	126.6(4)	F(7)-C(9)-C(6)	111.8(5)
C(22A)-H(22B)	0.96	C(1A)-C(2A)-H(2AA)	128.3	F(8)-C(9)-F(7)	106.7(5)
C(22A)-H(22C)	0.96	C(3A)-C(2A)-C(1A)	103.5(4)	F(8)-C(9)-F(9)	108.3(5)
F(1)-C(4)	1.319(6)	C(3A)-C(2A)-H(2AA)	128.3	F(8)-C(9)-C(6)	111.8(4)

F(2)-C(4)	1.309(6)	N(2A)-C(3A)-C(2A)	111.1(4)	F(9)-C(9)-F(7)	106.8(5)
F(3)-C(4)	1.345(6)	N(2A)-C(3A)-C(5A)	121.1(4)	F(9)-C(9)-C(6)	111.1(4)
F(4)-C(5)	1.328(7)	C(2A)-C(3A)-C(5A)	127.8(4)	F(10)-C(10)-C(8)	112.0(5)
F(5)-C(5)	1.343(7)	F(1A)-C(4A)-F(2A)	80.0(8)	F(11)-C(10)-F(10)	106.5(4)
F(6)-C(5)	1.343(6)	F(1A)-C(4A)-F(3A)	104.9(9)	F(11)-C(10)-F(12)	107.7(5)
F(7)-C(9)	1.339(7)	F(1A)-C(4A)-C(1A)	115.8(7)	F(11)-C(10)-C(8)	113.2(4)
F(8)-C(9)	1.328(6)	F(2A)-C(4A)-F(3A)	128.9(7)	F(12)-C(10)-F(10)	105.9(4)
F(9)-C(9)	1.333(6)	F(2A)-C(4A)-C(1A)	112.4(6)	F(12)-C(10)-C(8)	111.1(4)
F(10)-C(10)	1.352(7)	F(3A)-C(4A)-C(1A)	110.4(6)	N(5)-C(11)-C(12)	111.2(4)
F(11)-C(10)	1.329(6)	F(1B)-C(4A)-C(1A)	115.4(5)	N(5)-C(11)-C(14)	122.5(4)
F(12)-C(10)	1.342(6)	F(1B)-C(4A)-F(2B)	87.2(7)	C(12)-C(11)-C(14)	126.2(4)
F(13)-C(14)	1.328(6)	F(1B)-C(4A)-F(3B)	116.6(7)	C(11)-C(12)-H(12)	128.3
F(14)-C(14)	1.351(6)	F(2B)-C(4A)-C(1A)	112.5(5)	C(11)-C(12)-C(13)	103.4(4)
F(15)-C(14)	1.319(6)	F(2B)-C(4A)-F(3B)	112.0(6)	C(13)-C(12)-H(12)	128.3
F(16)-C(15)	1.337(6)	F(3B)-C(4A)-C(1A)	111.1(5)	N(6)-C(13)-C(12)	110.3(4)
F(17)-C(15)	1.349(5)	F(4A)-C(5A)-F(5A)	107.4(4)	N(6)-C(13)-C(15)	122.9(4)
F(18)-C(15)	1.339(5)	F(4A)-C(5A)-F(6A)	106.3(4)	C(12)-C(13)-C(15)	126.7(4)
F(19)-C(19)	1.313(6)	F(4A)-C(5A)-C(3A)	112.6(4)	F(13)-C(14)-F(14)	105.9(4)
F(20)-C(19)	1.334(6)	F(5A)-C(5A)-F(6A)	105.9(4)	F(13)-C(14)-C(11)	112.0(4)
F(21)-C(19)	1.315(6)	F(5A)-C(5A)-C(3A)	110.7(4)	F(14)-C(14)-C(11)	111.4(4)
F(22)-C(20)	1.344(6)	F(6A)-C(5A)-C(3A)	113.5(4)	F(15)-C(14)-F(13)	108.7(4)
F(23)-C(20)	1.331(6)	N(3A)-C(6A)-C(7A)	110.7(4)	F(15)-C(14)-F(14)	107.2(4)
F(24)-C(20)	1.327(6)	N(3A)-C(6A)-C(9A)	122.6(4)	F(15)-C(14)-C(11)	111.3(4)
O(1)-H(1)	0.865(10)	C(7A)-C(6A)-C(9A)	126.7(4)	F(16)-C(15)-F(17)	106.2(4)
O(2)-H(2)	0.865(10)	C(6A)-C(7A)-H(7A)	128.3	F(16)-C(15)-F(18)	106.7(4)
N(1)-N(2)	1.365(5)	C(6A)-C(7A)-C(8A)	103.3(4)	F(16)-C(15)-C(13)	112.5(4)
N(1)-C(1)	1.361(6)	C(8A)-C(7A)-H(7A)	128.3	F(17)-C(15)-C(13)	112.8(4)
N(2)-C(3)	1.346(6)	N(4A)-C(8A)-C(7A)	111.6(4)	F(18)-C(15)-F(17)	106.2(4)
N(3)-N(4)	1.360(6)	N(4A)-C(8A)-C(10A)	122.1(4)	F(18)-C(15)-C(13)	112.0(4)
N(3)-C(6)	1.337(6)	C(7A)-C(8A)-C(10A)	126.4(4)	N(7)-C(16)-C(17)	110.9(4)
N(4)-C(8)	1.346(6)	F(7A)-C(9A)-F(8A)	106.9(4)	N(7)-C(16)-C(19)	122.0(4)
N(5)-N(6)	1.358(5)	F(7A)-C(9A)-C(6A)	112.3(4)	C(17)-C(16)-C(19)	127.1(4)
N(5)-C(11)	1.347(6)	F(8A)-C(9A)-C(6A)	111.9(4)	C(16)-C(17)-H(17)	128.7
N(6)-C(13)	1.344(6)	F(9A)-C(9A)-F(7A)	107.7(4)	C(16)-C(17)-C(18)	102.7(4)
N(7)-N(8)	1.350(6)	F(9A)-C(9A)-F(8A)	106.6(4)	C(18)-C(17)-H(17)	128.7
N(7)-C(16)	1.347(6)	F(9A)-C(9A)-C(6A)	111.2(4)	N(8)-C(18)-C(17)	110.5(4)
N(8)-C(18)	1.339(6)	F(10A)-C(10A)-C(8A)	113.0(4)	N(8)-C(18)-C(20)	122.2(4)
N(9)-C(21)	1.137(7)	F(11A)-C(10A)-F(10A)	106.5(4)	C(17)-C(18)-C(20)	127.3(4)
N(1S)-C(1S)	1.189(14)	F(11A)-C(10A)-C(8A)	111.1(4)	F(19)-C(19)-F(20)	105.4(5)
C(1)-C(2)	1.377(7)	F(12A)-C(10A)-F(10A)	107.1(4)	F(19)-C(19)-F(21)	107.9(5)
C(1)-C(4)	1.491(7)	F(12A)-C(10A)-F(11A)	107.4(4)	F(19)-C(19)-C(16)	113.6(4)
C(2)-H(2B)	0.93	F(12A)-C(10A)-C(8A)	111.5(4)	F(20)-C(19)-C(16)	111.2(4)
C(2)-C(3)	1.386(7)	N(5A)-C(11A)-C(12A)	110.6(4)	F(21)-C(19)-F(20)	106.7(4)
C(3)-C(5)	1.483(7)	N(5A)-C(11A)-C(14A)	121.3(4)	F(21)-C(19)-C(16)	111.6(4)
C(6)-C(7)	1.388(7)	C(12A)-C(11A)-	128.1(4)	F(22)-C(20)-C(18)	110.0(4)

|					
		C(14A)			
C(6)-C(9)	1.500(7)	C(11A)-C(12A)-H(12A)	128.3	F(23)-C(20)-F(22)	106.6(4)
C(7)-H(7)	0.93	C(13A)-C(12A)-C(11A)	103.4(4)	F(23)-C(20)-C(18)	112.4(4)
C(7)-C(8)	1.387(7)	C(13A)-C(12A)-H(12A)	128.3	F(24)-C(20)-F(22)	106.0(4)
C(8)-C(10)	1.485(7)	N(6A)-C(13A)-C(12A)	110.6(4)	F(24)-C(20)-F(23)	107.5(4)
C(11)-C(12)	1.374(7)	N(6A)-C(13A)-C(15A)	121.4(4)	F(24)-C(20)-C(18)	113.9(4)
C(11)-C(14)	1.500(7)	C(12A)-C(13A)-C(15A)	127.9(4)	N(9)-C(21)-C(22)	178.2(6)
C(12)-H(12)	0.93	F(13A)-C(14A)-F(15A)	107.1(4)	C(21)-C(22)-H(22D)	109.5
C(12)-C(13)	1.392(7)	F(13A)-C(14A)-C(11A)	112.3(4)	C(21)-C(22)-H(22E)	109.5
C(13)-C(15)	1.473(7)	F(14A)-C(14A)-F(13A)	107.1(5)	C(21)-C(22)-H(22F)	109.5
C(16)-C(17)	1.385(7)	F(14A)-C(14A)-F(15A)	106.1(4)	H(22D)-C(22)-H(22E)	109.5
C(16)-C(19)	1.490(7)	F(14A)-C(14A)-C(11A)	113.5(4)	H(22D)-C(22)-H(22F)	109.5
C(17)-H(17)	0.93	F(15A)-C(14A)-C(11A)	110.5(4)	H(22E)-C(22)-H(22F)	109.5
C(17)-C(18)	1.404(7)	F(16A)-C(15A)-F(17A)	106.6(5)	N(1S)-C(1S)-C(2S)	176.0(12)
C(18)-C(20)	1.487(7)	F(16A)-C(15A)-F(18A)	106.1(5)	C(1S)-C(2S)-H(2SA)	109.5
C(21)-C(22)	1.455(8)	F(16A)-C(15A)-C(13A)	113.4(4)	C(1S)-C(2S)-H(2SB)	109.5
C(22)-H(22D)	0.96	F(17A)-C(15A)-F(18A)	106.4(5)	C(1S)-C(2S)-H(2SC)	109.5
C(22)-H(22E)	0.96	F(17A)-C(15A)-C(13A)	111.5(4)	H(2SA)-C(2S)-H(2SB)	109.5
C(22)-H(22F)	0.96	F(18A)-C(15A)-C(13A)	112.5(4)	H(2SA)-C(2S)-H(2SC)	109.5
C(1S)-C(2S)	1.430(18)	N(7A)-C(16A)-C(17A)	111.1(4)	H(2SB)-C(2S)-H(2SC)	109.5
Symmetry transformations used to generate equivalent atoms:					
#1 -x+1,-y+1,-z+1 #2 -x,-y+1,-z+2					

(B)
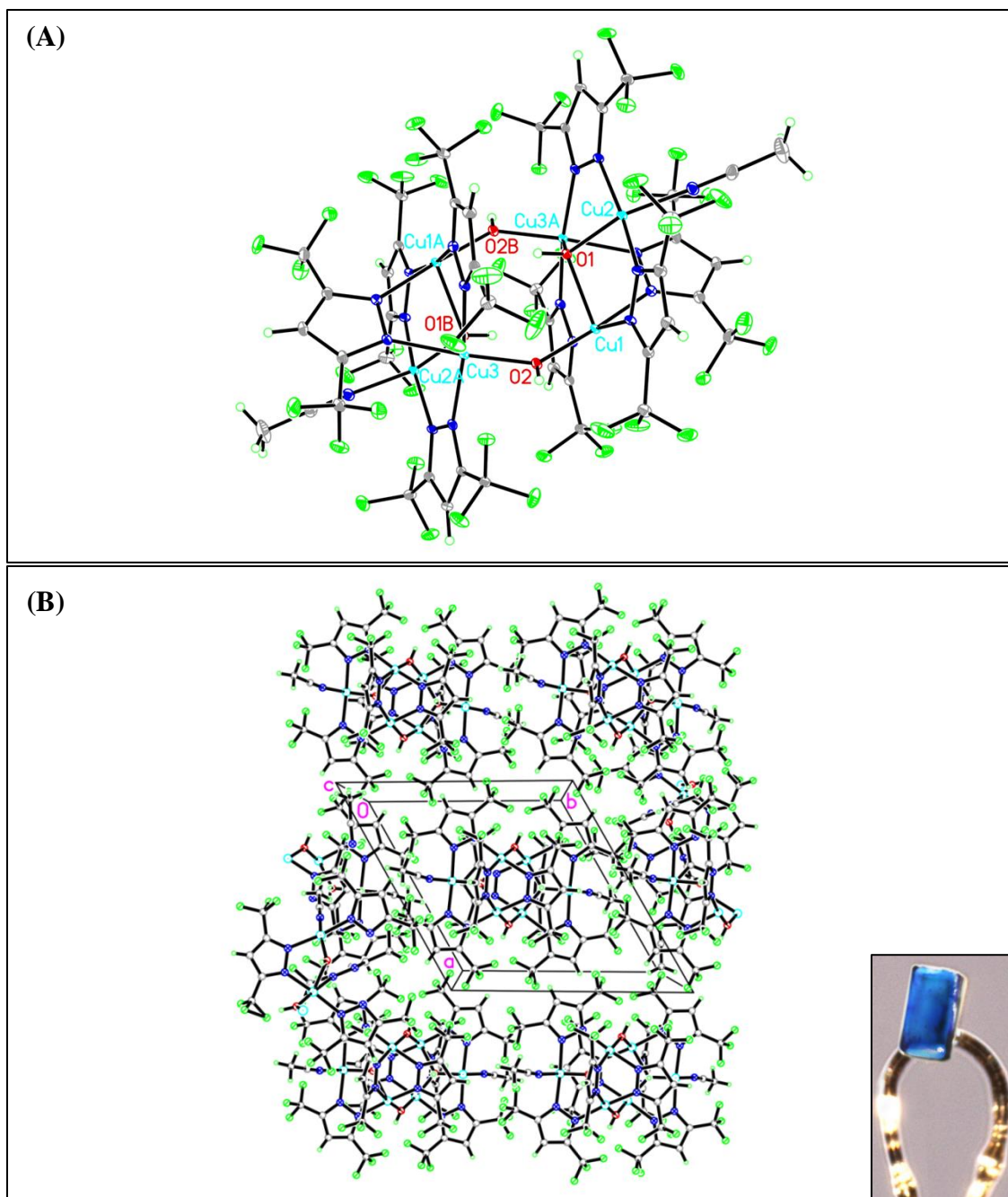
Figure 95. Crystal Structure of {Cu$_3$[3,5-(CF$_3$)$_2$Pz]$_4$(ACN)(OH)$_2$}$_2$ · ACN: **(A)** Symmetric Unit Cell and **(B)** Packing.

3.2.8.2 Elemental Analysis Data

In this section, the elemental analysis data for $\{Cu_3[3,5-(CF_3)_2Pz]_4(ACN)(OH)_2\}_2$ · ACN, shown in Table 16, are discussed, comparing the experimentally found data with the theoretical Anal. Calc.

The theoretical percentages of carbon (C), hydrogen (H), and nitrogen (N) were analytically calculated (Anal. Calc.) based on the empirical formula C46 H21 Cu6 F48 N19 O4 (MW = 2197.06 g/mol): C, 25.15; H, 0.96; N, 12.11. The empirical formula for the crystals accounts for the presence of an acetonitrile solvent molecule (C2 H3 N). The experimentally found data for the blue crystals (C, 25.44; H, 1.21; N, 12.79) relatively match that of the theoretical Anal. Calc. within ±0.29 for C, ±0.25 for H, and ±0.68 for N. The significant difference of ±0.68 for N between the theoretical Anal. Calc. and the experimentally found data hinted at the presence of an additional acetonitrile molecule.

The empirical formula for the blue crystals was adjusted in order to account for the presence of two acetonitrile solvent molecules (C2 H3 N) for every unit of $\{Cu_3[3,5-(CF_3)_2Pz]_4(ACN)(OH)_2\}_2$. The theoretical percentages of carbon (C), hydrogen (H), and nitrogen (N) were analytically calculated (Anal. Calc.) based on the "adjusted" empirical formula C48 H24 Cu6 F48 N20 O4 (MW = 2238.04 g/mol): C, 25.76; H, 1.08; N, 12.52. The experimentally found data for the blue crystals (C, 25.44; H, 1.21; N, 12.79) match that of the theoretical Anal. Calc. within ±0.32 for C, ±0.13 for H, and ±0.27 for N.

Table 16. Elemental analysis data for {Cu$_3$[3,5-(CF$_3$)$_2$Pz]$_4$(ACN)(OH)$_2$}$_2$ · ACN crystals: theoretical Anal. Calc. versus experimentally found data.

Elemental Analysis		
{Cu$_3$[3,5-(CF$_3$)$_2$Pz]$_4$(ACN)(OH)$_2$}$_2$ · ACN		
		Crystals
Empirical Formula: 2(C22 H9 Cu3 F24 N9 O2), C2 H3 N (MW = 2197.06 g/mol)		
Element	**Theoretical Anal. Calc.**	**Experimentally Found**
C	25.15%	25.44%
H	0.96%	1.21%
N	12.11%	12.79%
Cu	17.35%	
Empirical Formula: 2(C22 H9 Cu3 F24 N9 O2), 2(C2 H3 N) (MW = 2238.04 g/mol)		
Element	**Theoretical Anal. Calc.**	**Experimentally Found**
C	25.76%	25.44%
H	1.08%	1.21%
N	12.52%	12.79%
Cu	17.04%	

3.2.8.3 Characterization using FT-IR Spectroscopy

In this section, the IR spectrum for $\{Cu_3[3,5\text{-}(CF_3)_2Pz]_4(ACN)(OH)_2\}_2 \cdot ACN$ crystals, as shown in Figure 96, is discussed. The IR spectrum for the crystals feature the functional groups characteristic of the fluorinated-pyrazolate ($[3,5\text{-}(CF_3)_2Pz]^- = FPz^-$), hydroxo ($OH^-$), and acetonitrile (ACN) ligands: =C-H stretch (aromatic), C=C stretch (aromatic), C=N stretch (aromatic), C-C stretch (aromatic), C-N stretch (aromatic), C-F stretch, O-H stretch, C-H stretch (C-CH$_3$), and C≡N stretch.

Functional Groups	Expected Range (cm⁻¹)
=C-H stretch (aromatic)	3010-3100, 690-900
C=C stretch (aromatic)	1400, 1600
C=N stretch (aromatic)	1400-1620
C-C stretch (aromatic)	1400-1500
C-N stretch (aromatic)	1250-1335
C-F stretch	1000-1400
O-H stretch	3700-3584
C-H stretch (C-CH₃)	2862-2882, 2652-2972
C≡N stretch	2300-2200
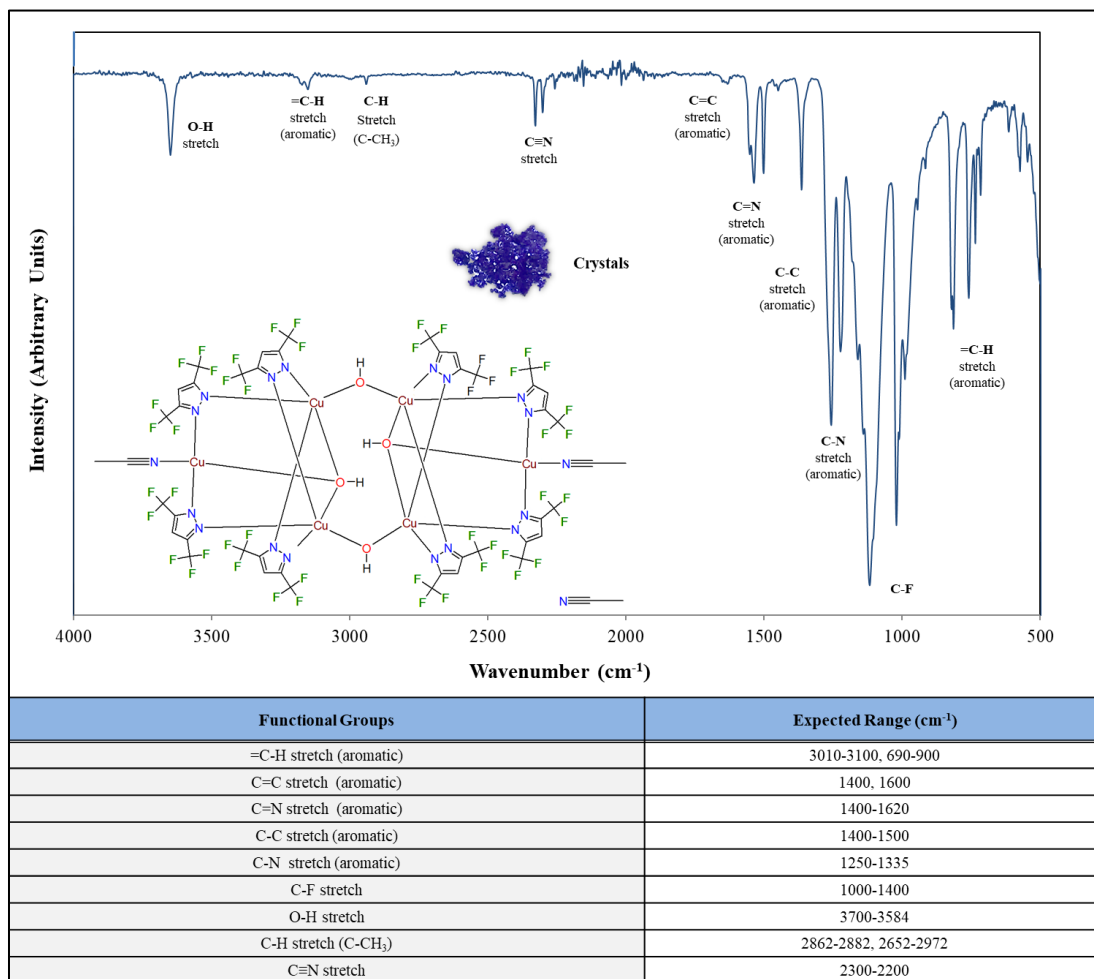
Figure 96. FT-IR spectra for $\{Cu_3[3,5\text{-}(CF_3)_2Pz]_4(ACN)(OH)_2\}_2 \cdot ACN$ crystals.

3.2.8.4 Characterization using TGA and DSC Analyses

In this section, the TGA and DSC analyses for the $\{Cu_3[3,5-(CF_3)_2Pz]_4(ACN)(OH)_2\}_2 \cdot$ ACN blue crystals (air dried), shown in Figures 97 and 98, are discussed.

Figure 97 shows the TGA analysis for the $\{Cu_3[3,5-(CF_3)_2Pz]_4(ACN)(OH)_2\}_2 \cdot$ ACN blue crystals in which a total weight loss of 89.75% was observed. The total weight loss was observed gradually over three weight loss drops, which were identified using the 1st derivative of the weight loss curve. The first weight loss of 19.31% was observed between 100.00°C and 203.94°C, with a 1st derivative peak (greatest rate of change on the weight loss curves) of 187.71°C. The second weight loss of 34.58% was observed between 203.94°C and 284.64°C, with a 1st derivative peak of 266.64°C. The third weight loss of 35.86% was observed between 284.64°C and 400.00°C, with a 1st derivative peak of 315.37°C. The first and second weight losses are most likely related to the partial sublimation of the $[3,5-(CF_3)_2Pz]^-$ ligands.

With regard to the emperical formula C44 H18 Cu6 F48 N18 O4 (MW = 2155.93.06 g/mol): C, 24.51; H, 0.84; N, 11.69, while accounting for the absence of the acetonitrile solvent molecule (C2 H3 N), the theoretical percentage of copper is 17.68%; however, the total weight loss of 89.75% was observed, which was primarily due to the sublimation of the fluorinated-pyrazolate ($[3,5-(CF_3)_2Pz]^-$), hydroxo (OH$^-$), and acetonitrile (ACN) ligands (total theoretical percentage of C, H, N and F of 82.32%). The remaining weight percentage of 10.25% following the aforementioned weight should theoretically be copper.

Figure 98 shows the DSC analysis for the $\{Cu_3[3,5\text{-}(CF_3)_2Pz]_4(ACN)(OH)_2\}_2 \cdot$ ACN blue crystals. Two broad endothermic events were observed. The first and second endothermic events were observed from 60°C to 210.53°C and from 210.53°C to 300°C, respectively, with peak maxima at 179.25°C and 283.01°C, respectively. Both endothermic events are most likely characteristic of partial sublimations (an endothermic event) of the fluorinated-pyrazolate ($[3,5\text{-}(CF_3)_2Pz]^-$) ligands. Moreover, the observed sublimation between 60°C to 210.53°C is in agreement with the TGA analysis regarding the first weight loss of 19.31% between 100.00°C and 203.94°C. Likewise, the observed sublimation between 210.53°C to 300°C is in agreement with the TGA analysis regarding the second weight loss of 34.83%, observed between 203.94°C and 284.64°C. Timelapse images of the blue crystals with regard to the increasing temperature are shown in Figure 98, in which the partial loss of the crystals blue color is observed by 179.25°C, followed by the complete loss of the crystals blue color by 283.01°C. The DSC analysis, as well as the timelapse images, show that the blue crystals begin to melt with decomposition around 300°C.
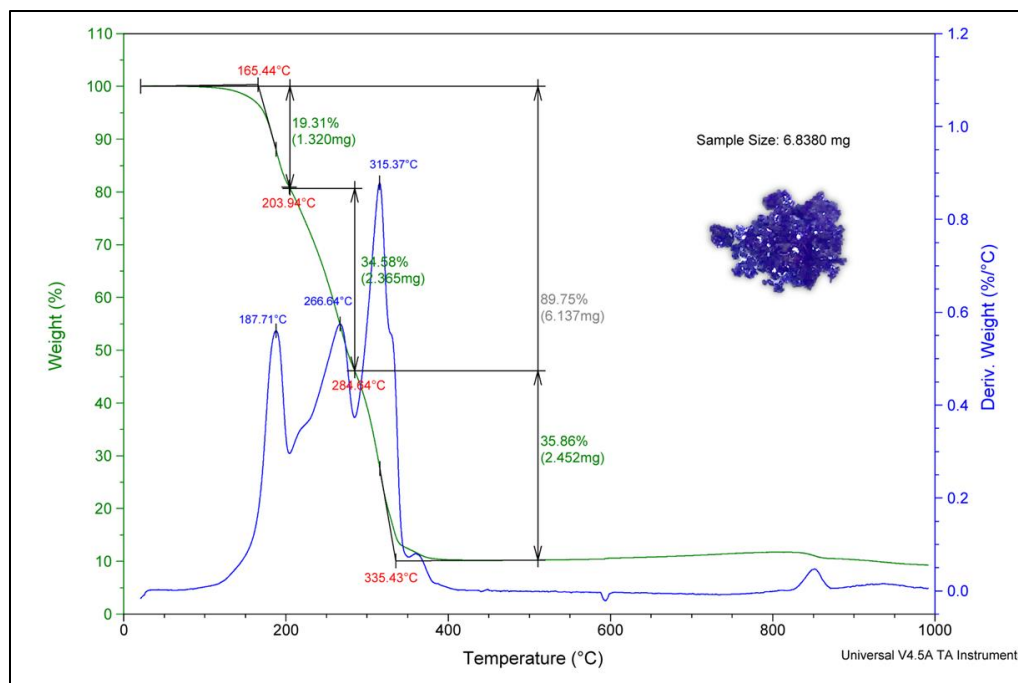
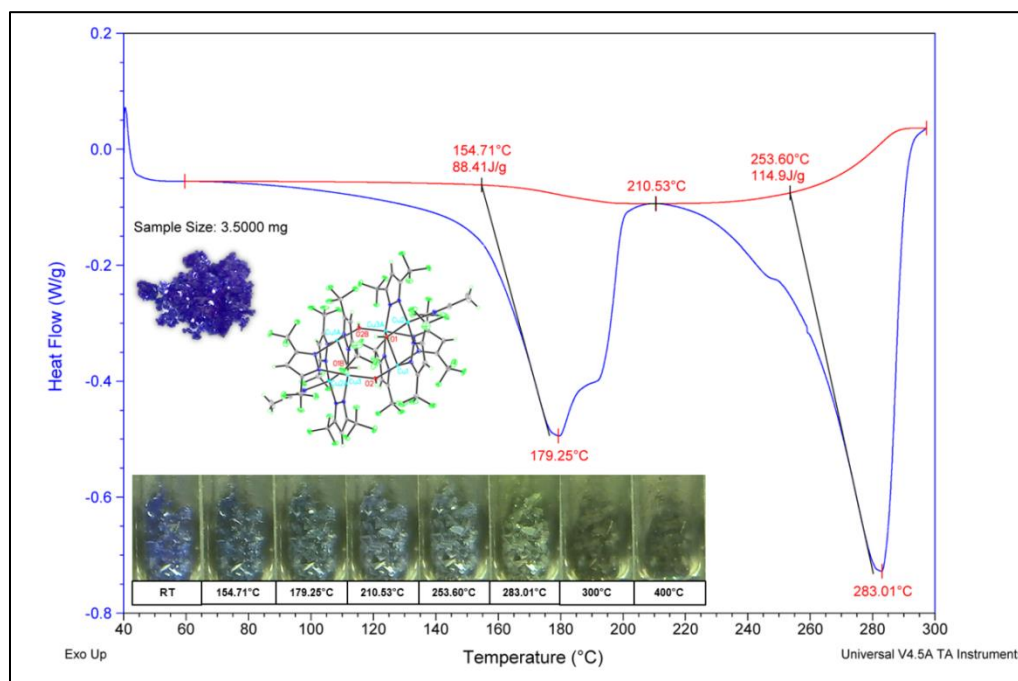**Figure 97.** TGA analysis of $\{Cu_3[3,5\text{-}(CF_3)_2Pz]_4(ACN)(OH)_2\}_2 \cdot ACN$ crystals.

Figure 98. DSC analysis of $\{Cu_3[3,5\text{-}(CF_3)_2Pz]_4(ACN)(OH)_2\}_2 \cdot ACN$ crystals.

3.2.9. Compound 9: {[CuI(PVP)] · 1.5 H$_2$O}$_\infty$

3.2.9.1 Elemental Analysis Data

In this section, the elemental analysis data for the {[CuI(PVP)] · 1.5 H$_2$O}$_\infty$ solvent-mediated powder are discussed, comparing the experimentally found data with the theoretical Anal. Calc., shown in Table 17.

The proposed structure of the product, {[CuI(PVP)] · 1.5 H$_2$O}$_\infty$, shown in Figure 99, is a based on a 1:4 ratio of CuI:PVP (for single units of 4-vinlypyridine); furthermore, three water molecules (H$_2$O) are included in the symmetric unit of the proposed structure in order to account for the (O-H) stretches observed in the IR spectra for both PVP the product. The theoretical percentages of carbon (C), hydrogen (H), and nitrogen (N) were analytically calculated (Anal. Calc.) based on the empirical formula C56 H62 Cu2 I2 N8 O3 (MW = 1276.05 g/mol): C, 52.71; H, 4.90; N, 8.78. The experimentally found data for the solvent-mediated powder (C, 52.76; H, 4.98; N, 8.82) match that of the theoretical Anal. Calc. within ±0.05 for C, ±0.08 for H, and ±0.04 for N.
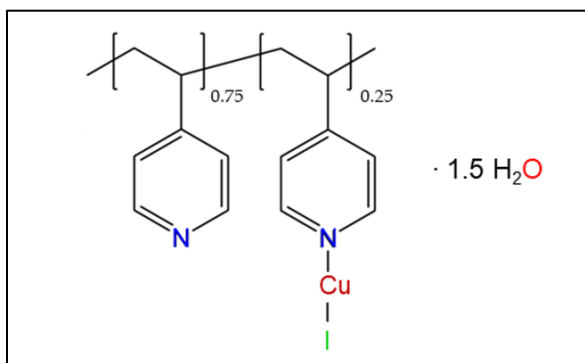

Figure 99. Proposed structure of {[CuI(PVP)] · 1.5 H$_2$O}$_\infty$, based on the 1:4 ratio of CuI:PVP (for single units of 4-vinlypyridine).

Table 17. Elemental analysis data for {[CuI(PVP)] · 1.5 H$_2$O]$_\infty$ solvent-mediated powder: theoretical Anal. Calc. versus experimentally found data.

Elemental Analysis		
{[CuI(PVP)]$_2$ · 3 H$_2$O]$_\infty$ = C56 C56 H62 Cu2 I2 N8 O3 (MW = 1276.04 g/mol)		
		Solvent-Mediated Powder
Element	**Theoretical Anal. Calc.**	**Experimentally Found**
C	52.71%	52.76%
H	4.90%	4.98%
N	8.78%	8.82%
Cu	9.96%	

3.2.3.2 Characterization using FT-IR Spectroscopy

In this section, the IR spectra for {[CuI(PVP)] · 1.5 H$_2$O}$_\infty$ solvent-mediated powder (and PVP), shown in Figure 100, are discussed. The IR spectra for the solvent-mediated powder and PVP are relatively identical to one another and feature the functional groups characteristic of PVP: =C-H stretch (aromatic), C=C stretch (aromatic), C=N stretch (aromatic), C-C stretch (aromatic), C-N stretch (aromatic), and C-H stretch (alkyl sp^3), and O-H stretch. Minor shifts in observed peaks and intensities are observed in the fingerprint region between 1,000 cm^{-1} and 1,500 cm^{-1}. An O-H stretch functional group is observed in the between 3,200 cm^{-1} and 3,500 cm^{-1} in both the IR spectra for the solvent-mediated powder and PVP, which may be attributed to the presence of water.
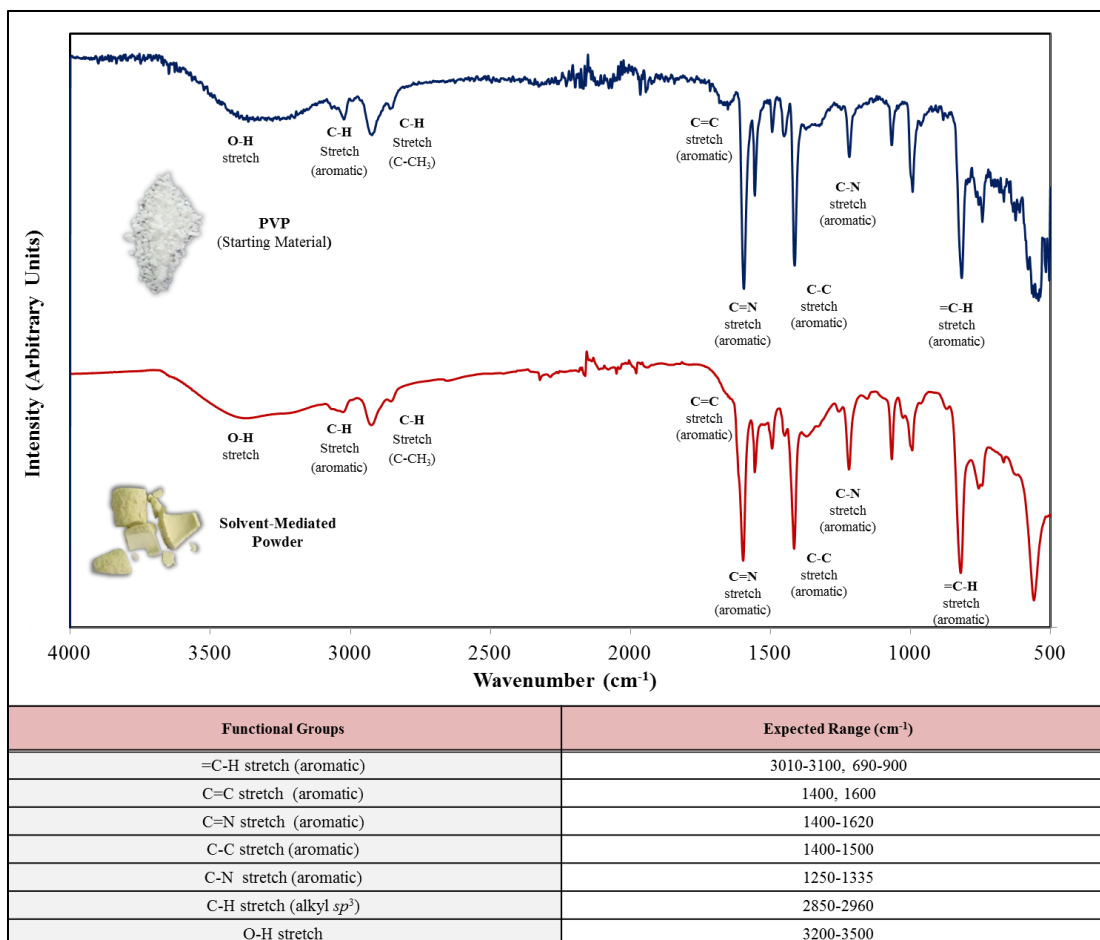
Functional Groups	Expected Range (cm^{-1})
=C-H stretch (aromatic)	3010-3100, 690-900
C=C stretch (aromatic)	1400, 1600
C=N stretch (aromatic)	1400-1620
C-C stretch (aromatic)	1400-1500
C-N stretch (aromatic)	1250-1335
C-H stretch (alkyl sp^3)	2850-2960
O-H stretch	3200-3500

Figure 100. Stacked FT-IR spectra for the $\{[CuI(PVP)] \cdot 1.5\ H_2O\}_\infty$ solvent-mediated powder and PVP.

3.2.3.3 Characterization using TGA and DSC Analyses

In this section, the TGA and DSC analyses for the $\{[CuI(PVP)] \cdot 1.5\ H_2O\}\infty$ solvent-mediated powder, shown in Figures 101 and 102, are discussed.

Figure 101 shows the TGA analysis for the $\{[CuI(PVP)] \cdot 1.5\ H_2O\}_\infty$ solvent-mediated powder in which a total weight loss of 79.30% was observed. The total weight loss was observed gradually over three weight loss drops, which were identified using the 1st derivative of the weight loss curve. The first weight loss of 4.215% was observed

between 24°C and 289.73°C, with a 1st derivative peak (greatest rate of change on the weight loss curves) of 45.29°C. The second weight loss of 61.61% was observed between 289.73°C and 500°C, with a 1st derivative peak of 382.65°C. The third weight loss of 13.48% was observed between 500°C and 1000°C, with a 1st derivative peak of 595.14°C.

With regard to the emperical formula C56 H62 Cu2 I2 N8 O3 (MW = 1276.05 g/mol): C, 52.71; H, 4.90; N, 8.78, while accounting for the presence of the three water molecules (H_2O), the theoretical percentage of copper is 9.97%. However, the total weight loss of 79.30% was observed, which was primarily due to the removal of the water molecules and the sublimation of PVP (total theoretical percentage of C, H, N and O of 70.13%). The first weight loss of 4.215% (between 24°C and 300°C) is characteristic of the removal of the water molecules, which have a theoretical percentage of 4.24%. The second weight loss of 61.61% (between 300°C and 500°C) is characteristic of the sublimation of PVP (completely sublimes between 300°C and 450°C), which have a theoretical percentage of 65.89%. The third weight loss of 13.48% (between 500°C and 1000°C) might possibly be characteristic of the sublimation of the remaining ~4.28% of PVP; meanwhile, the other ~9.20% might be characteristic of the partial release of iodide (I^-) in the form iodine (I_2). The remaining weight percentage of 20.70% following the aforementioned weight losses should theoretically be a mix of copper and copper(I) iodide.

Figure 102 shows the DSC analysis for the $\{[CuI(PVP)] \cdot 1.5\ H_2O\}_\infty$ solvent-mediated powder. A broad endothermic event was observed from 40°C to 231.12°C (with

a peak maximum at 97.22°C), which is most likely characteristic of desolvation (an endothermic event) of the water molecules. The observed desolvation between 40°C to 231.12°C is in agreement of the TGA analysis regarding the first weight loss of 4.215% between 24°C and 300°C, which was characterized as the removal of the water molecules.
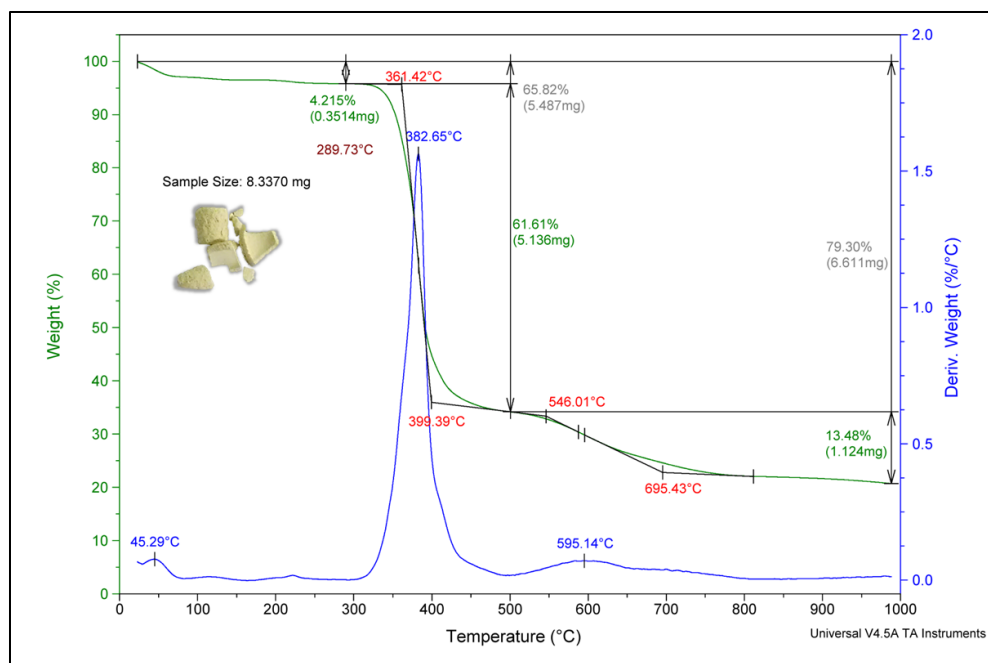

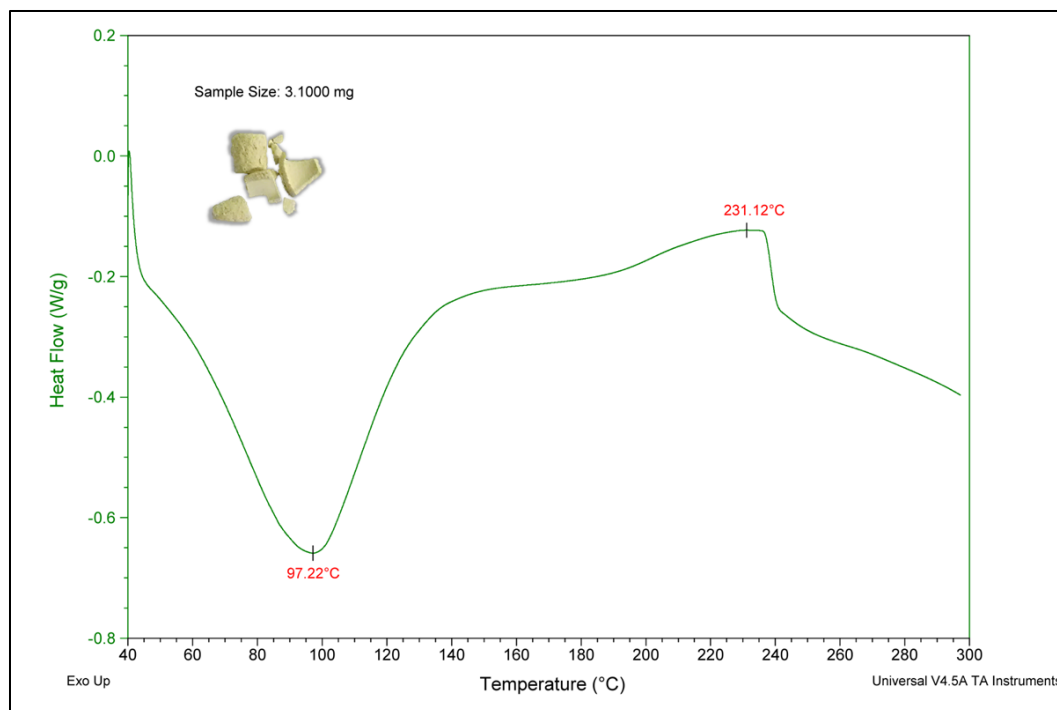**Figure 101.** TGA analysis of $\{[CuI(PVP)] \cdot 1.5\ H_2O\}_\infty$ solvent-mediated powder.

Figure 102. DSC analysis of $\{[CuI(PVP)] \cdot 1.5\ H_2O\}_\infty$ solvent-mediated powder.

3.2.3.4 Characterization using Photoluminescence

In this section, the photoluminescence of $\{[CuI(PVP)] \cdot 1.5\ H_2O\}_\infty$ solvent-mediated powder is discussed.

The solvent-mediated powder was checked under a handheld UV lamp for luminescence, under Short Wave UV ($\lambda_{ex} = 254$ nm) and Long Wave UV ($\lambda_{ex} = 365$ nm) at RT. As shown in Figure 103, at RT, strong, yellow photoluminescence was observed under 254 nm and 365 nm for solvent-mediated powder. After one to two days, the solvent-mediated powder exhibited photoluminescence quenching under both Short Wave UV ($\lambda_{ex} = 254$ nm) and Long Wave UV ($\lambda_{ex} = 365$ nm).

207

As shown in Figure 104, the photoluminescence of the 1:4 CuI:PVP (suspended in a solution of ACN and DCM) was measured at RT, using an excitation wavelength of λ_{ex} = 428 nm, producing an emission band with a maximum emission peak at λ_{em} = 554 nm.
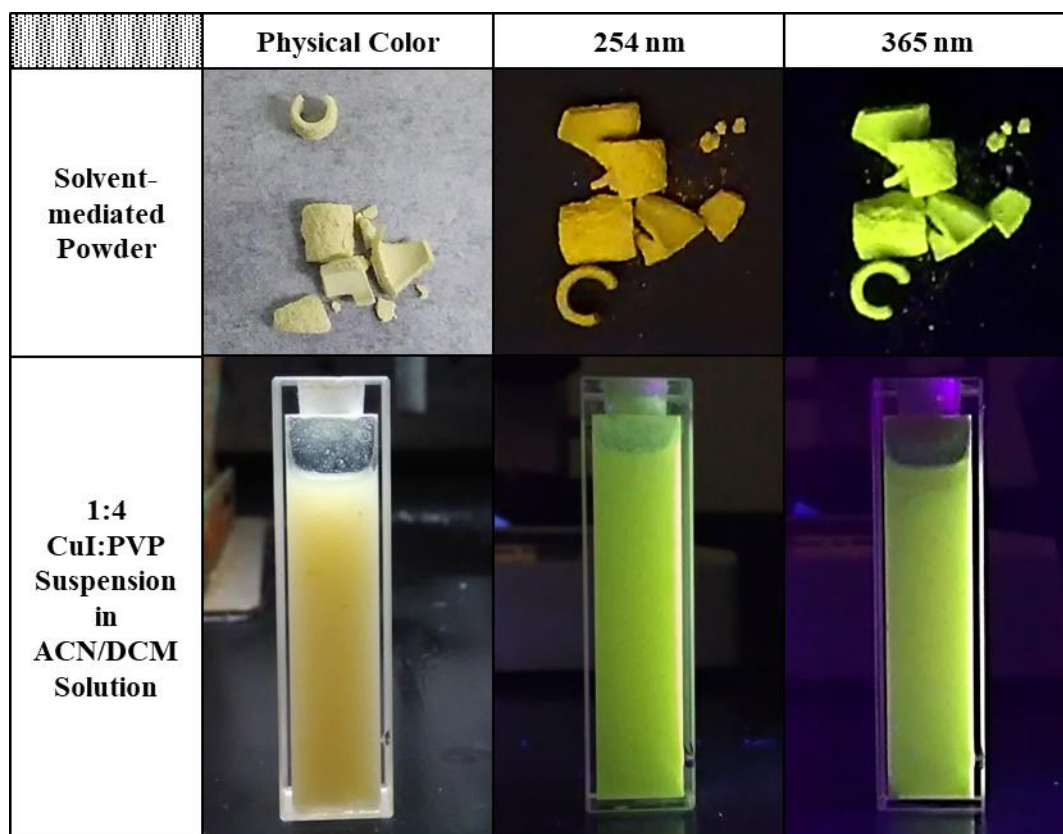
	Physical Color	254 nm	365 nm
Solvent–mediated Powder			
1:4 CuI:PVP Suspension in ACN/DCM Solution			

Figure 103. Photoluminescence of $\{[CuI(PVP)] \cdot 1.5\ H_2O\}_\infty$ solvent-mediated powder and 1:4 CuI:PVP (suspended in a solution of ACN and DCM) under Short Wave UV (λ_{ex} = 254 nm) and Long Wave UV (λ_{ex} = 365 nm), at room temperature (RT).
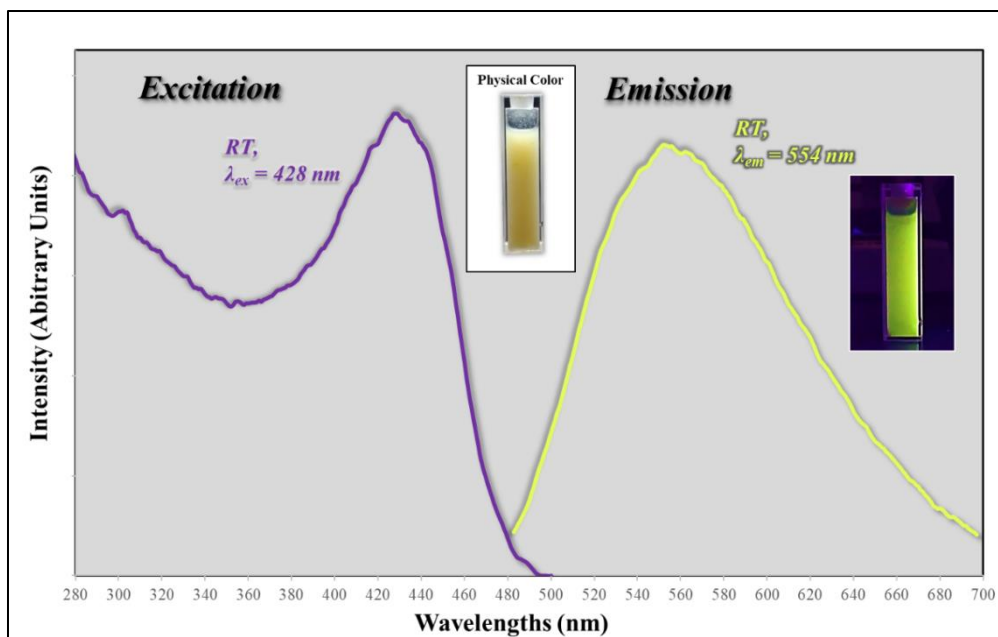
Figure 104. Photoluminescence spectra for 1:4 CuI:PVP (suspended in a solution of ACN and DCM), at room temperature (RT).

CHAPTER IV

CONCLUSION

In this work, six mixed-ligand copper(I) and silver(I) compounds with pyrazolate- and phenanthroline-based ligands, shown in Figure 105, were successfully synthesized in good yields while exploring alternative synthetic routes. The Cu(I) and Ag(I) compounds were thoroughly characterized with regard to their structural, physical, and photophysical properties.
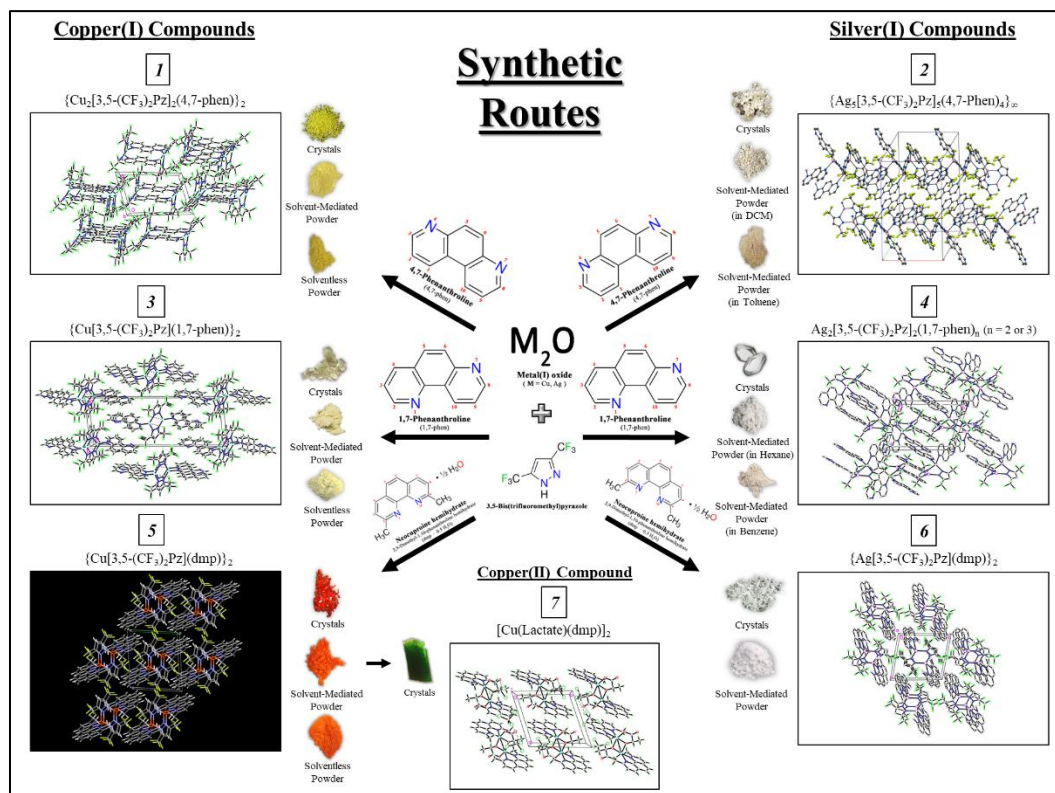

Figure 105. Synthetic Routes for Six Cu(I) and Ag(I) Compounds with Pyrazolate- and Phenanthroline-Based Ligands, and One Cu(II) Compound with Lactate- and Phenanthroline-Based Ligands.

4.1 Effects of Synthetic Routes

With regard to the effects of the synthetic routes, solvent-mediated versus solventless syntheses, the three Cu(I) compounds: {Cu$_2$[3,5-(CF$_3$)$_2$Pz]$_2$(4,7-phen)}$_2$, {Cu[3,5-(CF$_3$)$_2$Pz](1,7-phen)}$_2$, and {Cu[3,5-(CF$_3$)$_2$Pz](dmp)}$_2$, were synthesized via solvent-mediated and solventless syntheses, yielding both physically colored and photoluminescent solids, as shown in Figures 106 and 107. In contrast, the three Ag(I) compounds: {Ag$_5$[3,5-(CF$_3$)$_2$Pz]$_5$(4,7-phen)$_4$}$_\infty$, Ag$_2$[3,5-(CF$_3$)$_2$Pz]$_2$(1,7-phen)$_3$, and {Ag[3,5-(CF$_3$)$_2$Pz](dmp)}$_2$, were successfully synthesized via only solvent-mediated syntheses because the physical color of the solids, shown in Figure 106, are relatively colorless/off-white (resembling the physical color of one or both of the starting materials) and do not exhibit photoluminescence at RT or with heating. The solvent-mediated syntheses were monitored for completion via the change in physical color and/or the formation of precipitate; meanwhile, the solventless syntheses were monitored for completion via the change in physical color and/or the disappearance/appearance of luminescence. The six heteroleptic copper(I) and silver(I) compounds synthesized via solvent-mediated syntheses, were collected via filtration under vacuum. Two of the three Cu(I) compounds synthesized via solventless syntheses: {Cu$_2$[3,5-(CF$_3$)$_2$Pz]$_2$(4,7-phen)}$_2$ and {Cu[3,5-(CF$_3$)$_2$Pz](1,7-phen)}$_2$, were unwashed due being very air-sensitive in common solvents, while the air-stable Cu(I) compound: {Cu[3,5-(CF$_3$)$_2$Pz](dmp)}$_2$, was thoroughly washed with a suitable solvent.
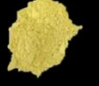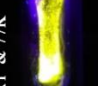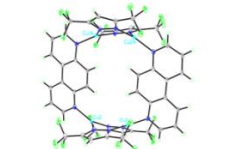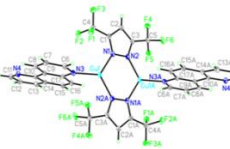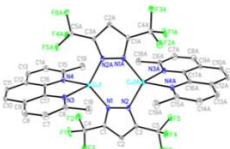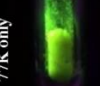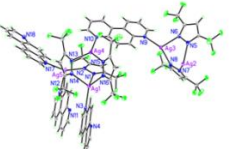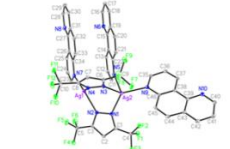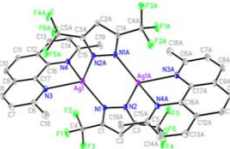
		Ligands					
		FPz + 4,7-Phen		**FPz + 1,7-Phen**		**FPz + dmp**	
Metal	**Cu(I)**	Physical Color	Luminescence	Physical Color	Luminescence	Physical Color	Luminescence
		Yellow	RT & 77K Yellow	Yellow	RT & 77K Yellow	Orange	RT & 77K Red
	Ag(I)	Physical Color	Luminescence	Physical Color	Luminescence	Physical Color	Luminescence
		Off-White	No Luminescence at RT or 77K	Off-White	77K only Green	White	77K only Green

Figure 106. Effect of metal and ligand on the physical colors, photoluminescence emission colors, and structures for the six Cu(I) and Ag(I) complexes and coordination polymers.

		Ligands					
		FPz + 4,7-Phen		**FPz + 1,7-Phen**		**FPz + dmp**	
Metal	**Cu(I)**	Solvent-Mediated	Solventless	Solvent-Mediated	Solventless	Solvent-Mediated	Solventless
		Yield = 84%		Yield = 81%		Yield = 79%	Yield = 69%
	Ag(I)	Solvent-Mediated	Solventless	Solvent-Mediated	Solventless	Solvent-Mediated	Solventless
		Yield = 77%	N/A	Yield = 75%	N/A	Yield = 61%	N/A

Figure 107. Effect of synthetic route for the six Cu(I) and Ag(I) complexes and coordination polymers.

With regard to the $\{Cu_2[3,5\text{-}(CF_3)_2Pz]_2(4,7\text{-phen})\}_2$ complex, the solvent-mediated powder was synthesized in a very good yield (yield 84%), experimental data/results for the solvent-mediated powder, solventless powder, and crystals are very similar and are in great agreement.

With regard to the $\{Ag_5[3,5\text{-}(CF_3)_2Pz]_5(4,7\text{-phen})_4$ coordination polymer, the solvent-mediated powder, synthesized using in dichloromethane, was synthesized in a very good yield (yield 77%). Meanwhile, the solvent-mediated powder, synthesized in toluene, was synthesized in a poor yield (yield 40%). The lower yield for the solvent-mediated powder, synthesized in toluene, was attributed to unavoidable loss due to the product's higher solubility in toluene, which resulted in significant loss during vacuum filtration. In addition, the experimental data/results for both solvent-mediated powders and the crystals are very similar and are in great agreement, while accounting for the absence/presence of solvent molecules.

With regard to the $\{Cu[3,5\text{-}(CF_3)_2Pz](1,7\text{-phen})\}_2$ complex, the solvent-mediated powder was synthesized in a very good yield (yield 81%), respectively. The experimental data/results for the solvent-mediated powder, solventless powder, and crystals are similar and are in good agreement, while considering the presence of impurities (due to excess ligand) in the crude solventless powder.

With regard to the $Ag_2[3,5\text{-}(CF_3)_2Pz]_2(1,7\text{-phen})_3$ compound, the solvent-mediated powder (filtered), synthesized using hexane was synthesized in a very good yield (yield 75%). The experimental data/results for the solvent-mediated powders and crystals are significantly different with regard to their elemental analysis data, IR spectra

(for fingerprint region), and TGA analyses, which suggests a difference in molecular structure. Furthermore, the elemental analysis confirms that the crystals are of the $Ag_2[3,5-(CF_3)_2Pz]_2(1,7-phen)_3$ structure, while the solvent-mediated powders are likely the Ag(I) analogues of the $\{Cu[3,5-(CF_3)_2Pz](1,7-phen)\}_2$ compound, possessing a $\{Ag[3,5-(CF_3)_2Pz](1,7-phen)\}_2$ structure.

With regard to the $\{Cu[3,5-(CF_3)_2Pz](dmp)\}_2$ compound, the solvent-mediated powder and solventless powder (washed) were synthesized in good yields (yields 79% and 69%, respectively). The experimental data/results for the solvent-mediated powder, solventless powder, and crystals are very similar with regard to their elemental analysis data and IR spectra; however, their TGA analyses were significantly different in terms of weight loss percentages. It is worth noting that the physical color of the powders and crystals vary slightly in that the powders appear orange in color while the crystals appear red in color (orange in color, under the microscope due to lighting). Although these differences are not completely understood, the presence of impurities and/or the presence of more than one polymorph of the $\{Cu[3,5-(CF_3)_2Pz](dmp)\}_2$ compound are possibilities.

Figure 108. Physical Color of $\{Cu[3,5-(CF_3)_2Pz](dmp)\}_2$ Crystals: Red (*right*); Orange (*left*), Under Microscope Lighting.

With regard to the {Ag[3,5-(CF$_3$)$_2$Pz](dmp)}$_2$ compound, the solvent-mediated powder was synthesized in a good yield (61%) despite unavoidable loss attributed to the solvent-mediated powder's solubility in toluene, resulting in some loss during vacuum filtration. The experimental data/results for the solvent-mediated powder and crystals are very similar with regard to their elemental analysis data and IR spectra; however, their TGA analyses were somewhat different in terms of their total weight loss percentages, which may suggest the presence of some impurities in the solvent-mediated powder.

4.2 Effect of Metal and Ligand: Physical and Photophysical Properties

The metal and ligand play significant roles in the formation of the six Cu(I) and Ag(I) compounds, which are visually evident in both their physical color (with regard to powder form) and photoluminescence, shown in Figures 106 and 107, respectively.

In comparison between the heteroleptic Cu(I) and Ag(I) compounds (compounds 1 and 2, respectively): {Cu$_2$[3,5-(CF$_3$)$_2$Pz]$_2$(4,7-phen)}$_2$ and {Ag$_5$[3,5-(CF$_3$)$_2$Pz]$_5$(4,7-phen)$_4$}$_\infty$, respectively, both were prepared in a similar manner, with the same ligands, and in the same molar ratios (1:3, metal to ligand); however, they differ in terms of their metal. This difference is visually apparent with regard to both physical color and photoluminescence. Moreover, the Cu(I) compound with 4,7-phen (compound 1, in powder form) exhibits a yellow physical color and yellow photoluminescence (at RT and 77K), while Ag(I) compound with 4,7-phen (compound 2, in powder form) exhibits an off-white physical color and no photoluminescence (at RT nor 77K).

Similarly, the heteroleptic Cu(I) and Ag(I) compounds (compounds 3 and 4, respectively): {Cu[3,5-$(CF_3)_2$Pz](1,7-phen)}$_2$ and {Ag[3,5-$(CF_3)_2$Pz](1,7-phen)}$_2$, respectively, were prepared in a similar manner (similar to compounds 1 and 2, respectively), and yet they exhibit a difference in physical color and photoluminescence, which is attributed to the effect of the metal. The Cu(I) compound with 1,7-phen (compound 3, in powder form) exhibits a yellow physical color and yellow photoluminescence (at RT and 77K), while Ag(I) compound with 1,7-phen (compound 4, in powder form) exhibits an off-white physical color and green photoluminescence (only at 77K).

Likewise, the Cu(I) and Ag(I) compounds (compounds 5 and 6, respectively): {Cu[3,5-$(CF_3)_2$Pz](dmp)}$_2$ and {Ag[3,5-$(CF_3)_2$Pz](dmp)}$_2$, respectively, were prepared in a similar manner (similar to compound 1), yet they exhibit a difference in physical color and photoluminescence, which is attributed to the effect of the metal. The Cu(I) compound with dmp (compound 5, in powder form) exhibits an orange physical color and red photoluminescence (at RT and 77K), while Ag(I) compound with dmp (compound 6, in powder form) exhibits a white physical color and green photoluminescence (only at 77K).

The ligand effect is visually apparent upon the comparison between the three respective Cu(I) compounds: {Cu$_2$[3,5-$(CF_3)_2$Pz]$_2$(4,7-phen)}$_2$, {Cu[3,5-$(CF_3)_2$Pz](1,7-phen)}$_2$, and {Cu[3,5-$(CF_3)_2$Pz](dmp)}$_2$, as well as the three respective Ag(I) compounds: {Ag$_5$[3,5-$(CF_3)_2$Pz]$_5$(4,7-phen)$_4$}$_\infty$, Ag$_2$[3,5-$(CF_3)_2$Pz]$_2$(1,7-phen)$_3$, and {Ag[3,5-$(CF_3)_2$Pz](dmp)}$_2$. The three Cu(I) compounds are physically colored (yellow, yellow,

and orange, respectively) and exhibit photoluminescence (yellow, yellow, and red, respectively). Interestingly, with respect to each Cu(I) compound, the physical color is similar to the photoluminescence emission color. On the other hand, the Ag(I) compounds are relatively similar in terms of physical color: white or off-white, yet differ in that the Ag(I) compound with 4,7-phen does not exhibit photoluminescence at RT or 77K, while the Ag(I) compounds with 1,7-phen and dmp exhibit green luminescence at 77K.

4.3 Effect of Metal and Ligand: Structural Properties

With regard to the six heteroleptic copper(I) and silver(I) compounds, the cyclic, trinuclear Cu(I)- and Ag(I)-pyrazolate precursors (starting materials), $\{[3,5-(CF_3)_2Pz]Cu\}_3$ and $\{[3,5-(CF_3)_2Pz]Ag\}_3$, respectively, were broken into dimeric units, singly and/or doubly bridged via the $[3,5-(CF_3)_2Pz]^-$ ligand.

The Cu(I) and Ag(I) compounds: $\{Cu_2[3,5-(CF_3)_2Pz]_2(4,7-phen)\}_2$ and $\{Ag_5[3,5-(CF_3)_2Pz]_5(4,7-phen)_4\}_\infty$, respectively, are different in their molecular structure despite using the same molar ratio of metal to ligand (1:3). The $\{Cu_2[3,5-(CF_3)_2Pz]_2(4,7-phen)\}_2$ compound exhibits a tetrameric, dimer-of-dimers structure composed of two pyrazolate-bridged dimer units, bridged via two 4,7-phen ligands. Meanwhile, the $\{Ag_5[3,5-(CF_3)_2Pz]_5(4,7-phen)_4\}_\infty$ coordination polymer exhibits a zigzag-like, polymeric structure composed of 3- and 4-coordinated Ag(I) centers, bridged via both 4,7-phen and $[3,5-(CF_3)_2Pz]^-$ ligands. In addition, each $\{Ag_5[3,5-(CF_3)_2Pz]_5(4,7-phen)_4\}$ unit exhibits $[Ag_2Ar_2]$ π-π stacked pairing.

The Cu(I) and Ag(I) compounds: $\{Cu[3,5\text{-}(CF_3)_2Pz](1,7\text{-phen})\}_2$ and $Ag_2[3,5\text{-}(CF_3)_2Pz]_2(1,7\text{-phen})_3$, respectively, are relatively similar in their molecular structure (for crystal) in that both compounds exhibit dimeric structures composed of a pyrazolate-bridged dimer unit. However, they differ in that the $\{Cu[3,5\text{-}(CF_3)_2Pz](1,7\text{-phen})\}_2$ compound consist of two 3-coordinated Cu(I) centers, with each center coordinated with a 1,7-phen ligand. Meanwhile, the $Ag_2[3,5\text{-}(CF_3)_2Pz]_2(1,7\text{-phen})_3$ compound consist of 3- and 4-coordinated Ag(I) centers, with the 3-coordinated Ag(I) center coordinated with one 1,7-phen ligand, and the 4-coordinated Ag(I) center coordinated with two 1,7-phen ligands. Furthermore, the packing of $Ag_2[3,5\text{-}(CF_3)_2Pz]_2(1,7\text{-phen})_3$ exhibits $[Ag_2Ar_2]$ π-π stacking pairs, as well as an End-Ar π-π stacking pair. Based on the elemental analysis data, the molecular structure for the Ag(I) compound with 1,7-phen in crystal form most likely differs from the molecular structure in powder form in that the powder structure may possibly resemble $\{Ag[3,5\text{-}(CF_3)_2Pz](1,7\text{-phen})\}_2$, the Ag(I) analogue of $\{Cu[3,5\text{-}(CF_3)_2Pz](1,7\text{-phen})\}_2$, possessing two 3-coordinated Ag(I) centers with two $[3,5\text{-}(CF_3)_2Pz]^-$ and two 1,7-phen ligands.

The Cu(I) and Ag(I) compounds: $\{Cu[3,5\text{-}(CF_3)_2Pz](dmp)\}_2$ and $\{Ag[3,5\text{-}(CF_3)_2Pz](dmp)\}_2$, are analogous in structure. In addition, both compounds exhibit the same dimeric structures composed of a pyrazolate-bridged dimer unit, and each 4-coordinated metal(I) center is coordinated with a dmp ligand via bidentate chelating.

4.4 Synthesis of Copper(II)-Lactate Compound via Copper Catalysis: Acetone to Lactate Conversion

An alternative method for the crystallization of the $\{Cu[3,5-(CF_3)_2Pz](dmp)\}_2$ complex inadvertently resulted in the synthesis of the dimeric, copper(II)-lactate complex: $[Cu(Lactate)(dmp)]_2$, shown in Figure 105 as compound 7. The introduction/formation of the deprotonated lactate $(CH_3CH(O^-)COO^-)$ ligand was traced to the use of excess acetone and the presence of O_2 (from air), which has been reported by Diaconu et al.[38] According to the literature, a mononuclear copper(I) complex with a tris(pyrazolyl)borate ligand was reacted with acetone (in excess) in the presence of air (at 25°C), leading to the coordination of acetone's oxygen atom with the Cu(I) center and the eventual conversion of the coordinated acetone to protonated lactate, $(CH_3CH(OH)COO^-)$, as shown in Figure 109.[38]

Regarding the $[Cu(Lactate)(dmp)]_2$ complex, the coordination of the acetones' oxygen atoms with the Cu(I) centers, followed by the conversion of the acetones to protonated lactates, likely occurred stepwise, leading the removal of the two fluorinated-pyrazolate ligands, $[3,5-(CF_3)_2Pz]^-$. The resulting pyrazolate ligands, in turn, deprotonated the coordinated $(CH_3CH(OH)COO^-)$ ligands, thus allowing for the deprotonated oxygen atoms to further coordinate with the adjacent copper centers.
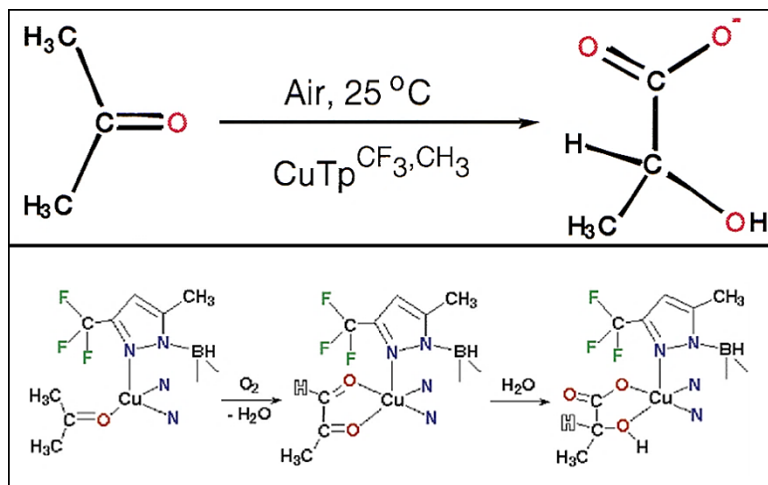
Figure 109 Mechanism of acetone to lactate conversion via copper catalysis.[38]

The resulting crystallization/synthesis produced a mixture of [Cu(Lactate)(dmp)]$_2$ green crystals and {Cu[3,5-(CF$_3$)$_2$Pz](dmp)}$_2$ red crystals (and/or orange powder). Although the [Cu(Lactate)(dmp)]$_2$ green crystals were never weighted out, the yield was considered to be very poor. Elemental analysis data was experimentally obtained for the [Cu(Lactate)(dmp)]$_2$ green crystals with the least amount of impurities. Moreover, the elemental analysis data suggested that chloroform was present with [Cu(Lactate)(dmp)]$_2$ in a 1:4 molar ratio, rather than a 4:1 molar ratio as shown in the x-ray crystallographic data. The difference in the molar ratio of chloroform to [Cu(Lactate)(dmp)]$_2$ was understandable considering that the green crystal were very unstable out of solution. Due to the very poor yield, the green crystals were only characterized via single crystal X-ray diffraction, elemental analysis, and FT-IR spectroscopy.

4.5 Copper(I/II) Complexes and Metallopolymers using FPz⁻ and PVP

In addition to the aforementioned Cu(I) and Ag(I) compounds, this work explored the syntheses of copper(I) iodide-base Cu(I/II) complexes and metallopolymers with a pyrazolate-based ligand ($[3,5-(CF_3)_2Pz]^- = FPz^-$) and poly(4-vinylpyridine) (PVP), shown in Figure 110.
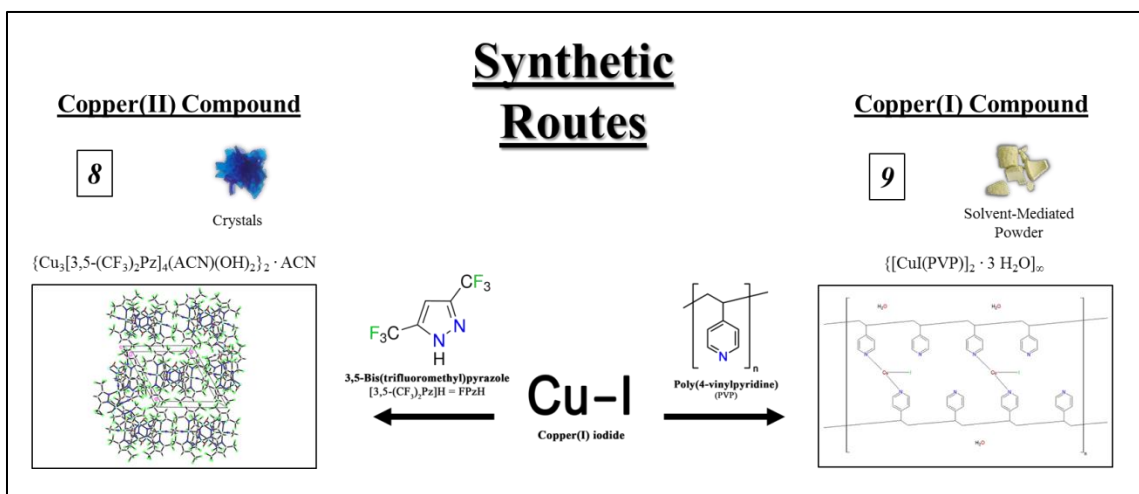
Figure 110. Synthetic routes for copper(I) iodide-based Cu(I/II) compounds and metallopolymers with pyrazolate ligands and poly(4-vinylpyridine).

With regard to the syntheses of homoleptic copper(I) iodide-base complexes and metallopolymers with (FPz^-), various solvent-mediated and solventless syntheses were attempted while varying the molar ratio, temperature, and duration of the reactions; however, the reactions did not yield a product. Interestingly, this inadvertently led to the synthesis of a heteroleptic, hexameric (hexanuclear) copper(II)-pyrazolate complex: $\{Cu_3[3,5-(CF_3)_2Pz]_4(ACN)(OH)_2\}_2 \cdot$ ACN, composed of two trinuclear $Cu_3(\mu_3-O(H))$ core units, bridged via two μ-hydroxo (μ-OH) ligands. $\{Cu_3[3,5-(CF_3)_2Pz]_4(ACN)(OH)_2\}_2 \cdot$ ACN was collected as blue crystals via gravity filtration,

resulting in a poor yield (yield 39%). The $\{Cu_3[3,5\text{-}(CF_3)_2Pz]_4(ACN)(OH)_2\}_2 \cdot ACN$ blue crystals were thoroughly characterized using single crystal X-ray diffraction, elemental analysis, FT-IR spectroscopy, thermogravimetric analysis (TGA), and differential scanning calorimetry (DSC).

The syntheses of new copper(II)-pyrazolate complexes with $Cu_3(\mu_3\text{-}O(H))$ cores have recently been reported and utilized as secondary building units (SBUs) for the development of new metal organic frameworks (MOFs), as shown in Figure 111.[39-41] The trinuclear $Cu_3(\mu_3\text{-}O(H))$ cores are formed via the central bridging ligand: μ_3-hydroxo (μ_3-O(H)), which is coordinated with three Cu(II) centers; moreover, this typically occurs via the reaction of Cu(II) compounds with an appropriate ligand(s), such as a pyrazole or 1,2,4-trazole, although alternative synthetic routes utilizing various strong acids (HCl, $HClO_4$, etc.) and a strong base (NaOH) with pyrazolate-based ligands have been explored.[39-42] Ferrer et al. reported the syntheses of three trimeric copper(II) complexes with $Cu_3O(H)$ cores, shown in Figure 112, using the 1,2,4-triazole derivative ligand: Haat (3-acetylamino-1,2,4-triazole), in aqueous solutions of $Cu(CF_3SO_3)_2$, $Cu(NO_3)_2 \cdot 3H_2O$, and $Cu(ClO_4)_2 \cdot 6H_2O$.[42] Furthermore, the syntheses of the aforementioned trinuclear copper(II)-triazolate complexes were performed in a similar manner as that of the hexanuclear copper(II)-pyrazolate complex: $\{Cu_3[3,5\text{-}(CF_3)_2Pz]_4(ACN)(OH)_2\}_2 \cdot ACN$, in that the molar ratio of metal-to-ligand of 1:2 was used, and the compounds were precipitated out as blue crystals from standing solutions (at RT) and only after extended durations of syntheses (20 days up to 2 months).[42]
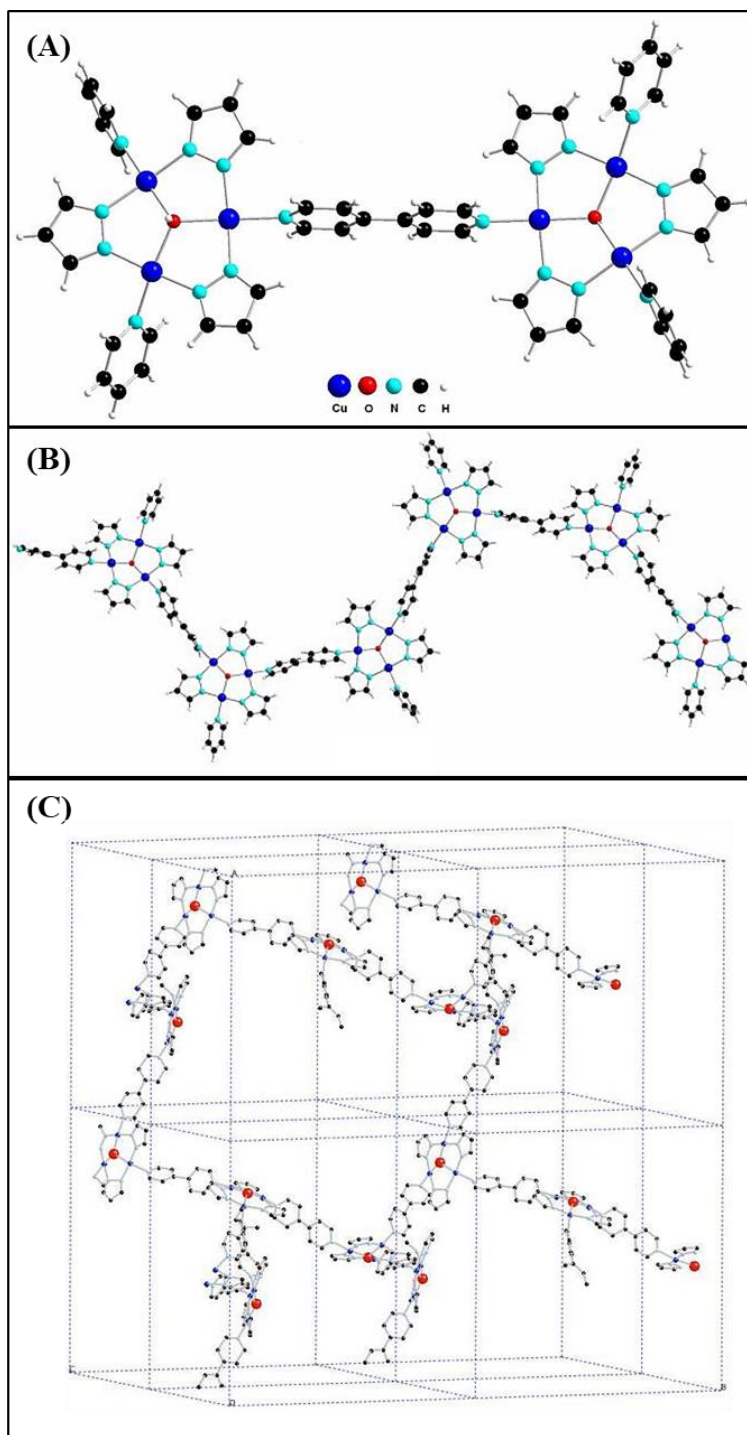
Figure 111. Copper(II)-pyrazolate complex with $Cu_3(\mu_3\text{-O(H)})$ cores utilized as a secondary building unit (SBUs) for the development of new metal organic frameworks (MOFs): **(A)** a secondary building unit (SBU), **(B)** 1-D coordination polymer (1-D chain), and **(C)** 3 –D coordination polymer (3-D lattice).[39]
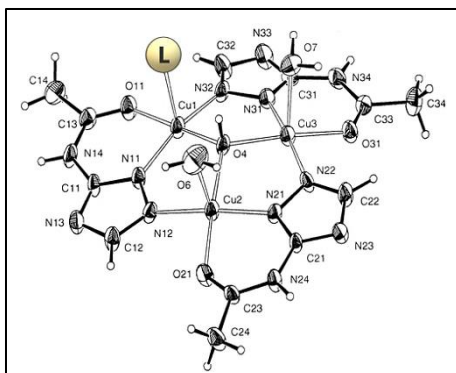
Figure 112. General structure of trinuclear copper(II)-triazolate complexes with $Cu_3(\mu_3\text{-}O(H))$ cores (L = CF_3SO_3, NO_3, ClO_4).[42]

With regard to the syntheses of homoleptic copper(I) iodide-base metallopolymer with poly(4-vinylpyridine) (PVP), various solvent-mediated syntheses were attempted while varying the molar ratio and solvents of the reactions. A 1:4 molar ratio of CuI:PVP (for single units of 4-vinlypyridine) resulted in the synthesis of a yellow colored, solid in good yield (yield 66%). The 1:4 CuI:PVP product was thoroughly characterized using elemental analysis, FT-IR spectroscopy, thermogravimetric analysis (TGA), and differential scanning calorimetry (DSC), which allowed for the determination of a proposed structure, $\{[CuI(PVP)] \cdot 1.5\ H_2O\}_\infty$, shown in Figure 99. Although the solvent-mediated powder initially exhibited strong, yellow photoluminescence in solid-state, the photoluminescence was completely quenched after one to two days. Photoluminescence at RT was measured for 1:4 CuI:PVP (suspended in a solution of ACN and DCM) using an excitation wavelength of λ_{ex} = 428 nm, producing an emission band with a maximum emission peak at λ_{em} = 554 nm. 1:4 CuI:PVP (suspended in a solution of ACN and DCM) did not exhibit course- nor fine-tuning with regard to either varying the excitation wavelength (λ_{ex}) or temperature.

REFERENCES

(1)   Rawashdeh-Omary, M. A. Remarkable Alteration of Photophysical Properties of Cyclic Trinuclear Complexes of Monovalent Coinage Metals Upon Interactions with Small Organic Molecules. *Comment Inorg. Chem.* **2012**, *33*, 88–101.

(2)   Dias, H. V. R.; Diyabalanage, H. V. K.; Rawashdeh-Omary, M. A.; Franzman, M. A.; Omary, M. A. Bright Phosphorescence of a Trinuclear Copper(I) Complex: Luminescence Thermochromism, Solvatochromism, and "Concentration Luminochromism". *J. Am. Chem. Soc.* **2003**, *125*, 12072–12073.

(3)   Dias, H. V. R.; Diyabalanage, H. V. K.; Eldabaja, M. G.; Elbjeirami, O.; Rawashdeh-Omary, M. A.; Omary, M. A. Brightly Phosphorescent Trinuclear Copper(I) Complexes of Pyrazolates: Substituent Effects on the Supramolecular Structure and Photophysics. *J. Am. Chem. Soc.* **2005**, *127*, 7489–7501.

(4)   Dias, H. R.; Polach, S. A.; Wang, Z. Coinage Metal Complexes of 3,5-Bis(trifluoromethyl)pyrazolate Ligand: Synthesis and Characterization of {[3,5-$(CF_3)_2$Pz]Cu}$_3$ and {[3,5-$(CF_3)_2$Pz]Ag}$_3$. *J. Fluor. Chem.* **2000**, *103*, 163–169.

(5)   Omary, M. A.; Rawashdeh-Omary, M. A.; Gonser, M. W. A.; Elbjeirami, O.; Grimes, T.; Cundari, T. R.; Diyabalanage, H. V. K.; Gamage, C. S. P.; Dias, H. V. R. Metal Effect on the Supramolecular Structure, Photophysics, and Acid−Base Character of Trinuclear Pyrazolato Coinage Metal Complexes. *Inorg. Chem.* **2005**, *44*, 8200–8210.

(6)   Rawashdeh-Omary, M. A.; Rashdan, M. D.; Dharanipathi, S.; Elbjeirami, O.; Ramesh, P.; Dias, H. V. R. On/Off Luminescence Vapochromic Selective Sensing of Benzene and Its Methylated Derivatives by a Trinuclear Silver(I) Pyrazolate Sensor. *Chem. Commun.* **2011**, *47*, 1160–1162.

(7)   Zhang, J.-P.; Zhang, Y.-B.; Lin, J.-B.; Chen, X.-M. Metal Azolate Frameworks: From Crystal Engineering to Functional Materials. *Chem. Rev.* **2011**, *112*, 1001–1033.

(8)   Monica, G. L.; Ardizzoia, G. A. The Role of the Pyrazolate Ligand in Building Polynuclear Transition Metal Systems. In *Progress in Inorganic Chemistry*; Karlin, K. D., Ed.; John Wiley & Sons: New York, 1997; Vol. 46, pp 151–238.

(9)   Evans, W. Preparation and Investigation of Monodentate and Bridging Pyrazole Complexes. *J. Chem. Educ.* **2004**, *81*, 1191–1192.

(10)   Trofimenko, S. The Coordination Chemistry of Pyrazole-Derived Ligands. *Chem. Rev.* **1972**, *72*, 497–509.

(11)   Wang, C.; Liu, D.; Lin, W. Metal–Organic Frameworks as a Tunable Platform for Designing Functional Molecular Materials. *J. Am. Chem. Soc.* **2013**, *135*, 13222–13234.

(12)   Summers, L. A. The Phenanthrolines. In *Advances in Heterocyclic Chemistry*; Katritzky, A. R.; Boulton, A. J., Eds.; Academic Press: New York, 1978; Vol. 22, pp 1-69.

(13)   Pavic, A.; Glišić, B. Ð.; Vojnovic, S.; Warżajtis, B.; Savić, N. D.; Antić, M.; Radenković, S.; Janjić, G. V.; Nikodinovic-Runic, J.; Rychlewska, U.; Djuran, M. I. Mononuclear Gold(III) Complexes with Phenanthroline Ligands as Efficient Inhibitors of Angiogenesis: A Comparative Study with Auranofin and Sunitinib. *J. Inorg. Biochem.* **2017**, *174*, 156–168.

(14)   Bonacorso, H. G.; Andrighetto, R.; Frizzo, C. P.; Zanatta, N.; Martins, M. A P. Recent Advances in the Chemistry of 1,10-phenanthrolines and Their Metal Complex Derivatives: Synthesis and Promising Applications in Medicine, Technology, and Catalysis. *Targets in Heterocyclic Systems*, **2015**, *19*, 1-27.

(15)   Rogers, H. M.; Arachchige, S. M.; Brewer, K. J.; Swavey, S. Polyatomic Bridging Ligands. In *Reference Module* in *Chemistry, Molecular Sciences and Chemical Engineering*; Reedijk, J., Ed.; Elsevier: Waltham, Massachusetts, 2014; pp 135-157.

(16)   Stanojević, I.; Savić, N.; Crochet, A.; Fromm, K.; Djuran, M.; Glišić, B. Synthesis and Structural Analysis of Polynuclear Silver(I) Complexes with 4,7-Phenanthroline. *J. Serb. Chem. Soc.* **2019**, *84*, 1-11.

(17)   Savić, N. D.; Vojnovic, S.; Glišić, B. Ð.; Crochet, A.; Pavic, A.; Janjić, G. V.; Pekmezović, M.; Opsenica, I. M.; Fromm, K. M.; Nikodinovic-Runic, J.; Djuran, M. I. Mononuclear Silver(I) Complexes with 1,7-Phenanthroline as Potent Inhibitors of Candida Growth. *Eur. J. Med. Chem.* **2018**, *156*, 760–773.

(18)   Capano, G.; Chergui, M.; Rothlisberger, U.; Tavernelli, I.; Penfold, T. J. A Quantum Dynamics Study of the Ultrafast Relaxation in a Prototypical Cu(I)–Phenanthroline. *J. Phys. Chem. A* **2014**, *118*, 9861–9869.

(19)   Garakyaraghi, S.; Mccusker, C. E.; Khan, S.; Koutnik, P.; Bui, A. T.; Castellano, F. N. Enhancing the Visible-Light Absorption and Excited-State Properties of Cu(I) MLCT Excited States. *Inorg. Chem.* **2018**, *57(4)*, 2296–2307.

(20)   Xu, S.; Wang, J.; Zhao, F.; Xia, H.; Wang, Y. J. Photophysical Properties of Copper(I) Complexes Containing Pyrazine-Fused Phenanthroline Ligands: A Joint Experimental and Theoretical Investigation. *Mol. Model*. 2015, *21*, 313.

(21)   Samia, A. C. S.; Cody, J.; Fahrni, C. J; Burda, C. The Effect of Ligand Constraints on the Metal-to-Ligand Charge-Transfer Relaxation Dynamics of

Copper(I)-Phenanthroline Complexes: A Comparative Study by Femtosecond Time-Resolved Spectroscopy. *J. Phys. Chem. B* **2004**, *108*, 563-569.

(22) Capano, G.; Rothlisberger, U.; Travernelli, I.; Penfold, T. J. Theoretical Rationalization of the Emission Properties of Prototypical Cu(I)–Phenanthroline Complexes. *J. Phys. Chem. A* **2015**, *119*, 7026-7037.

(23) Riesgo, E. C.; Credi, A.; Cola, L. D.; Thummel, R. P. Diastereoselective Formation and Photophysical Behavior of a Chiral Copper(I) Phenanthroline Complex. *Inorg. Chem.* **1998**, *37*, 2145–2149.

(24) Płotek, M.; Dudek, K.; Kyzioł, A. Selected Copper(I) Complexes as Potential Anticancer Agent. *CHEMIK.* **2013**, *67*, 1181–1190.

(25) Marzano C.; Pellei M.; Tisato F.; Santini C. Copper Complexes as Anticancer Agents. *Anti-Cancer Agents Med. Chem.* **2009**, *9*, 185–211.

(26) Galindo-Murillo, R.; Garcia-Ramos, J. C.; Ruiz-Azuara, L.; Cheatham, T. E.; Cortes-Guzman, F. Intercalation Processes of Copper Complexes in DNA. *Nucleic Acids Res.* **2015**, *43*, 5364–5376.

(27) Chikira, M.; Ng, C. H.; Palaniandavar, M. Interaction of DNA with Simple and Mixed Ligand Copper(II) Complexes of 1,10-Phenanthrolines as Studied by DNA-Fiber EPR Spectroscopy. *Int. J. Mol. Sci.* **2015**, *16*, 22754-22780.

(28) Omary, M. A.; Rawashdeh-Omary, M. A.; Diyabalanage, H. V. K.; Dias, H. V. R. Blue Phosphors of Dinuclear and Mononuclear Copper(I) and Silver(I) Complexes of 3,5-Bis(trifluoromethyl)pyrazolate and the Related Bis(pyrazolyl)borate. *Inorg. Chem.* 2003, *42*, 8612–8614.

(29) Neogi, S.; Schnakenburg, G.; Lorenz, Y.; Engeser, M.; Schmittel, M. Implications of Stoichiometry-Controlled Structural Changeover Between Heteroleptic Trigonal $[Cu(phenAr_2)(py)]^+$ and Tetragonal $[Cu(phenAr_2)(py)_2]^+$ Motifs for Solution and Solid-State Supramolecular Self-Assembly. *Inorg. Chem.* **2012**, *51*, 10832–10841.

(30) Almotawa, R. M.; Aljomaih, G.; Trujillo, D. V.; Nesterov, V. N.; Rawashdeh-Omary, M. A. New Coordination Polymers of Copper(I) and Silver(I) with Pyrazine and Piperazine: A Step Toward "Green" Chemistry and Optoelectronic Applications. *Inorg. Chem.* **2018**, *57*, 9962–9976.

(31) Uppiah, D. J.-N.; Bhowon, M. G.; Laulloo, S. J. Solventless Synthesis of Imines Derived from Diphenyldisulphide Diamine or *p*-Vanillin. *E-J. Chem.* **2009**, *6*, S195-S200.

(32) Baláž, P.; Achimovičová, M,; Baláž, M.; Billik, P.; Cherkezova-Zheleva, Z.; Criado, J. M.; Delogu, F.; Dutková, E.; Gaffet, E.; Gotor, F. J.; Kumar, R.; Mitov,

I.; Rojac, T.; Senna, M.; Streletskiikl, A.; Wieczorek-Ciurowam, K. Hallmarks of Mechanochemistry: From Nanoparticles to Technology. *Chem. Soc. Rev.* **2013**, *42*, 7571-7637.

(33)   Dikarev, E. V.; Goroff, N. S.; Petrukhina, M. A. Expanding the Scope of Solvent-Free Synthesis: Entrapment of Thermally Unstable Species. *J. Organomet. Chem.* **2003**, *683*, 337-340.

(34)   Saikia, L.; Baruah, J.; Thakur, A. A Rapid, Convenient, Solventless Green Approach for the Synthesis of Oximes Using Grindstone Chemistry. *Org. Med. Chem. Lett.* **2011**, *1*, 12.

(35)   Safko, J. P.; Kuperstock, J. E.; Mccullough, S. M.; Noviello, A. M.; Li, X.; Killarney, J. P.; Pike, R. D. Network Formation and Photoluminescence in Copper(I) Halide Complexes with Substituted Piperazine Ligands. *Dalton Trans.* **2012**, *41*, 11663.

(36)   Hobbollahi, E.; List, M.; Monkowius, U. Poly(4-Vinylpyridine) as Ligand for Au(I) and Zn(II) Cations: Luminescent Metal-Containing Polymers. *Monatshefte für Chemie - Chemical Monthly* **2019**, *150*, 877–883.

(37)   Rawashdeh-Omary, M. A.; López-De-Luzuriaga José M.; Rashdan, M. D.; Elbjeirami, O.; Monge, M.; Rodríguez-Castillo María; Laguna, A. Golden Metallopolymers with an Active T1State via Coordination of Poly(4-Vinyl)Pyridine to Pentahalophenyl-Gold(I) Precursors. *J. Am. Chem. Soc.* **2009**, *131*, 3824–3825.

(38)   Diaconu, D.; Hu, Z.; Gorun, S. M. Copper-Based Bioinspired Oxygenation and Glyoxalase-Like Reactivity. *J. Am. Chem. Soc.* **2002**, *124*, 1564-1565.

(39)   Rivera-Carrillo, M.; Chakraborty, I.; & Raptis, R. G. Systematic Synthesis of a Metal Organic Framework Based on Triangular $Cu_3(\mu_3\text{-}OH)$ Secondary Building Units: From a 0-D Complex to a 1-D Chain and a 3-D Lattice. *Cryst. Growth Des.* **2010**, *10*, 2606-2612.

(40)   Casarin, M.; Cingolani, A.; Nicola, C. D.; Falcomer, D.; Monari, M.; Pandolfo, L.; Pettinari, C. The Different Supramolecular Arrangements of the Triangular $[Cu_3(\mu_3\text{-}OH)(\mu\text{-}pz)_3]^{2+}$ (pz = Pyrazolate) Secondary Building Units. Synthesis of a Coordination Polymer with Permanent Hexagonal Channels. *Cryst. Growth Des.* **2007**, *7*, 676-685.

(41)   Nicola, C. D.; Garau, F.; Gazzano, M.; Monari, M.; Pandolfo, L.; Pettinari, C.; Pettinari, R. Reactions of a Coordination Polymer Based on the Triangular Cluster $[Cu3(\mu3\text{-}OH)(\mu\text{-}pz)3]2$ with Strong Acids. Crystal Structure and Supramolecular Assemblies of New Mono-, Tri-, and Hexanuclear Complexes and Coordination Polymers. *Cryst. Growth Des.* **2010**, *10*, 3120-3131.

(42)   Ferrer, S.; Haasnoot, J. G.; Reedijk, J.; Müller, E.; Cingi, M. B.; Lanfranchi, M.; Lanfredi, A. M. M.; Ribas; J. Trinuclear N,N-Bridged Copper(II) Complexes Involving a Cu3OH Core: $[Cu_3(\mu_3\text{-}OH)L_3A(H_2O)_2]A\cdot(H_2O)_x${L = 3-Acetylamino-1,2,4-triazolate; A = CF_3SO_3, NO_3, ClO_4; x= 0, 2} Synthesis, X-ray Structures, Spectroscopy, and Magnetic Properties. *Inorg. Chem.* **2000**, *39*, 1859-1867.